Rigid inclusions under wind turbine foundation : Experimental behaviour and numerical studies

Adnan Sahyouni

N°d'ordre NNT : 2023ISAL0116

THESE de DOCTORAT DE L'INSA LYON, membre de l'Université de Lyon

Doctoral School N° 162
Mécanique, Energétique, Génie Civil, Acoustique

Specialty/ Civil Engineering

Soutenue publiquement le 11/12/2023 par:
Adnan Sahyouni

Rigid inclusions under wind turbine foundation: experimental behaviour and numerical studies

Devant le jury composé de :

Zachert, Hauke	Professeur des Universités	TU Darmstadt	Rapporteur
Salciarini, Diana	Maître de Conférences HDR	UniPG	Rapporteure
Kotronis, Panagiotis	Professeur des Universités	Centrale Nantes	Examinateur
Thorel, Luc	Directeur de Recherche	Uni Eiffel	Examinateur
Grange, Stéphane	Professeur des Universités	INSA-LYON	Directeur
Briançon, Laurent	Maître de Conférences HDR	INSA-LYON	Encadrant
Burtin, Pierre	Ingénieur Etudes Principal	MENARD	Invité
Racinais, Jérôme	Directeur de l'ingénierie	MENARD	Invité
Prunier, Florent	Maître de Conférences HDR	INSA-LYON	Invité
Silvani, Claire	Maître de Conférences	INSA-LYON	Invitée

Département FEDORA – INSA Lyon - Ecoles Doctorales

SIGLE	ECOLE DOCTORALE	NOM ET COORDONNEES DU RESPONSABLE
ED 206 CHIMIE	**CHIMIE DE LYON** https://www.edchimie-lyon.fr Sec. : Renée EL MELHEM Bât. Blaise PASCAL, 3e étage secretariat@edchimie-lyon.fr	**M. Stéphane DANIELE** C2P2-CPE LYON-UMR 5265 Bâtiment F308, BP 2077 43 Boulevard du 11 novembre 1918 69616 Villeurbanne directeur@edchimie-lyon.fr
ED 341 E2M2	**ÉVOLUTION, ÉCOSYSTÈME, MICROBIOLOGIE, MODÉLISATION** http://e2m2.universite-lyon.fr Sec. : Bénédicte LANZA Bât. Atrium, UCB Lyon 1 Tél : 04.72.44.83.62 secretariat.e2m2@univ-lyon1.fr	**Mme Sandrine CHARLES** Université Claude Bernard Lyon 1 UFR Biosciences Bâtiment Mendel 43, boulevard du 11 Novembre 1918 69622 Villeurbanne CEDEX e2m2.codir@listes.univ-lyon1.fr
ED 205 EDISS	**INTERDISCIPLINAIRE SCIENCES-SANTÉ** http://ediss.universite-lyon.fr Sec. : Bénédicte LANZA Bât. Atrium, UCB Lyon 1 Tél : 04.72.44.83.62 secretariat.ediss@univ-lyon1.fr	**Mme Sylvie RICARD-BLUM** Laboratoire ICBMS - UMR 5246 CNRS - Université Lyon 1 Bâtiment Raulin - 2ème étage Nord 43 Boulevard du 11 novembre 1918 69622 Villeurbanne Cedex Tél : +33(0)4 72 44 82 32 sylvie.ricard-blum@univ-lyon1.fr
ED 34 EDML	**MATÉRIAUX DE LYON** http://ed34.universite-lyon.fr Sec. : Yann DE ORDENANA Tél : 04.72.18.62.44 yann.de-ordenana@ec-lyon.fr	**M. Stéphane BENAYOUN** Ecole Centrale de Lyon Laboratoire LTDS 36 avenue Guy de Collongue 69134 Ecully CEDEX Tél : 04.72.18.64.37 stephane.benayoun@ec-lyon.fr
ED 160 EEA	**ÉLECTRONIQUE, ÉLECTROTECHNIQUE, AUTOMATIQUE** https://edeea.universite-lyon.fr Sec. : Philomène TRECOURT Bâtiment Direction INSA Lyon Tél : 04.72.43.71.70 secretariat.edeea@insa-lyon.fr	**M. Philippe DELACHARTRE** INSA LYON Laboratoire CREATIS Bâtiment Blaise Pascal, 7 avenue Jean Capelle 69621 Villeurbanne CEDEX Tél : 04.72.43.88.63 philippe.delachartre@insa-lyon.fr
ED 512 INFOMATHS	**INFORMATIQUE ET MATHÉMATIQUES** http://edinfomaths.universite-lyon.fr Sec. : Renée EL MELHEM Bât. Blaise PASCAL, 3e étage Tél : 04.72.43.80.46 infomaths@univ-lyon1.fr	**M. Hamamache KHEDDOUCI** Université Claude Bernard Lyon 1 Bât. Nautibus 43, Boulevard du 11 novembre 1918 69 622 Villeurbanne Cedex France Tél : 04.72.44.83.69 direction.infomaths@listes.univ-lyon1.fr
ED 162 MEGA	**MÉCANIQUE, ÉNERGÉTIQUE, GÉNIE CIVIL, ACOUSTIQUE** http://edmega.universite-lyon.fr Sec. : Philomène TRECOURT Tél : 04.72.43.71.70 Bâtiment Direction INSA Lyon mega@insa-lyon.fr	**M. Etienne PARIZET** INSA Lyon Laboratoire LVA Bâtiment St. Exupéry 25 bis av. Jean Capelle 69621 Villeurbanne CEDEX etienne.parizet@insa-lyon.fr
ED 483 ScSo	**ScSo**[1] https://edsciencessociales.universite-lyon.fr Sec. : Mélina FAVETON Tél : 04.78.69.77.79 melina.faveton@univ-lyon2.fr	**M. Bruno MILLY** (INSA : J.Y. TOUSSAINT) Univ. Lyon 2 Campus Berges du Rhône 18, quai Claude Bernard 69365 LYON CEDEX 07 Bureau BEL 319 bruno.milly@univ-lyon2.fr

[1] ScSo : Histoire, Géographie, Aménagement, Urbanisme, Archéologie, Science politique, Sociologie, Anthropologie

Acknowledgments

Reflecting on my PhD journey, I now see the profound value of acknowledgments. Regardless of our knowledge background, passion, or dedication, we all face moments of doubt. Acknowledgments serve to honour those extraordinary people who turn our uncertainties into strength.

I express my deepest gratitude to the jury members, whose valuable feedback and presence significantly enriched my doctoral journey. I extend special thanks to Professor Hauke Zachert from TU Darmstadt for engaging discussions on ground improvement techniques within my thesis. I am also grateful to Dr. Diana Salciarini from Università degli Studi di Perugia, Italy, for her insights into macroelement analysis. I hope they enjoyed their time in Lyon as much as I valued their input. My meeting with Professor Luc Thorel in Nantes, beside the centrifuge a year before my defense, was a good moment of scholarly exchange that I hold in high regard. Additionally, I extend special thanks to Professor Panagiotis Kotronis for his enriching discussions on FEM and macroelement modeling.

My PhD journey received incredible support from my advisors. Dr. Laurent Briançon, your commitment to my thesis work and field research was invaluable. Our travels across various regions of France not only enriched my research journey but also deepened my love and appreciation for French culture, which has become a beloved second culture to me. Prof. Stéphane Grange, your expertise and insights, particularly in macroelement development, have significantly shaped both my dissertation and my career perspective. Your innovative approaches to solving complex problems and your academic enthusiasm have been truly invaluable. I also want to extend heartfelt thanks to Florent Prunier and Claire Silvani for their valuable time and insights throughout my doctoral studies. Your mentorship has been essential to my academic and personal growth.

I am compelled to express special thanks to my colleague at Menard, Pierre Burtin, whose extensive expertise in ground improvement and truly remarkable personality have significantly inspired and guided me. My continued interactions with you, Pierre, particularly at Menard, are greatly cherished, and I am profoundly grateful for your support. Jérôme Racinais, the importance of your contributions to my studies is immense, matched only by the grace and humanity you exhibit in our work together. It is an absolute pleasure to collaborate with you. Benoit Quandalle, my former R&D manager, the mentorship you've provided has been crucial to my development. The depth of knowledge and insights I have gained from you are deeply valued and will be carried with me in my future endeavors. Stéphane Brûlé, our discussions, though sometimes brief, on the challenges of research were extremely insightful. I am sincerely grateful for the wisdom shared during those conversations. Thank you to Cyril Plomteux for the unmatched technical moments discussing with you, such a big deal for me. Thank you to every colleague of Menard France; you were just great!

To my fellow PhD students at the Geomas Laboratory at INSA Lyon, your friendship and support have truly made a difference. It’s challenging to acknowledge everyone individually without missing someone, but I deeply cherish the moments we shared, be it burning the midnight oil in the lab, gatherings at our places, or relaxing times at Kelly’s bar in Lyon's second district. I promise to individually recognize each of you in due time (Natalia, Nicole, Rosy, Nour, François, Danai, Atefeh, Thomas, Hamza, Julien, Nissrine, Alex, Gianluca, Janet, Clara, José & Thomas). To the permanent staff and professors at the GEOMAS Lab, your influence and presence will be sorely missed. A special shout-out to Jean-François, for the invaluable discussions we had in the lab and the memorable basketball games we attended together. A heartfelt thanks also goes to Irini, Noureddine, Mario, and Stéphane for their support and guidance.

To my wife, Dr. Layal Chamma, your unwavering support has been my foundation, and I vow to be the same for you for all our days.

To my mother, the epitome of unconditional love, you deserve more thanks than I can ever express. To my beloved father, whom I lost during my third year of this journey, your absence has left a void in my heart. It's been a struggle to move past this loss, a struggle that continues. I hope you're at peace wherever you are.

To my lifelong friends (no need to name as they know who they are ;)), your constant support and friendship have meant the world to me.

I cannot conclude my acknowledgments without expressing my gratitude towards France, my beloved second country, and the unforgettable moments spent in Lyon. Those years rank among the best of my life, and I promise to return at every opportunity. I'm also thankful to Menard Oceania and Sydney, my third home, for their warm welcome and the chance to engage in fascinating geotechnical projects. Born Lebanese, my assimilation into French culture has been so complete that it became a humorous point at my workplace in Australia to "suppress the Frenchman in me." This experience has transcended an academic journey; it has been a profound exploration of culture and personal growth, immensely enriched by the diverse group of people I've had the privilege to meet and learn from.

Thank you for taking the time to read my acknowledgments. I hope you enjoy reading my thesis and find it both informative and engaging.

Abstract

Wind turbines stress their foundations in relatively atypical, distinguishing them from other conventional structures. The extensive range of loading scenarios outlined by manufacturers results in a diverse array of design approaches for turbine foundations. Among the myriad of geotechnical solutions available to support such structures, ground improvement techniques, particularly the use of rigid inclusions, have gained prominence. This method has seen a significant rise in application across Europe and globally, with its adoption in onshore wind farms being particularly notable.

The growing utilization of rigid inclusions, coupled with extensive research in the field, has led to a deeper understanding of their physical principles across various applications. The research interest of this work lies in the analysis of the complexity of load transfer from wind excitations and the effects of the structure on the soil reinforced by rigid inclusions. The load distribution between the soil and the inclusions involves several interaction mechanisms between the different structural components, including the gravity foundation, the load transfer platform, the soil, and the inclusions. An attempt is made to simplify these complex mechanisms by considering each component separately, thanks to the multiaxial research conducted in this dissertation: (1) Instrumentation of a real scale wind turbine foundation in addition to monitoring a static load test on an isolated column adjacent to the wind turbine platform. (2) Nonlinear finite element modelling, including soil laboratory tests, unit cells in axisymmetric modelling, and three-dimensional approach (3) Development of a novel macroelement for rigid inclusions under a gravity foundation to account for the various interactions and constrain the geometric effect, as a contribution to the design approaches.

The key findings of this work can be summarised as follows: (1) The experimental work has allowed to validate the initial assumptions of the project, to quantify the load transfer to the rigid inclusions and the interaction between the columns and the soil. The stored monitoring data were used to address several subjects, including determining the moment load at the base of the foundation as a function of wind speed. (2) Soil models were derived by simulating soil laboratory tests using the finite element method. The experimentally calibrated numerical modelling showed good agreement with the available measurements and highlighted the boundary conditions in the two-dimensional models that are overcome in the three-dimensional modelling. (3) The comparison of the macroelement results with the finite element modelling was very satisfactory and validated the model with incomparable time difference.

This dissertation contributes to the FEDRE (Fondations d'Eoliennes Durables et REpowering) project, aiming also to assist in increasing the presence of wind turbines in the French landscape. It supports the repowering strategy of existing structures, contributing to global sustainability and environmental friendliness. The findings presented in this dissertation are intended as a significant contribution to the repowering phase of onshore wind turbines established on rigid inclusions.

Résumé

Les éoliennes sollicitent leurs fondations de manière relativement atypique par rapport à d'autres structures courantes. Les cas de charges fournis par le fabricant englobent des milliers de scénarios différents, ce qui conduit à des approches de conception relativement inhabituelles pour les fondations de l'éolienne. Parmi les différentes solutions géotechniques pour supporter de telles structures, les techniques d'amélioration du sol occupent une part importante. Les inclusions rigides sont considérées comme l'une des plus répandues dans ce domaine, et le nombre de projets en Europe et dans le monde augmente de manière significative.

La forte augmentation des projets d'inclusions rigides ainsi que leurs antécédents travaux de recherche ont permis une meilleure compréhension de leur concept physique dans diverses applications. L'intérêt de cette recherche réside dans l'analyse de la complexité du transfert de charge lors des sollicitations de l'éolienne et des effets de la structure sur le sol renforcé par des inclusions rigides. La répartition des charges entre le sol et les inclusions implique plusieurs mécanismes d'interaction entre les différents composants structuraux, notamment la semelle en béton, la plateforme de transfert de charge, le sol et les inclusions. Une stratégie a été suivie pour simplifier ces mécanismes complexes en considérant chaque composant séparément, grâce aux recherches multiaxiales menées dans cette thèse : (1) Instrumentation d'une fondation d'éolienne en vraie grandeur ainsi qu'un essai de chargement statique sur une colonne isolée adjacente à la plate-forme de l'éolienne. (2) Modélisation non linéaire par la méthode des éléments finis, calibrée par des essais de laboratoire des sols et l'essai de chargement statique, incluant une modélisation axisymétrique de cellules élémentaires et une approche tridimensionnelle. (3) Développement d'un nouveau macroélément pour modéliser les inclusions rigides sous une semelle gravitaire afin de tenir compte des différentes interactions et particularités géométriques, dans le but de compléter les approches de dimensionnement.

Les principales conclusions de cette recherche sont les suivantes : (1) Le travail expérimental a permis de valider les hypothèses initiales du projet, de quantifier le transfert de charge vers les inclusions rigides et l'interaction entre les colonnes et le sol. L'ensemble des données récoltées a été utilisé pour aborder plusieurs sujets, notamment la détermination du moment au niveau de la base de la fondation en fonction de la vitesse du vent. (2) Les lois de comportement des sosl ont été calibrées en simulant des essais de laboratoire à l'aide de la méthode des éléments finis. La modélisation numérique ajustée expérimentalement a montré une bonne concordance avec les mesures disponibles et a souligné les conditions aux limites dans les modèles bidimensionnels qui sont surmontées dans la modélisation tridimensionnelle. (3) La comparaison des résultats du macroélément avec la modélisation par éléments finis a été très satisfaisante et a validé la nouvelle approche avec un temps de calcul incomparablement plus rapide.

Cette thèse fait partie du projet FEDRE (Fondations d'Éoliennes Durables et REpowering). Les résultats présentés dans cette thèse doivent être considérés comme une contribution à la phase de repowering des éoliennes terrestres fondées sur des inclusions rigides.

Table of Contents

List of Figures

List of Tables

CHAPTER 1

Introduction and problem statement

1.1 General context

Ground improvement and ground reinforcement techniques are essential geotechnical solutions for addressing complex land-related challenges, including stability concerns, insufficient bearing capacity, and excessive settlement. These methodologies, developed by visionary engineers in the 20th century, have undergone significant advancements over the last three decades. This progress is attributed to their successful implementation, numerous advantages, and the ongoing evolution of the research base. Moreover, ground improvement and ground reinforcement are gaining importance over traditional geotechnical methods due to their cost-effectiveness and reduced carbon footprint, considerations that are becoming pivotal in shaping modern global policies. Recent data from the National Renewable Energy Laboratory (NREL, 2014) suggest that employing ground improvement techniques can reduce expenses associated with critical infrastructure, such as wind turbine foundations, by as much as 30%. This cost-saving potential underscores the growing reliance on ground improvement projects, with approximately 80% of onshore wind turbines in Europe based on shallow foundations often requiring ground improvement techniques, as reported by the European Wind Association (EWA, 2009).

The rigid inclusion technique, introduced in the early 1990s as an alternative to deep foundation systems, stands as a significant approach in the field of soil reinforcement. It is particularly favoured for use in compressible soils, aiming to increase their bearing capacity and reduce the settlement of overlying structures. In simple terms, the method involves the creation of a reinforced soil matrix—comprising soil and inclusion elements—that is not rigidly connected to the superstructure, thereby improving the native soil characteristics. Since its development, the rigid inclusion technique has been successfully applied to a wide range of construction projects, from technically demanding and heavy construction sites to various types of infrastructure. This includes transportation, ports, coastal infrastructure, dams, mining, industrial, commercial, residential projects, and energy sectors, including wind farms.

The advantages of this technique are diverse, emphasizing economic and environmental benefits. Economically, it offers rapid installation, eliminates the need for rigid connections like steel reinforcement, and streamlines superstructure construction, thereby reducing project timelines and enhancing compatibility across various construction environments. From an environmental perspective, it requires less materials compared to alternative methods and reduces dependence on manufactured products, which greatly diminishes the environmental footprint and significantly cuts down on the carbon emissions linked to construction projects.

In the effort to reduce global carbon emissions, onshore wind turbines have become an essential component of renewable energy strategies and are gaining importance in the construction sector. This trend has contributed to an increase in ground improvement projects that support the foundations of wind turbines. The use of rigid inclusion techniques in these projects not only highlights their environmental benefits but also represents a notable contribution to renewable energy infrastructure. This approach demonstrates a significant connection between sustainable construction practices and the growth of green energy solutions, underscoring the importance of sustainable building practices in advancing the expansion of renewable energy.

The sustainability of onshore wind turbine structures, which provide clean energy, is conventionally limited by their lifespan, typically around 20 years (IEC 61400-3, 2005). Recent studies suggest this lifespan could be slightly extended based on several factors, including the structure's fatigue life. Given the pressing environmental challenges, it is imperative to sustain renewable power generation by replacing or upgrading wind turbines that have reached the end of their operational life, a process known as re-equipping or repowering. This strategy is particularly crucial in Europe to reduce reliance on fossil fuels. In 2016, 12% of wind turbines in Europe had been operational for at least 15 years. This figure is expected to rise significantly by 2030 (Figure 1-1), indicating an increased need for repowering to not only maintain but also potentially increase future energy production, as projected in the wind energy scenarios for Europe by 2030 (Figure 1-2).

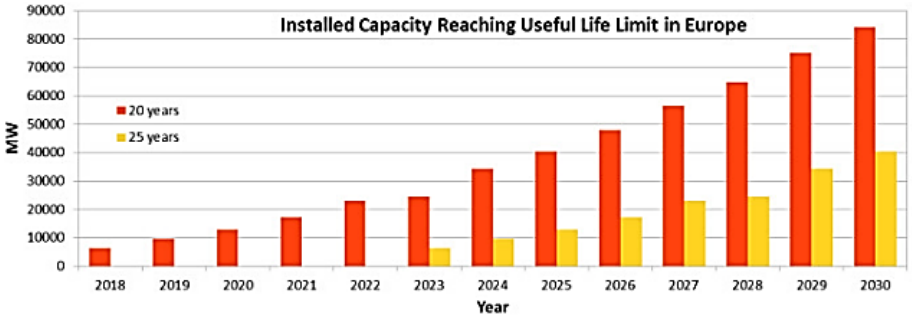

Figure 1-1: Installed wind power capacity in Europe reaching the end of its useful life (Martínez et al., 2018).

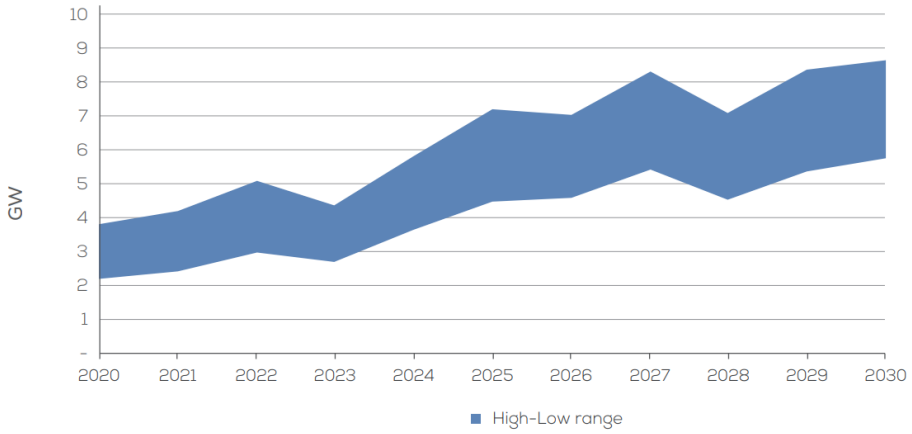

Figure 1-2: Repowering volumes in Europe to 2030 (WindEurope, 2017).

Re-equipment phases, commonly referred to as "Repowering" could also be seen as an opportunity to replace old generations of wind turbines with new machines that produce more energy. The increase in the energy capacity of wind turbines in recent years is closely related to advances in technology as well as the significant increase in the size of wind turbine components (Figure 1-3), such as the rotor and shaft (González and Lacal-Arántegui, 2016), which results in additional load on the supporting soil. One of the studies shows that the invention of multi-megawatt wind turbines has led to a doubling of tower height and rotor diameter and an eightfold increase in rated power over the last 35 years (Enevoldsen and Xydis, 2019).

In two different contexts, both onshore wind turbines and rigid inclusions markets are growing rapidly. Not only are both fulfilling with the relative reduction of carbon emissions compared to other corresponding technologies, but the current hot topic of repowering is an important field that links both techniques in this dissertation within the ongoing research project FEDRE (Fondations d'Eoliennes Durables et REpowering). The main objective of the project is to study an onshore wind turbine foundation underlined by rigid inclusions in order to propose innovative repowering solutions that reuse the existing foundations instead of demolishing them completely.

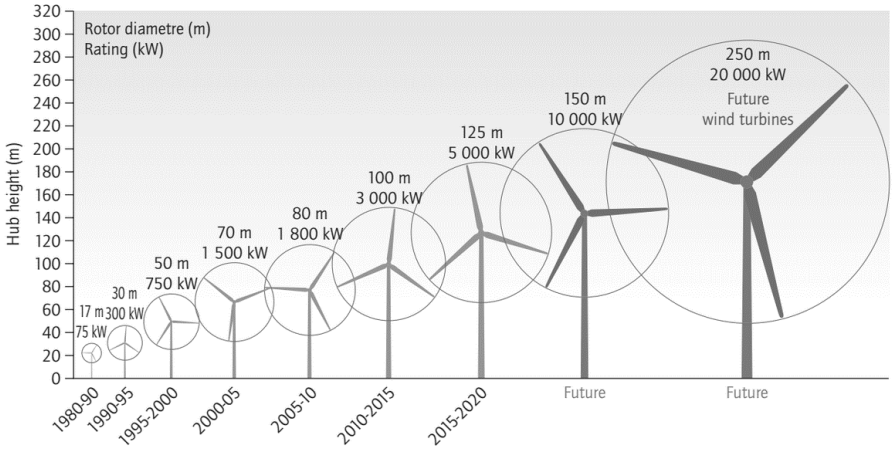

Figure 1-3: Evolution of wind turbine size and future prospects (IEA, 2013).

Among the possible solutions, rigid inclusions are an important factor and the key to success in the repowering phase since there is no structural connection between the soil and the concrete foundation. In this case, the rigid inclusions that reinforce the first version of the foundation remain intact and it is logistically possible to execute new columns to cover the additional area of the foundation (Figure 1-4).

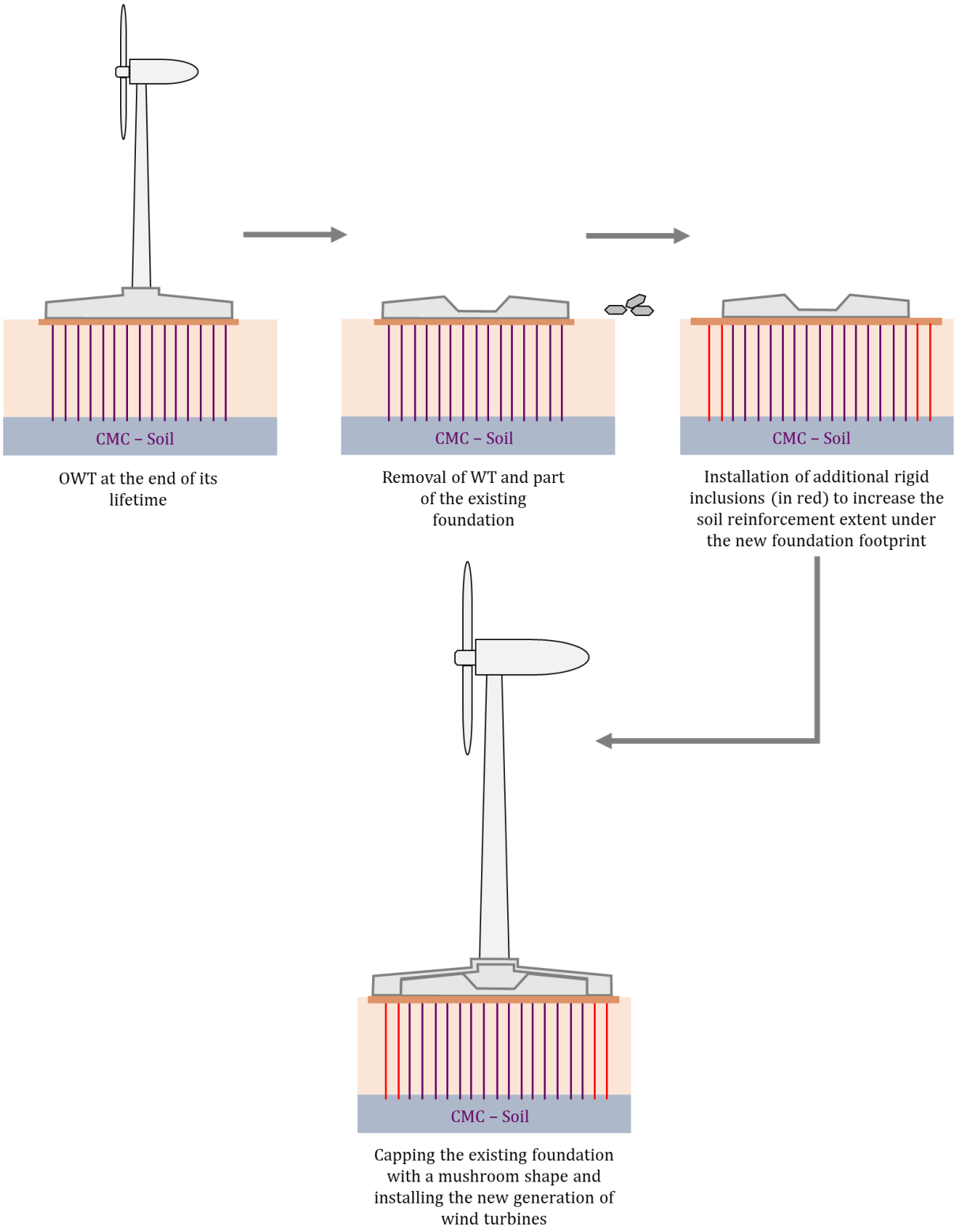

Figure 1-4: Repowering strategy of FEDRE project.

1.2 FEDRE Project

FEDRE (Fondations d'Eoliennes Durables et REpowering) is an ongoing research project with an industrial background investigating the OWT gravity foundations supported by RIs. The project has two main focuses: First, it aims to find an innovative solution for the reuse of gravity foundations by replacing wind turbines at the end of their lifetime with new generations of onshore wind turbines that are relatively massive compared to the old generation. Second, it explores the possibility of optimising the design of current onshore wind turbine foundations to support multiple generations of wind turbines in the future as part of the proposed repowering solution will be explored. The project targets three markets: environmental, economic, and applied research.

1.2.1 Environment

Regarding the environmental aspect, repowering strategies will result in less concrete being used for foundations. This means that less cement will be produced, since one ton of cement needed to produce reinforced concrete requires the emission of approximately 807 kg of CO2 (Chen et al., 2010). In addition, the production of green energy is maintained and increased, reducing fossil energy.

1.2.2 Economic

Regarding the economic market, a rough estimate of the construction work for an onshore wind turbine can be up to 10% of the total cost, i.e., 100 k€ per installed MW. The repowering of an existing foundation would allow a saving of about 1/4 to 1/3 of the construction cost, i.e. between 150 and 200 k€ for the change from a 3 MW to a 5 MW wind turbine.

For the French market, where the installed base is known, repowering could concern 1,200 to 1,300 wind turbines out of 3,200 wind turbines reaching an age of 20 years by the end of 2029. Thus, repowering could generate in 2029 in France a turnover of about 8 000 k€ and 50 jobs in the different partners of the FEDRE project (14 k€ per installed turbine MW).

By 2028/2030, repowering in Europe is expected to include a capacity of 6 000 MW. With a market share of 5%, which is realistic given the international activities of the various partners, the projected export turnover would be in the order of 4,200 k€.

By reducing this total cost and in the context of accelerating repowering projects, this will lead to a very important outcome for the economic balance of the projects. Moreover, it will serve as an advertisement for onshore wind energy in France and lead to more investments in renewable energies.

1.2.3 Research field

The project strategy is divided into six segments, each representing a different subject area that facilitates the transition from research to industry in order to achieve the project's objectives.

These segments leverage the expertise of our industrial partners and the research-driven focus of the project. The structure of this alignment is as follows:

- **GEOMAS at INSA Lyon**: A research laboratory specializing in civil engineering and materials, with a particular emphasis on the rigid inclusion technique, as evident through various research activities related to ASIRI and ASIRI+.
- **MENARD GROUP:** A world specialist in foundation solutions based on ground improvement and reinforcement technologies, actively engaged in Design & Build projects, as well as in selected research activities related to ground improvement.
- **ANTEA GROUP:** An international engineering and environmental consulting firm.
- **NORDEX SE:** A European firm specializing in the design, sale, and manufacturing of wind turbines.
- **CTE WIND:** An engineering firm focused on designing wind turbine foundations.
- **PAREX:** A Leading Manufacturers of Construction Materials.

The main components of the project are outlined as follows: (1) The demonstrator, (2) the physical modelling, (3) the numerical modelling of the mechanisms observed and highlighted in the first two cases, (4) the transfer from research to engineering, (5) the developing for solutions to improve the maintenance and reuse of foundations for repowering phases, (6) the valorisation of the project. At the end of the project, this study will allow FEDRE to propose repowering solutions tailored to each case after auscultation of the foundation and surrounding soil. These solutions could be implemented at the end of the project on one or more of their wind turbines to be repowered. The foundational research of this project is being conducted through two doctoral theses: one focuses on the study of concrete gravity foundations (Modu, 2022), while the other pertains to the current dissertation. Both are under the supervision of the GEOMAS laboratory.

1.3 Scientific context

The load transfer from a superstructure to a soil reinforced by rigid inclusions is governed by the interaction mechanisms between the foundation and the reinforced soil elements (soil- inclusion), (Briançon, 2002). The interaction mechanisms, referred to in this dissertation as soil-structure interaction, depend on several factors, such as the type of foundation capping the inclusions, the presence or absence of the LTP below the foundation, the type of soil, the type of loading, and the interaction with the surrounding soil. Each of these elements has been the subject of research. ASIRI (2013) synthetized most of the previous research in addition to the usual international standards such as Eurocode 7 (EN 1997-1, 2004, 2009, 2013) investigate the interactions in such a combined system. The main contribution of ASIRI (2013) was the introduction of standardised design methods for rigid inclusions, which differ mainly in the type of application and foundation behaviour. Three different design methods have been proposed: analytical, numerical, and homogenization. The analytical models are considered very advantageous for rigid inclusions, since their input parameters are directly linked to the in-situ tests for engineering use. They are also relatively easy to implement to solve most of the common situations. For numerical computation, it is recommended using an axisymmetric approach over a unit cell in which the rigid inclusion is centred in a soil volume below the foundation. Although this modelling approach takes more time and requires soil laboratory data rather than direct in-situ parameters, it provides more comprehensive information than average settlement and maximum stress within the inclusion. Regarding the homogenization methods, they are mostly based on the concept of

multiphase modelling (De Buhan, 2005), which takes into account the interaction between the soil and rigid inclusions. These methods have evolved over the years and are advantageous compared to the three-dimensional FEM due to their lower computational time. However, these methods are relatively less explored and are more focused on research than engineering applications.

Due to the complex loading of wind turbines, the mechanism of load transfer is becoming more challenging. In this case, the simulation of soil-structure interaction with the analytical models and the FEM recommended in ASIRI (2013) using unit cells could not be easily applied. These models are essentially used in the case of vertical loading or uniformly distributed contact pressure at the base of the foundation. However, an extension of the analytical model, called the biphasic model (Cuira and Simon, 2009), allows adding an overturning moment and a horizontal load at the base of the foundation during an iterative analysis without considering the geometric effect. The application of the analytical models in the case of OWT is described in (Aguado et al., 2012). Moreover, the use of 3D FEM could be an alternative solution in this case, but not on an engineering scale since such modelling could take several days of simulations and engineers would have less opportunity to perform sensitive analyses. On the other hand, the durability of the OWT foundation remains an open question. Recent studies suggest that the durability of OWT can be extended if various factors such as design methods, construction, and maintenance are considered. In the FEDRE project, reusing the foundations of OWT is one of the main scientific challenges, and rigid inclusions are considered key to success in the repowering process.

To address the scientific challenges associated with the estimated soil-structure interaction, a monitoring plan was developed to track load transfer from the wind turbine to the gravity foundation and then to the reinforced soil. The stress under the studied gravity foundation was assumed to be trapezoidal during the operation of the wind turbine and triangular in an accidental case. This hypothesis was analysed using the monitoring data and numerical modelling. The loads imposed by the wind turbine, which is underlined by a variation of stresses on the rigid inclusions, are verified and applied to numerical models. In addition, the soil models are calibrated experimentally by simulating laboratory soil tests in cyclic and static domain. The behaviour of the interface between the rigid inclusions and the surrounding soil is calibrated using a static loading test on an isolated column.

To overcome the limitations of analytical models through an iterative analysis with geometric effect, a macroelement approach is proposed. This type of modelling allows the behaviour of the reinforced soil and foundation system to be reproduced at the macroscopic scale, using multiple elements to simulate the soil-inclusion interaction. A novel multiscale macroelement for a soil reinforced by rigid inclusions under axial loading, horizontal loading and a moment is developed and validated numerically and then experimentally. The model consists of an array of biphasic columns formulated using the MATLAB toolbox ATL4S (Grange, 2018), and accounts for the defined soil-structure interactions in the case of rigid inclusions.

Thus, the overall objective of this research is to improve the understanding of the interaction mechanisms of a soil reinforced by rigid inclusions under wind turbines and to propose several numerical methods suitable for solving this problem.

1.4 Scope of work

The objective of the current research is to evaluate the behaviour of Controlled Modulus Column (CMC)-type rigid inclusions under the foundations of onshore wind turbines. The scope of this work is extensive, incorporating various topics to address challenges such as complex loading, soil-structure interactions, post-treatment data, soil models, and nonlinear finite element modelling.

The dissertation is structured into five chapters, positioned between the introductory and concluding chapters. Each chapter includes a literature review pertinent to its field. The main research subject is explored through various methodologies, including real field observations, soil investigations, analytical analyses, numerical modelling, and the macroelement approach.

Chapter 1, provides background information on FEDRE project and repowering strategies.

Chapter 2, introduces the rigid inclusions technique, complex loading, current design methods, wind energy and the complex loading on its structures. This chapter also discusses the concept of soil-structure interaction as applied in this thesis. It outlines the study's purpose and objectives and concludes with a statement identifying the current gap in the literature, which this research aims to address by introducing various research axes.

Chapter 3, focuses on real-scale instrumentation of a wind turbine during the construction phase up to commissioning and in the first years of its lifetime. The objective of the monitoring carried out in September 2019 in northern France is to follow the load transfer from the foundation to the reinforced soil, the deformations and the responses to the complex cyclic loads induced by the wind, as well as the different operating modes of the wind turbine. Different measurement techniques were used with different types of sensors, such as: Earth pressure cells, vibrating wire extensometers, strain gauges, accelerometers, inclinometers, and optical fibres. The measurements are analysed by synchronizing them with the SCADA system of the wind turbine. The main result of this work is the qualitative and quantitative evaluation of the stress distribution in the head region of the rigid inclusions and its evolution as a function of wind direction and wind speed. In addition to the qualitative reflection of the high rigidity of the gravity foundation. The measurements of the optical fibres installed inside the rigid inclusions represented the soil-structure interaction between the soil and the inclusion. At the end of the FEDRE project, the overall result of the real scale monitoring will help to propose a structural health monitoring (SHM) approach to optimize the maintenance of the wind turbines and extend their lifetime. The results of the measurements will not only feed into the numerical models of the wind turbine foundations (another research focus of the project) but could also help to evaluate the capabilities of the current foundation for a new generation of wind turbines with likely larger loads.

Chapter 4, details the numerical modelling of rigid inclusions under the gravity foundation of wind turbines using nonlinear finite element methods. The objective of the project is to create an experimentally calibrated model while simulating the soil-structure interaction. To this end, the interface between the inclusion and the soil was first calibrated using a static load test on an instrumented isolated rigid inclusion. Several nonlinear soil models were also defined to characterise the behaviour of the soil volume under complex loading conditions based on the

modelling of the available laboratory soil tests. Finally, the numerical model results were tested against the available real field monitoring measurements by comparing the results.

Chapter 5, proposes a novel multiscale macroelement approach for soil reinforced with rigid inclusions under wind turbines, that accounts for vertical loading and large overturning moment. The model incorporates the soil-structure interaction a ground reinforced by rigid inclusions. A key highlight of this model is the adaptable friction law at the inclusion-soil interface, enabling its applicability to diverse load conditions. The formulation is thoroughly explained, and comprehensive comparisons are made with numerical simulations and a selection of actual measured data.

Chapter 6, summarizes the general conclusions and perspectives of the thesis.

CHAPTER 2

General literature review

2.1 Renewable Energy

Renewable energy is now a global necessity to reduce pollution and combat global warming. Switching to green energy and limiting carbon dioxide emissions are top priorities for most countries. In 2015, 190 countries signed the (UNFCCC, 2015), in which renewable energy plays a key role in implementing the conference's climate change-focused commitments. In light of this agreement, European countries set three targets (EU Climate Action, 2018): (1) reduce greenhouse gas emissions by at least 40% in 2030 and 80% in 2050 compared to 1990 levels; (2) increase the share of renewable energy in total energy consumption by at least 32% in 2030; (3) increase the efficiency of renewable energy by 27% in 2030. Incidentally, the energy sector in Europe is responsible for more than 75% of greenhouse gas emissions. Therefore, renewable energies are the solution to make the European Green Deal a reality.

The main renewable energy sources are biomass, photovoltaic (PV), solar thermal, hydropower, wind power, ocean energy, and geothermal energy (Turner, 1999; Edenhofer et al., 2011). Investments in renewable energy sources are influenced by various factors, such as the policies of each country (Apergis and Pinar, 2021), the reduction of energy dependence, especially in Europe (Marques et al., 2011), and the resource wealth of the regions. For example, solar, wind, and bioresources in the Middle East and North Africa; solar, wind, hydro, wave, and tidal power for Asia and Oceania; geothermal, solar, wind, and bioresources for the Sahara and North America; and wind, solar, hydro, wave, tidal, geothermal, and bioresources for Europe (Adekoya et al., 2021).

In the period from 2010 to 2020, the installed renewable energy capacity in Europe grew from 322 GW to 610 GW, contributing to 22% of the total global installed capacity (IRENA, 2018). As can be seen in (Figure 2-1), the expected growth of renewables in Europe is mainly driven by solar PV, offshore wind, and onshore wind, which account for almost the same share of electricity generation in the 2050 energy transition scenario. Currently, this growth is not homogeneous across European countries, with wind power much more prevalent than solar energy in Scandinavian countries, with wind capacities of 1565 MW, 6434 MW, 838 MW and solar capacities of 35 MW, 153 MW, and 27 MW in Finland, Sweden, and Norway, respectively, in 2016 (Energy, 2018; Steigen, 2018; Cohen et al., 2021). The Scandinavian countries are not expected to be major players in the PV market. However, they represent an interesting example of the potential of PV, especially in combination with the increasing popularity and share of electric vehicles. In Germany, the installed capacity of solar and wind power plants is almost equal (Salm et al., 2016). However, this is not the norm, as across the EU-28, wind capacity is about 50% larger than solar capacity, with 154,325 MW wind turbines installed and 103,114 MW solar turbines installed (as of 2016) (Energy, 2018).

In France, renewable energies are growing rapidly and the reliance on their technologies is becoming increasingly important, as we can see from the negative indices of the non-renewable (Figure 2-2), which represent, for example, the change in net capacity in 2019.

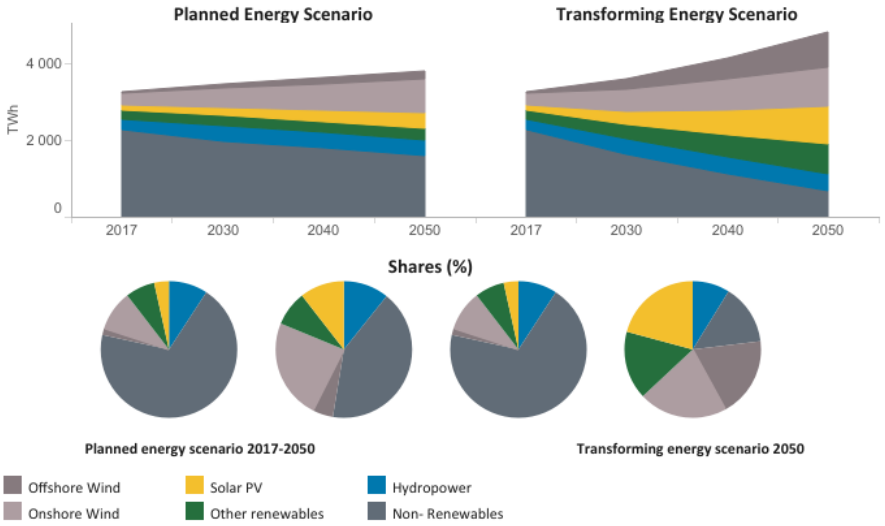

Figure 2-1: Electricity generation, Eu-28 transforming 2050 (IRENA, 2018).

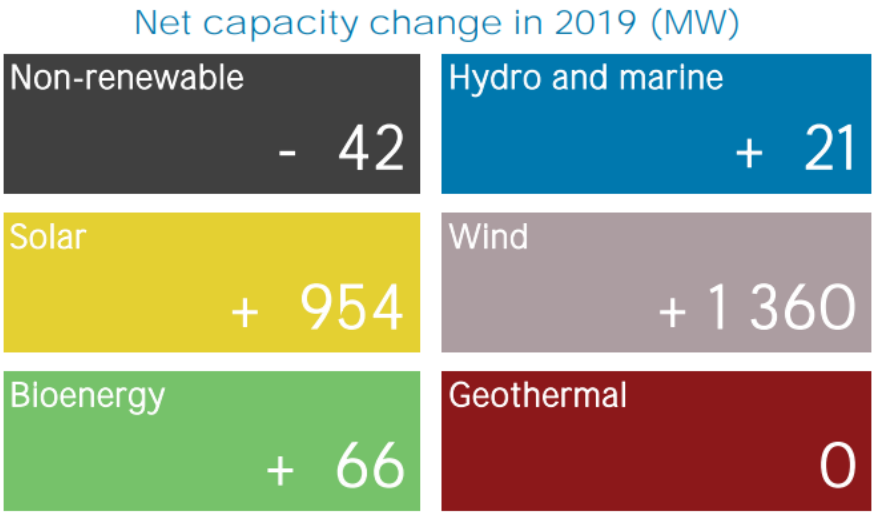

Figure 2-2: Net capacity change in France 2019 (IRENA, 2018).

2.1.1 Wind Energy

Wind energy is a fast-growing sector in Europe, and the region is one of the largest producers of wind energy in the world. In Europe, installed wind energy surpassed any other form of electricity generation in 2017, accounting for 55% of total installed electricity capacity (WindEurope, 2017). Cumulative annual installation in Europe shows linear growth (Figure 2-3(a)). In 2023, the total installed capacity will exceed 250 GW, with Europe alone accounting for about 21% of the cumulative installed capacity worldwide. The trend toward increased use of wind energy in Europe is expected to continue as countries strive to reduce their carbon emissions and seek a

more sustainable energy mix. Total installed capacity is expected to increase linearly to 3200 GW by 2030 (Figure 2-3(b)) to meet the fossil-free energy target by 2050.

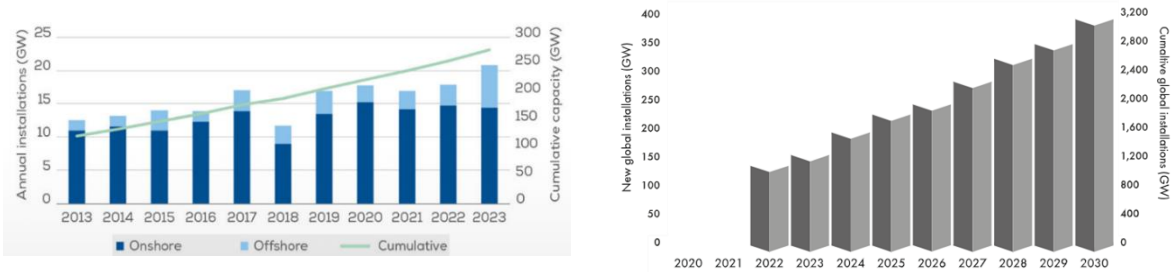

(a) (b)

Figure 2-3: (a) Gross annual and cumulative installation of wind energy in Europe (WindEurope), (b) Cumulative wind energy installation in the world including the gap each year to meet net zero by 2050 scenarios (GWEC).

2.1.2 French Market

Wind energy plays an important role in France's energy mix. With a total installed capacity of 18.7 GW as of 2021, the installed wind energy capacity in Europe is mixed, with 5 countries accounting for about 65% of the total installed capacity on the continent. France is currently the fourth largest country in Europe in terms of the number of wind turbines installed, with a very high proportion of onshore versus offshore turbines. The expansion of wind energy in France is partly taking place through the renovation of existing farms that have reached the end of their useful life, allowing an increase in the amount of energy generated while maintaining the same number of towers. Overall, the transition from 15 GW in 2018 to 34.1 GW in 2028 will result in the wind fleet growing from 8000 towers at the end of 2018 to about 14500 in 2028, an increase of 6500 towers.

2.2 Ground Improvement & Soil Reinforcement

Ground improvement methods have evolved considerably over the past five decades. They are now recognized as a major sub-discipline of geotechnical engineering (Schaefer et al., 2012). Ground improvement is used primarily because of the increasing need to use marginal sites for new construction and to mitigate the risk of failure or potential poor performance (Bird et al., 2005).

The increase in ground improvement applications is also related to their economic and environmental benefits. In some of these techniques, no materials are mixed or drilled into the soil, the mechanical properties of the soil are improved by the mechanical action of the equipment (Figure 2-4). Converting large areas of difficult soil conditions into buildable areas is one of the incomparable advantages of soil improvement over traditional geotechnical solutions. There are numerous soil improvement solutions. Their categories, functions and methods are summarized in (

Table 2.1).

Soil reinforcements techniques are used to improve the strength and stability of soil in construction projects. Their definition overlaps with ground improvement methods, but both have different concepts in geotechnical engineering based on the type of soil and project conditions (

Table 2.2). In the first method, vertical or horizontal reinforcing elements are placed in the soil. In the second, the internal structure of the soil is modified in place to increase its compactness. This is done either by reducing the volume of the voids, for example by applying an aggregate to a saturated soil and allowing the water to settle under positive pressure - in this case we speak of soil consolidation - or by vibrating the soil so that it compacts due to the rearrangement of the grains using the techniques of dynamic compaction. Soil reinforcement techniques are widely used and surround us every day in classic construction projects (foundations, retaining walls, road embankments, railroad tracks, etc.). And for difficult areas (polluted soils, areas prone to flooding, very massive construction areas, etc.). Some of the reference projects for soil improvement and soil reinforcement can be found in (Briançon et al., 2018).

Figure 2-4: Menard's "Giga" compactor drops a 200-ton weigh (Nicholson, 2014).

Table 2.1: Ground Improvement Categories, Functions and Methods (Schaefer et al., 2012)

Category	Function	Methods
Densification	Increase density, bearing capacity, and frictional strength; increase liquefaction resistance of granular soils; decrease compressibility, increase strength of cohesive soils	Vibrocompaction Dynamic compaction Blasting compaction Compaction grouting Surface compaction (including rapid impact compaction)
Consolidation	Accelerate consolidation, reduce settlement, increase strength	Preloading without drains Preloading with vertical drains Vacuum consolidation Electro-osmosis
Load Reduction		Geofoam

	Reduce load on foundation soils, reduce settlement, increase slope stability	Foamed concrete Lightweight fills, tire chips, etc.
Reinforcement	Inclusion of reinforcing elements in soil to improve engineering characteristics; provide lateral stability	Mechanical stabilized earth Soil nailing/anchoring Micro piles Columns (aggregate piers, stone columns, geotextile encased columns, sand compaction piles, jet grouting) Fibre reinforcement Column supported embankments with load transfer platforms Geosynthetic reinforced embankment
Chemical Treatment	Increase density, increase compressive and tensile strength, fill voids, form seepage cutoffs	Permeation grouting with particulate or chemical grouts Bulk filling Jet grouting Compaction grouting Deep soil mixing-wet and dry Fracture grouting Lime columns
Thermal stabilization	Increase shear strength, provide cutoffs	Ground freezing Ground heating and vitrification
Biotechnical stabilization	Increase strength, reinforcement	Vegetation in slopes as reinforcing Microbial methods
Miscellaneous	Remediate contaminated soils	Electrokinetic methods, chemical methods

Table 2.2: Recommended ground improvement/reinforcement techniques based on the ground type (modified after Racinais et al., 2016).

Peat	Clay	Silt	Sand	Gravel	Rock fill
Consolidation (Preloading + Vertical Drains)					
Menard Vacuum					
			Rapid Impact Compaction		
			Dynamic Compaction		
			VibroCompaction		
Dynamic Replacement Pillars					
	Stone Columns				
Controlled Modulus Columns (CMC)					
Soil Mixing					
	Jet Grouting				

The oldest known techniques for ground reinforcement date back to Roman times, when vertical wooden elements were utilized to distribute or transfer structural loads to larger or more robust areas of the ground. Below is one of the major soil reinforcement techniques that strengthen the soil through the injection of relatively stiffer materials into the ground (Menard Group):

- Rigid inclusions, also referred to CMC, is a ground reinforcement technique with objective of improving the quality of poor soils and eliminate the necessity for deep foundations through reinforcing the ground under shallow rigid foundation or flexible foundation through installing concrete columns into the ground utilizing either soil displacement or soil extraction techniques and therefore ensure the optimal distribution of the superstructure's load between the inclusions and the soil. This technique will be elaborated upon in this thesis.

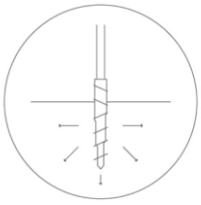

- Stone columns, also known as vibro-replacement, is a ground reinforcement technique also used to improve the load-bearing capacity and reduce the settlement of soils under poor conditions. This technique involves inserting relatively large-diameter columns filled with crushed stone into the ground and compacting them in layers to increase soil stability. Stone columns improve drainage, reduce the risk of liquefaction during seismic events, and are commonly used in constructing foundations for buildings, roads, and embankments. A variation of this technique, combining rigid inclusions and stone columns, is referred to as bi-modulus columns. This approach features a Controlled Modulus Column (CMC) as the bottom part, capped with a stone column.

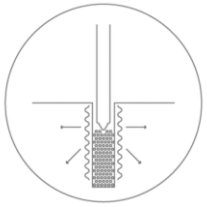

- Soil Mixing is a ground reinforcement technique designed to reduce settlement under structures, improve soil bearing capacity, promote stability, lower the risk of liquefaction, and facilitate mass stabilization. Additionally, it serves to decrease earth pressure behind retaining structures and functions as a groundwater barrier, among other benefits. This method entails mixing the soil at either shallow or deep levels with a binder agent, which is introduced into the soil matrix using specialized mixing tool equipment.

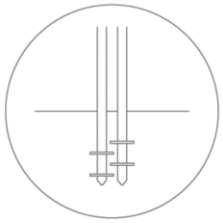

- Jet grouting is a ground reinforcement technique employed for a diverse array of applications, including the control and reduction of settlement beneath structures, improving ground bearing capacity, creation of impervious barriers for deep excavations, installation of retaining walls, underpinning of existing structures, reinforcement of soils around existing utility lines and buried infrastructures, and operations in challenging access conditions such as limited headroom and cramped spaces. This method entails drilling into the soil and injecting grout at high pressure, possibly combined with air or water, to mix with the soil and form columns or masses of a homogenized, high-strength soil-cement material.

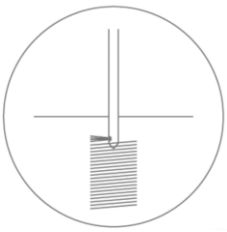

2.2.1 Rigid Inclusions

2.2.1.1 Foundation types

The choice of foundation type plays a crucial role in the design and construction of structures. It depends on several factors, including soil conditions, bearing capacity and type of structure, and loading. The four main types of foundations used in geotechnical engineering are shown in (Figure 2-5).

Shallow foundation, is designed to transfer the load of a structure to the soil layer near the ground surface. It is a common type of foundation for the construction of buildings and structures. If the stability and settlement of the structure are not guaranteed, other foundation solutions must be chosen.

Deep foundation, by definition, a foundation in which depth exceeds width. They are designed to transfer the entire loads of a structure to deeper soil or rock layers with better properties when soil conditions at the surface are insufficient to withstand the loads. Load transfer to deeper strata is accomplished by means of rigid elements connected to the structures, the piles.

Mixed foundation, or pile raft foundation is a type of foundation that combines elements of shallow and deep foundations. This type of foundation is characterized by a shallow foundation that covers a large portion of the structure and is supported by piles that are structurally connected to the raft. Part of the loads introduced by the structure is transferred to the soil under the cap. The advantage is that the load transferred at each pile head is reduced.

The alternative of shallow foundations, deep foundations and mixed foundations presents its advantages by increasing the stability of the structures and reducing the additional settlements. However, the disadvantages of these techniques are their complexity in execution and their high cost. This is because special equipment must be used and a lot of time must be scheduled during construction. On the other hand, deep foundations are often subject to additional loads, such as lateral loads and dynamic loads, which must also be considered during design.

The rigid inclusions technique, offers an innovative middle ground between shallow and deep foundations, aimed at reducing settlement and increasing the bearing capacity of soil foundations underneath superstructures. It can be seen similar to the mixed foundation, but without a structural connection with the foundation above, typically using a load transfer platform instead. The technique's main allure is its construction simplicity, coupled with a significant reduction in the diameter and length of columns compared to conventional piles. This ensures remarkable efficiency, even in the face of challenging soil conditions.

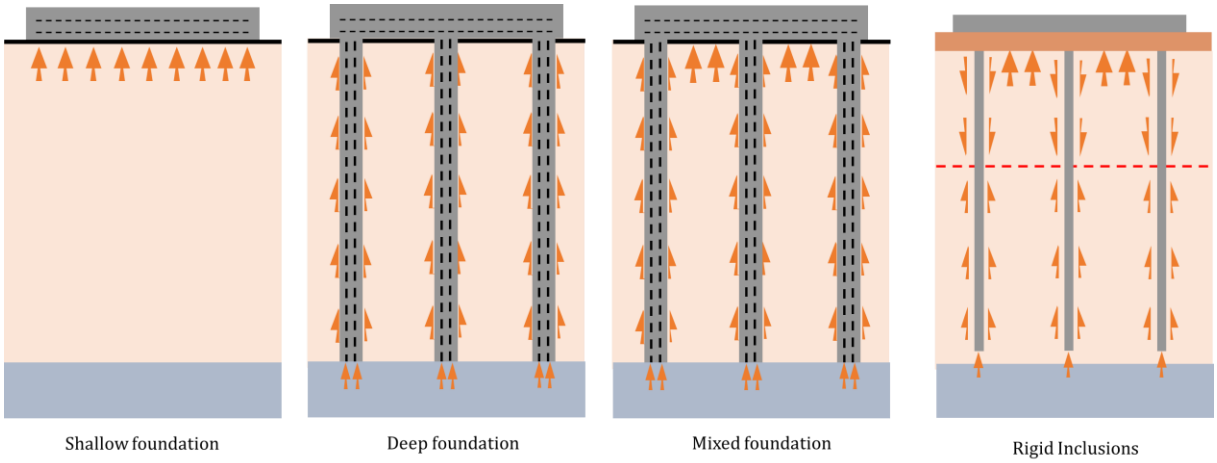

Figure 2-5: The various types of foundations (Modified after ASIRI, 2013).

2.2.1.2 Overview and Statistics

In this project we are interested in the rigid inclusion technique. This technique is initially used in unfavourable soil conditions, including loose/soft fine-grained soils and organic soils (Briet and Plomteux, 2010; Currie et al., 2015). The technique, which is now widely used, has evolved greatly since the 1990s in terms of the number of projects undertaken and the areas of application (Racinais et al., 2016). Applications include all areas of construction: residential, industrial, commercial, road embankments, railroad embankments, storage tanks, onshore wind turbines, etc. (ASIRI, 2013).

As previously stated, the number of CMC projects being undertaken at onshore wind turbines is significant. For example, at the time of their construction, the Fantanele and Cogealac projects were considered the largest onshore wind farms in Europe with a total capacity of 600 MW (Briet and Plomteux, 2010). In France, more than 85% of wind turbines are supported by shallow foundations (Nardelli, 2019). Furthermore, rigid inclusions were employed in 10% of all wind turbine foundations, doubling the proportion of classic deep foundations. Some interesting data (Figure 2-6) illustrate the proportion of rigid inclusions supporting gravity foundations OWT in France.

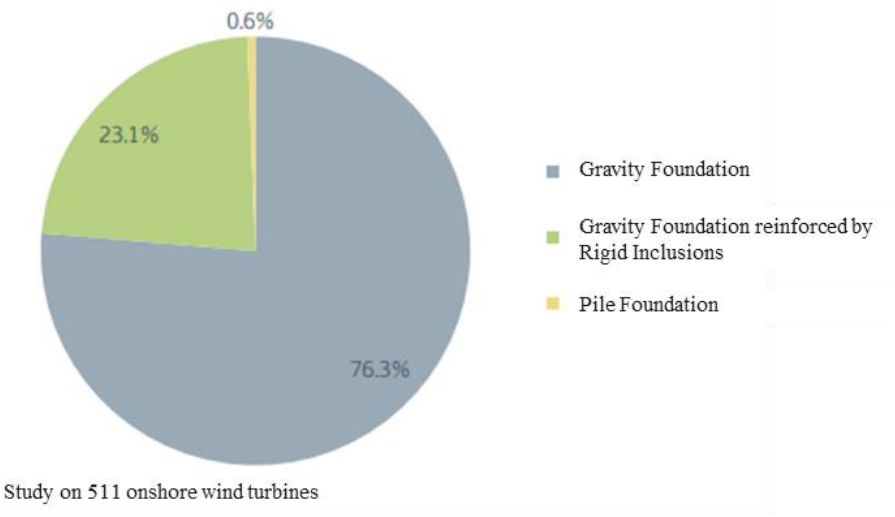

Figure 2-6: Statistics of Antea Group since 2013 (Antoinet and Marthe, 2016).

2.2.1.3 History & Development

Reinforcing soil with rigid inclusions is a technique that is not relatively recent. In the modern world, several application projects using RIs were carried out before the 1960s, but without necessarily the same design methods that we know today. One of the earliest research papers that summarised this technique and its applications is (Schlosser et al., 1983). The technique was defined as a special and new field of soil improvement and was discussed at international conferences starting in 1977. The authors mentioned that 35 papers on soil reinforcement were submitted to the proceedings of the VIII ECSMFE conference in 1983. Several points were covered in the abstract, such as: Soil Reinforcement Interaction, Behaviour and Design Methods, and Case Studies and Control Methods. The abstract classified soil reinforcement in terms of foundations, walls, and slope stabilization.

A network of rigid inclusions as we know it today was clearly described by (Combarieu, 1988) in the case of embankment. The research paper describes the design methods for rigid inclusions under high embankments based on the state of the art at that time. The conclusions state that soil settlement is significantly reduced, lateral movement is limited, and the stability of the embankment is ensured in the short and long term when rigid inclusions are employed. Subsequently, the design of rigid inclusions under slab on ground and footings was described in (Combarieu, 1990). The work includes the modelling of vertical rigid inclusions under footing by introducing an analytical model to estimate the limit load and settlements of a foundation resting on rigid inclusions. Several literature reviews, numerical models, and analytical models then detailed various applications of rigid inclusions, some of which are discussed in the following section. The state-of-the-art report on the construction process (Chu et al., 2009) has listed the latest developments in construction methods and engineering techniques, as well as some reference projects around the globe.

In France, the ASIRI national project (ASIRI, 2013) published recommendations for the design, construction, and control of rigid inclusions, which are considered the most advanced regulations on the subject at the global level. The project involved the evaluation of a series of physical experiments, numerical models, experimental models, and real-world monitoring as a

fundamental step toward understanding the mechanisms at work in this innovative foundation system. The applied research program presented here was made possible by the broad range of skills of the project participants, who came from both academic and professional backgrounds.

The project carried out between 2005 and 2011 contributed greatly to the developments of rigid inclusions. The main objective of this program was to overcome the lack of generally accepted references for the design or execution of this reinforcement technique. Given the magnitude of the task to be accomplished, the emphasis was placed on the behaviour under vertical, static and uniform loads, which is precisely applicable to the majority of structures for which this technique is used: the case of embankments in the central section, the case of extended foundations such as slabs (Figure 2-7).

The industrial success of the application of rigid inclusions has led to the proposal of this technique for other structures outside the scope of ASIRI. To this end, a research project is being carried out within ASIRI+ to address the application of the recommendations or more complex loads, such as:

- Thin embankment where controlling the differential settlement is essential
- Structures that transfer cyclic loads to the reinforced soil mass (e.g., wind turbines)
- Foundations of structures that must support dynamic and non-vertical loading in seismic situations
- Foundations founded directly on rigid inclusions without load transfer platform.

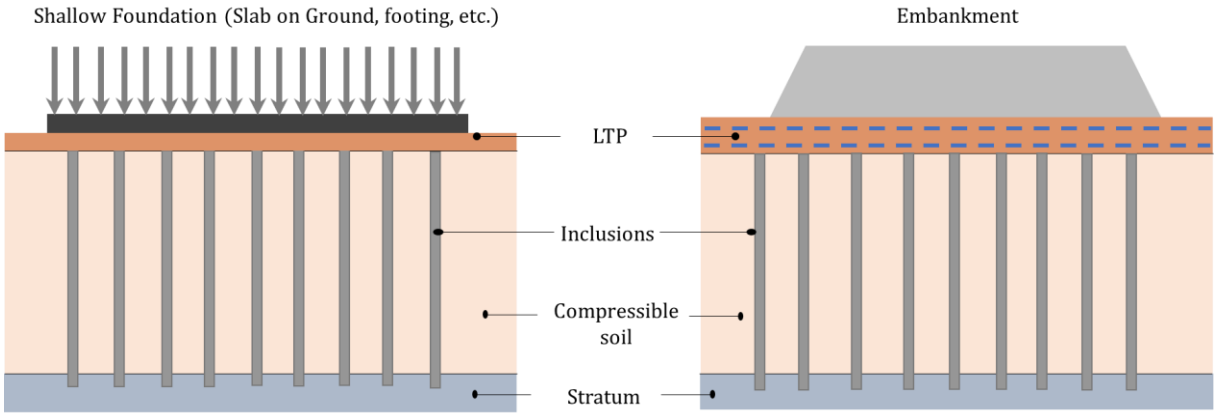

Figure 2-7: Soil reinforcement by rigid inclusions

2.2.1.4 Concept

Rigid inclusions consist of continuous, slender elements, usually made of cement. Their geometrical sections can often be cylindrical and typically vertical. The network of supports follows a regular mesh pattern determined by the engineering design. The term rigid refers to the higher rigidity of the column relative to the surrounding soil. This is independent of the cement or concrete strength of the columns or whether or not steel reinforcement is installed inside the columns.

The fundamental difference between piles and rigid inclusions is expressed not only by the presence of a connection between the piles and the foundation, but also the resultant interaction mechanisms, despite some conceptual similarities. In general, the design of piles assumes that

they carry 100% of the applied load. This assumption leads to focus on the interaction between the piles and their interfaces with the soil without emphasizing on the load transfer (Figure 2-8 (a)). The fact that the inclusions are not connected to the superstructure, as well as their effect on creating a new soil matrix with a different rigidity due to the presence of the columns, lead to a load transfer between the elements (soil, inclusions, load transfer platform, foundation) (Figure 2-8 (b)). These interaction mechanisms from the core of soil-structure interaction in case of rigid inclusions.

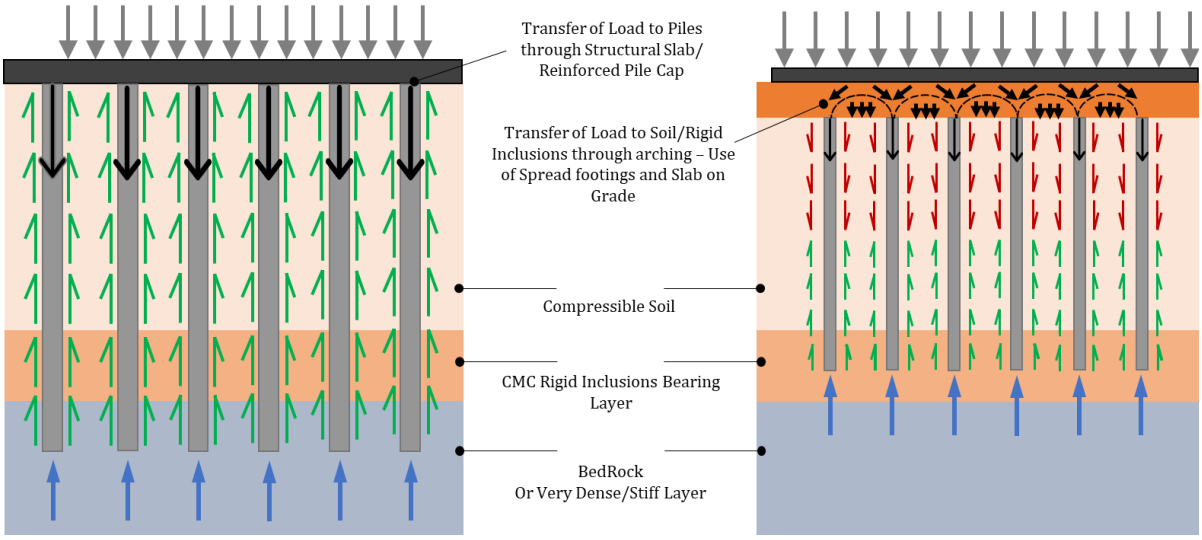

Figure 2-8: (a) Simplification of load transfer in a foundation connected with piles, (b) Simplification of the load transfer in a soil reinforced by RIs

2.2.2 CMC

The technique of rigid inclusions, increasingly used in many countries, has many different names: piled-embankment, column-supported embankment, geosynthetic reinforced pile supported (GRPS), pile-supported earth platform, or soil column reinforcement. Rigid inclusions are also referred to as columns, pile-like inclusions, or non-contact settlement-reducing piles in a general sense; in reference to some of the commonly used installation techniques; and controlled modulus columns (CMCs), which are known by (Menard Group). A CMC is a type of rigid enclosure made of mortar, concrete, or other specific material. They could also be classified as semi-rigid inclusions, since some of the literature distinguishes between rigid and semi-rigid inclusions without always having a clear conventional difference. However, the design of CMCs is mainly based on (ASIRI, 2013) in accordance with the Eurocodes (Racinais et al., 2016). The diameter of the columns can vary from 250 mm to 450 mm and the length can be up to 50 m. CMCs are generally divided into two families in terms of design and execution conditions:

- Drilled CMC with soil displacement where the soil is displaced laterally and virtually no excavation is produced. It belongs to Class 3, Category 7 of Annex A of NF P94-262 (2012). This technique requires the use of tools specifically designed for this purpose, i.e., drills or auger tools with reverse pitch in the displacement area (Figure 2-9).
- Drilled CMC with soil displacement, where the soil is replaced by column material. It belongs to Class 2, Category 6 of Annex A of NF P94-262 (2012).

Both types are equipped with monitoring devices that provide a variety of information that is published at the end of each project and tracked by engineers. This data is important to comply with the design plans and to control the execution in order to comply with the standards.

(a) (b)

Figure 2-9: (a) CMC with soil displacement, (b) typical CMC AUGER (Varaksin et al., 2014).

Rigid inclusions have been used mainly for road embankment construction in Europe since their development in the 1970s (Briançon, 2002). Nowadays, however, the technique is used in almost all types of structures (Table 2.3). The number of projects worldwide using CMC in all types of applications is extremely increasing (Figure 2-10), and this number is constantly growing due to the successful application of the technique in terms of its benefits and reference projects. This development has contributed to the continuation of the project (ASIRI, 2013) with the ongoing research project (ASIRI+, 2018).

All types of soil conditions are an area of application for rigid inclusions. In practice, however, their economic utility remains limited to soft or medium soils, most of which are compressible, i.e., clay, silt, or peat.

Table 2.3: Fields of application of RIs

RIs application	References
High Speed Train	(Alexiew and Vogel, 2002),(Burtin and Racinais, 2016)
Highway	(Combarieu and Frossard, 2003), (Plomteux and Lacazedieu, 2007), (Van Eekelen and Brugman, 2016)
Industrial Buildings and Warehouses	(Racinais and Plomteux, 2011), (Briançon et al., 2015)
Tanks	(U. S. Okyay and Briançon, 2012), (Racinais et al., 2016)
Bridges	(Pecker, 2004)
Wind turbines	(Plomteux and Ciortan, 2010), (Sahyouni et al., 2022)

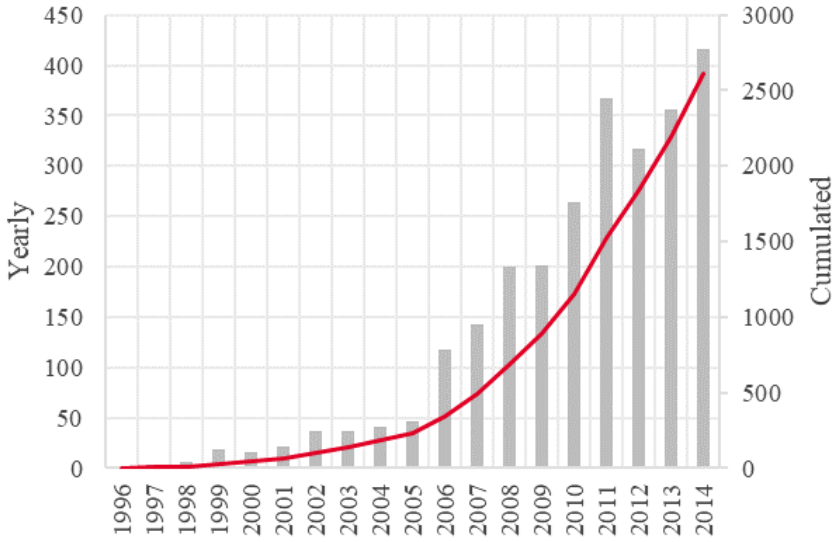

Figure 2-10: Development of CMC projects around the world (Racinais et al., 2016).

2.3 Onshore Wind Turbines

Wind turbines are machines designed for the purpose of generating electrical energy by converting the kinetic energy of the wind. This concept has been around for centuries and has its origins in the use of windmills, which extracted mechanical energy from the wind to perform industrial processes (Burton et al., 2011).

OWT consist of several key components (Figure 2-11), each of which plays a critical role in power generation. The main components include the rotor, nacelle, tower, yaw mechanism, brakes, gear box, generator, transformer, controller, and blades. The rotor, which is the most visible part of the turbine, consists of several blades that rotate and capture wind energy. The nacelle, located at the top of the tower, houses the generator, transformer, and controller. The yaw mechanism helps the rotor align with the wind direction, while the tower supports the weight of the nacelle and rotor. The generator converts the rotor's mechanical energy into electrical energy, which is then sent to the transformer for conversion into high voltage for remote transmission. The controller regulates the rotor speed and power output to ensure optimal power generation and safe turbine operation. These components work together to efficiently harness wind energy and convert it into electricity. The invisible part of the wind turbine consists of the foundation and the connection to the electric grid.

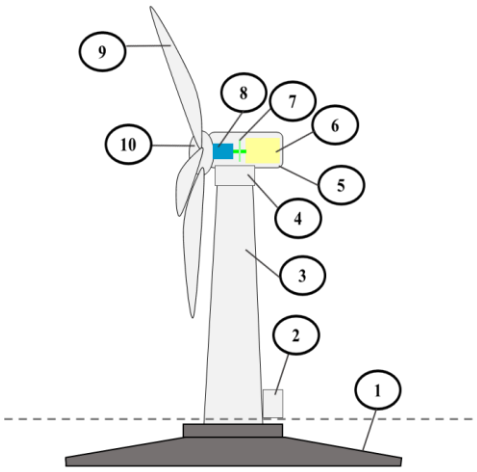

1. Foundation
2. Connection to the electric grid
3. Tower
4. Yaw control
5. Nacelle
6. Generator
7. Electric or mechanical brake
8. Gearbox
9. Rotor blade
10. Rotor hub

Figure 2-11: Wind turbine components.

Modern onshore wind turbine towers come in various configurations such as tubular steel towers, steel lattice towers, concrete-steel composite towers, and a wooden tower concept. The 3-blade horizontal axis rotor mounted on a tubular steel tower is considered the most efficient and practical method for wind turbine design (Risø and Veritas, 2002) in terms of how the structure supports and resists loads.

2.3.1 Complex loading

The structural design of wind turbines, defined by their slender configurations and heavy rotating components, places them under various loading conditions. These conditions are primarily driven by wind actions and can be categorized as follows: wind action (aerodynamic loads), operational loads, gravitational loads, along with a multitude of environmental factors.

Wind action significantly impacts the rotor blades, turbine tower, and the foundation of the wind turbine. The cyclic unpredictable nature of wind, varying both in space and time, adds to the complexity of its impact. Wind direction can change throughout the entire 360° spectrum, and this is further complicated by fluctuating wind speeds. To manage this unpredictability, it's crucial to employ a count method such as statistical analysis for addressing the variability of wind loadings. This approach aids in estimating the variable forces exerted by the wind on a structure (Hansen, 2015). In accordance with international standards such as (IEC 61400-1), wind turbines are designed to endure a multitude of load cases, including extreme wind gusts and diverse environmental conditions. Moreover, the wind's extended lever arm generates considerable overturning moments at the base of the foundation. These moments are cyclical and manifest varying characteristics throughout the turbine's operational life. Various simplified methodologies have been employed to predict wind load and transform it into a spectrum of moments impacting the foundation plane (Bhattacharya et al., 2013; Lombardi et al., 2013; Arany et al., 2015; Guo et al., 2015; Yu et al., 2015; Gupta, 2020). Depending on the characteristics of the wind load and the resultant moments, the cyclic loading can be categorized as either one-way or two-way.

Operational loads, also known as rotor loads, are the forces and moments acting on the rotor blades due to their aerodynamic interaction with the wind. These loads are characterized by their

frequency and are commonly referred to in literature as "1P" and "3P" loadings (Figure 2-12). "1P" denotes the rotational frequency of the rotor for one complete cycle, while "3P" corresponds to the frequency of a single blade passing (in a wind turbine with three blades). The rotation of the wind turbines is influenced by wind speed, with typical operational speeds ranging from a cut-in wind speed of 3.0 m/s to a cut-out wind speed of 25 m/s. These operational loads are crucial in determining the dynamic response of the wind turbine's foundation system, as the excitation they produce can resonate with the natural frequency of the turbine structure.

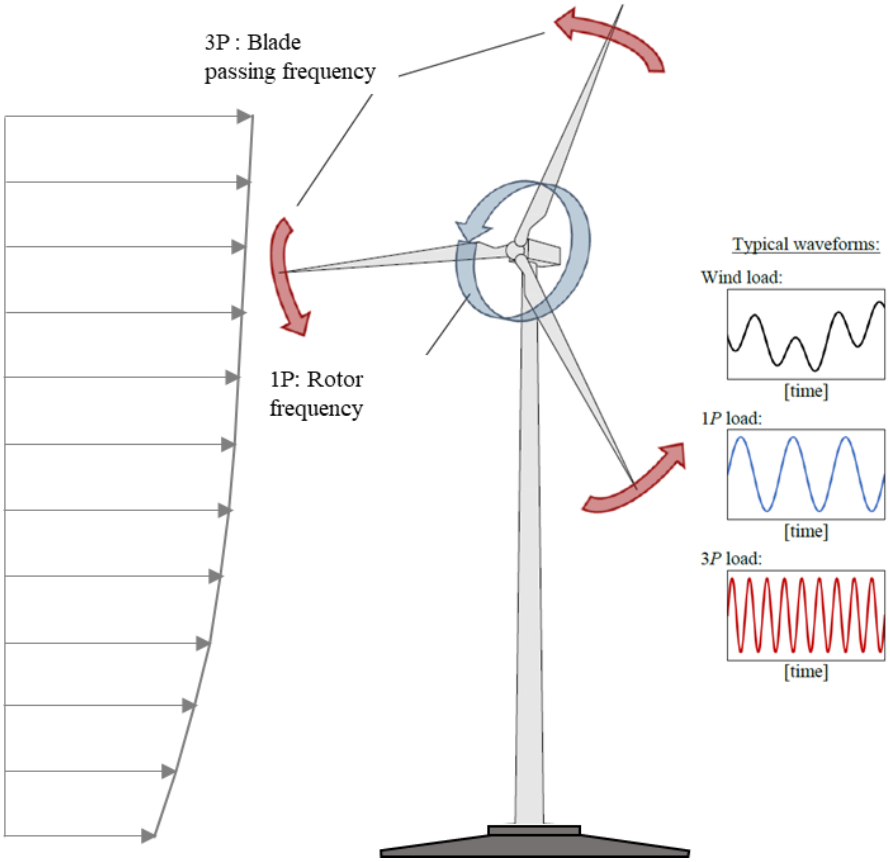

Figure 2-12: Typical loading in onshore wind turbines.

The permanent gravity load consists of the total weight of all the wind turbine components, encompassing the tower, nacelle, rotor blades, and additional structural elements. It also incorporates the weight of the gravity foundation itself, as well as the backfill material applied over the foundation. This backfill serves to enhance the foundation's resistance against the overturning moment induced by the wind.

Environmental factors such as temperature variations, atmospheric pressure, lightning, icing, and seismic activities may impact the behaviour and performance of wind turbines over their lifespan. These factors can have significant implications on the structural integrity, operational efficiency, and overall durability of the turbines.

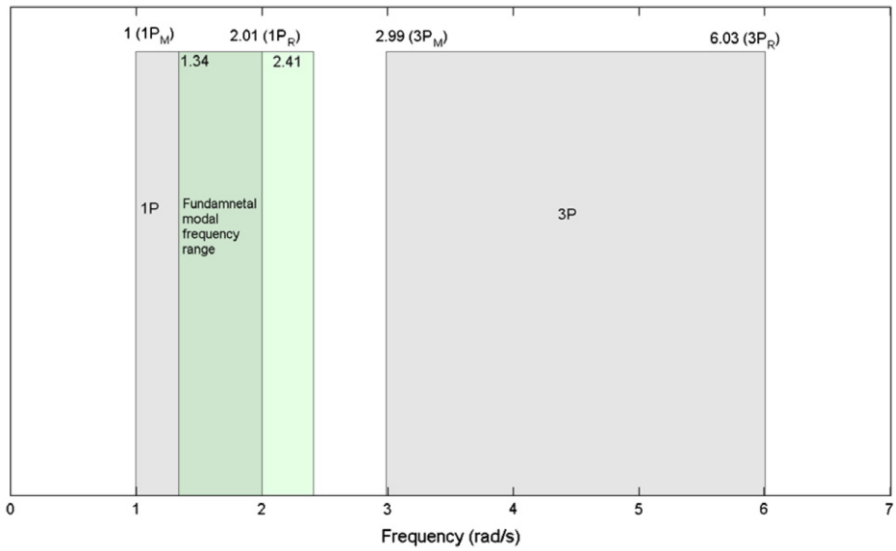

Figure 2-13: Frequency spectrum of 1P and 3P in relation to the fundamental modal frequency range, incorporating Soil-Structure Interaction (Harte et al., 2012).

To capture the essential characteristics of wind loading and its cyclic effects from a soil-structure interaction perspective, the simplification method of Nikitas et al. (2016) helps to decipher the loading scenarios acting on wind turbine foundations from the soil-structure interaction perspective. The method is based on dividing the model into two sub-models: cyclic and dynamic. (1) the behaviour of the foundation/soil under cyclic loading, leading to fatigue problems; (2) the behaviour of the foundation/soil considering the changing stiffness of the whole system to account for resonance problems dynamically (Figure 2-14). This simplification has been considered in numerous research papers, such as (Gupta, 2020), who performed 3D numerical modelling of a monopile for an offshore wind turbine by applying a simplified cyclic loading scenario to represent the pile and soil and ignoring the dynamic effect of 1P and 3P.

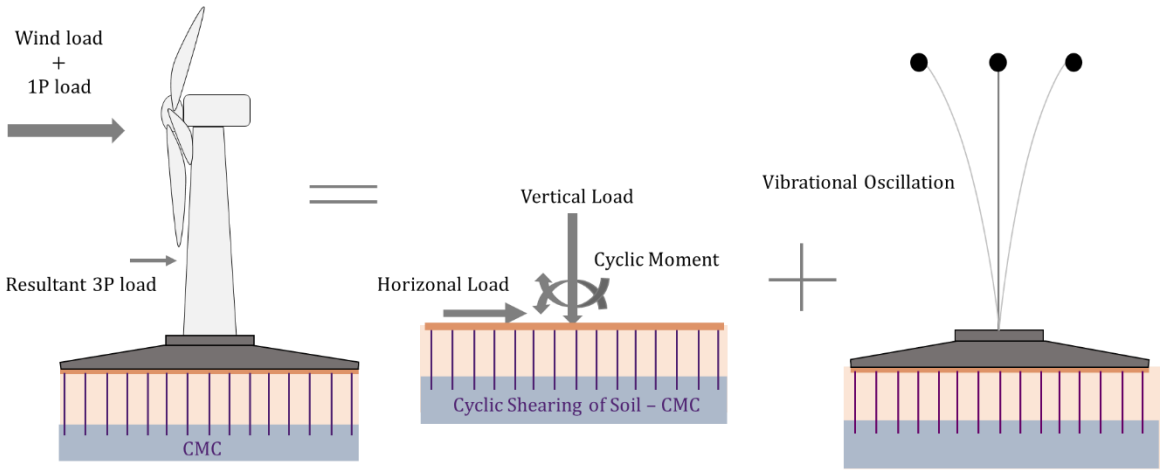

Figure 2-14: An analysis of the OWT model in the context RIs, edited after (Nikitas et al., 2016).

2.3.2 Cyclic loading

The field of cyclic loading is indeed a significant research area in geotechnical engineering. The behaviour of soils and foundation systems under cyclic loading conditions is complex and presents unique challenges that require thorough investigation and understanding. Cyclic loading

can occur due to various factors, such as, wind-induced vibrations, wave action, traffic loading, and other. There can be some ambiguity and confusion regarding the terminology used to describe different types of loadings, such as cyclic loading, dynamic loading, and repeated loading. Based on (Peralta and Achmus, 2010), the cyclic loading is distinguished from dynamic loading in terms of frequency, inertia, and strain accumulation (Table 2.4). Distinguishing between two-way and one-way cyclic loading is also of paramount importance. Two-way cyclic loading, as the name suggests, involves loading in both the positive and negative directions. Conversely, one-way cyclic loading, while still cyclic, has its cycles predominantly in one direction.

Table 2.4: Loadings definition

Repeated load	Cyclic	Cyclic-Dynamic	Dynamic
Frequency	0 – 1 Hz	1 – 10 Hz	>10 Hz
Inertia	Negligible	Relevant	Relevant
Strain accumulation	Predominantly plastic	Plastic and elastic	Predominantly elastic

The nature of the cyclic loadings, identified through their varying frequencies and cycle counts, differs significantly across different projects. In onshore wind turbine, the cyclic overturning moment is calculated with a frequency of 0.01 (Lopez-Querol et al., 2017). Although offshore wind turbines are assumed to have a higher wind amplitude and may experience sudden gusts, which is not the case for onshore wind turbines (Pytlik, 2016), many studies have found that the prevailing frequency of the gusty wind is much lower than the wave loads. In some studies, the frequency of wind loading is considered so low that the inertial effects in the soil region are negligible and the cyclic loading is considered quasi-static (Seymour, 2018), although the structure undergoes dynamic amplification due to this loading frequency. The 1P and 3P loads are less pronounced compared to the wind loads. Only 0.02% of the total bending moment at the mudline of the offshore structure results from the 1P loading, while less than 1% results from the 3P loading (Arany et al., 2015).

The frequency of cyclic loads on wind turbines is significantly high. Over a 20-year lifespan, a typical wind turbine might experience between 100 million and 1 billion load cycles (Janssen et al., 2012). The table below (Table 2.5) highlight the high number of cycles wind turbine structures experienced compared to other structures.

Table 2.5: Range of the number of load cycles for structures (Göransson and Nordenmark, 2011)

Low Cycle $<10^3$	High Cycle $10^3 - 10^7$	Very High Cycle $10^3 - 10^7$
Earthquake loading	Bridges	Mass transport systems
Storm loading	Airport pavements	Wind power plants
Wind loading		Offshore structures

The impact of cyclic actions on both the structure and the terrain correlates with the cycle count. Research literature seems to have limited studies examining how geomaterials respond to extensive cyclic actions (Pytlik, 2016). Cyclic loading can have significant effects on the strength and deformation properties of the soil such as (Puech and Garnier, 2017):

- Shear strength deterioration, potentially diminishing the load-bearing ability.

- Rise in excess pore pressures, decreasing effective stresses, possibly leading to liquefaction.
- The fluctuation of clay soil's shear strength based on the shearing speed.
- The long-term "fatigue" effects on soils and interfaces after numerous cycles, potentially augmenting prolonged displacements.

In the context of shallow foundations, the impact of cyclic loading can lead to an increase in the displacements and influences the foundation performance (Zachert et al., 2011). Various analytical models have been formulated to represent this effect such as Byrne et al., (2002). Similarly, the hypoplasticity concept using the concept of a macroelement, as showcased by (Salciarini and Tamagnini 2009).

In the context of deep foundation, mainly piles foundation it's essential to differentiate between two primary types of loadings on piles: lateral and axial loading. Lateral loading has gained significant attention due to its relevance in offshore platforms and wind turbines supported by monopiles. Noteworthy research initiatives like PISA project (Pile Soil Analysis) have been undertaken with the objective of proposing innovative design methodologies for offshore wind turbine monopile foundations (Byrne et al., 2015) under rather monotonic loading, particularly the PISA design model which captures intricate soil-monopile interactions. The "SOLCYP" project (Puech and Garnier 2017) introduced a guideline-based design approach for piles undergoing extensive cyclic loading over extended periods both axial and lateral cyclic loading using real in-situ and experimental tests. Their study not only delved into understanding displacement accumulation but also provided analytical techniques to address the decline of lateral skin friction on the pile shaft. In the offshore wind sector, the effects of high cyclic accumulation have been extensively researched - a depth of research not as prevalent in onshore wind. Various methods and models have been developed, such as the high cyclic accumulation model using finite elements, which was able to reproduce the experimental behaviour for monopiles (Zachert et al., 2016; Zachert and Wichtmann, 2020), in addition to the macro-element approach discussed in Chapter 5.

In the context of gravity foundation underlined by a soil reinforced with rigid inclusions, the loading is not directly associated with the foundation load. Instead, the load is transferred from the rigid foundation to the load transfer platform. As a result, unlike piles which may experience two-way loadings, these rigid inclusions are subjected exclusively to compressive forces (Figure 2-15).

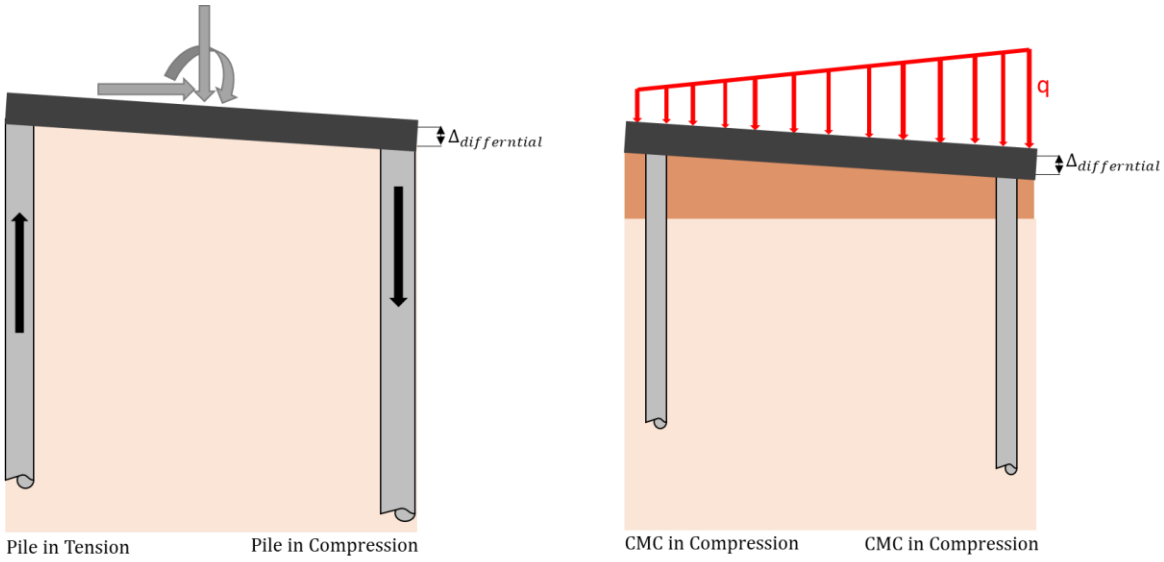

(a) (b)

Figure 2-15: Simplified Load Comparison for Piles (a) vs. Rigid Inclusions (b).

While current international geotechnical engineering design codes don't specifically address this aspect of loading, some hint at potential cyclic loading effects on foundation soil, particularly concerning diminished bearing capacity (Eurocode 7, 2007). On the other hand, industrial research recognizes the importance of studying and addressing cyclic loading through guidelines, research projects, and specialized practices (API RP2A-WSD, 2007; API, 2GEO, 2011; API RP2A-WSD, 2007)

2.3.3 OWT Foundations

The foundation consists of the upper part of the base, which ensures the connection with the mast, and the foundation elements, which transfer the loads to the ground. The types and shapes of wind turbine foundations depend on the load of the wind turbine and the site conditions. They could be defined as follow (Aguado et al., 2012), refer to (Figure 2-16):

- Gravity foundations
- Gravity foundations on soil reinforced by stone columns
- Gravity foundations on soil reinforced by rigid inclusions
- Deep foundations, such as piles
- Mixed or composite foundations

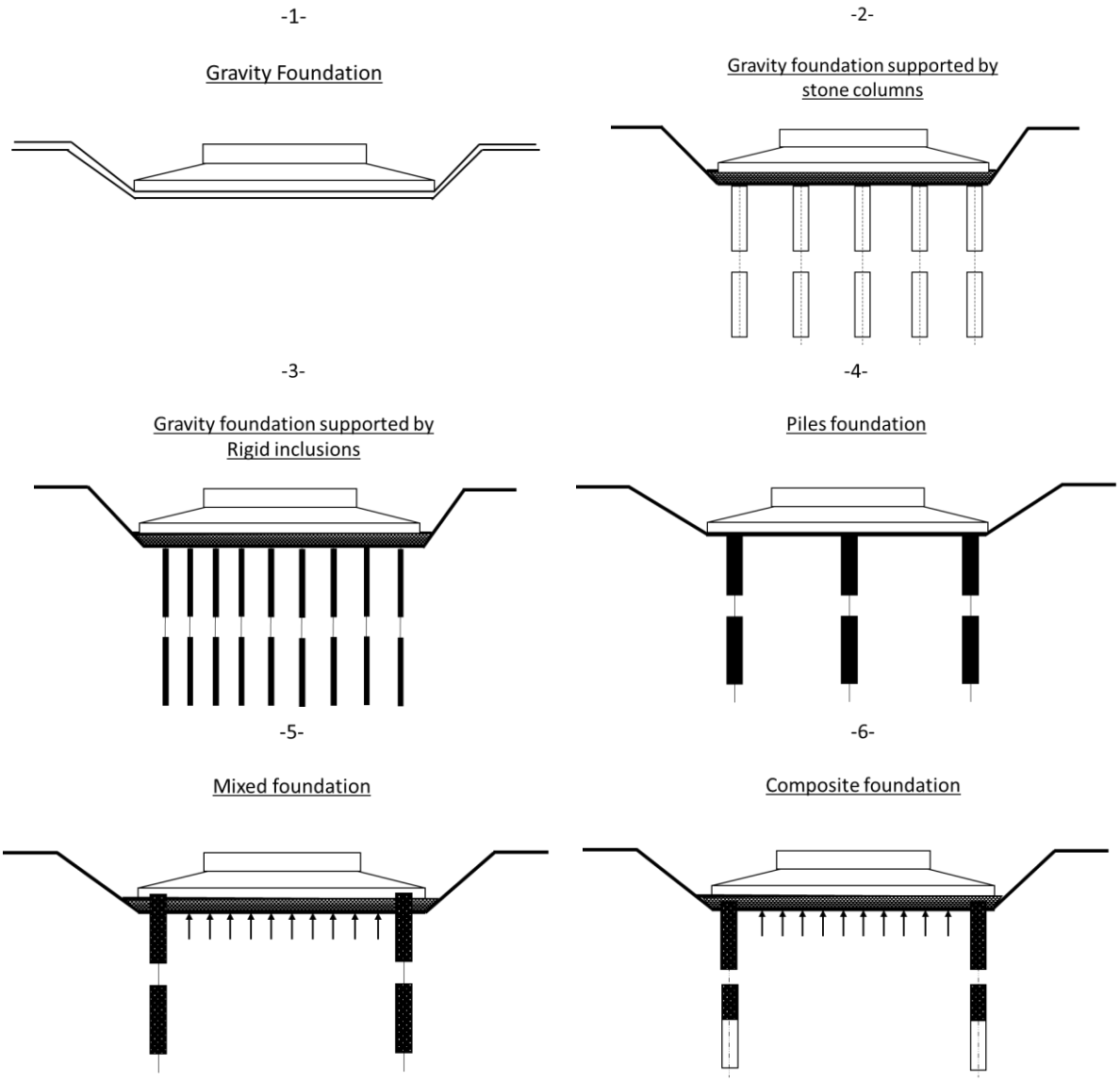

Figure 2-16: Principles of different foundation types for onshore wind turbines (modified after Aguado et al., 2012).

2.3.3.1 Design and considerations

Geotechnical design of foundations for onshore wind turbines is currently based on recommendations that include design and control of foundations for wind turbines. The following are the most frequently cited documents in chronological order.

The Danish Wind Industry Association, in cooperation with Risø National Laboratory, has developed a standard for wind turbine design (Risø and Veritas, 2002). The code focuses on wind turbine design and certification, with emphasis on structural design, load calculations, and safety considerations. The standard covers all aspects of wind turbine design, including the structural design of the tower, blades, and foundation, as well as electrical and control systems. It provides guidelines for calculating the loads acting on the wind turbine, taking into account factors such as wind speed and turbulence.

The National Committee of Soil Mechanics has published recommendations (Aguado et al., 2012) that relate to the design and control of wind turbine foundations. These may be included within the scope of these regulations or alternative rules proposed for very large or unusual structures in geotechnical category 3 (Eurocode 7 EN 1997-1, 2005, Section2). The measures for the design, calculation, construction, and inspection of wind turbine foundations are based primarily on the applicable codes, and additional provisions have been included in this text to address the unique characteristics of this type of structure. These recommendations apply to horizontal axis wind turbines located upstream (the rotor blades are on the side of the tower facing the wind) or downstream. They apply to industrial wind turbines with a rotor axis greater than 12 meters above the platform. All verifications are proposed in these recommendations for the main load cases.

The American Society of Civil Engineers and the American Wind Energy Association published recommendations in 2011 (ASCE–AWEA, 2011): Recommended practice for compliance of large land-based wind turbine support structures. This guidance document provides conservative recommendations for the sizing and deployment of land-based wind turbines. The purpose of this document is to provide those responsible for the validation process in the construction of a wind turbine with elements that clarify the relevant and appropriate standards to be used in design and applied to verify structural capacity to ensure that wind turbine structures that have received a construction permit have a minimum level of safety against failures that may occur during their service life. one chapter deals specifically with foundations and states that foundation fatigue should be considered in design. However, these recommendations are general in nature and do not address design details.

The International standards organisation DNV GL has published a standard for the certification of wind turbines (DNV-ST-0126). It is considered a global provider of renewable energy consulting and certification services. It presents pragmatic design approaches and can be applied, for example, to steel and concrete masts, shallow and deep foundations in the onshore sector. This standard also includes requirements for materials, design and maintenance. The section on foundations is particularly specified:

- Crack control requirements
- Consideration of fatigue models for substructure
- Requirements for the quality of mortars for wedging

Concerning the geotechnical design, we find in this standard:

- The consideration of the impact of dynamic loads
- New safety coefficients to be applied
- Requirements to apply the observational method for the design

The International Electrotechnical Commission (IEC) has published a series of international standards that provide guidelines (IEC 61400-1) for the design, manufacture, and testing of wind turbines. The first edition of the IEC 61400 series was published in 1993. It was followed by several updates through 2019. Part 6 of the code provides guidelines for the design of foundations for onshore wind turbines. It includes geotechnical considerations based on Eurocode 7, such as soil conditions, foundation design, and installation requirements.

2.3.3.2 French guidelines

The design of onshore wind turbines with soil reinforcement using rigid inclusions in France is primarily guided by two key references: CFMS (2011)and ASIRI (2013). These documents provide specific recommendations and guidelines for the design of such foundations.

The operational and environmental load cases for wind turbines are defined in the standard (IEC 61400-1 (Edition 3), 2005), which includes an estimated number of load cases ranging from 2000 to 6000. These load cases are classified into eight design load cases (DLC), which represent the most likely conditions that a wind turbine may experience throughout its operational life. These design load cases are as follows:

1. Power production
2. Power production with occurrence of a fault
3. Start-up
4. Normal shutdown
5. Emergency shutdown
6. Standstill (stop or reduced speed)
7. Standstill and fault conditions
8. Transportation, assembly, maintenance, and repair

The manufacturer typically defines an additional design load case, "Lift-off." This load case encompasses 99% of the wind turbine's production duration and is used as a quasi-permanent service load design condition. When the wind turbine is shallow founded (with or without prior soil reinforcement). The design load cases (DLC) must be classified according to standard design loads as follow:

- Quasi-permanent (QP) SLS and Rare (R) SLS
- Fundamental (Fund) ULS and Accidental (Acc) ULS

The weighting factors listed in (Table 2.6) are taken from the CFMS (2011) to define loads at SLS and ULS.

Table 2.6: Partial weighting factors according to CFMS (2011)

Load case	Limit states	F_Z	H	M	Water
DLC_{QP}	ULS_{Fund}	1.0 or 1.35	1.8	1.8	1.125 x 1.05
	SLS_{perm}	1.0	1.0	1.0	1.0
DLC_{Rare}	ULS_{Fund}	1.0 or 1.35	1.5	1.5	1.125 x 1.05
	SLS_{Rare}	1.0	1.0	1.0	1.0
DLC_{Acc}	ULS_{Acc}	0.9 or 1.1	1.1	1.1	1.0

The geotechnical design of a gravity foundation is based on the mobilization of the bearing capacity of the underlying soil, its resistance to overturning, and the control of its uplift under different load cases. The conditions to be checked are typically expressed in terms of the compressed area compared to the total area. When the wind turbine is in the power production phase, corresponding to the "service wind" conditions, the foundation must remain fully

compressed, meaning that no uplift is allowed. The prevention of uplift is based on ensuring a maximum eccentricity do not exceed the D/8, where “D” is the equivalent diameter of the foundation. The eccentricity, denoted as "e," is defined as the ratio between the overturning moment (M) and the vertical force (V).

This estimate of uplift does not consider the stiffness of the underlying soil and any soil-structure interaction. It is a purely conservative geometric approach to controlling uplift. The contact pressure at the base of the foundation is related to the values of eccentricity and can be seen in different configurations (Figure 2-17). The stress ranges in green and red are calculated based on a geometric interpretation. The green region represents the compressed region. The gap, on the other hand, indicates the loss of contact and the uplift of the soil. ((Figure 2-17 (b)) represents the uplift of the foundation from the ground and a gap at the contact area. Since the subsoil under the foundation cannot withstand a tensile load, the contact area between the foundation and the soil is reduced (red area).

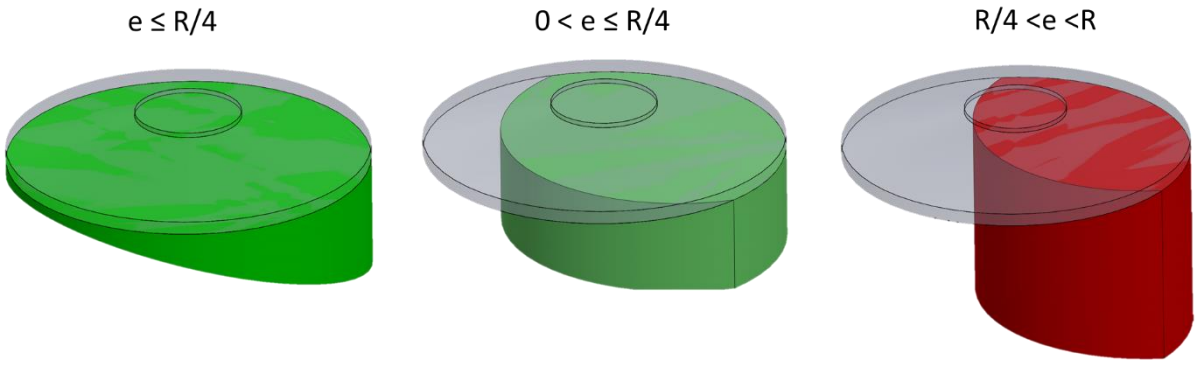

Figure 2-17: Stress distribution at the base of a foundation subjected to eccentric loading.

The geotechnical design of a wind turbine foundation aims to ensure the following:

- The soil is capable of supporting the vertical and horizontal static or transient loads imposed by the wind turbine throughout its lifespan
- The displacements, including absolute and differential settlements, remain compatible with the proper functioning of the wind turbine during its lifespan
- Resonance phenomena between the foundation and the supporting soil are avoided.

In addition to verifying the conditions related to uplift, the geotechnical design requirements for foundations are defined by normative documents, particularly the standards (NF P94-261, 2012) and NF P94-262 (2012). They also include specific requirements from the turbine manufacturers, which can vary in nature, such as:

- Maximum allowable rotation angle of the wind turbine tower during service
- Long-term absolute and/or differential settlements
- Maximum stress applied to the soil by the foundation
- Static rotational stiffness
- Dynamic rotational stiffness for shallow foundations or horizontal/vertical stiffness for deep foundations.

In the case of rigid inclusions, the above point is also considered. A global bearing capacity is evaluated at the contact pressure surface with respect to the corresponding load combinations, in addition to the local bearing capacity represented by the tributary area of the rigid inclusion, which is expected to be highly loaded. The soil-structure interactions can be reported to the structural engineer by specifying the equivalent vertical, horizontal, and rotational stiffness of the reinforced soil block under the foundation.

2.4 Soil - Structure - Interaction

Oddly enough, every structure built on earth ultimately rests on the ground unless it does not float or falls over. With rapid technological advances, structures have become increasingly sophisticated. The natural conditions to which they are exposed also require a deep understanding of the behaviour of the materials and the system to ensure safety and durability. Most building materials that make up a structure are specified and manufactured for a specific purpose, while soils are complex materials that form the traditional foundation and must be tested to identify, evaluate, and use effectively or not depending on their properties. Therefore, understanding the response of the soil to the superstructure and the response of the superstructure to physical phenomena emanating from external hazards, especially natural ones, is a priority in conceptual engineering. In reality, current study methods, where loads are well controlled and we are not in a large project exposed to external hazards, tend to decouple the geotechnical model from a structural model (Figure 2-18). In other words, soil-structure interaction (SSI) aims to overcome the limitation of decoupling models by incorporating whole-system analysis. However, the definition of SSI cannot be easily generalised, but depends on the particular case study. It is quite clear that the concept of soil-structure interaction refers to static and dynamic phenomena mediated by a compliant soil and a stiffer superstructure, but the discipline encompasses so many different aspects, sometimes closely related, that it is indeed difficult to give a convincing definition in a few words (Kausel, 2010). The term interaction is the essential one, because it clarifies that not only the nature of the soil has an influence on the behaviour of the structure, but also the structure has an influence on the behaviour of the soil, which can change the components of the excitation. Some of the main problems that constitute the theory of SSI can be seen as follows (Kausel, 2010):

- Response of a soil domain to external dynamic or static sources acting near - or on - the surface
- Response of soil to ground vibrations induced by earthquakes or other sources, such as fast-moving trains, even before any structures are in their path
- Response of rigid, ideally massless structures to ground waves passing beneath them
- Response of ideally massless foundations, piles, or caissons embedded in compliant soils, triggered by static, harmonic, or transient loads acting directly on those foundations
- Additional deformation of the soil in the vicinity of a structure due to the response to the inertia of the structure itself.

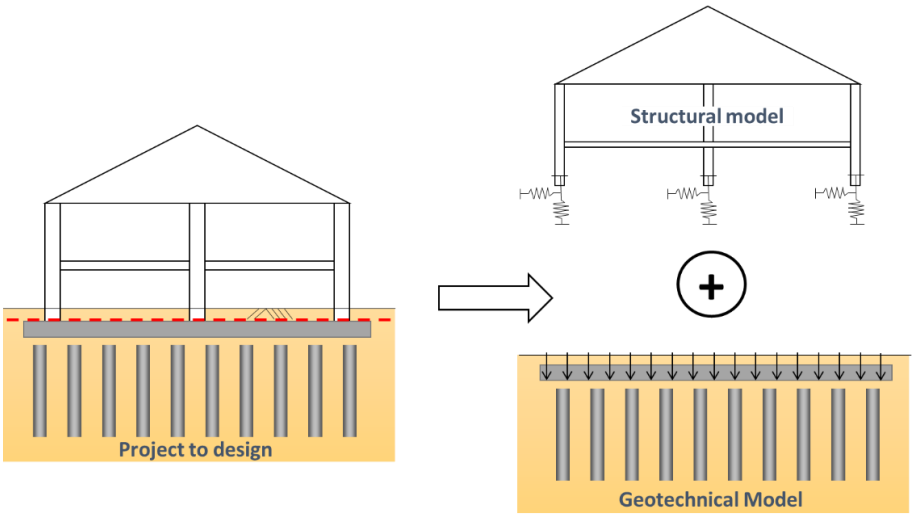

Figure 2-18: Usual decoupling of "geotechnical" and "structural" models, edited after (Cuira and Simon, 2016).

The SSI is an intensively researched area to improve this discipline. There are several methods that SSI can be considered. They range from linearity (simplified methods) to nonlinearity of system behaviour and from static to dynamic- cyclic loading. Several methods can be considered for SSI, which are distinguished as follows: direct approach, substructure method, hybrid approach, and macroelement hybrid model. It is known that these methods are used in the field of earthquake control, but that is not our focus in this dissertation. In general, for soil-pile foundations as well as soil – rigid inclusions, the focus is on the soil-structure interface of nonlinearity that arises at this stage due to the effect of cyclic loading, rather than the governing nonlinearity of the system in a general soil-structure interaction as defined by (Kausel, 2010). SSI is usually limited to buildings designed in earthquake zones. However, wind turbines are themselves a rotating machine loaded by the wind and are designed to withstand continuous vibration-induced forces during their lifetime. Early studies have shown that the response of a structure to a dynamic wind load can be influenced by SSI (Novak and El Hifnawy, 1988). The literature on the dynamic interaction of wind turbines considering SSI is limited (Harte et al., 2012). SSI will be crucial in the dynamic treatment of the frequency of the wind turbine system (wind, blade and rotor rotation) based on rigid inclusions and, on the other hand, how the reinforced soil affects this frequency when the wind turbine is located in a seismic area. On the other hand, the soil – inclusion – LTP – structure will almost fall under the same methods with different boundary conditions to evaluate the interaction of the soil reinforcement under a static, dynamic or cyclic structure.

2.4.1 Dynamic SSI- Soil reinforcement by RIs

In the dynamic domain, particularly in earthquake-prone areas, rigid inclusions have been used successfully for various types of structures, including those that pose a high risk to people, such as residential buildings and bridges. The technique has been extensively researched in the static domain, while in the dynamic domain, as with many traditional construction techniques, it is still relatively recent, although numerous research and construction projects have been conducted in this area. The mechanical behaviour of rigid inclusions has traditionally been compared to pile foundations in the dynamic domain, as deep foundation techniques share some similarities in such

mechanisms in terms of shaft friction and base resistance. However, rigid inclusions are a technique intermediate between shallow and deep foundations, which makes them more advantageous than other techniques under certain conditions related to site characteristics.

Nevertheless, several research projects are underway in different areas (static, dynamic, and cyclic) to optimize design methods and investigate important considerations for such complex loading. Pile foundations have failed several times in earthquakes, while rigid inclusions have not experienced any failures (Jimenez, 2019). There is no comparison because rigid inclusions are a relatively new technique that is less used compared to piles, but it is worth noting how important this technique is to improve research projects in this area. One of the most interesting examples of the use of rigid inclusions technique in earthquake zones is the Rion-Antririon project in Greece (Pecker, 2000). The bridge was designed for difficult environmental conditions and is located in one of the most vulnerable earthquake zones in Europe, where the maximum ground acceleration is about 0.48g. The earthquakes that have occurred since commissioning have not damaged the structure. As for the integrity of the rigid inclusions, there are no data to verify this as they have not been instrumented. In addition, in the city of Morelia, in west-central Mexico, which is considered an area of high seismic risk, a huge construction project with 76 buildings was founded on rigid inclusions (Paniagua et al., 2007).

Two key mechanisms are generally involved in the interaction between soil, foundation, and structure under dynamic, mainly seismic loading: kinematic and inertial interaction(Gazetas and Mylonakis, 1998; Wolf, 1985). These two phenomena are considered in the use of pile foundations and also in soil reinforcement by rigid inclusions:

- The kinematic interaction corresponds to the reaction of the foundation in the absence of the structure. We must imagine that the difference in stiffness between the columns and the soil and the rigid foundation leads to a difference between the motion of the soil in the free field and in the presence of the columns (Pecker, 2011). The greater the difference in stiffness values between these two components, the greater the difference in the motion we get. The length of the RIs is a factor that affects the wavelengths of the dominant seismic frequencies (ASIRI+, 2018).
- Inertial interaction reflects the dynamic interaction between the structure and the foundation, as the movement of the structure generates inertial forces that are transmitted through the foundation to the ground. This results in additional dynamic forces on the soil-foundation system. The use of SSI aims to reduce the probability of resonant frequency of the structure by taking into account the damping phenomena due to the nature of the material and geometric properties.

Despite the similarity between the behaviour of piles and rigid inclusions under dynamic loads. Soil reinforcement with rigid inclusions has advantages for construction in earthquake-prone areas. In terms of seismic loading, this type of reinforcement is comparable to an isolation system at the base of the structure. The LTP creates a zone of energy dissipation between the structure and the rigid elements. And since the inertia generated by the structure is not directly transferred to the inclusions, as is the case with piles, this results in a reduction of inertial forces.

In the case of OWT, where the structure is not located in an earthquake prone zone, a dynamic analysis with SSI is essential to avoid resonance problems between the natural frequency of the

wind turbine system and the turbine excitation frequencies. This aspect of dynamic evaluation of wind turbines is still very recent in the onshore sector, compared to what has been done recently for offshore turbines as well. The following articles address the literature review on dynamic analysis of onshore wind turbines using SSI, as well as numerical and analytical applications using degrees of multi-freedom (Harte et al., 2012; Michel et al., 2018; Gravett and Markou, 2021)
In the context of soil-structure interaction with rigid inclusions, various interactions can be observed through load transfer mechanisms and the type of superstructure loading. Two distinct categories can be identified: embankments and footings. The focus of this dissertation is on the soil-structure interaction of gravity foundations under wind turbines. It is important to note that the complex loading conditions associated with wind turbine foundations add complexity to the soil-structure interaction analysis.

The previous sections of the dissertation provided an overview of the static and dynamic features of the problem. A general definition of static soil-structure interaction will be outlined and followed throughout the study. This will lay the foundation for the subsequent analysis and exploration of the specific aspects of soil-structure interaction in the context of gravity foundations under wind turbines.

2.4.2 Footings

The rigid inclusions under footings are usually covered with a layer of granular material called a "load transfer platform" or LTP, playing a major load in the soil-structure-interaction. This layer allows load transfer at the top of the inclusion and associated soil volume, reducing and homogenising the surface settlement. For rigid inclusions under footings, the LTP is usually made of granular material to improve the mechanical properties in shear strength, since load transfer is governed by this phenomenon. The thickness of the LTP is considered small relative to the length of the inclusions and the usual interval is between 0.4 to 0.8 (m). The LTP plays an important role in ensuring load transfer mechanism. Its presence in numerous RIs projects has made it a research topic for many authors, since it is responsible for the redistribution of load components between the soil and the RIs. It has been discussed that the materials that make up the LTP and their thickness have a direct influence on the efficiency of load transfer, as these properties can increase the stresses at the heads of the inclusions and decrease the stresses in the soil. The LTP play an important role in preventing punching phenomena through the inclusions in the structure by absorbing the loads transferred from the inclusion heads, thus ensuring efficient foundation performance (ASIRI, 2013; ASIRI+, 2018; Garcia et al., 2021).

In the case of a gravity foundation, the interaction between inclusions – soil vs LTP – structure could be determined based on the load transferred at the base of the foundation and its dissipation in the LTP. This allows the stress distribution between the components of the soil reinforcement with a specific deformation propagation according to a scheme with planes of equal settlements: one at the base of the foundation (an essential hypothesis in the current simplified design methods), one in the neutral plane and one under the end of the column where the settlement profile is again homogeneous (Figure 2-19).

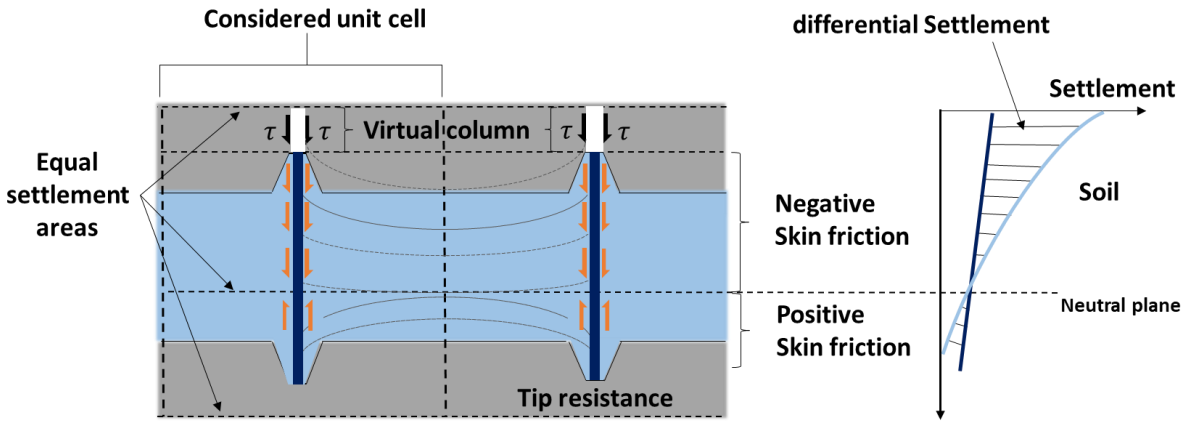

Figure 2-19: Settlements, load transfer behaviour and planes with equal settlements in the RI grid, edited after (Bohn, 2015).

Another type of interaction can be seen at the level of the soil – inclusion, where negative skin friction occurs when the soil settles to a certain depth relatively more than the column, and positive skin friction occurs when the settlement phenomena are reversed.

The presence of different elements that make up the concept of soil reinforcement technique by RIs leads to different interactions at the substructure level before the coupling between the geotechnical and structural models. The general interactions that constitute the concept of this technique were summarised by (Briançon, 2002) and presented in (ASIRI, 2013) as follows:

1. Interaction between the structure and the LTP, depending on the thickness, the material properties of the LTP, and the stiffness of the foundation.
2. Interaction between the LTP and the reinforced soil matrix, which consists of the compressible soil layer and the rigid inclusions.
3. Interaction at the interface between the compressible soil and the inclusions
4. Interaction between the tip of the inclusions and the anchored soil layer.

The configuration of the OWT foundation reinforced by RIs (Figure 2-14) reflects a complex loading to which the foundation and the soil below are subjected, including a high overturning moment. Therefore, a three-dimensional geotechnical model must account for several interactions that may not be considered by only using the unit cell model. Two other important physical phenomena that must always be considered when designing a 3D problem are highlighted below:

5. Interaction between the individual cells described by a soil/shear effect at the interface between two units, when a possible differential settlement could occur due to the trapezoidal load transfer at the base of the foundation as a result of the high overturning moment (Figure 2-20 (a)).
6. Interaction of the soil reinforcement with the external unloaded soil mass, since the foundation and rigid inclusions are in fact finite elements and are not implemented in a repeated infinite domain (Figure 2-20 (b)).

To summarize the key interactions to consider when designing and evaluating RIs under a gravity foundation separated by an LTP, designers are encouraged to consider the six interactions shown in (Figure 2-21). Each of these key phenomena was considered in the development of the

macro- element in this chapter when the asymmetric configuration was achieved and converted to a three-dimensional configuration of the geotechnical model.

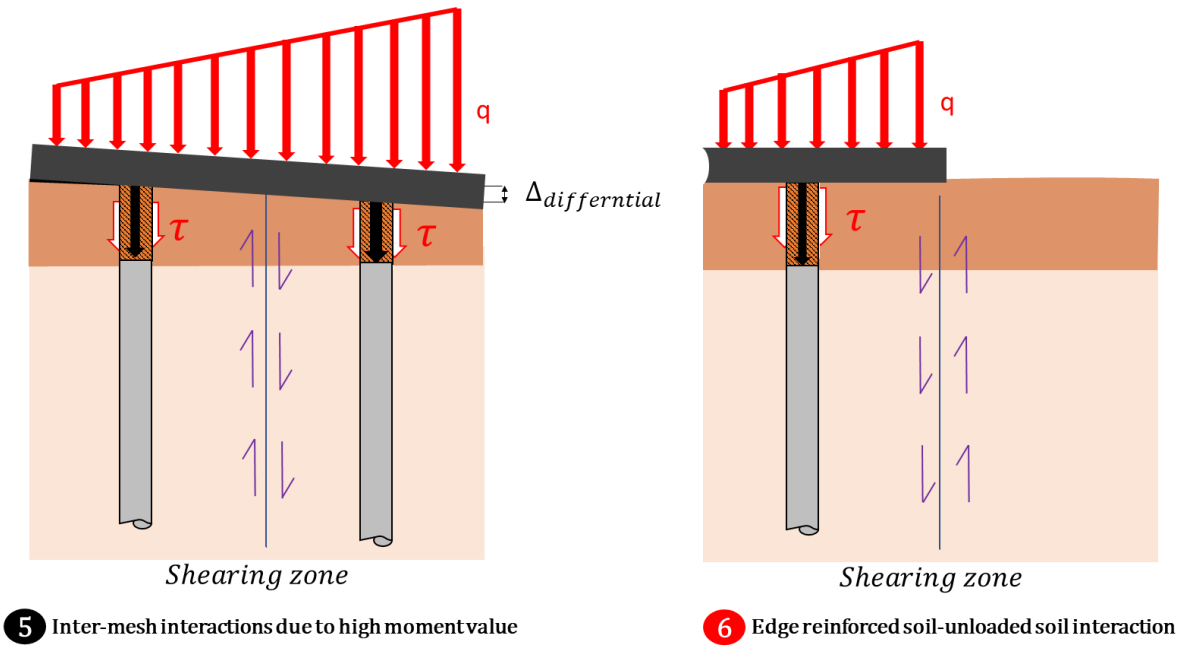

(a) (b)

Figure 2-20: Proposed two additional simplified interaction phenomena for consideration in the modelling of RIs under OWT foundations.

This list of interactions is usually represented by analytical models and numerical analyses such as the finite element method and the finite difference method. In numerical models, the interface between soil-inclusion vs LTP – structure, the contact elements, represents this mechanism and the soil is usually represented by an elasto-plastic constitutive law. In the static domain, the behaviour of soils reinforced by rigid inclusions has been studied in numerous research projects. These include real-scale measurement devices and physical modelling for almost all domains (ASIRI, 2013).

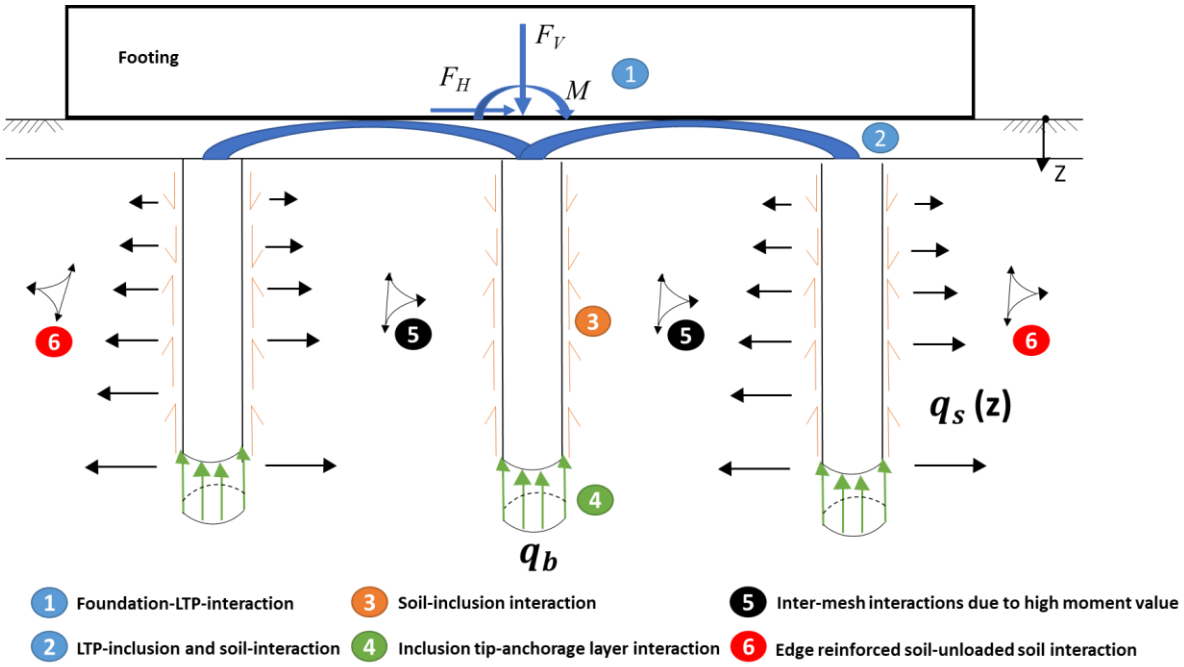

Figure 2-21: Soil reinforcement by RIs interactions under a gravity foundation in a 3D configuration.

2.4.3 Design and considerations of rigid inclusions

The design methods for a gravity foundation reinforced by rigid inclusions can be divided into three types (ASIRI, 2013): analytical, numerical, and homogenization models. Numerical models are considered direct methods that do not require stepwise modelling. However, some of the commonly used analytical models require some decoupling of the geotechnical model to perform the overall calculations, which are referred to as indirect methods. In between, there are hybrid models that combine direct and indirect methods, especially the homogenization methods for rigid inclusions. In the following section, the differences between the methods are explained and it is shown that another approach, such as the macroelement, which is intermediate in its simplification and robustness between the direct and indirect methods and is consistent with the current methods for rigid inclusion design, could be interesting.

2.4.4 Direct methods

By definition, direct methods consist of modelling the soil, foundation components, and superstructure in a single step (Kramer, 1996). If we project this concept to OWT foundations by RIs, in this way the load transfer mechanisms and the physical and geometric nonlinear phenomena can be accounted for, such as the eccentricity and stress concentration in the foundation of the onshore wind turbine in addition to the nonlinear phenomena at the interface between soil and inclusions. There is also the possibility of considering the effects of cyclic loading and material fatigue. The finite element method (FEM) and the finite difference method (FDM) are well suited for the linear and nonlinear behaviour of complex or arbitrarily shaped structures founded on soil layers with inhomogeneous and anisotropic material properties. In the field SSI, FEM are widely used methods (Karabalis and Beskos, 1984), where the problems are treated at the local level (constitutive laws for stress and strain). In the case of RIs, there are a large number

of publications using both methods FEM & FDM for various structural applications considering the modelling of the structure and the underlying reinforced medium.

The computational method is well represented in modelling soils reinforced by rigid inclusions under a gravity foundation. According to (ASIRI+, 2018), numerous reference works have been performed using finite element and finite difference software. Numerical analyses are performed at the scale of the structure. Most models are performed in three dimensions or with an asymmetric model. For example, the FEM protocol consists of various structural elements (beams, embedded beams, volumes, etc.). The interaction with these elements and the surrounding soil is represented by the meshing procedure, which generates a finite number of nodes. Each node can be assigned several degrees of freedom, depending on the boundary conditions of the model. There are two common methods: nodes can be associated with structural elements and soil mass if they are assumed to behave in the same way, or strong mesh refinement must be performed to distinguish their behaviour. Another common method is to introduce interface elements to indicate the different properties between the two domains (soil and structural elements) and easily control a phenomenon such as sliding or detachment. The interface element could be crucial in such an application, e.g., cyclic loading, to consider the loading history at each cycle and predict the behaviour of the columns in relation to the adjacent soil. The interface elements are recommended to significantly reduce the sensitivity of the load-settlement calculation (Wehnert, and Vermeer, 2004). The FEM method for rigid inclusions under shallow foundations is presented in detail in Chapter 3 of the dissertation. As for rigid inclusion analysis including soil-structure interaction under dynamic conditions, some of the related research can be found in these publications (Pecker, 2000; Hatem, 2009; Rangel-Núñez et al., 2008; Awwad and Donia, 2016; Mánica Malcom et al., 2016; ASIRI+, 2018; Zhang et al., 2022; Jawad et al., 2023).

2.4.5 Indirect methods

Indirect methods, by definition, consist of decomposing the problem in question into several submodels where in each a specific method could be employed. This approach is used in both static and dynamic domains. This approach aims to study separately the structure and the reinforced soil in the case of rigid inclusions (Figure 2-22), or sometimes it is more of an iterative design process. If we are referring to a dynamic problem as example, the geotechnical model could first be used to define a set of “dynamic” stiffnesses (linear or nonlinear) that may include frequency effects (dynamic impedances). The stiffnesses or impedances are then introduced into the structural model to simulate the ground response. The latter leads to the definition of the seismically induced torsion at the base of the structure. After several iterations between the structural and geotechnical models, it may be necessary to adjust the values of the stiffnesses (or impedances) that depend on the distribution of rigid inclusions, a distribution that must be adjusted for load descent. Finally, the adjusted structural model allows the dimensioning of the structure. In OWT, the decoupling method (Figure 2-14) is a perfect example of disentangling the physical phenomena to evaluate the overall behaviour of the soil-foundation system under such complex loads. In the following sections, the iterative methods used in the simplified methods for rigid inclusions are presented in detail.

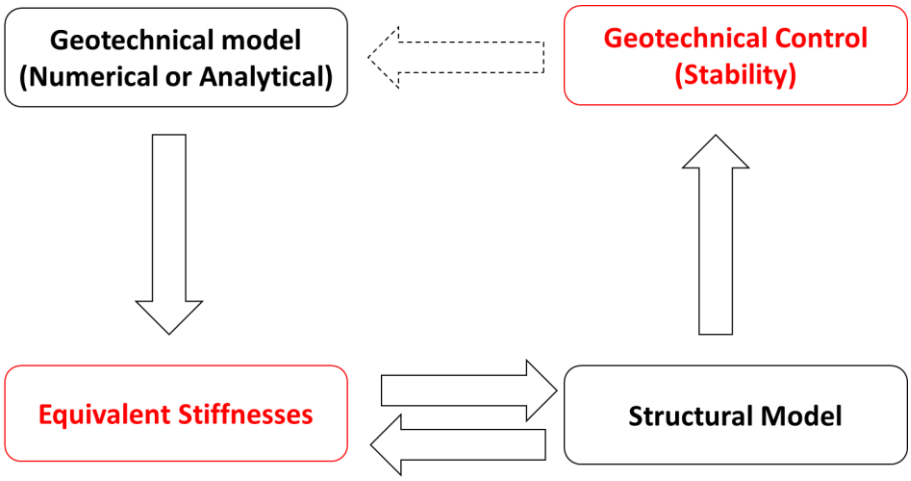

Figure 2-22: Ordinary iterations between the geotechnical model and the structural model.

2.4.6 Analytical methods

Several analytical approaches focus on rigid inclusion design and attempt to understand the interactions within the soil reinforcement matrix. These methods aim to capture the mechanisms of interaction between the soil and the inclusion. Effective strategies such as load transfer methods like the "t-z" and "p-y" methods are often used to integrate this interaction along the inclusion interface and at its base resistance in the anchorage layer. Boundary conditions play a critical role in these approaches, especially in the context of soil reinforcement with rigid inclusions, whether in foundations, embankments, slab on grade, and similar applications.

The first level of interaction, soil – inclusion, is represented by the t-z method, which is used to estimate the displacement of a rigid inclusion using a nonlinear shape under axial loading. The results are found to be satisfactory as they are intensively compared with experimental and numerical results. The semi-empirical mobilization laws proposed by (Frank and Zhao, 1982) are one such method originally proposed for piles into fine or granular soils. They are based on the evaluation of a large number of piles loading tests before covering the main soil classes and the piles with and without soil displacement. The physical parameters of the method are based on the Menard modulus "E_m" from the pressuremeter a common in-situ used in Europe and especially in France. The model of (Frank and Zhao, 1982) is highly recommended for describing the interactions that develop over the height of an isolated inclusion, as well as for representing the behaviour of a group of inclusions by a slight modification, as integrated in the following analytical methods MV2 or MV3, applied within an axisymmetric model of the inclusion within a given group, adjusting the curve of frictional mobilization to account for the group effect between adjacent inclusions (ASIRI, 2013).

The second level of interaction, load transfer from the foundation to the reinforced soil through the arching effect in the LTP, is also represented analytically by the technique of a fictitious column consisting of an extension of the rigid inclusions in the LTP and made of LTP material (Combarieu, 1988). As described in detail in (ASIRI, 2013), the method was modified (Combarieu, 2007, 2008) to overcome some of the limitations in the case of rigid inclusions (Figure 2-23). In applying the method, a distinction was made between embankment and rigid slabs. In the latter case, an equal settlement condition of column and soil is considered at the upper boundary of the system (Figure 2-19), and the mobilization law used for the mobilized friction

between fictitious column and LTP can be equated to the law described for a granular soil by using the equation (2.1), (NF P94-262, 2012).

$$\tau = k \tan \delta \, \sigma'_v \tag{2.1}$$

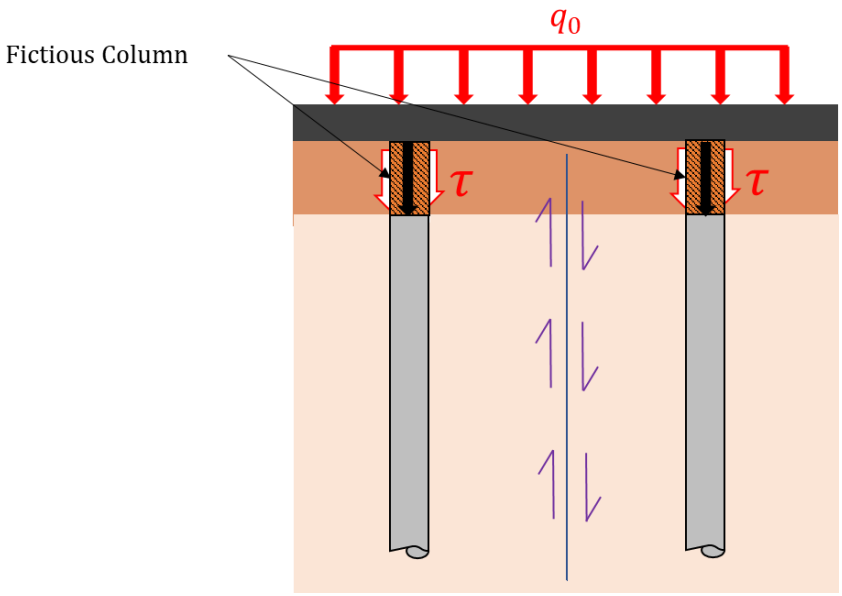

Figure 2-23: Modelling LTP as fictitious columns as an extension of RIs.

2.4.7 Simplified methods

The load transfer methods incorporated into the design methods for rigid inclusions are presented analytically as a series of MV and MH models, where "V" represents vertical loading and "H" represents horizontal loading at the base of the foundation. Each model in the series MV or MH can be used interchangeably to account for a combination of loads. A detailed presentation of these methods and their calculation steps can be found in (ASIRI, 2013).

The MV1 model (Combarieu, 1990) aims to calculate the load- settlement of a foundation reinforced by rigid inclusions under a vertical load in two stages by interpolating between a case without inclusions and one with inclusions. Although the model takes the group effect of the inclusions into account, one of the limitations is that only a centred axial load can be applied and the settlements of the LTP, directly related to the stress concentration on the inclusion head, are neglected.

The MV2 model (Glandy and Frossard, 2002) is a biphasic model that examines the interaction between the domain of inclusions and the complementary soil. The model is proposed for foundations with a uniform settlement condition at the base and is an iterative method that can be used to determine the distribution of forces and settlement profiles of the two domains. One of the main limitations of the model is its validity only by imposing a vertical uniform loading on the top of the unit cell. that it does not consider the group effect. This should be considered separately by adjusting the mobilization laws used.

The MV3 model (Simon, 2010) consists in assimilating the volume of soil reinforced by the inclusions at the base of the foundation with an equivalent homogeneous monolith. The study of an isolated inclusion in the centre of a unit cell reinforcement mesh allows the determination of the properties of the equivalent monolith, a monolith surrounded by the surface of the foundation. The MV3 model is suitable for simulating a footing reinforced by RIs. This method requires several calculation steps (Figure 2-24). In the first step, an inclusion with the surrounding soil is calculated as if it were in an infinite grid (without any interaction with the environment). From this step, an equivalent oedometric modulus E* under vertical loading is calculated and used for the second step, in which the soil and the columns under the foundation are considered as one block. The settlement of the latter is calculated as a large equivalent unit cell without reinforcement and with an external skin friction at the edge of the monolith for a soil-soil friction. The last step corresponds to the calculation of the load-settlement curve of the inclusion in a soil volume under the hypothesis of equal settlements at the base of the foundation, so that the load at the top of the column corresponds to the results of the settlement of the soil volume from step 2. In this step, the fictitious column method is applied by expanding the inclusion in the LTP to ensure the load transfer mechanisms under the foundation. One of the main advantages of this method is the ability to account for group effects within the load transfer methods and load-settlement profile for the rigid inclusions and soil.
Limitation: As a coherence test, a second MV3 should be performed without considering rigid inclusion. The settlement calculated at step 2 using a module E (not E*) must be compared to the settlement of a footing using a reputable analytical method. The settlement criteria imposed to calibrate the shear forces acting on the model borders in order to achieve the same settlement estimated analytically, leads to a several iterative calculations.

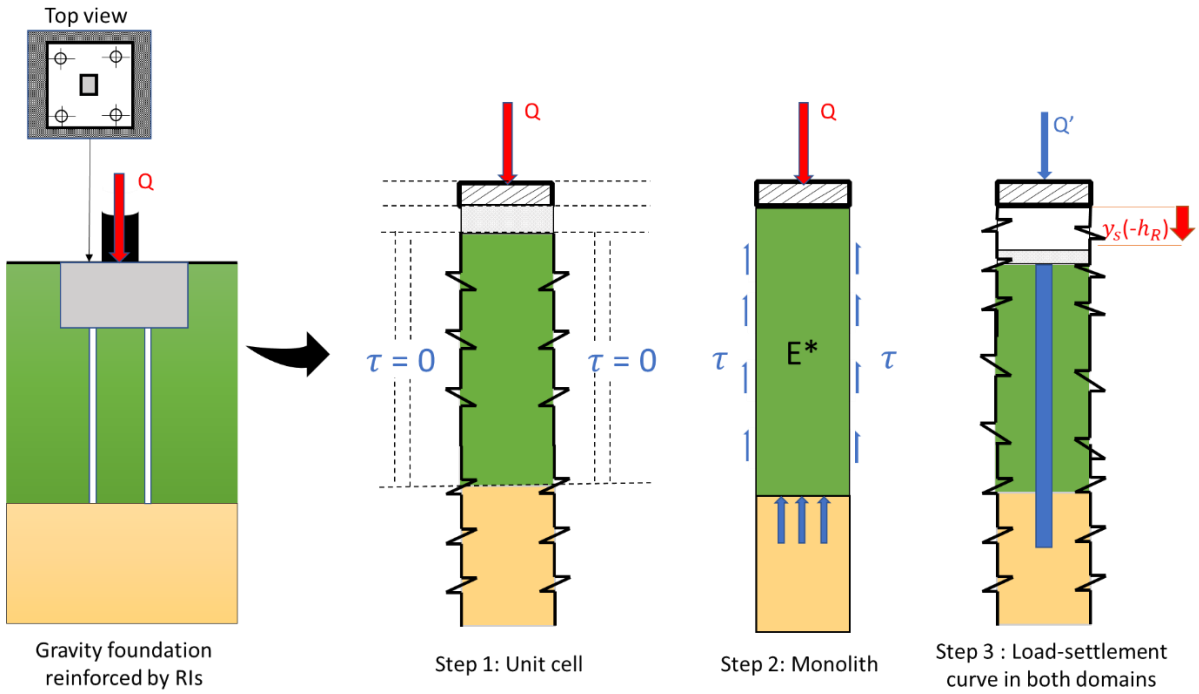

Figure 2-24: Modelling of a foundation reinforced with RIs using the analytical model MV3.

The series of MH models that consider the horizontal load and moment at the base of the foundation are also divided into MH1 to MH3, with different solutions in terms of estimating the shear stress in the soil and along the RIs. The MH3 model is a continuation of the MV3 model with

two successive additional steps (Figure 2-25). It consists of studying the lateral displacement of the monolith and the rotation of the foundation under a combination of horizontal loading and a moment {H, M} acting on the base of the foundation (Simon, 2010).

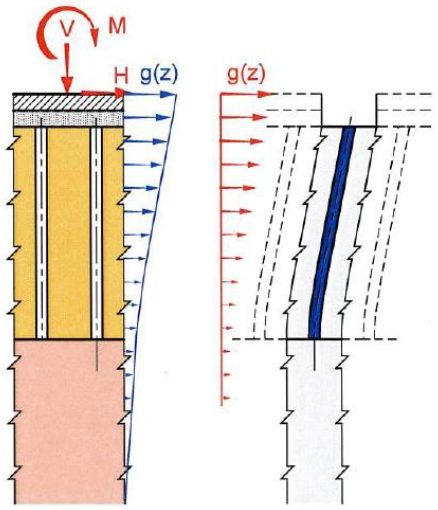

Figure 2-25: Additional steps to consider lateral load and moment in the MV3 model (Simon, 2010).

The listed analytical models represent the current simplified models used in the design of rigid inclusions under a rigid foundation, which could be iterative models under the title of indirect methods. The model proposed by (Simon, 2010) is considered state of the art in simplified methods, since it uses several calculation steps to determine the load distribution within the rigid inclusions and the soil under a complex load represented by a vertical, horizontal, and a moment at the base of the structure. The model is considered an interesting alternative to more complex methods such as FEM &FDM, since it is simply based on the usual tools of deep foundation design and is able to consider, in a three-dimensional framework, the interactions that develop firstly within the volume reinforced by the inclusions and secondly between this reinforced volume and the surrounding block (Simon, 2010).

2.4.8 Partial conclusions

The simplified methods serve as design methods for various rigid inclusions applications. Their implementation in design tools usually requires a mathematical solver. Despite the simplification of the application of these methods compared to the direct methods, since they involve a step-by-step calculation to achieve the design. Their scope is limited within a geometric barrier, and each approach must be mastered by the user and adapted to the specifics of the project and the types of tests to be performed. In addition, (ASIRI, 2013) has listed several verifications that must be performed after applying these methods, especially when a load other than the centred vertical axial load is applied. Nevertheless, these methods have paved the way for advances in RI design, as their results cover several approaches, such as:

- The load transfer mechanism inside the LTP,
- the load transfer by friction (positive and negative) at the interface between the soil and the inclusion's shaft,
- the load transfer at the inclusion tip into the anchorage layer,

- the load and settlement profiles of the soil and the inclusions,
- the settlement of the soil layers under the inclusions,
- the interaction of the reinforced matrix with the unloaded soil mass beyond the foundation.

A combination of the MV3 and MH3 analytical models could be relevant in the case of the OWT foundation. However, the nature of the loading at the base of the foundation leads to multiple applications of such simplified methods to design different unit cells of RIs based on the stress level at their head according to the configuration of the rigid inclusions. An example of the generalised resulting uniform trapezoidal stress at the base of the foundation is shown in (Figure 2-26 (a)). It reflects the multiple modelling that must be performed in this case, as a typical stress distribution below the foundation requires multiple modelling to achieve this type of stress (Figure 2-26 (b)). Another major limitation, the implementation of the CMCs under the WT foundation is various with narrow spacing at the edge of the foundation and larger spacing next to the centre of the foundation (Figure 2-26) which is not possible to consider using the MV3 model.

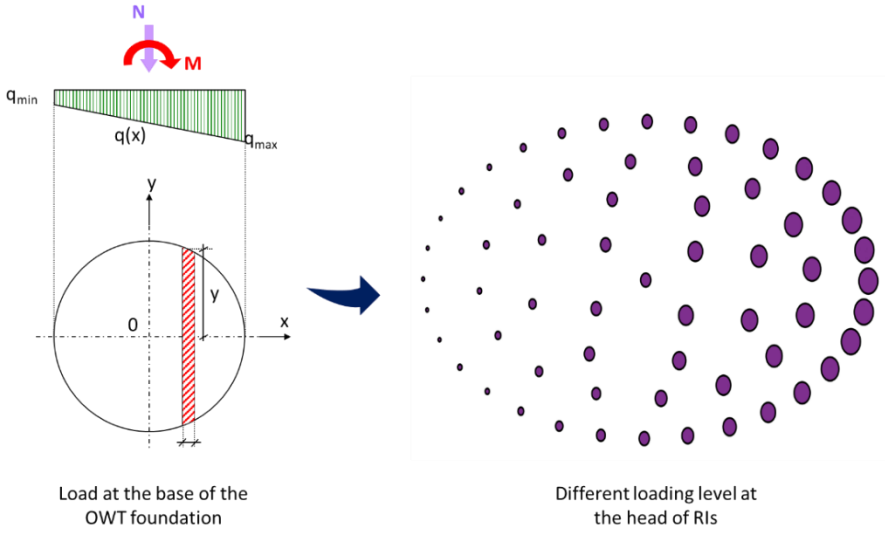

Figure 2-26: (a) Generalized loading under the foundation of a wind turbine, (b) heterogeneous stress level at the head of the inclusions.

2.4.9 Multiphase approach

The simulation of the interaction between the soil and the pile group, leading to an estimation of the settlements of a deep foundation is an important geotechnical area where different methods have been applied. In this context, several models for soil reinforcement by rigid inclusions have been developed. Originally called "hybrid models", they were developed by (Griffiths et al., 1991) and (Clancy and Randolph, 1993) for the design of mixed foundations and are based on an extension of the "hybrid method" proposed by (Chow, 1986) for the analysis of pile groups. It consists of discretizing the rigid elements into one-dimensional beam elements that are loaded only in tension and compression. The interaction with the soil mass is accounted for by springs schematizing lateral friction ("t-z" load transfer curves), as in deep foundations, and the soil mass is integrated by linear elastic equivalent springs. These models were applicable only to axial loads, that is, to short, simple calculations for vertical settlements. To extend their application, a three-

dimensional simulation of this type of structure was performed by (Vetter, 1998) using the finite element method, in which both the soil and the piles were discretized separately, resulting in a long computation time due to the thousands of elements created for the mesh. To overcome these limitations, a so-called ''multiphase model'' for pile-reinforced soil was proposed to predict the global response of pile foundations under purely vertical (Sudret and De Buhan, 2001) or combined loads (Hassen and De Buhan, 2005).

In the case of soil reinforcement by rigid inclusions, the homogenization method was introduced as an alternative to the finite element methods. It consists in understanding the reinforced composite soil as a homogeneous one within an anisotropic medium due to the rigid inclusions. The idea of using a classical homogenization method to model a reinforced structure by rigid inclusions is valid if two conditions are met: (1) the reinforcing inclusions are periodically arranged in the solid; (2) the characteristic scale of the reinforcement (e.g., the distance between two adjacent inclusions) can reasonably be considered sufficiently small compared to the overall dimensions of the structure (Thai Son, 2009). Due to its analytical formulations, a classical homogenization model has the great advantage of being easy to implement. Nevertheless, a classical homogenization method is usually based on the implicit assumption of perfect adhesion between the inclusions and the surrounding soil, which is not the case for the design methods at the interface between soil and inclusions. Furthermore, the shear and bending effects in the rigid inclusions cannot be represented.

A multiphase approach consists of an efficient alternative to the classical homogenization method by replacing one phase of an anisotropic medium with two different geometrically superimposed continuous media in mutual interaction, called "phases", which represent the soil or network of reinforcing inclusions at the macroscopic level. In the case of RIs, several multiphase models (De Buhan and Sudret, 2000; Sudret and De Buhan, 2001; Bennis and De Buhan, 2003) provide a mechanically consistent framework for developing appropriate design methods with a drastically reduced computational cost compared to that required for direct numerical simulations. The multiphase model is based on a change of scale to avoid the heavy task of treating soil and reinforcement inclusions separately. In this way, the model benefits from the advantages of the homogenization method without its limitations, while considering the interactions between soil and inclusions that are inaccessible in the homogenization method.

2.4.10 Two-phase model

A two-phase model is a version of the multiphase modelling approach in which only two phases are represented by separate homogenization of the soil and inclusions in the two-phase domain (Figure 2-27). The model represents the heterogeneity of the system by assuming that at each spatial point of the entire reinforced volume, two phases, the matrix and the reinforcement, represent the soil and the inclusions, respectively. The kinematics of the two-phase model are considered separately for each phase. In the matrix phase, a displacement vector is calculated for each spatial value. In the reinforcement phase, a beam type is used to represent the displacement and rotation of the inclusions at their two ends.

The two-phase model developed by (Hassen and De Buhan, 2005) represents the continuation of the analytical formulation for the multi-phase models (De Buhan and Sudret,

2000). It is based on the principle of the virtual work method of a system in a two-phase environment using a variational formulation and assuming perfect adhesion with the surrounding soil. The solution of the variational problem was achieved by a discretization in a finite element framework to find the displacement and rotation fields that minimize the potential energy functional in an approximated space contained in the set of kinematically admissible fields. The finite element method was represented by an equivalent equal meshing in both phases with 3 degrees of freedom for plane deformation and one for rotation along the vertical axis.

The principle of virtual work of the two-phase model (Sudret, 1999) is illustrated in the following equations:

$$\varepsilon\left(\underline{\xi}^m, \underline{\xi}^r, \omega^r\right) = W(\underline{\xi}^m, \underline{\xi}^r, \omega^r) \; - \; \phi(\underline{\xi}^m, \underline{\xi}^r, \omega^r) \tag{2.2}$$

Where W is the deformation energy of the two-phase domain and ϕ is the external load potential, that leads to:

$$W\left(\underline{\xi}^m, \underline{\xi}^r, \omega^r\right) = \int_{\Omega} \Psi\left(\underline{\xi}^m, \underline{\xi}^r, \omega^r\right) \mathrm{d}\Omega + \int_{\Sigma} \psi^p(\Delta\underline{\xi}) \, d\Sigma \tag{2.3}$$

$$\begin{aligned}(\underline{\xi}^m, \underline{\xi}^r, \omega^r) = \int_{\Omega} \left(\rho^m \, \underline{F}^m \, . \underline{\xi}^m + \rho^r \, \underline{F}^r \, . \underline{\xi}^r\right) \mathrm{d}\Omega + \int_{\partial\Omega_T^m} \underline{T_d^m} . \underline{\xi}^m dS \\ + \int_{\partial\Omega_T^r} \underline{T_d^r} . \underline{\xi}^r dS + \int_{\partial\Omega_T^r} C_d^r \, \omega^r dS\end{aligned} \tag{2.4}$$

The two-phase model (Hassen and De Buhan, 2005) provides a good basis for a powerful method with low computational cost and an easy integration possibility into a finite element calculation code such as the software package CESAR-LCPC (Bourgeois et al., 2006). One of the main limitations of the model is the nature of the plane deformations of the problem, which require periodic assimilation of the rigid inclusions in the reinforcement phase, as well as the assumed perfect bond condition, where there is no possibility of slip between soil and reinforcement, and the limitation of access to the information along the inclusions.

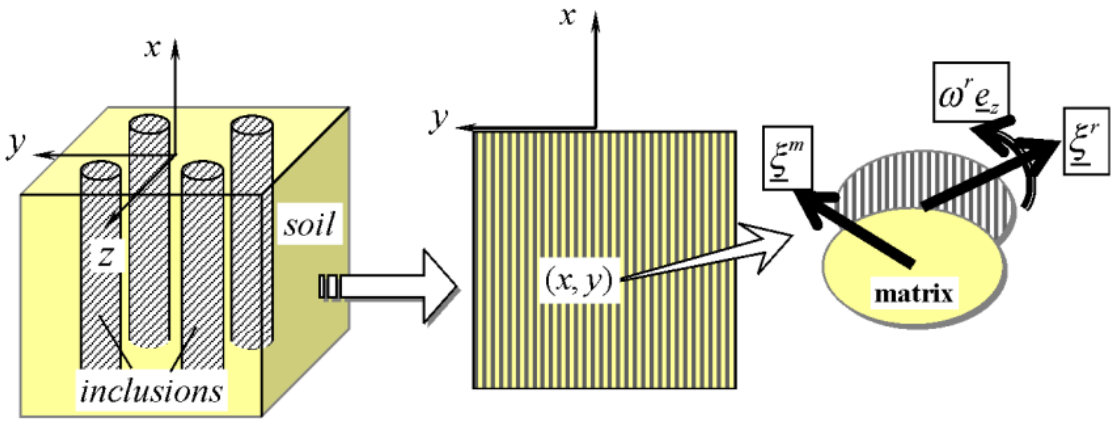

Figure 2-27: Principle of multiphase modelling of a soil reinforced by linear inclusions (Hassen and De Buhan, 2005).

On the other hand, the development of the two-phase model continued. The theoretical and numerical framework of the model has been extended to the elastic plastic soil model (Thai Son et al., 2009). This work has made it possible to develop, both theoretically and numerically, the most complete version of the multiphase model to describe the elasto-plastic behaviour as well as the failure behaviour of soil reinforcement by rigid inclusions. This model allows to consider, at the macroscopic level, not only the interaction between soil and inclusions, but also the bending and shear effects on the columns. The model was tested in different configurations, which allowed a good understanding of its capacity and identified different factors such as the response of the model (soil reinforcement by RIs) to lateral loading. Throughout the validation of the model, it has been pointed out that adding transverse interactions between the two phases could be more valuable in case where the inclusions are inclined and not verticals, and a perfect adherence could be fine for the vertical inclusions. Another significant improvement of the two-phase modelling for rigid inclusions (Bourgeois et al., 2012) was the introduction of the interaction laws between the reinforcement and the soil at the level of the column tip as a function of the diameter, length, and spacing of the inclusions, resulting in a complete evaluation of the stiffness and yield strength parameters that govern the interaction laws (shaft and tip). The two-phase modelling was evaluated in the dynamic domain based on a linear elastic behaviour of the different components of the structure accounting for the longitudinal interaction between the two phases, as well as shear and bending of the inclusions (Nguyen et al., 2016).

Out of chronological order, the two-phase model is a highly recommended approach in the field of soil reinforcement by RIs. An equivalent simplified approach has been developed at the level of an axisymmetric model with a purely vertical loading and an interaction between the two domains determined by the load transfer curves at the interface and at the level of the peak between the two phases (Cuira and Simon, 2009). The developed model has proven its performance through a series of validations with experiments and direct numerical methods.

2.5 Conclusions

The onshore wind energy sector is experiencing significant growth, driven by both environmental concerns and evolving political landscapes. In this context, the utilization of rigid inclusions in wind turbine applications is rapidly increasing. The loading on wind turbines is characterized by cyclic loading acting on the foundation with a high overturning moment.

This chapter focuses on the interactions and mechanisms involved in the use of rigid inclusions under wind turbine loading. Various methods and considerations for designing rigid inclusions are discussed, considering the specific requirements of wind turbine foundations. By addressing these design considerations, the chapter sets the stage for introducing the macroelement modelling approach as well the soil-structure-interaction in FEM.

CHAPTER 3

Field Monitoring

3.1 Introduction

One of the main components of this dissertation is the field monitoring of a real scale wind turbine built on a soil reinforced by rigid inclusions to observe and analyse the load transfer from the wind turbine structure to the bottom of the foundation to the rigid inclusions. This should allow a better understanding of the mechanisms of load transfer in case of RIs reinforcing OWT foundation in order to go propose repowering solutions in a methodology consisting at the same time optimize the design of the future wind turbines and to determine the capacity of an existing foundation to be retrofitted.

This field monitoring project extends the ASIRI initiative (ASIRI+, 2018) by assessing complex load dynamics specific to Rigid Inclusions (RIs). The primary objective is to observe the transfer of loads from the foundation to the reinforced soil, capture deformation patterns, and analyse responses to the intricate cyclic loads generated by wind and the various operational modes of wind turbines. A comprehensive array of measurement techniques employing diverse sensor types was deployed, including earth pressure cells, vibrating wire strain gauges, standard strain gauges, accelerometers, inclinometers, and fibre optics for precise strain measurements. To interpret the collected data, an algorithm was developed to delineate the behaviour of rigid inclusions, ensuring independence from variable factors such as wind direction. This algorithm also facilitates the synchronization of measurements with the wind turbine's Supervisory Control and Data Acquisition (SCADA) system, allowing for a holistic analysis of the RI's performance under operational conditions.

This research direction is significantly motivated by factors that are pertinent to both the inaugural FEDRE project and the broader geotechnical community. It draws inspiration from the foundational principle articulated by Lord Kelvin (1824-1907): "If you cannot measure it, you cannot improve it." This maxim underscores the critical importance of quantifiable metrics in enhancing and refining geotechnical methodologies and practices.

The number of projects reinforcing OWT foundations with rigid inclusions has increased dramatically over the past decade due to several successful factors compared to other geotechnical solutions. Real-scale instrumentation will provide an important database for fitting and comparing numerical models and analytical solutions.

Repowering projects to maintain and increase wind energy production will increase incredibly in Europe in the coming years. Therefore, the field monitoring will help to find solutions for a possible optimization of the current design and propose an innovative ecological repowering solution for the current OWT foundations. Regardless of the repowering solutions, rigid inclusions

will play an important role as the inclusions are not structurally connected to the gravity foundation, so partial or complete demolition of the foundation will not affect the inclusions.

The complexity of wind turbine loading, including low-amplitude cyclic loading with a very large number of cycles, can lead to fatigue of wind turbine components, the concrete foundation, and the soil. Long-term monitoring will allow to follow the effects of such loading on each component to be analysed and to draw conclusions about the behaviour of the geotechnical and structural solution, which will help to adjust the numerical modelling and redirect the use of some analytical solutions.

In the field of geotechnical engineering, there are no standardised international codes, either at the European level or on other continents, that explicitly describe the design procedures and verifications when complex loads such as cyclic loads are the main load on the foundation. However, several national recommendations exist to help engineers manage the design of complex loads for offshore and onshore wind turbines. Increased field monitoring for particular geotechnical projects would complement these recommendations and provide a platform for future international codes.

3.2 Overview

Instrumentation consists primarily of real-time data to measure physical properties in a field of interest. In the early 1920s, the importance of soil testing and instrumentation in geotechnical engineering was historically highlighted and explored by Karl Terzaghi (1883-1963) through his research findings and strategies. He referred to the collection of experimental data and the subsequent development of a theory to explain the measured data. In his presentation, Peck, (1993) describes that Terzaghi turned to a mathematical theory only after he had achieved a complete understanding of the phenomenon based on an intensive study of data from tests on real foundation materials. Soil identification recognition has evolved with the development of instrumentation in the field, culminating at that time in the instrumentation of triaxial tests to measure soil properties (Bishop and Henkel, 1957), which represented a turning point in laboratory testing and the advanced method of evaluating soil behaviour.

The use of instrumentation is not limited to validation of theories and advances in soil characterization. As geotechnical scales expand and man-made structures such as tunnels, towers, offshore structures, wind turbines, and others evolve, and as new geotechnical solutions are invented, particularly in the area of ground improvement, instrumentation becomes increasingly important to optimise design and ensure the safety and durability of structures. One of the most recent examples is the monitoring of the challenging "Burj Khalifa" construction project (Abdelrazaq, 2012; Russo et al., 2013), the tallest structure ever built, where the foundation was monitored to evaluate its behaviour and compare it with the design method and combine it with more innovative new design approaches. In addition, a branch of geotechnical instrumentation called the observational method (Peck, 1969; Allagnat, 2005), mentioned in Eurocode 7 as an acceptable verification method for limit states, aims to create an interactive design and construction control method that links design with observed performance during construction to allow for pre-planned design changes during construction. The method essentially involves the creation of a preliminary design based on known data at that time, a monitoring plan to verify the

allowable behaviour of the structure during construction, and a contingency plan that goes into effect if the established limits of allowable behaviour are exceeded. Despite its importance in dealing with uncertainties in geotechnical design, the observational method is not a common practise due to its unclear definition and methodology, including the design and interpretation of the data (Spross and Johansson, 2017), and the various requirements, including project stack holders, that must be directly implemented.

New technologies are constantly pushing the boundaries of what can be measured and monitored. In recent years, it has become possible to transmit measurement data wirelessly and collect data from satellites (Yu et al., 2020). The development of post-treatment data using Big data and machine learning is also a turning point in the history of monitoring. One of the successful applications of machine learning in geotechnical engineering is a challenging project to predict soil properties using the measurement database (Santamarina et al., 2019; Liu and Lacasse, 2022). As an example, in the rigid inclusions field, Menard's has developed a project called OMNIBOX™ that aims to consolidate collected data from in-situ testing and real-time machine data for their rigid inclusions project to provide real-time prediction of key soil properties through machine learning algorithms that benefit both the design and construction phases by bringing them as close as possible to where most production decisions are made, namely the rig.

The instrumentation of a wind turbine and its foundations foreseen in the FEDRE project will allow to establish a solid experimental basis for the wind turbine repowering project through continuous measurements of the different structural components (turbine, gravity foundation, rigid inclusions and soil). It is also possible to derive an approach for "structural health monitoring".

3.3 Field instrumentation

In the realm of geotechnical engineering, true scale measuring instruments are indispensable. They provide foundational support for the preliminary design of facilities or remediation projects, ensuring safety, aiding in the reduction of construction costs, and facilitating the control of construction procedures. Moreover, these measurements play a crucial role in guaranteeing satisfactory long-term performance, offering legal certainty to owners responsible for construction, and driving forward the advancement of geotechnical engineering practices. As (Dunnicliff, 1993) articulated, instrumentation emerged as a pivotal solution for administrators, engineers, and researchers who were grappling with significant challenges in infrastructure projects at the time. The topic of field instrumentation in geotechnical engineering has been a subject of extensive discussion across numerous research endeavours. Documenting instrumentation projects is vital for enhancing structural health monitoring within specific areas of interest and contributing to the evolution of state-of-the-art practices in the field.

3.3.1 Instrumentation planning

Deploying real-scale instrumentation transcends mere instrument selection; it encompasses a thorough, sequential technical process that starts with defining the objective and culminates in the application of the collected data. For any geotechnical field instrumentation project, the

following questions must be answered prior to the site mission (Dunnicliff, 1993; Indicator, 2004; EN ISO 18674-1, 2015; Briançon, 2020):

- The reasons for instrumentation?
- what is to be measured?
- how is it to be measured?

To accurately address these inquiries, it is advisable to adhere to the following process, which encapsulates key components of the monitoring project as outlined by (Thomas H, 1985; Dunnicliff, 1993; ASIRI, 2013; Briançon et al., 2016; Briançon, 2020). Building on these foundational elements, the instrumentation of a real-scale wind turbine was undertaken in this study.

3.3.1.1 Type of monitoring

The geotechnical solution requiring instrumentation is subject to specific conditions, including the natural phenomena under investigation and the variables to be measured—such as groundwater level, pore water pressure, earth pressure, total stress, vertical and horizontal deformation, inclination, acceleration, etc. Additionally, the stratigraphy of the subsoil, environmental conditions, and the proposed construction methodology must be clearly defined prior to the commencement of monitoring. In this phase, the geotechnical engineer assumes a critical role, as the determination of the necessary measuring equipment typically falls within their purview.

3.3.1.2 Auscultation plan

The auscultation plan is designed to ensure high-quality monitoring of the physical parameters for each type of structure. It involves meticulously determining the placement of instruments and the number of measurement points to optimize planning and avoid positions that could result in ambiguous or even misleading data. Making predictions is often crucial to refine the selection of instruments and their specifications, as well as to identify which variables need measuring. These predictions can be based on the current state of the art in the field or through numerical analysis of the project. Furthermore, the designer must consider the potential for sensor failure for various reasons, particularly during construction phases, to mitigate risks effectively.

3.3.1.3 Choosing instrumentation

As mentioned earlier, each project has a unique set of critical parameters. Based on the variables to be measured and the predictions, the selection of sensors is adjusted to meet the specific requirements. Many parameters can influence the type of instrumentation, such as:

- Sensor specifications: Considerations such as the measurement range, precision, and resolution are crucial.
- Environmental conditions: Factors like temperature, corrosion, and exposure to water are important. Sensor datasheet will specify its tolerance to various conditions.

- Field conditions: Modifications may be required for sensor installation, for example, equipping accelerometers with a cone-shaped mounting to secure them underground.
- On-site personnel and resources: It's essential to assess whether the necessary skills for device installation are available and if initial measurements for calibration can be coordinated with the construction phases.

In integrating instruments within the auscultation plan, it is vital to acknowledge that the introduction of sensors might alter the stiffness of key structural elements within the geotechnical solution. This alteration could impact the load transfer from the superstructure to the rigid inclusions, potentially leading to inaccurate measurements. Special care must be taken to mitigate such effects to ensure the reliability of the monitoring data.

3.3.1.4 Acquisition Data devices

Measurements in the field of geotechnical monitoring can vary widely, ranging from point measurements, which are collected manually on-site at specific times, to continuous measurement strategies that are crucial during both the construction phases and the initial serviceability phase of a project. The conditions encountered on a construction site differ significantly from those in a laboratory setting, often making direct access to sensors challenging. This necessitates an automated system for reading and centralizing measurements, a task that extends beyond the mere collection of data. The primary function of data acquisition devices is to communicate with sensors, allowing for the configuration of measurement frequencies, the establishment of monitoring schedules, and the integration of alerts for immediate action in case of anomalies, thereby minimizing the risk of data loss during critical periods. Additionally, some of these devices are equipped with wireless technology, enabling data transmission via email or real-time updates through a mobile application, enhancing the accessibility and management of project data.

3.3.2 Guidelines for soil reinforcement by rigid inclusions

In this study, we focus on the behaviour of rigid inclusions beneath a gravity foundation for supporting the latest generation of onshore wind turbines. The development of the rigid inclusion technique is grounded in a robust experimental foundation that encompasses physical modelling, laboratory tests, and real-scale instrumentation. The comprehensive instrumentation efforts undertaken prior to the publication of (ASIRI, 2013) are documented within this book. Drawing on insights from this project, along with the guidelines for ground improvement outlined by (Briançon, 2020), the instrumentation activities discussed in this chapter are currently being implemented.

This section does not outline a specific objective for overseeing soil reinforcement projects. Instead, its purpose is to shed light on the various tests and controls conducted during construction phases. Like any geotechnical work, this technique necessitates thorough construction supervision, control, and maintenance, all in alignment with the stipulations of Eurocode 7, Section 4.

Adhering to the tests and controls related to soil reinforcement during the execution phase is crucial for identifying key focus areas within the overall field instrumentation project for this technique. The tests outlined in (ASIRI, 2013) below detail the phenomena and physical parameters that should be considered, either wholly or partially:

- static load tests on an isolated inclusion, or on a group of inclusions,
- inspections of the integrity of inclusions shafts,
- execution controls,
- load transfer platform checks,
- controls of geotextiles or geogrids.

The objectives of the requirements outlined are to guarantee superior structural integrity in geotechnical project undertakings, encompassing both design and construction stages. Nonetheless, post-delivery, the measurement of physical quantities often becomes less frequent. To facilitate deeper analysis, there may be a need for more comprehensive, project-specific instrumentation that monitors soil reinforcement activities during construction and assesses the structure's serviceability thereafter. Field measurements enhance the comprehension of mechanisms occurring within and among the different components of the reinforced soil, ensuring the proposed design aligns with anticipated outcomes.

3.3.2.1 Measurement criteria

The formulation of this question might appear straightforward, yet its resolution can be complex. Instruments are specifically designed to measure one or more physical variables to facilitate the understanding of a particular phenomenon. Consequently, it is imperative to precisely identify this phenomenon and eliminate any extraneous influences that may obfuscate the results' interpretation. Occasionally, the variable of interest could also be geometric, such as boundary conditions. Specifically, within the realm of rigid inclusions, the selection of measurements, the types of sensors to be used, and the avoidance of confounding factors have been thoroughly delineated based on extensive research conducted in this field. Essential guidelines beneficial for the execution of instrumentation projects in this area have been established (ASIRI, 2013) and are expounded upon below and in the sections that follow. These guidelines are pertinent to a wide range of projects, including high embankments, railroad embankments, wastewater treatment plant reservoirs, industrial slabs, and gravity foundations.

The primary parameters to be measured during field monitoring are significantly influenced by the structural components of the project (including the substructure, foundation, and superstructure), the type of load, the project's initial concept, and the available budget. This is because the instrumentation system—comprising sensors, data acquisition units, materials, and the numerous on-site interventions—is typically costly. For soil reinforcement projects utilizing rigid inclusions, the measurement of certain critical variables is indispensable (ASIRI, 2013; Briançon, 2020), including:

1. Load transfer to the rigid inclusions.
2. Settlement of both the soil and rigid inclusions.

Additionally, other monitoring parameters may also be vital, with their relevance varying according to the type of structure and soil profile. These include:

3. Settlement across the soil profile.
4. Stress beneath the foundation.
5. Deformation of the Long-Term Performance (LTP) layer and gravity foundation.
6. Pore pressure within the soft soil layers.
7. Lateral displacements and inclination angles of the rigid inclusions at the structure's perimeter.

These variables collectively facilitate a deep understanding of a project geotechnical performance, ensuring the effectiveness of the design and the structural integrity. Additional measurements might also be relevant, including deformation along rigid inclusions and data from high-frequency sensors, particularly significant when inclusions are subject to cyclic dynamic loads. Discussions on these types of measurements appear at the end of the chapter, within the context of structural monitoring for onshore wind turbine foundations reinforced by rigid inclusions.

3.3.2.2 Measurement methodologies

Having identified the variables to be measured, the next question is which sensors provide the most accurate and reliable parameters and whether they are suitable for geotechnical applications. The state of the art in geotechnical instrumentation is becoming increasingly important, as reporting on the measurements, the challenges, and the success or failure of the instrumentation helps avoid many problems and questions on construction sites.

Regarding the settlement measurements, the type of sensors used must be adapted to the expected level, which is usually a low value in the soil reinforcement. The settlements can be measured along the vertical and/or horizontal profiles. A distinction can be made between punctual and vertical profile measurements. In the case of the former, it is usually used at the point of interest to validate one or more measurement points and get a millimetric precision. In the case of the vertical profile, it is a useful information to assess the settlements of one or more soil layers to globalize the behaviour of the soil under structural loading. An overview of these sensor types, which are suitable for the case of rigid inclusions under gravity foundations, are summarized in (Table 3.1).

Table 3.1: Real-scale Instrumentation of rigid inclusions in case of gravity foundation

Measurement type	Devices	Applications
Punctual	Hydraulic Transmitters	Briançon et al., (2015)
Vertical profile	Magnetic extensometer/multi-point extensometer	(Briançon et al., 2015)
Inclination	Inclinometer	Baroni et al., (2016); Pham et al., (2019); Bohn et al., (2022)

Regarding stress measurement, total stress cells, also known as Earth Pressure Cells (EPC), are commonly used for stress measurements in deep basements, diaphragm walls, and tunnels, especially where new construction activities may redistribute stress to existing structures. Such sensors are commonly used in soil reinforcement to measure load transfer from gravity foundations to rigid inclusions.

Regarding the deformation, strain is one of the most important variables in field monitoring. For an axial component, deformation is generally defined as the change in length of a component divided by the original length. However, in a field such as soil, the three orthogonal deformations and the corresponding shear deformations are also important. In all cases, knowledge of the deformation allows a transformation into load, pressure, strain, inclination or torque, depending on the geometric configuration of the deformation measurement. One of the most valuable and widely used sensors in all fields of geotechnical engineering is the Vibrating Wire Strain Gages (VWSG), as it is easy to install and has high accuracy and durability (Bordes and Debreuille, 1984; Simon et al., 2015). The use of such instruments is very reliable in pile construction (Bartz and Blatz, 2022), as these instruments are highly resistant to environmental effects and the transfer of loads from them in piles is very practical. Another tool for measuring strain is fibre optic sensors, which provide continuous, precise, and high accuracy in heterogeneous soil media (Kania et al., 2020) .An overview of the state of the art of this technology is given in the following section.

3.3.3 Optical fibre sensors

Distributed Fibre Optic Deformation Sensors (DFOS) offer new possibilities in geotechnical field instrumentation. By incorporating fibre optic technology within geotechnical structures, they enable the collection of precise, spatially detailed data. These sensors are characterized by their ease of installation and the flexibility to process data even before being deployed in the field. Conceptually, DFOS can be likened to embedding thousands of strain gauges within a single cable, elevating monitoring capabilities to a new level. Their design allows for installation in challenging and confined spaces that are inaccessible to traditional sensors. Moreover, DFOS enhance the longevity of structures by offering efficient early warnings for potential geotechnical instabilities.

The fundamental principle of optical fibre involves transmitting a signal, represented by light, from its source to the endpoint and back. Optical fibres are distinguished by their capacity to carry a significantly larger amount of information across vast distances within remarkably short durations, outperforming other sensor types (Awad, 2001). Essentially, optical fibres operate on the principles of light physics. Light is known to travel in free space at a velocity of approximately $c = 3.10^8 \mathrm{m}/s$. As it propagates and encounters different media with different densities and refractive indices, it is reflected or refracted, in whole or in part, within a certain ratio between the two phenomena. The propagation of light within an optical fibre is primarily directed by total internal reflection, a process facilitated by the carefully layered materials composing the optical fibre cable (Figure 3-1). Furthermore, it is crucial to acknowledge the scattering phenomena that occur when a light pulse interacts with the medium's particles and acoustic waves. The scattered light traveling in the opposite direction of the initial propagation (towards the source) is termed "backscattering," a phenomenon that plays a critical role in various applications, notably in fibre optic sensing.

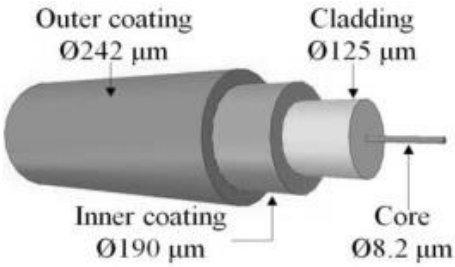

Figure 3-1: Illustration of a single-mode glass fibre coated with a two-layer polymer coating (Tan et al., 2021).

Fiber optic sensing technology has its roots in the advancements of fibre optic technology, becoming increasingly prominent in the instrumentation field due to its capability to measure variables such as strain, temperature, pressure, and more. This is achieved by modulating the light's intensity, phase, polarization, wavelength, or propagation time within the fibre sensors, coupled with signal processing techniques tailored to the specific technology applied. In the evolution of fibre optic sensing, a variety of sensors were developed (Culshaw, 2000) prior to the advent of distributed sensing technology, also known as DFOS. This technology capitalizes on backscattering and the modulation of backscattered radiation, which is initiated by a forward-directed optical beam, typically for detecting temperature or strain fields. Three primary backscattering processes are employed (Figure 3-2):

1. Rayleigh scattering: This generates the strongest signal among the three methods, although the returned intensity merely reflects the intensity that reached the scattering point. Consequently, systems relying on Rayleigh backscatter need to modulate this intensity through an additional mechanism.
2. Brillouin scattering: This method produces an offset frequency spectrum that correlates directly with the acoustic phonon spectrum within the fibre, offering insights into various physical conditions.
3. Raman scattering: This approach samples the optical phonon spectrum, which can distinctly measure the temperature at the scattering point.

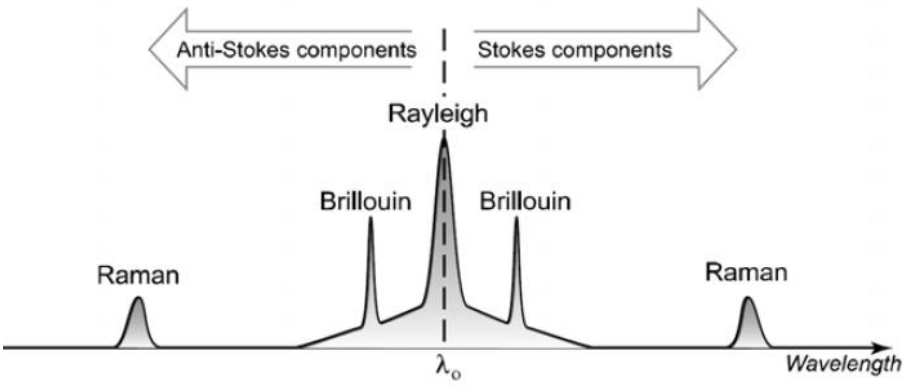

Figure 3-2: Raman, Brillouin and Rayleigh scattering in the optical fibres (Thévenaz and Niklès, 2007).

DFOS measurements consist of the measurement of physical variables by a large number of gauges continuously aligned along a fibre. We can imagine that the functionality consists in determining the distance travelled by the light in the fibre at time "t" to the measurement point by one of the backscattering techniques. Thanks to these distance measurements, the spatial

distribution is reconstructed for the physical quantity to be measured. In practise, there are two different methods for measuring distance in an optical fibre: Optical Time Domain Reflectometry "OTDR" (Barnoski and Jensen, 1976) and Optical Frequency Domain Reflectometry (OFDR). In OTDR, light pulses are repeatedly injected into the optical fibre. Each of these light pulses is reflected from the internal defects of the fibre structure. The pulse and the backscattered light are attenuated. Thus, it is possible to determine both the distance travelled in the optics and the actual measurement by time domain analysis. In OFDR (Eickhoff and Ulrich, 1981), the system is divided into two subclasses: coherent and incoherent. Most OFDR systems based on Rayleigh scattering are classified as coherent OFDR, while incoherent OFDR is mainly used for systems based on Raman or Brillouin scattering (Khadour and Waeytens, 2018). In the coherent OFDR method, a linear, frequency-modulated light pulse is transmitted into the fibre. This method requires a tuneable laser on as wide a band as possible that is free of mode hopping. The wave emitted by the laser is split into a reference signal and another measurement signal, which is injected into the fibre under test. Then the signals are mixed in a coupler and the interference signal is detected. The OFDR technology has significantly higher spatial resolution and exponentially more measurement points than OTDR technology (Bao et al., 2014). The combination of high spatial resolution, fast update rate, additional number of sensors, and complete distribution distinguishes OFDR technology as the most sophisticated technology on the market.

In addition to the DFOS, there is another technique in fibre optic sensing that is related to the single measurement sensor. It consists of returning the strain value at a fibre section with a measurement length that can vary from a few millimetres to several tens of meters, depending on the technology used. Multiplexing several individual measurement sensors results in quasi-distributed sensors. Most fibre optic sensors for single measurements are based on fibre Bragg grating and interferometry (Iten, 2012). A table of comparison (Table 3.2) rewritten after (Boldyreva, 2016), showed the different measurements techniques.

To narrow down the fibre optic sensing technique, the advancement of this technique leads to a variety of measurement techniques, the most important of which are listed in Table 3.2. The application of OFDR Brillouin OTDR is very extensive and touches all geotechnical fields: gravity foundations, pile foundations, ground improvements, tunnels, pipes and wind turbines. Field instrumentation with fibre optic sensors has recently developed very intensively. Here are some research papers that refer to the state of the art and summarise the cited applications of fibre optic technology (Iten, 2012; Kechavarzi et al., 2015; Caponero, 2020; Bado and Casas, 2021).

Table 3.2: Performance comparison of different fibre optic sensing techniques.

Parameter	Raman OTDR	Brillouin OTDR	Rayleigh OFDR	Bragg grating
Range	1-30 km	100 km	100 m	100 Channels
Spatial resolution	1 cm-17 m	1 m	1 mm	10 cm
Temperature resolution	0.1^0C	1^0C	0.1^0C	0.01^0C
Deformation resolution	-	10 $\mu m/m$	1 $\mu m/m$	0.1 $\mu m/m$

Rayleigh OTDR sensor technology is relatively new to the market compared to Brillouin OTDR, but is used for numerous geotechnical monitoring applications. In this work, we address

this technology for measuring rigid inclusions and gravity foundations. One of the applications of this technology is field instrumentation of ground improvements with the installation of fibre optic cables to measure the deformation of geosynthetics in soil reinforcement by rigid inclusions under embankment (Briançon and Simon, 2011, 2017). DFOS technology is widely used in pile foundations nowadays because it allows continuous measurement of the pile profile and provides an actual strain profile of the pile, which is not possible with conventional monitoring instruments, even when multiple instruments are installed in the instrumented piles (Figure 3-3). The strain profile is created by connecting the measurement points (Sienko et al., 2019).

One of the reference works that interested us, since it uses the same DFOS technology, is the research work of Kania et al., (2020), which uses OFDR DOFS to monitor the strains and temperature inside different steel piles and CFA piles subjected to a static load test. The authors provide some recommendations for installation to ensure correct measurement and to facilitate post-treatment data. Moreover, the instrumentation of several concrete piles of a realistic tour is performed with the same technology and the measured strain profiles are compared with numerical models (Milane, 2021).

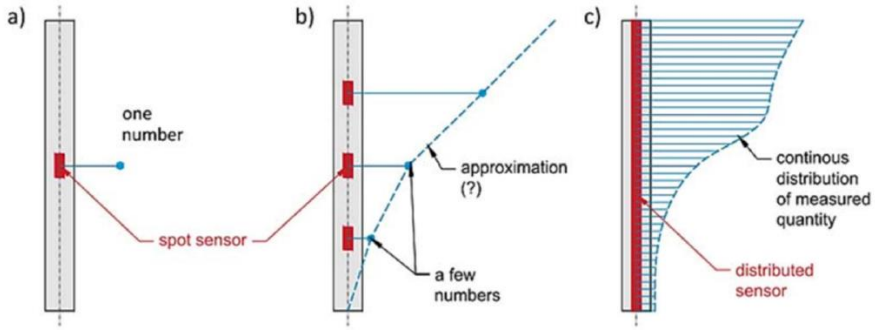

Figure 3-3: Measurement schemes for concrete piles: (a) punctual, (b) quasi-continuous, (c) distributed (Sienko et al., 2019).

3.4 Monitoring background

Onshore wind turbines are comprehensively monitored through an integrated system known as SCADA, aimed at facilitating control, assessing performance, and guiding maintenance activities based on actual data. Contemporary wind turbines (WTs) typically log over 200 variables at frequencies ranging from every 1 to 10 minutes via their SCADA systems (Blanco et al., 2018). Recorded data encompass a wide array of parameters including temperature, air density, acceleration, rotor speed, wind speed and direction, nacelle orientation, blade pitch angles, energy output, among others. Several of these parameters prove crucial within the framework of structural health monitoring systems. Various methods and algorithms exist for the meaningful interpretation of these data in design analysis (Yang et al., 2013). Nonetheless, information garnered from the SCADA system does not pertain to the turbine's foundation or the underlying soil.

Geotechnical and structural field monitoring of onshore wind turbine foundations remains relatively nascent, especially when compared to their offshore counterparts, largely because

incidents of failure attributable to soil-structure interaction are comparatively rare for onshore wind turbines.

In this section (Table 3.3) outlines selected research focusing on the geotechnical/structural dynamics of foundations. These studies primarily investigate the fatigue behaviour of concrete foundations subjected to fluctuating wind loads, along with degradation and cracking at the junction with the wind turbine shaft. A notable study listed in (Table 3.3) examined soil stress and settlement beneath gravity foundations, showcasing how these metrics evolve throughout construction and beyond the turbine commissioning. These observations highlight the foundation rigidity and the resultant soil-structure interaction. Conversely, an analysis integrating these measurements with data on wind direction and speed across the turbine operational lifespan is not extensively covered in the literature.

Table 3.3: Synthesis of field-monitoring of OWT

References	Wind turbine	Monitored components	Sensors	Motivation	Major results
Hassine, (2011)	1.5 MW turbine & 2.3 MW	- Concrete foundation	- EPC at the base of the foundation - strain gauges on the foundation rebars, - load cells at the anchor bolts	Load and Fatigue in onshore concrete foundation	- Highlighting the crucial importance of the pedestal reinforcement against the wind load - Estimation of the rotational stiffness of the OWT foundation
Currie et al. (2015)	2.0 MW turbine	- Embedded ring concrete foundation	- LVDT Displacement sensors	Damage around the bottom flange of the embedded ring	- Validation of a developed low-cost wireless structural integrity monitoring for the SHM in embedded ring concrete foundation
He et al. (2019)	1.5 MW turbine	- Embedded ring concrete foundation	- Vibrating wire sensor - Strain gauge	Damage around the bottom flange of the embedded ring	- Relating the degradation of concrete in the measured areas to the effect of repeated loads. - Load identifications (Moments and shear forces) through the strain measurements - SHM for embedded ring concrete foundation
Perry et al. (2017)	80 m tour height	- Octagonal gravity foundation (external) - Turbine tower	- Fibre Bragg gratings inside the tower and at the concrete face of the foundation	Cracked wind turbine foundations	- The foundation crack opening displacements respond linearly to tower strain and do not change by more than ±5 µm.

					- Lateral crack displacements were found to be negligible
Rubert et al. (2017)	–	- Gravity foundation (reinforcement bars) - Turbine tower	- Fibre Bragg gratings at the steel reinforcement (Radial and vertical) and at the turbine tower	Foundation steel reinforcement strain	- Measurements of foundation strains did not exceed 95 με and showed a strong correlation with measured tower displacements.
Yilmaz et al. (2022)	-	- Gravity foundation - Soil profile	- Deformation meter (strain gauge) below the foundation - EPC at the base of the foundation	Monitor pressure and deformation responses of lean clay foundation soils	- Fluctuations in pressure and deformation in the foundation and in the soil based on their positions due to the wind direction. - The strain due to the wind load is dissipated at 1.7 m depth below the foundation.

Regarding real-scale monitoring of a wind turbine foundation supported by rigid inclusions, a study on an OWT gravity foundation on rigid inclusions was carried out at a site in France from 2009 to 2012, spanning the turbine construction and service life (Haza Rozier et al., 2012). The wind turbine shaft extends 78 m in height, and the foundation diameter measures 16.7 m. The 84 rigid inclusions of CMC type, installed by Menard Company, match the CMCs instrumented in this project. The compressible soil beneath the foundation is identified as silt and compact clay. Two levels of measuring devices were installed under the wind turbine foundation to monitor load transfer and foundation settlement (Table 3.4). A critical outcome of this instrumentation was the observation of minimal foundation settlements due to the rigid inclusions, with settlements of 1 cm noted post-construction, remaining unchanged throughout three years of monitoring. However, significant stress variations were recorded at the rigid inclusions head due to loading from the wind turbine. Notably, the deformation of the rigid inclusions could not be determined as the measurements from the VWSG were not traceable.

Table 3.4: Sensors configuration (Haza Rozier et al., 2012)

Below the gravity foundation		**At the head level of the RIs**	
Sensors	Specifications	Sensors	Specifications
8 EPC	Selected positions	14 EPC	Equivalent diameter of the RIs, selected RIs
11 Transmitters	Selected positions	8 Transmitters	On the soil between the instrumented RIs
		2 VWSG	Inside one RI

As for field monitoring of rigid inclusions, various projects have been conducted around the globe for different applications of RIs. In (ASIRI+, 2018), 24 studies were reported in which field monitoring of rigid inclusions took place. Most of these projects focused on the embankment rather than gravity foundations, in part because embankment projects are typically associated with relative megaprojects, so there is a real scientific motivation for instrumentation and publication of results. The following references include instrumented real-scale projects of rigid inclusions using concrete slabs as foundations (Briançon et al., 2015; Umur Salih Okyay and Briançon, 2012) and gravity foundations (Baroni et al., 2016; Bohn et al., 2022). However, it is interesting to note that physical modelling occupies an important part of the research in this field, as shown by the following works (ASIRI+, 2018; Rivera Rojas, 2019).

3.5 Monitored wind turbine foundation

3.5.1 Case study: Wind turbine E6 at Ecoust Saint-Mein

The foundation of a wind turbine built on soil reinforced by rigid inclusions has been instrumented and the installation of sensors took place from September to October 2019. The instrumented N117/3600 wind turbine, built by NORDEX & ACCIONA (Table 3.5), was erected in the park of Ecoust-St-Mein, northern France. The features of the gravity foundation designed by CTE WIND are shown in the (Figure 3-4). The installed RIs are of the CMC type, drilled with soil displacement, designed and constructed by Menard according to Class 3 Category 7 as defined in

Annex A of standard (NF P94-262, 2012). The number of rigid inclusions with a diameter of 360 mm and an average depth of 10 m executed under the gravity foundation is 64.

Table 3.5: OWT N117/3600 (Nordex & Acciona)

Nominal power	3.6 MW
Cut-in wind speed	3.0 m/s
Cut-out wind speed	25 m/s
Rotor Diameter	116.8 m
Operation range rotational speed	7.9 -14.1 rpm
Shaft height	91 m
Total height	117 m

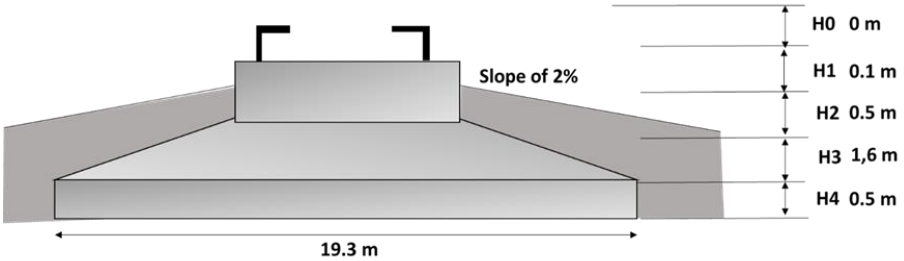

Figure 3-4: Gravity foundation of "E6".

The gravity foundation is supported by rigid inclusions, type CMC. The base of the concrete foundation is situated 1.7 meters below the surface, with the foundation's depth reaching approximately 2.7 meters. Beneath the base of the concrete foundation lies a 10-centimeter-thick layer of lean concrete, followed by an 80-centimeter-thick Load Transfer Platform (LTP). The upper boundary of the CMCs aligns with the bottom of the LTP layer. The arrangement of the CMCs beneath the gravity foundation is illustrated in (Figure 3-5). The load-bearing area allocated to each CMC, based on their placement within specified radii beneath the circular footing, is determined by the results of the design analysis.

The geotechnical conditions of the site at the preliminary design phase are defined as follows:

Table 3.6: Preliminary geotechnical design parameters

Soil type	Top Level [m]	Bottom Level [m]	Pressuremeter Moduls (MPa)	Unit Weight (kN/m^3)	Lateral Skin Friction (kPa)
Load Transfer Platform	-1.8	-2.6	12.5	19	-
Loose Silt	-2.6	-4.5	8	18	65
Compact Clayey Silt	-4.5	-10	16	18	78
Compact Horizon	-10	-23	22	18	114
Intact Chalk	-23	Deep Layer	940	19	170
CMC	-2.6	-11	-	22	-

Radius	Number of CMCs
8.8	25
7	19
5	13
2.5	6
0	1

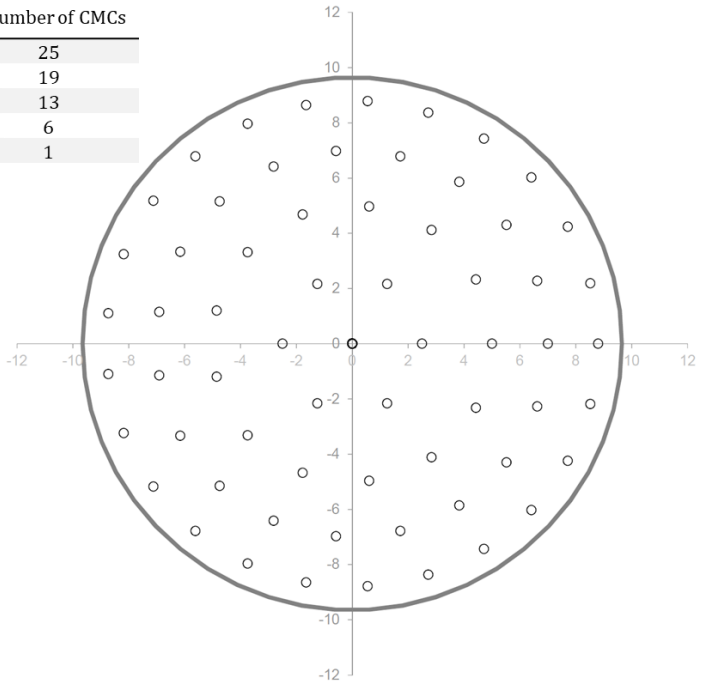

Figure 3-5: CMC Layout.

3.5.1.1 Objective of the instrumentation

The purpose of the instrumentation set up is, on the one hand, to follow the load transfer and settlements in the reinforced soil and, on the other hand, to understand the behaviour of the foundation. Thus, two different measuring devices have been used:

- the first consists in following the load transfer in the foundation of the wind turbine,
- the second consists in measuring the load transfer in the soil reinforced by rigid inclusions and its settlements.

In this dissertation, only the sensors at the soil reinforcement level are presented. The sensors within the gravity foundation are cited in Modu(2022).

3.5.1.2 Instrumentation at the RIs level

Several sensors were installed at the rigid inclusion level (Figure 3-6):

- EPC, located on the top of the inclusions (measuring the total vertical stress),
- Settlement sensors (to measure the differential settlements between the soil and the inclusions),
- DFOS placed within selected inclusions (deformation measurements),
- a downhole inclinometer oriented against the prevailing wind direction.

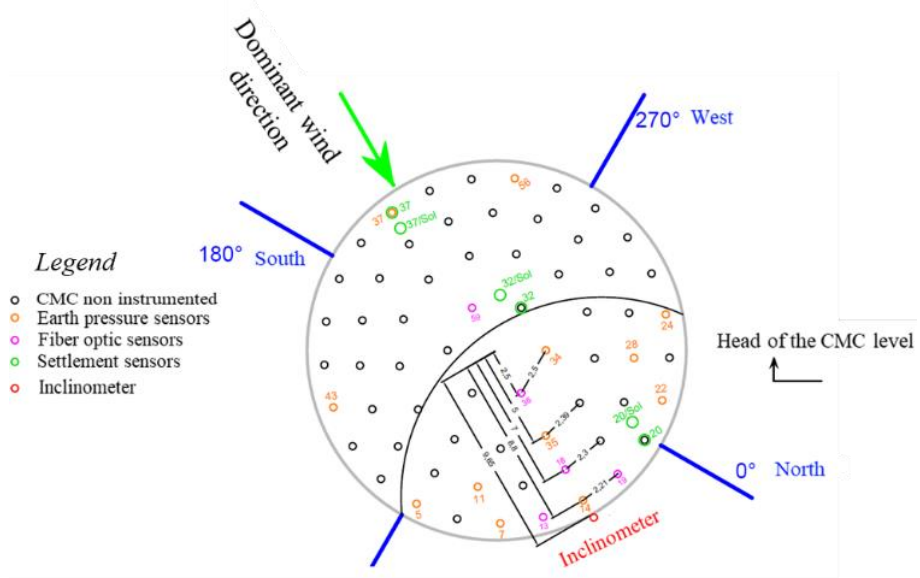

Figure 3-6: Top view of the positions of the sensors at the level of the head of the rigid inclusions.

3.5.1.2.1 Stress measurement

A total of 12 sensors were installed at the heads of the rigid inclusions, which have the same cross-section as the columns to perfectly cover the load transfer to the RIs. EPC with a pressure range of 50 bars are used (manufactured by GLOTZL). Each sensor is positioned horizontally at its location on a sand bed and then covered with sand. The electrical cables are laid in trenches, routed through the cover, and connected to the acquisition device (Figure 3-7). The sensors are particularly concentrated on the inclusions of the zone that are most exposed against the prevailing wind direction (Figure 3-6).

(a) (b)

Figure 3-7: (a) EPC installed at the top of the RIs with an equivalent diameter, (b) wiring to the acquisition units.

3.5.1.2.2 Soil/IR differential settlement measurement

Soil settlement is measured with 6 hydraulic transmitters with a range of 0.1 bar (manufactured by SISGEO), connected in series, first via a hydraulic line to a tank filled with antifreeze mounted on a bracket outside the structure's right-of-way, and second via an electrical line to the

acquisition device (Figure 3-8). The transmitter measures the pressure variations between its position and the level of the tank. Each transmitter is connected to the atmospheric pressure through a capillary connected to the electrical cable. Three zones were targeted to measure the different soil/inclusion settlements (Figure 3-6).

(a) (b)

Figure 3-8: (a) Hydraulic transmitters installed at level of the RI, (b) wiring to the acquisition units.

3.5.1.3 Instrumentation at the load transfer platform level

Several sensors were installed on the load transfer platform:

- EPC mounted on the top of the LTP (measuring the total vertical stress),
- Settlement sensors located on the top of the LTP (differential settlements soil/inclusion).

3.5.1.3.1 Stress measurement

A total of 6 sensors were installed on the load transfer platform (Figure 3-9). These sensors were installed in an overlay above the LTP with respect to the instrumented inclusions below the LTP with a range of 10 bars. The same installation protocol as the first EPC in Section 3.5.1.2.1 is followed here. The sensors are also heavily distributed in the zone, which is considered to be highly condensed due to the theoretical prevailing wind direction. In particular, the sensors are located at the inclusions of the most heavily loaded zone.

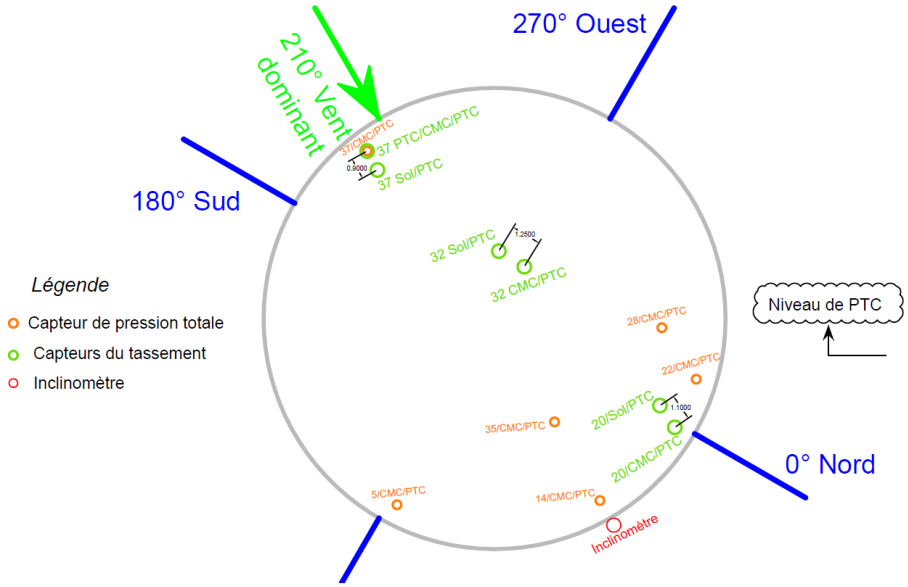

Figure 3-9: Top view of the positions of the sensors above the LTP.

3.5.1.3.2 Soil/IR differential settlement measurement

The settlement sensors installed on LTP (Figure 3-9) to measure the settlement of the gravity foundation are in the same type and number of the sensors installed in the previous section.

3.5.1.4 Deformation measurements of rigid inclusions using DFOS

Five optical fibres were inserted into rigid inclusions to measure their deformation (Figure 3-6). The setup, tested for the first time at the instrumented wind turbine site, was also the first time DFOS was used in unreinforced RIs. The optical fibres were attached to a series of metal rods, each 1 m long. Each time the metal roads are injected into the freshly poured concrete, the optical fibre cable is attached to the next row of metal tubes until the systems in the centre of each instrumented RI are fully penetrated (Figure 3-10).

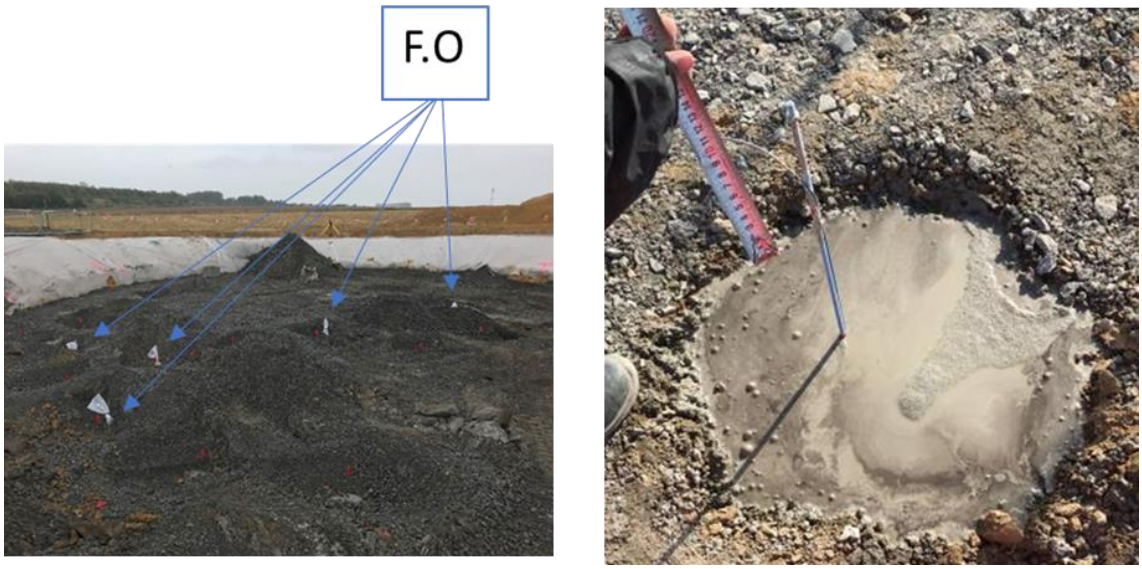

(a) (b)

Figure 3-10: (a) DFOS placed in fresh concrete, (b) preparation of LTP platform for DFOS (installed in selected RIs) cabling outside foundation area.

Optical fibres with Rayleigh backscatter technology using an optical setup based on OFDR technology is used to measure the strain of the RI. The optical interrogator allows distributed measurements of deformation and temperature along a simple optical fibre. The latter can be bonded to or even embedded in the structure, for example in concrete or composites, with thousands of measurement points, with centimetric or even millimetric resolution and over very long distances.

3.5.1.5 Measurement of horizontal displacement

The inclinometer tube was installed in a 15 m deep borehole in accordance with standard (EN ISO 19674-3, 2017)(Figure 3-11). These provisions are supplemented as follows:

- The main direction is parallel to the axis of horizontal force application,
- the drilling is carried out under the cover of a protective casing,
- the equipment is then lowered under the protection of the casing to reach its theoretical height,
- the equipment is sealed along its entire length between the bottom of the borehole and the planned level of earthworks by grouting from the bottom of the borehole while the temporary casing is raised,
- the tube is extended during backfilling.

Figure 3-11: Position of the inclinometer.

3.5.2 Monitoring in static and dynamic conditions

The physical variables measured during geotechnical monitoring can be analysed in both domains - static and dynamic. In the static domain, the measurements can determine the effects of the vertical load, i.e., the self-weight of the structure, and the overturning moments resulting from the wind load acting on the structure. The fact that the wind is a dynamic variable leads to a cyclic effect in the operation of the wind turbine, which generates rocking motions on the structure. The resulting measurements in the dynamic domain could evaluate the "real" loading rate acting on the foundation and consequently on the rigid inclusions represented in the dynamic variation of stress and settlements synchronized with the load and its frequency, which in turn could be useful to identify the cyclic loading and therefore its effects on the structural and geotechnical components and the stiffness of the system (wind turbine-foundation-reinforced soil). The identification of the dynamic/cyclic loading during the variation of the mean wind speed and wind fluctuations is interesting to evaluate the effects of wind loading and wind turbine rotation on the soil during the measurements and during the modelling and small laboratory by simulating the same site conditions.

3.5.2.1 Frequencies measurement at the base of the WT

The measurement of the frequencies at the base of the shaft is one of the variables that allow to measure the loading rate acting on the gravity foundation, coming from the wind load and the rotation of the turbine rotor. For this purpose, a triaxial capacitive accelerometer (manufactured by SDI) with an input range of +/- 2g is used, located at the bottom of the shaft WT (Figure 3-12). The sensor is capable of detecting low frequencies with high resolution in a range (0 to 250 HZ) that is close to the expected natural and exit frequencies of an OWT.

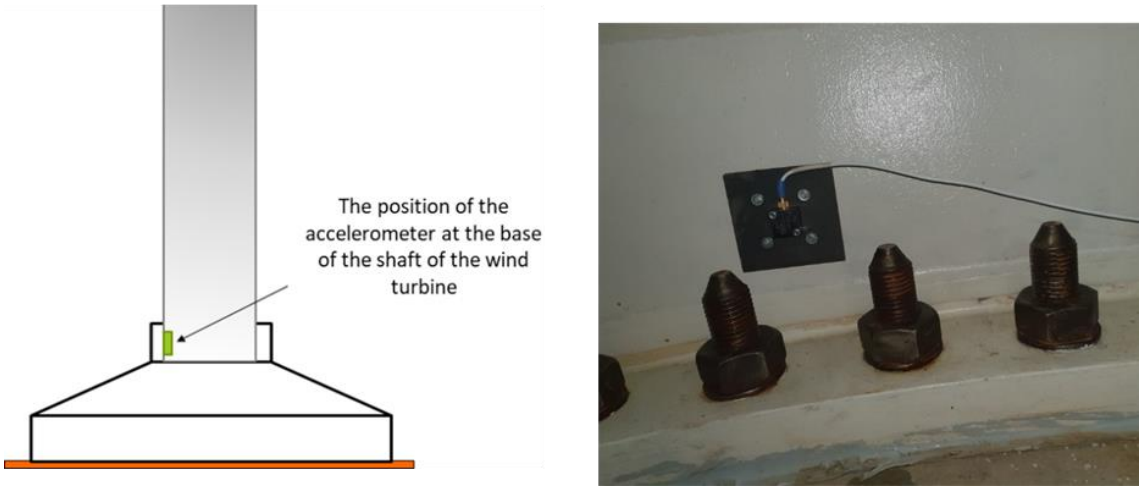

(a) (b)

Figure 3-12: (a) Position of the accelerometer, (b) Installed sensor at the base of the WT.

3.5.2.2 Diverse instruments

In addition to the embedded sensors in the system, this work used an external sensor to monitor the dynamic aspect of the wind turbine. With these instruments, a test campaign was carried out in which we tried to synchronise all possible dynamic measurements, such as: the fibre optics in the RIs, the EPC with a very high acquisition rate, and the accelerometers. In parallel, a radar interferometry was installed to monitor the turbine and geophones on the gravity foundation and the ground next to it.

The interferometry radar is of the IBIS FS type (Figure 3-13 (a)) and allows the simultaneous measurement of the displacement of several points in real time with an accuracy of 1/100 mm and the derivation of the vibration frequencies of structures up to 200 Hz.

Another type of external instrumentation used in the field was several geophones placed on the foundation of the wind turbine (Figure 3-13(b)) to dynamically characterize the substructure and superstructure. For this purpose, three velocimeters were integrated, covering a range from low vibrations ± 0.5 mm/s to high vibrations ± 5 cm/s, and also equipped with three accelerometers allowing operational registration of frequencies between 0.1 Hz and 1024 Hz.

(a) (b)

Figure 3-13: (a) The interferometry radar, (b) The geophone instruments.

3.5.3 Synthesis of the installed instruments

In summary, two levels of sensors were installed in the geotechnical part of the structure (the hidden part) at the pile head level and under the gravity foundation, at the top of the LTP (Figure 3-14). The total number of sensors installed in this area is summarized in the following (Table 3.7), indicating the number of sensors still working after the construction phase and until today, and the number of damaged sensors.

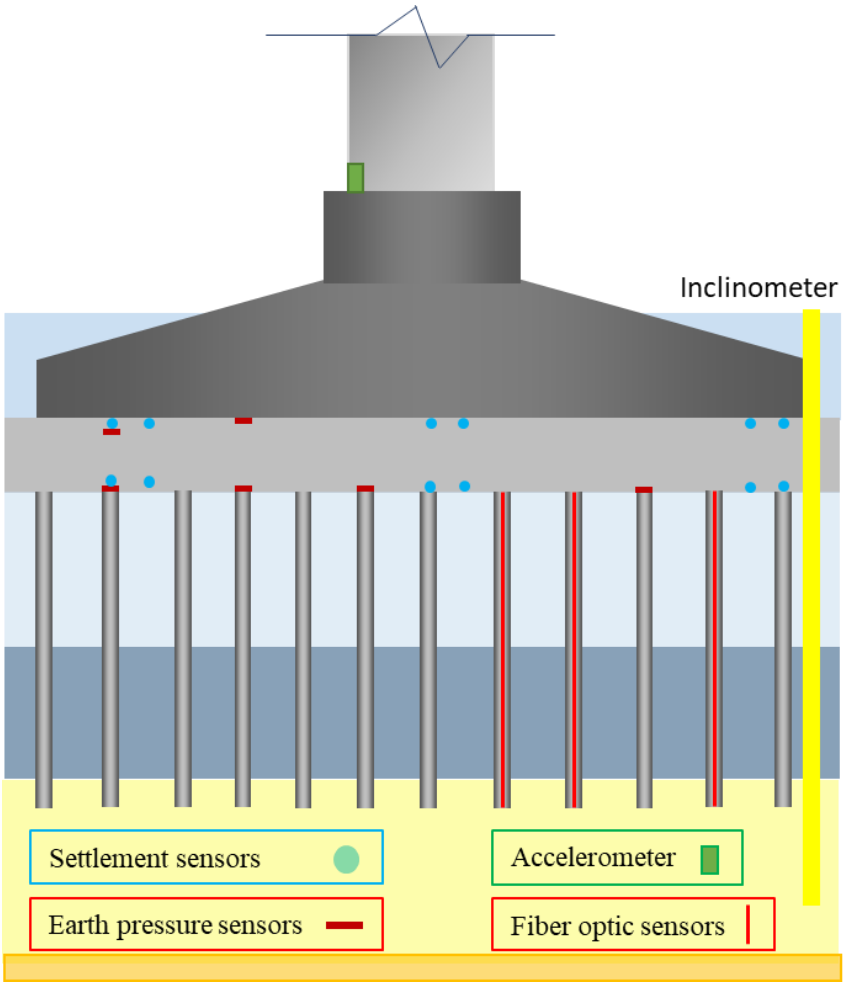

Figure 3-14: Elevation section showing the positions of the instruments used in this study.

Table 3.7: Installed sensors

Installed sensors	Functional sensors
18 (Earth Pressure Sensors)	16, continuous measurements
12 (Hydraulic Settlement Sensors)	10, erroneous measurements
2 Accelerometers	2, punctual measurements
20 (Vibrating Wire Strain Gages)	19, continuous measurements
13 (Fibre Optics)	9, punctual measurements

3.5.4 Acquisition devices

On the one hand, acquisition devices should be adapted to the way sensors are used to collect data. On the other hand, the selection of acquisition devices must be optimized to achieve the desired sampling rate, especially when many sensors are connected to the acquisition devices and a very high sampling rate is required for modal analysis. Nowadays, many types of acquisition devices can interrogate numerous types of sensors and adding conditioners could make some originally incompatible sensors compatible again. In this work, automatic data loggers were used for the installed sensors (Table 3.8), except for the inclinometer, which was measured manually with the inclinometer probe.

Table 3.8: Data acquisition devices

Data logger	Sensors type
DataTaker DT85GM	EPC, hydraulic transmitters.
SdiLogger	Accelerometer
LUNA ODiSI 6100	Optical fibres

The DataTaker is a well-known device for measuring a variety of sensors, such as all electrical sensors and, in the model used, a variety of geotechnical sensors, such as VWSG and other geotechnical sensors. The instrument has an integrated programming language that provides a user-friendly interface and allows programming of all available sensors for its 16 analogue channels. It also has an integrated cellular modem that allows automatic transmission of data. A DataTaker central unit is installed and, in conjunction with three modules (extensions), allows the connection of 73 sensors. The acquisition unit is a sensitive element of the monitoring equipment and must be installed in a cabinet that protects it from environmental influences. In this project, the equipment was installed in a base with a diameter of 1 m, a few decimeters from the edge of the foundation, with all the cables of the sensors embedded under the foundation exiting at this point (Figure 3-15).

The DFOS used in this work, based on OFDR Rayleigh scattering technology, could be interrogated by several optical acquisition systems already on the market, such as the OdiSi B, OBR 4600, and OdiSi 6100. The latter was used for the monitoring work (Figure 3-16) as it offers the possibility to monitor up to 100 m DFOS with an accuracy up to 1με, a measurement up to 0.65 mm and a sampling rate up to 250 HZ. This OdiSi system is characterized by its advanced programming software, which offers the possibility of streaming and visualizing data in real time, as well as the possibility of localizing the measurement, which was very useful in our case, since the optical fibres installed in the RIs, which have an average length of 10 m, were extended by an average of 25 m to leave the cable in an area accessible for the measurements.

The power supply of the monitoring data loggers must be sized according to the power requirements, depending on the number of sensors and their type. The data logger devices installed in the concrete base (Figure 3-15) are powered by direct energy from the wind turbine. Measurements with the OdiSi 6100 were taken on time every time a test campaign was programmed on the site, on average 6 times per year. These devices were also powered by the energy generated by the wind turbine or by a private portable power supply.

(a) (b)

Figure 3-15: (a) The wiring of the embedded sensors towards the concrete base, (b) the two extensions of the DataTaker installed in the base.

(a) (b)

Figure 3-16: (a) an example of a measurement campaign, (b) the DFOS monitoring data in real time.

3.5.5 Measurements

3.5.5.1 EPC at the level of RIs

Measurements began since the installation of the sensors, before the construction of the gravity foundation, to follow the evolution of the stress measurements. Unfortunately, a technical error in the power supply to the sensors rendered the EPC measurements unusable during all phases of construction. The correction was made when installation of the WT began, not before because of the COVID pandemic. The EPC measurements at the top of the RIs shown in (Figure 3-17) represent the measurement after the wind turbine was built at a wind speed of less than 3m/s. Some discrepancies were noted between the measured total vertical stresses for the instrumented CMCs before the wind turbine was placed in service. These discrepancies decreased after the wind turbine was commissioned and measurements were taken while the machine was running in OFF mode and at low wind speed through selected events in 2020 and 2021 (Figure 3-17). In addition to the differences in the stress at the head of the RIs seen in the following two figures, the measurements of the neighbouring RIs are redundant (Figure 3-18).

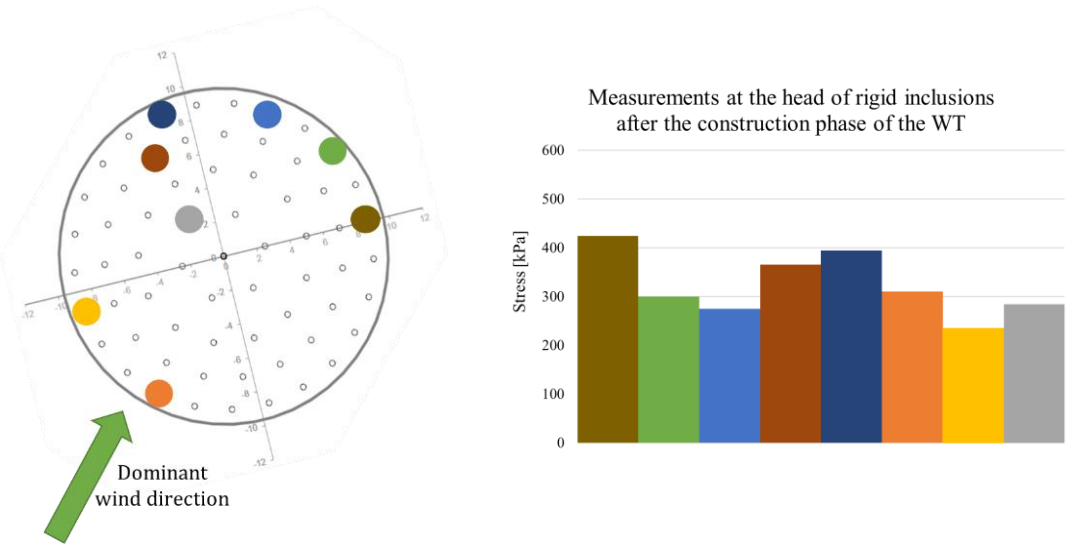

(a) (b)

Figure 3-17: (a) Positions of the RIs, (b) Total vertical stress.

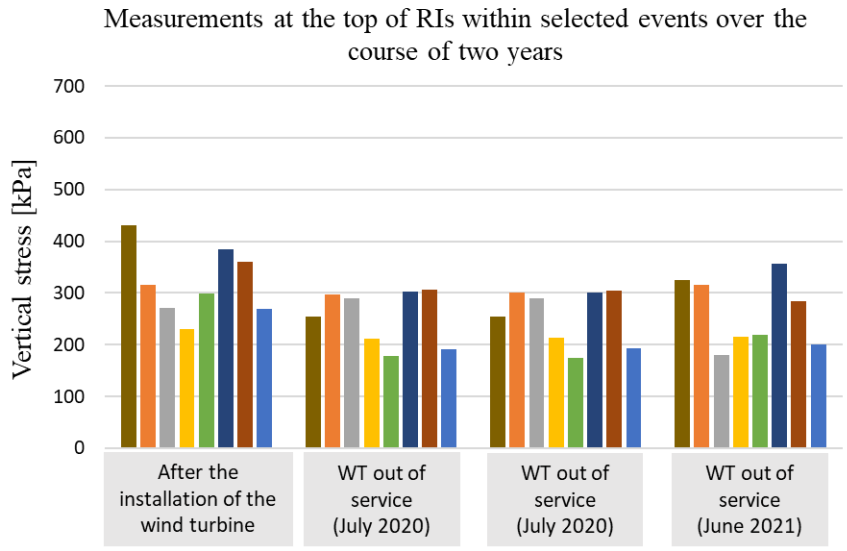

Figure 3-18: Comparison of the stress measurement at the top of RIs estimated in the static domain (without wind influence and without rotational motion).

In addition to the stress measurements outlined previously, the diagrams provided next illustrate readings from two sensors positioned diametrically opposite each other "24" and "43" (Figure 3-19). The reason for highlighting these particular measurements lies in their consistently higher readings across all events monitored, in terms of both absolute stress levels and variability, compared to the readings from other sensors. This focus helps our understanding of the overall stress distribution, offering insights into the average stress levels depicted in the diagrams. Notably, when the wind turbine is inactive, the stress measurements from all sensors tend to align closely (Figure 3-20). This uniformity contrasts with the operational state of the wind turbine, during which the behaviour of sensors "24" and "43" significantly diverges from the rest but following the same global trend (Figure 3-21).

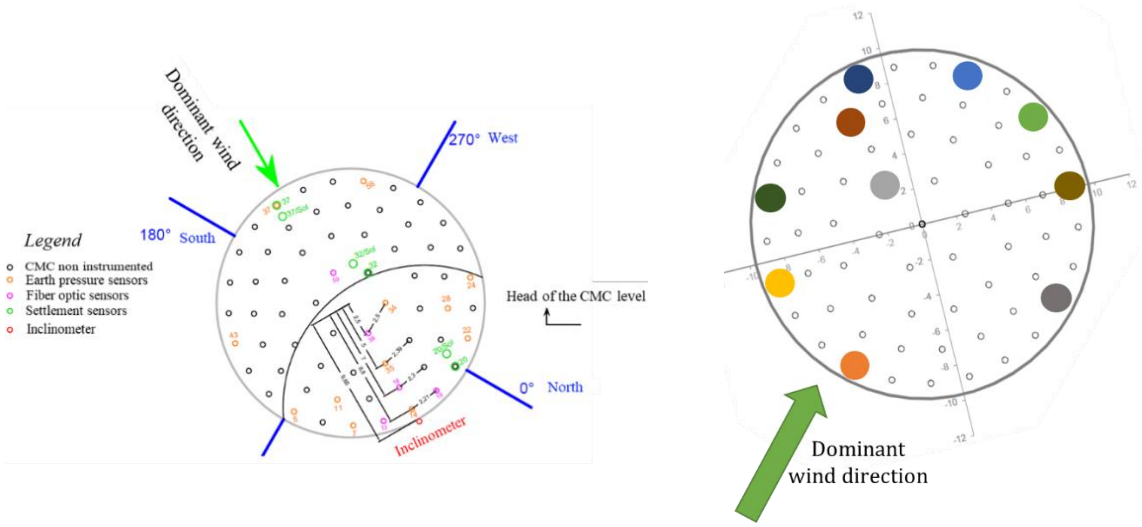

(a) (b)

Figure 3-19: (a) Numbers of the instrumented RIs, (b) Colour code for the instrumented RIs.

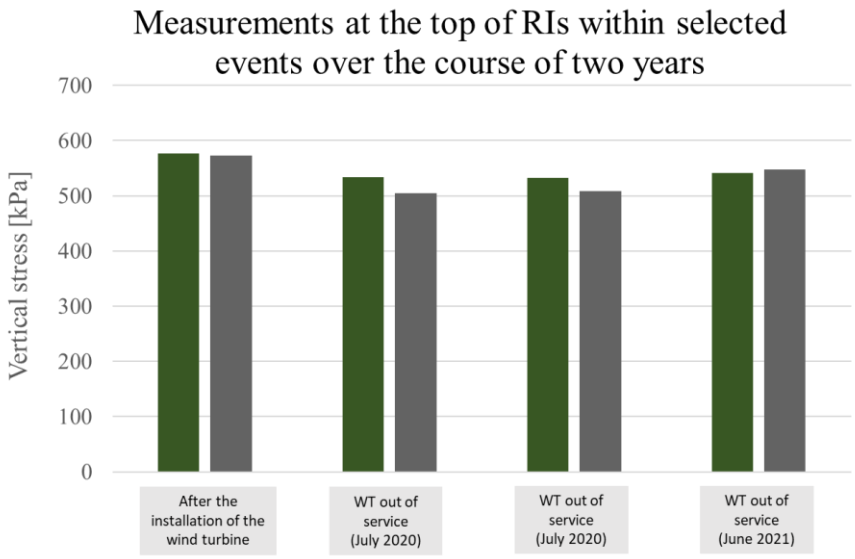

Figure 3-20: Increased values of two EPC for diametrically opposed RIs (43 & 24).

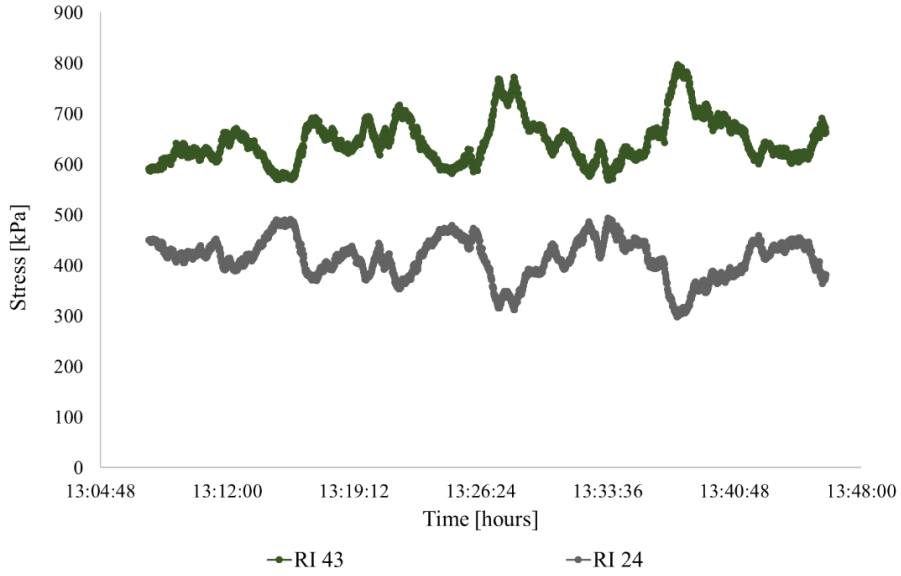

Figure 3-21: Behaviour of rigid inclusions (43 & 24).

After the first official start-up of the wind turbine on June 17, 2020, the measurements are directly disturbed, as we can see from (Figure 3-22). Using the examples of RI "37" and RI "14", we can visually observe that they are subject to a perfect inverse behaviour. Their positions show that they are diametrically opposed under the foundation of the wind turbine (Figure 3-19). The first interpretation shows that the wind direction during the period in question was opposite to the theoretically prevailing wind direction. When RI "37" reached its highest stress level, the wind came from the northeast, while RI "14" reached its highest value from the southwest. This measurement reflects the hypothesis of a trapezoidal stress distribution under the wind turbine foundation when its surface is 100% compressed.

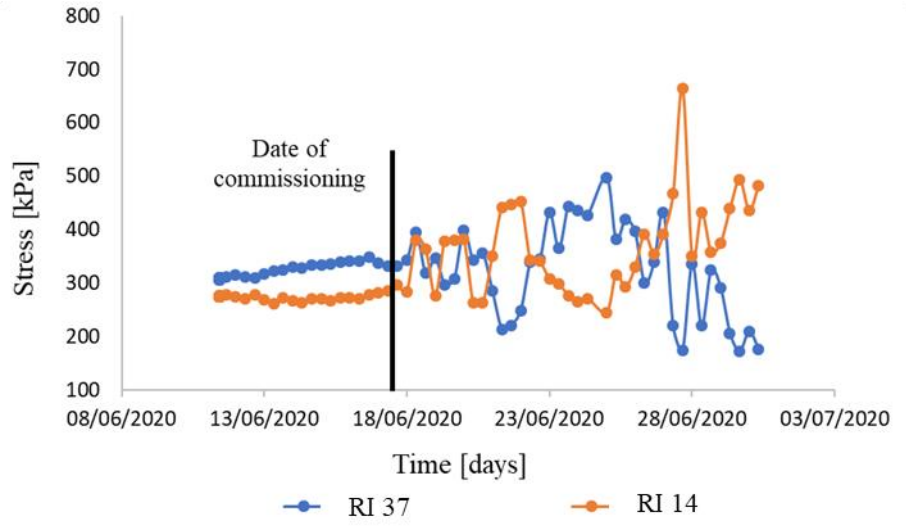

Figure 3-22: Vertical stress at the top of the RIs directly after commissioning of the wind turbine (RI 14 & RI 37)

A measurement campaign conducted on site on July 21, 2020 included a ON / OFF test of the wind turbine, with the sampling rate for the EPC of 1 Hz controlled directly on site. The collected

recordings reflect the load transfer to the head of the RIs based on their positions and again illustrate the inverse behaviour of the diametrically opposed RIs. Another interesting aspect is that the stress values measured at the top of the RIs return to their quasi-static values when the wind turbine is shut down, since the wind speed at the time of measurement is relatively low, averaging 6 m/s (Figure 3-23). This aspect can highlight the combined effect of the wind and the rotational effect of the turbine, and also distinguishes between two expected load transfer regimes from the wind turbine foundation to the rigid inclusions during the lifetime of the wind turbine. The phenomenon of recovery of the same measured magnitude at the head of the rigid inclusions during the two OFF periods (Figure 3-23) has also been observed in monitoring of rigid inclusions under a water tank, where earth pressure cells record approximately the same vertical stresses after loading and unloading cycles (Umur Salih Okyay and Briançon, 2012).

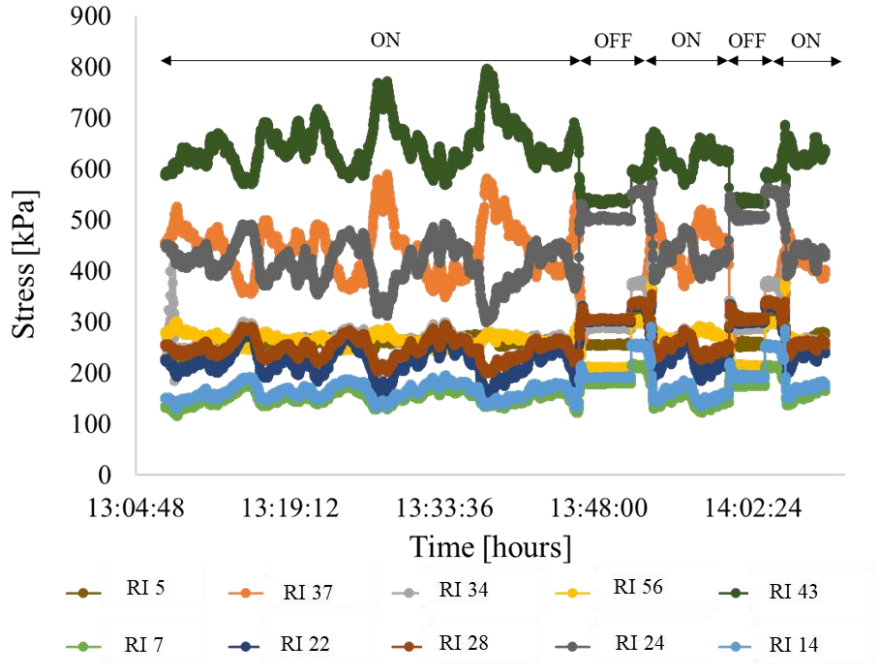

Figure 3-23: Vertical stress at the head of the RIs ON /OFF-Test

On the other hand, the readings during the periods of OFF reflect the redundancy of the measurements. An example of this is RIs "14 & 17", which are adjacent to each other on the plan (Figure 3-24) and the symmetrical shape of the arching effect between these two inclusions during the ongoing measurements, which also give some indication of the symmetry of the arching effect between the soil and the RIs, a conceptual phenomenon in soil reinforcement. The measurement of RI "37" was added to show how the diametrically opposed RIs behave in a precise inverted form. Regarding the stress level, we can observe that the RI 37 is more stressed, which is logical since the foundation exerts compressive stress on its side and slightly relieves the zone of RIs "14 & 17", and since the foundation cannot pull these inclusions since there are no structural connections between the foundation and the rigid inclusions. This effect has been statistically studied and will be shown in the next sections. The redundancy of the sensors is also shown in a continuous measurement over several months (Figure 3-25), the stress is of course not static, which leads to the fluctuations of the stress. However, the stress level of the sensors in these periods is very similar in terms of the severity of the events that could be detected in the series of measurements. The serial number in (Figure 3-25) corresponds to measurements taken at interval of 10 minutes.

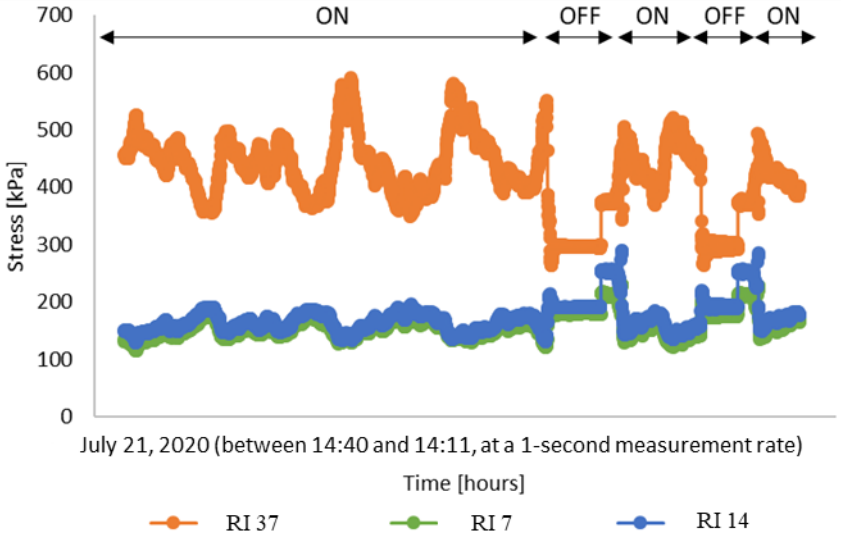

Figure 3-24: EPC measurements on selected RIs to illustrate the wind direction effect.

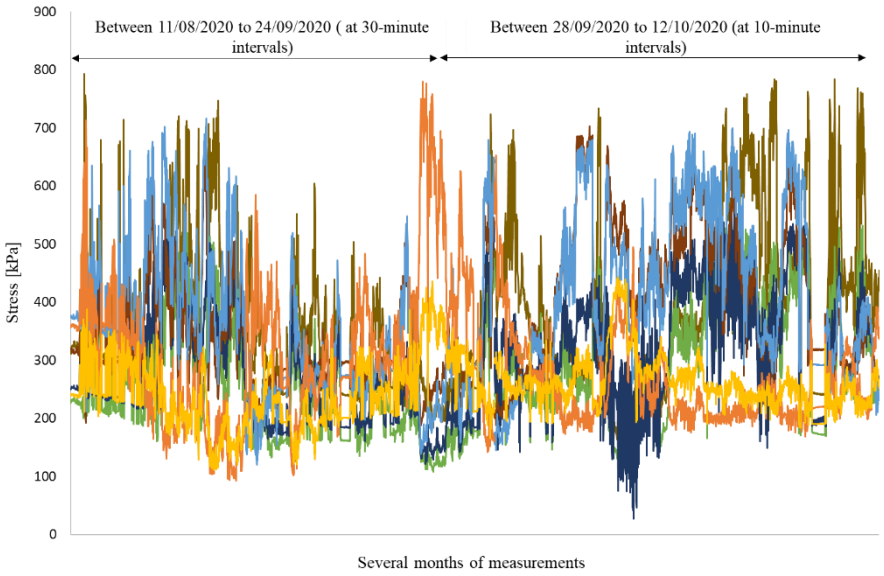

Figure 3-25: Continuous EPC measurements at the top of RIs over a long period of time.

The EPC measurements, shown in the (Figure 3-26), illustrate approximately two months of continuous measurements. At each significant peak, the various factors such as wind speed and wind direction are determined. Again, the influence of such factors on the behaviour of the RIs can be seen continuously in the increase and decrease of the stress reflecting the load from the gravity foundation.

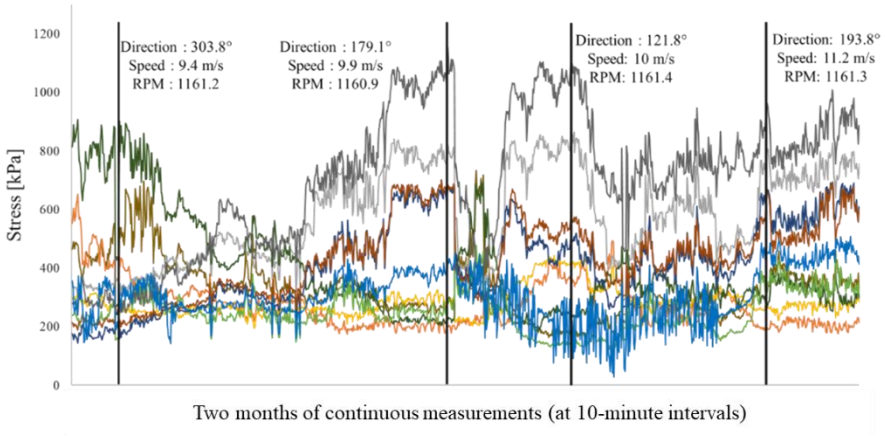

Figure 3-26: Measurements between September and November 2020.

To account for all sensors in the data analysis, and especially because the construction phase measurements have been lost, the following strategy is used to represent the measurements as vertical stress variation, i.e., the stress measurement at time "t" minus the initial stress measurements after the construction phase from WT. In a small exercise to illustrate how wind direction directly affects the measurements, the EPC measurements at the head of the RIs: 43, 24 (diametrically opposed) are shown in (Figure 3-27). In this particular example, some data is recorded to control the wind direction. As we can see, the wind direction at 250 degrees cancels the variations of the two inclusions, since the direction is orthogonal to these inclusions. However, with wind direction near 160 degrees and 350 degrees, the variation in stress is greatest in these data intervals.

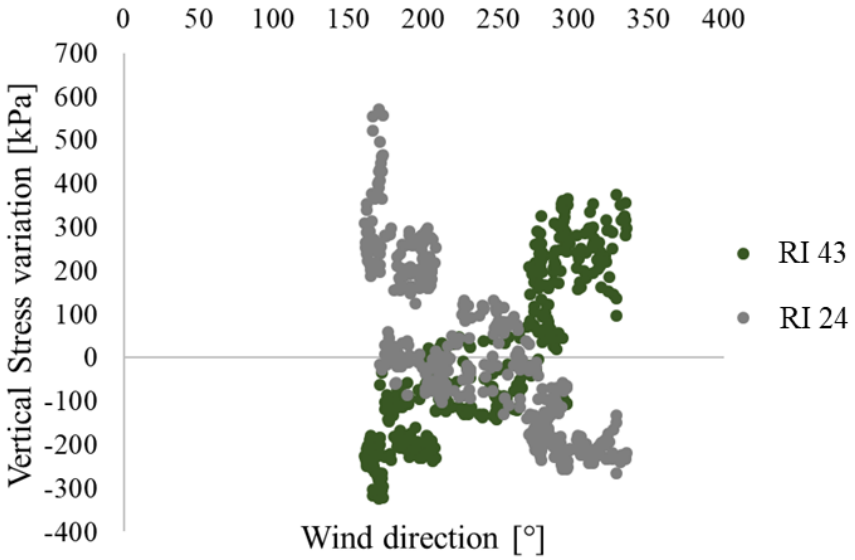

Figure 3-27: Stress variation of two EPC in a defined time interval with different wind direction.

3.5.5.2 EPC below the foundation

Measurements of the EPC below the foundation are compared with the superimposed EPC at the top of the RIs. Unfortunately, the EPC below the foundation was delivered directly to the site at the same time as the installation. However, it was delivered with a measurement range of 0-10 bars instead of 0-5 bars, which is very high compared to the estimated measurements of 0.5 bar

at dead load and up to 3 bars at high wind load. As a solution, the EPC measurements below the foundation labelled "F" are weighted by a constant factor of 22, (above which the values of F28 exceeds the values of R28) to be compared with the measurements at the top of the RIs (Figure 3-28), which means that the values of the EPC below the foundation shall not be taken into consideration. The EPC measurements at positions 14, 22, 28, and 37 are very similar at both levels (RI & F), with trends following each other exactly in the corresponding RI and foundation plots.

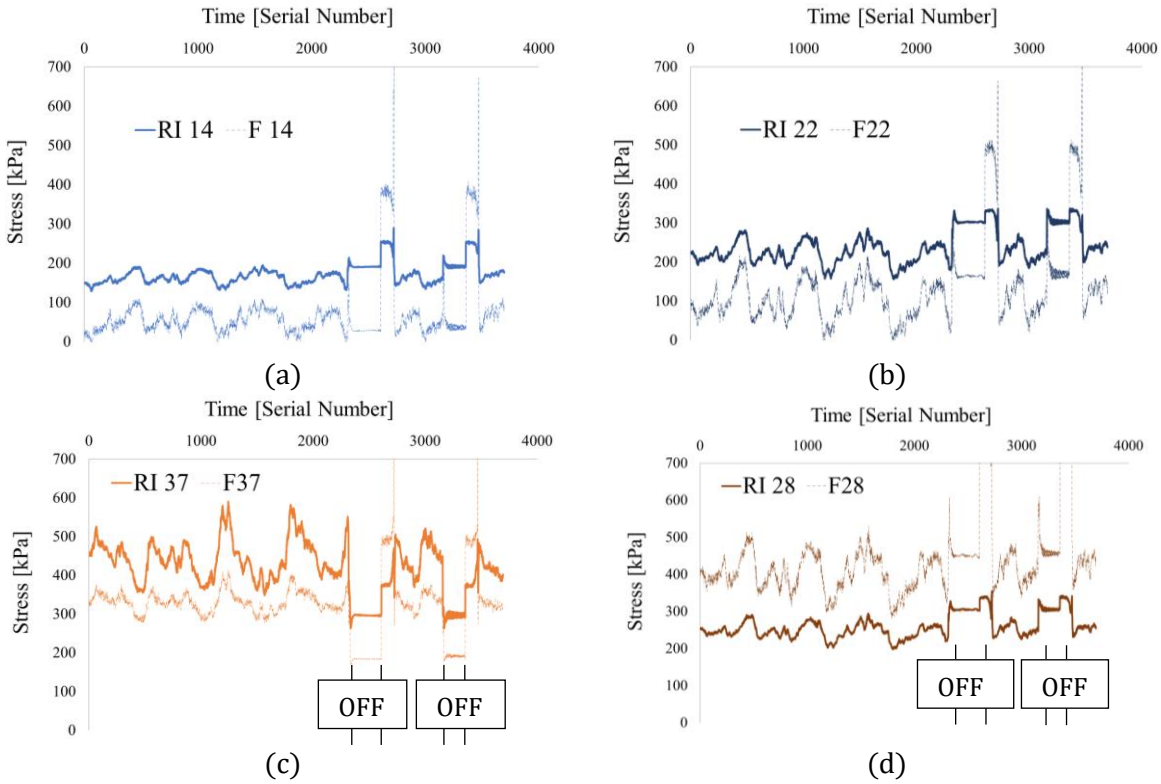

Figure 3-28: Comparison EPC measurements of selected positions at the base of the gravity foundation and at the top of the RIs.

Qualitatively, several physical phenomena can be identified from the superposition of the measurements (Figure 3-28):

- The behaviour of the RIs directly followed the behaviour of the foundation, since the shapes of the loading curves due to the wind loading and the rotation of the wind turbine are the same. This means that during compression (since we have a 100% compressed area under the foundation at this loading rate), the RIs behave as if they were notionally extending through the LTP, and due to the arching effect, the load is immediately transferred to the RIs, from where the high difference in stress level is concentrated as a load transfer to the relatively rigid elements 'RIs" within the soil matrix.
- The influence of wind direction is also evident in the results for position 37 (Figure 3-28 (c)) compared to the other windows in the figure, which reflect an identic behaviour of the EPC at the top of the RIs and below the foundation, both opposite to position 37.
- Each time the wind turbine starts to rotate after the period OFF in the following seconds, the EPC registers a slight vertical stress jump before the stress level stabilises again. This phenomenon is more pronounced for the EPC below the foundation and less pronounced

for the EPC at the top of the RIs. This damping of the stress levels could be dissipated in the soil between the RIs.

3.5.5.3 Statistical analysis

The variety of changes in vertical stress at the head of RIs makes it too difficult to understand the overall behaviour of RIs over time in a single graph because too many factors interact in wind turbines, such as machine production, rotor speed, wind direction, and wind speed. Therefore, the interpretation of the RIs monitoring data in this case requires the parallel observation of multiple data to draw a point-by-point conclusion at each time "t" of the measurements, which is a tedious process. As a qualitative solution, the EPC measurements are directly coupled with the SCADA measurement system to track how the wind turbine loading, especially the wind load, permanently affects the load transfer to the rigid inclusions. The coupling process was performed using the principal component analysis (PCA). A technique used to reduce the dimensionality of such data sets, increasing interpretability while minimising information loss. The added dataset was the wind direction, wind speed, and measured stress variation at the head of the RI (time (t) of sensor measurement minus self-weight of the structure) during the wind turbine operating period for three consecutive months. As a result, the diametrically opposed RIs (Figure 3-29) are statistically inversely proportional throughout the measurement period (Figure 3-29 (a)). On the other hand, the adjacent RIs represent the positively correlated vectors (RIs 22, 28, 34 and 24). Thus, the conclusion from the application of this method is that the behaviour of the diametrically opposite CMCs is quantitatively and qualitatively inversely proportional during the operation of the wind turbine, while the neighbouring RIs have no wind influence.

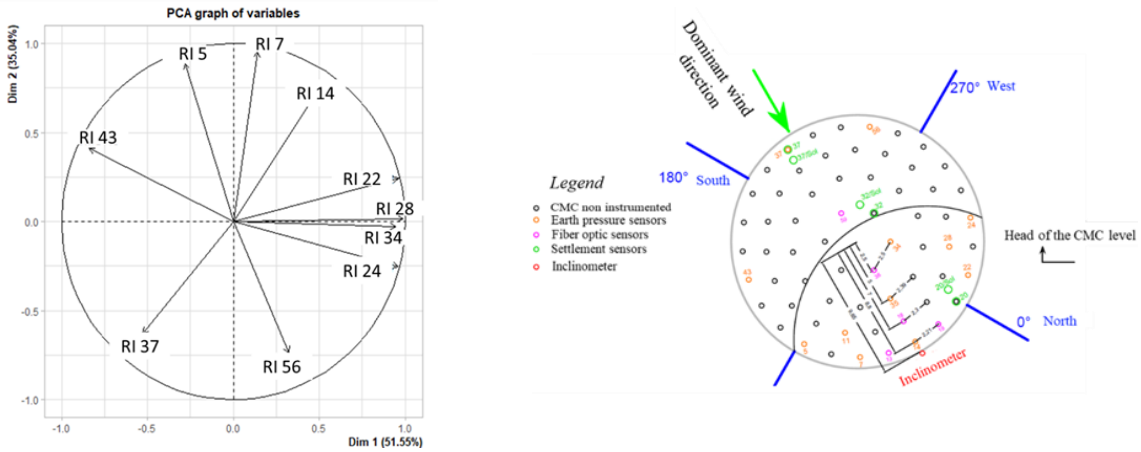

(a) (b)

Figure 3-29: PCA analysis for the RIs behaviour under the wind turbine foundation.

3.5.5.4 Algorithm of post-treatment

The statistical analysis using the PCA method is interesting to identify the factors involved in the variations of the measurements during the lifetime of the wind turbine. However, the main objective of field monitoring is to obtain a quantitative measurement to compare with design methods and understand the mechanisms of load transfer. Considering the loss of several sensors and measurements (Table 3.7) and the difficulties in analysing the measurements due to the

fluctuating external load, a post-processing algorithm was carried out, the basic idea of which is explained below.

The instrumented wind turbine operates in a wind speed range between 2.5 m/s and 25 m/s. It reaches its rated power (3.6 MW) at a wind speed of 13.5 m/s. During the operation of the wind turbine, the nacelle rotates with the yaw angle in a time-dependent manner to counteract the maximum wind speed in order to achieve the maximum speed for the production of the machine. Therefore, the post-treatment methods must account for this rotation each time, as the wind direction has a direct effect on the measurements. To quantify the varying loading effect on the EPC at the top of the RIs, the RIs and corresponding sensors are positioned to rotate against the main wind direction each time, so the measurements in this case are seen to be independent of this factor. Accordingly, the following transformation is applied:

$$\begin{bmatrix} X'^{(t,\theta)} \\ Y'^{(t,\theta)} \end{bmatrix} = R(\theta).\begin{bmatrix} X(t) \\ Y(t) \end{bmatrix} \quad (3.1)$$

$$R(\theta) = \begin{bmatrix} \cos(\theta) & \sin(\theta) \\ -sin(\theta) & \cos(\theta) \end{bmatrix} \quad (3.2)$$

The X and Y matrices contain the coordinates of the RIs including the EPC since they have the same diameter as the RIs, the X' and Y' matrices contain the new coordinate-transformed constraint data, and θ is the average 10-minute angle between the sensor datum and the wind direction. In addition to EPC measurements and wind direction and speed, other SCADA measurements are also included, such as rotor rotation speed, blade pitch angles of and wind turbine energy consumption, to create different analysis scenarios. All data are synchronized simultaneously, and the plan and motivation for the post-treatment method are shown in (Figure 3-30).

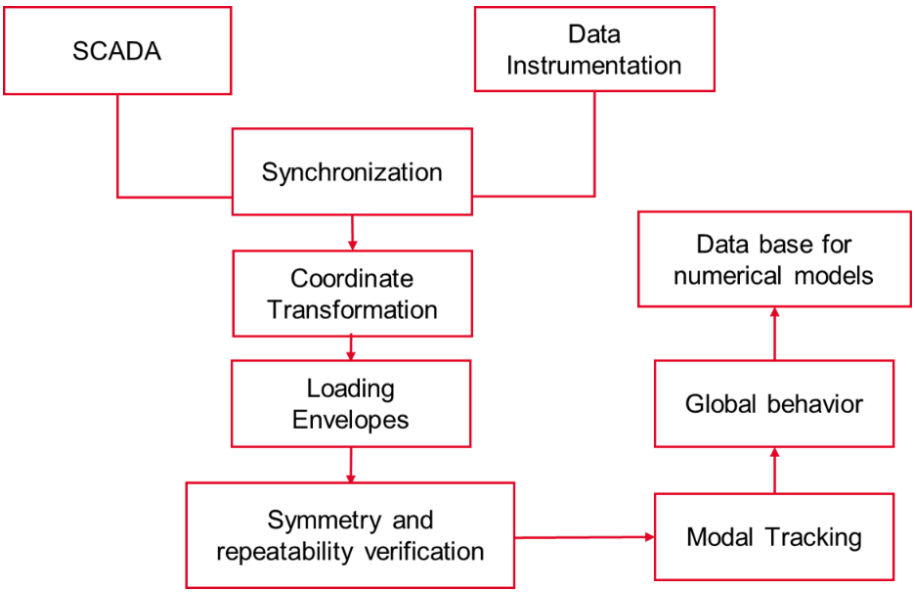

Figure 3-30: Post-treatment methods for EPC measurements.

Post-treatment data were performed to illustrate the results of the algorithm. The X-axis of the Figure 3-31 represents the 360 degrees of the plan on which the RIs are located, and the Y-axis represents the variation of the stress measured with the EPC. The data shown were measured several months (unfiltered data) after the official commissioning of the wind turbine. It is can be seen that the main wind direction in this measurement interval is between 170 and 190 degrees, where the maximum stress variation occurs. This maximum decrease drastically to the left and right as we move away from the main wind direction to reach the minimum in the opposite wind direction. In between, we could observe a small stress variation reflecting the RIs, which are less affected by the wind direction due to their position.

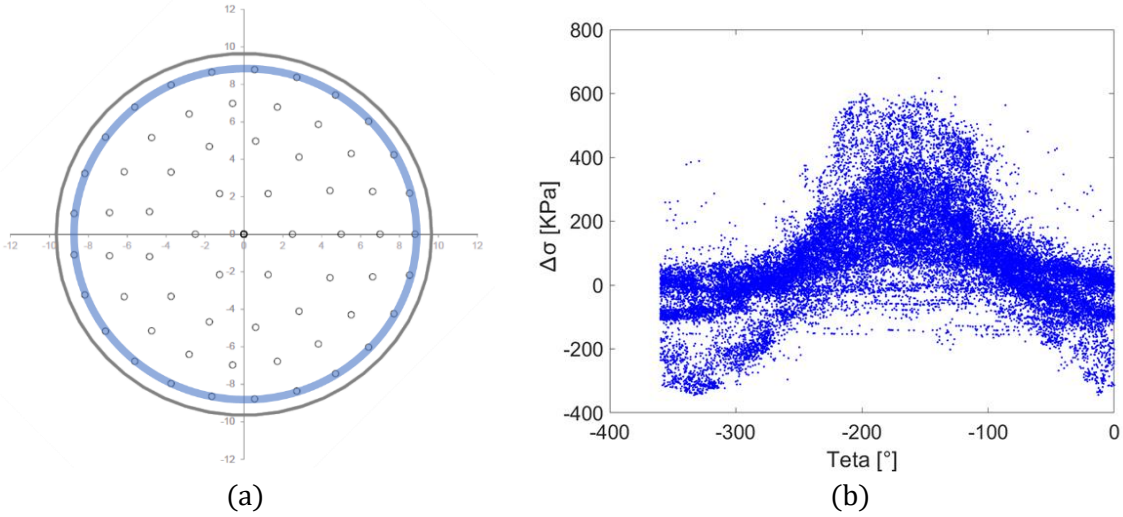

Figure 3-31: (a) Outer diameter of the RIs, (b) Stress variation at the top of RIs.

In a three-dimensional system, the data show how the stress varies inversely from the diametrically opposite position at the head of the rigid inclusions for the RIs on the outer circle of the RIs (Figure 3-32). Although the general trend of the graph is clear enough. It is important to note that the data shown here is unfiltered raw data after processing by the algorithm. Therefore, synchronisation with SCADA measurements between wind direction and nacelle direction could sometimes be difficult, so some of the points shown here do not match the expected global shape.

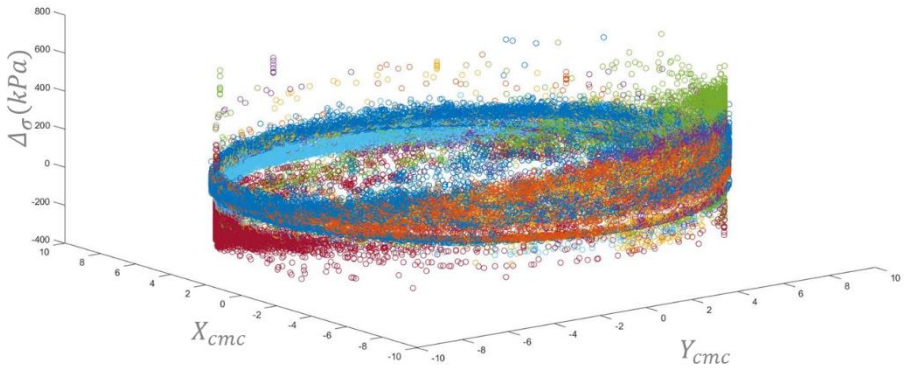

Figure 3-32: 3D stress variation over the head of the RIs (outer diameter).

Interpreting the data, it is noticeable that the stress variations correlate with the square of the velocity (Figure 3-33). Here we have plotted different wind directions and the corresponding stress variations and velocity variations.

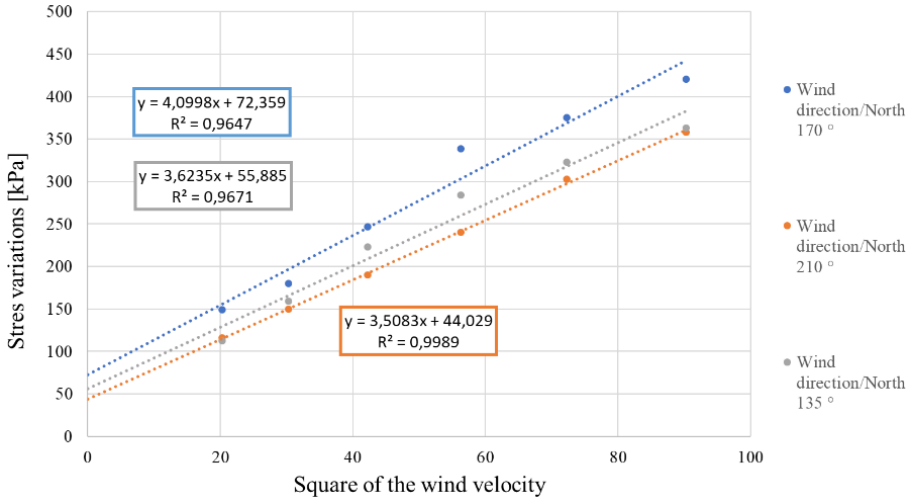

Figure 3-33: Measurement of EPC fluctuations as a function of the square of the wind speed.

To create a sort of envelope based on the stress variation and independent of the wind direction, it is normalized by dividing it by the corresponding velocity square to obtain a 2D stress envelope. In this way, the measurements are combined into a curve that parallels the cyclic effects of the wind turbine loading. This type of curve is useful because it allows the calculation of the moment acting at the base of the wind turbine foundation based on equation (3.3) proposed by (Mirza and Brant, 2009). In this way, several useful information such as the moment, stress variation and stress level can be presented in one graph (Figure 3-34). The envelope curve is the result of the analysis of several months of continuous measurements. During this time, all wind directions were recorded, as you can see from Figure 3-35 (a), where the wind came from all directions. The symmetry of the stress variation across the top of the RIs can also be seen in Figure 3-35 (b), where we observe a normal distribution resulting from the number of stress variations recorded in a given period, which in turn illustrates the quasi-opposite behaviour of the RIs under the wind turbine's gravity foundation during the operating period. The 3 plans in Figure 3-34 (b) reflect the stress path as maximum, average, and minimum. The equation of each plan could be written as the shape of the maximum and minimum stress distribution under gravity (equation (3.3)).

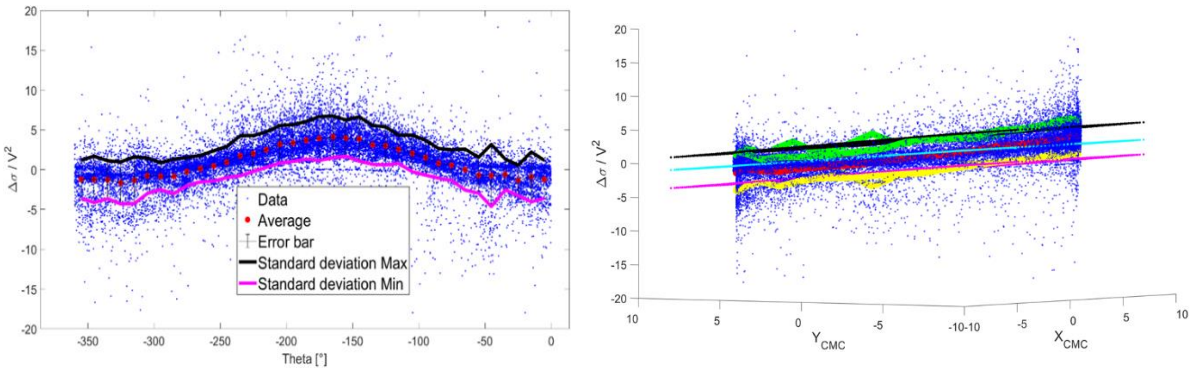

(a) (b)

Figure 3-34: (a) 2D Stress envelope based on normalized EPC measurements, (b) 3D Stress envelope based on normalized EPC measurements.

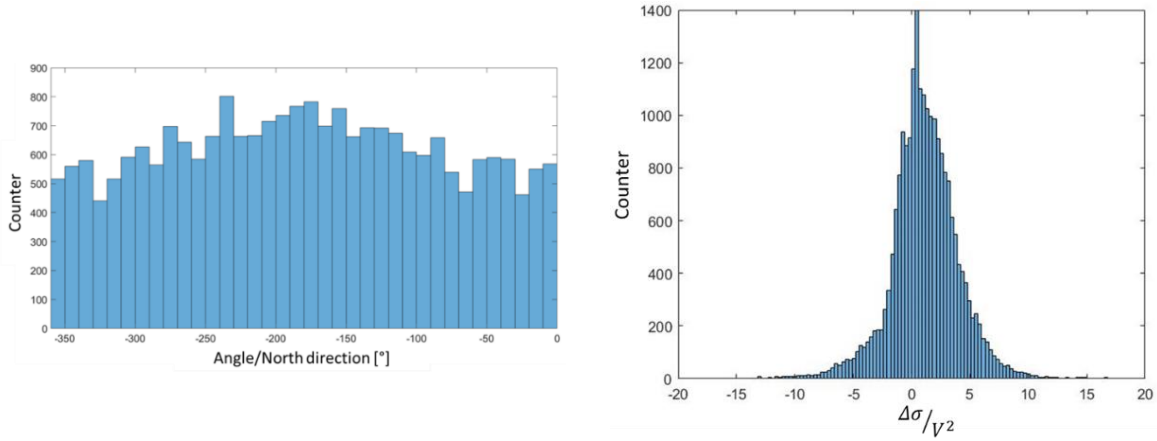

(a) (b)

Figure 3-35: (a) Statistical analysis of the wind direction that occurred during the envelope studies, (b) the normal distribution of the normalized stress variation during the interval of the studies.

3.5.5.5 Moments calculations

In a wind turbine project, foundation design criteria are established simultaneously with several load combinations to be tested, which are typically extreme and not justified for the geotechnical design scope. These load combinations are also typically used in research (i.e., outside of engineering design) when modelling wind turbine foundations (Pham, 2018) or when attempting to increase overturning moments to achieve failure (Mohamed and Austrell, 2018), or in the quasi-static values also issued by the wind turbine manufacturer (Seymour, 2018), or when specialised wind turbine design and analysis software such as "GH Bladed" (Zhou et al., 2021) or open-source code for wind turbine dynamics simulation (openFAST) are considered. Independent of the mentioned separate programmes, the overturning moment can also be estimated with theoretical background. However, the inclusion of structural and aerodynamic damping requires a complex study due to the interaction between the fluid and the structure and the complexity of the wind turbine. A coupling between computational fluid dynamics and structural dynamics was developed by Bailly (2014), with parameters estimated based on a literature review. The study found that the resultant load carried by the foundation in normal operation is less important than the resultant force specified by the wind turbine manufacturer.

In a field monitoring project of a real scale wind turbine, the calculation of the overturning moment is challenging because it cannot be measured directly by sensors and additionally the dynamic effects have to be considered. The overturning moment was derived from field monitoring by using measured axial stress increments and assuming a plane strain (He et al., 2019). In the current project, it was found that the stress distribution at the outer perimeter of the RIs appears to be correlated as a trapezoidal stress distribution in the case of a fully compressed region, i.e. 100% foundation-soil contact (Figure 3-36), and that the stress path recorded at the top of the rigid inclusions closely follows that located directly below the gravity foundation. Therefore, the overturning moment at the base of the foundation was calculated for different wind speed intervals (Figure 3-37).

The Figure 3-36 described the location of the calculated the load descent {V, H, M}, and the moment calculations were done as following:

A linear vertical stress was assumed under the gravity foundation, therefore the equation proposed by (Mirza and Brant, 2009):

$$q_{max/min} = \frac{V}{A} \pm \frac{M}{I/_{\upsilon}} \tag{3.3}$$

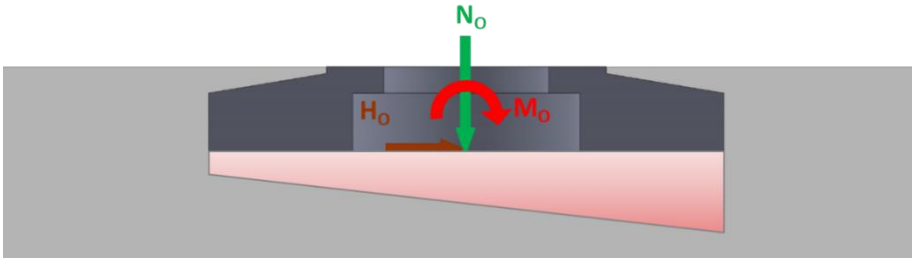

Figure 3-36: Position of the calculated load Descent at the base of the gravity foundation.

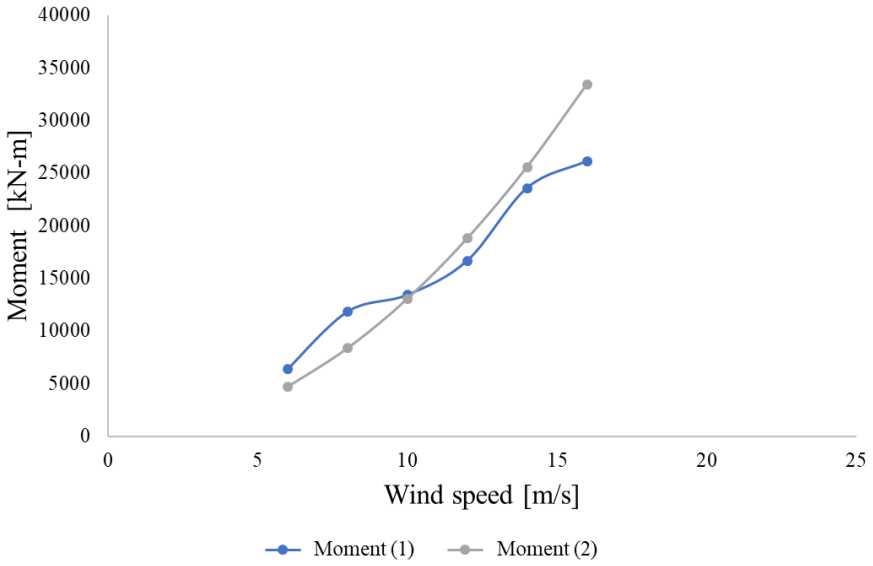

Figure 3-37: Calculated overturning moment.

For the specific location of the instrumented wind turbine, the manufacturer informed us that the average annual velocity is 8.5 m/s. Therefore, three different moments were determined for three different interval wind speeds (Table 3.9). The values of the moments calculated in this chapter are used in the numerical simulations (FEM and macroelement modelling). The designations below are used when comparing the results of the numerical models to refer to the values of the load applied to the wind turbine.

Table 3.9: Overturning moments derived from instrumentation measurements

Average wind speed (m/s)	Designation	Moment [kN.m]	Horizontal Force [kN]	Vertical Force [kN]
6	M_6	7000	77	4095
12	M_12	17300	190	4095
16	M_16	30000	330	4095

It is important to note that the values of overturning moment and horizontal forces derived from the measurements are compared with the available data in the literature. In the study of He et al., (2019), an overturning moment of 16000 kN.m and a horizontal force of 150 kN are calculated for a wind speed of 12 m/s based on real-scale measurements. This reference provides an indication of the expected magnitudes of these load components under specific wind conditions.

3.6 DFOS

3.6.1 Deformation

The soil-structure interaction at the level of soil-inclusion is achieved through DFOS. The installed sensors aim to first determine the deformations in the RIs as a function of wind loading and then derive the axial loading to investigate the concept of rigid inclusions and quantify the negative and positive skin friction. As we will see in finite element chapter, skin friction is very important to calibrate the numerical moment and properly estimate the bearing capacity of the isolated columns.

The measured deformation of a selected rigid inclusion numbered 13 is shown in the (Figure 3-38). The different magnitude of deformation in 2020, which correlates with the wind direction, shows that the wind direction was in the same position as the rigid inclusion on July 21, which explains the lowest magnitude of deformation among the others. The negative skin friction and positive skin friction are determined by the measurements (Figure 3-38), which reflect the relative displacement between the inclusion and the soil, which is negative at the beginning and becomes positive after reaching the maximum deformation at a height of about 3.5 m in this case. The measurements are used to determine the relative displacement between the inclusion and the soil. It should be noted that the first meter of measurements is not shown because it could be considered tricky. It has also been reported that the DFOS in piles may not be clear to analyse in the first part of it close to the head of the column.

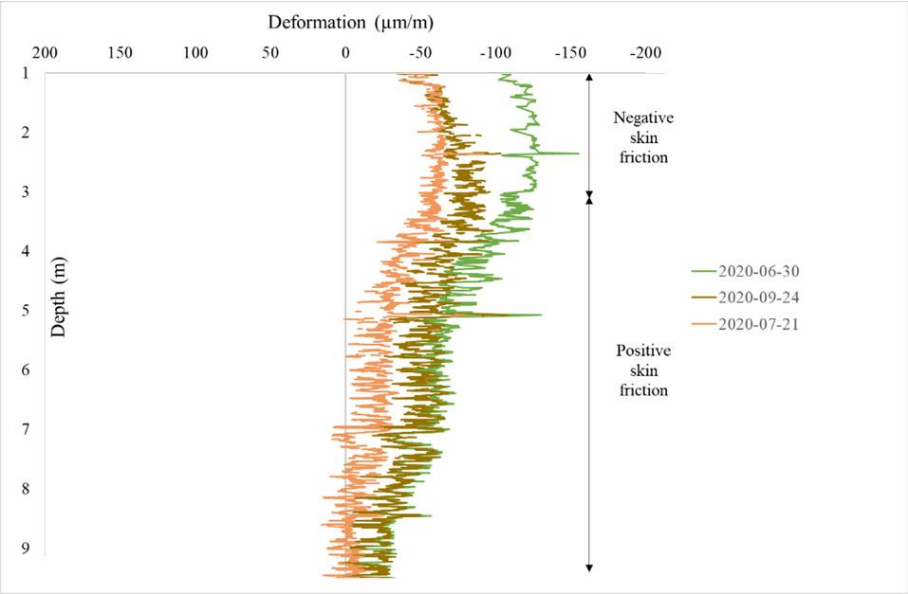

Figure 3-38: DFOS in RI 13.

3.6.2 Axial load

The axial stress distribution can be calculated using the DFOS, assuming that the deformation is in the elastic range. This exercise is performed for RI 13 (Figure 3-39). In this example, the ON / OFF test performed on the wind turbine on July 21, 2020 (Figure 3-38) is shown using the measured deformation through the optical fibre. The wind direction was from the northeast at the time of the measurement, which explains that the axial load in RI 13 increases when the machine is set to OFF. It is interesting to note that this increase does not only occur at the head of the rigid inclusion, but throughout the entire profile, as can be seen in Figure 3-39. This means that the behaviour along the column: LTP, friction at the interface and bearing resistance are solicited by the wind direction and speed. It has been reported (Sienko et al., 2019) that the variations in the calculated axial load have some local extremes that have been attributed to a reduction in the stiffness of the column (presumably due to the reduction in the cross-sectional area of the pile or the elastic modulus of the concrete). This could also be the reason for the discrepancies in this case (unfiltered data are presented in this chapter). However, it should be noted that in the case of rigid inclusion, steel reinforcement is not included and the cross-sectional area of the column is small compared to classical piles, so the estimated concrete modulus is less complicated to estimate/control.

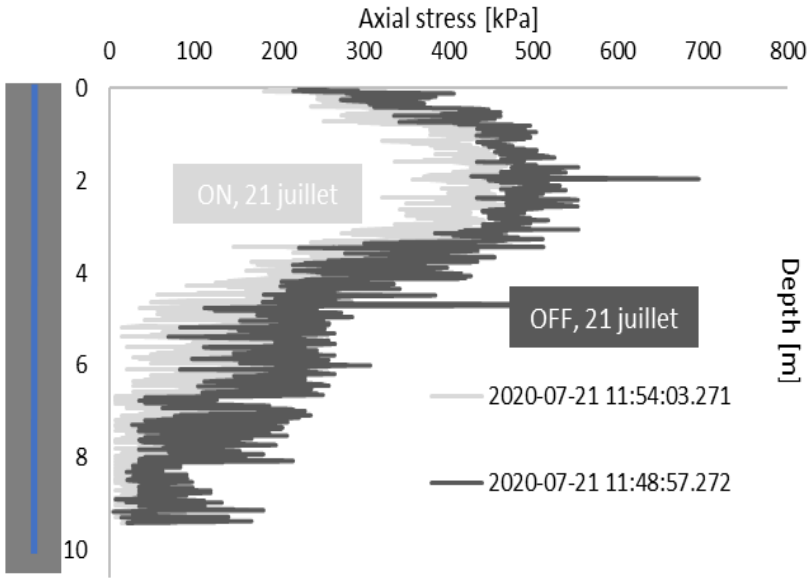

Figure 3-39: Vertical axial stress inside the rigid inclusion during the ON/OFF test.

3.7 Static Test Load

3.7.1 Introduction

A static load test “SLT” until failure was carried out on an isolated rigid inclusion marked "IR1" type CMC with soil displacement on a platform located near the instrumented wind turbine to have a similar geotechnical condition as the soil profile under the concrete foundation. The main objective of this test is not only to test the bearing capacity of the column, but also to use the measurements as a solid data base to calibrate the numerical model used to simulate the static load test. When multiple physical variables affect the soil-structure interaction, calibration of the numerical models is required. The following strategy is followed: After the soil model(s) is selected based on laboratory experimental tests, it is assigned to the RI-soil interface and the adjacent soil and compared with the static load test results to validate and then calibrate as necessary. Then, the validated constitutive law is used a second time to simulate the soil in a 3D model representing the onshore wind turbine and its foundation system, taking complex loads into account (Figure 3-40).

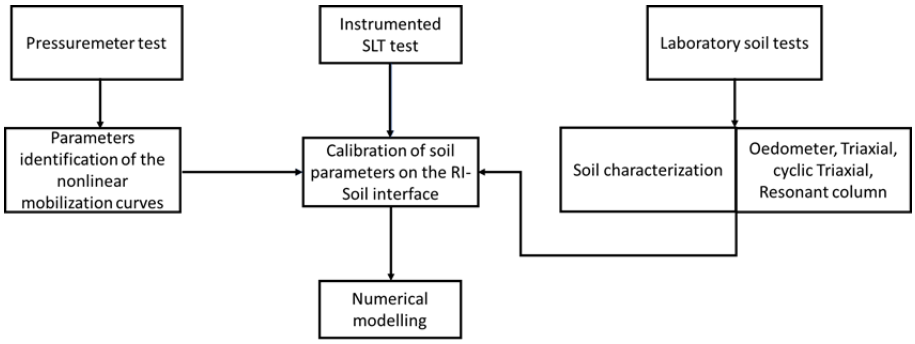

Figure 3-40: Strategy for applying the SLT in the numerical models.

3.7.2 Background

Combining instrumentation with static load testing is one way to optimize pile and rigid inclusion design. The classical static load test usually measures only the load-settlement relationship. However, if the column is instrumented, axial friction mobilization curves q_s as a function of pile displacement can be calculated. Experimental SLT plays an importance to assess the following characterizations of an isolated column: its capacity, behaviour and pile integrity (Poulos, 1989). The instrumentation of piles has experienced an evolution. Simple tell-tales have been first utilized to measure the relative pile deformation to the pile head (Dunnicliff, 1993). Vibrating wire strain gauges is commonly installed throughout the length of the piles to measure the strain punctually (Dunnicliff, 1993; Fellenius, 2002; Siegel and McGillivray, 2009; Burlon et al., 2014). Recently, a successful application of the OFDR DFOS in the geotechnical field led to using this technology to instrument the piles (Bersan et al., 2018; Sienko et al., 2019; Kania et al., 2020).

The main advantage of the DFOS is the continuous strain measurement through the entire length of the fiber which lead to a very high resolution, so an accuracy in estimating the shaft skin friction. Both techniques: Brillouin scattering (Kechavarzi et al., 2015; Mohamad et al., 2017) and Rayleigh back scattering (Briançon et al., 2016; Kania et al., 2020) were brought into play in the case of piles. In FEDRE project, Rayleigh technology has been utilized and a spatial resolution of 2.6 mm have been achieved thanks to the ODiSI-6000 measurement system. In case of rigid inclusions, the use of FO in real scale instrumentation is relatively recently introduced.

3.7.3 Test RI

The test setup consists in the use of eight reaction columns, four on either side of the IR1 and a stiff loading beam. The horizontality of the loading system was controlled, the head of the IR1 was lowered to a depth of 20 cm, and the perfect flatness of the jack's bearing surface was ensured by adding a layer of sand between the head of the column and the loading plate and checked by a level (Figure 3-41). The pressure was controlled by a manometer and the force was measured with a precise load cell with a capacity of 2000 kN.

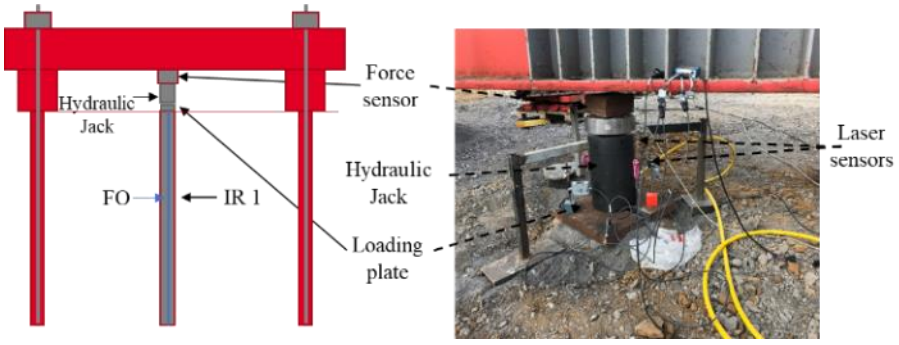

Figure 3-41: Illustration of the static load test setup.

The originality of the test is in the use of a 12 m optical fibre positioned inside the column to measure the strain distribution along the IR1 during the loading increments. Rayleigh backscattering technology based on OFDR (Optical Frequency Domain Reflectometry) was chosen to follow these deformations with a spatial resolution of 2.6 mm and an acquisition frequency of 250 Hz thanks to the optical interrogator ODiSI-6000. The placement for the fibre optic in rigid

inclusions was experienced for the first time on this site, where the optical fibre was taped to 1 m long threaded rods connected to each other during insertion into the fresh concrete.

3.7.4 Bearing capacity

The bearing capacity of an isolated column during the SLT is controlled by two parameters: the limit value of skin friction q_s and the limit end-bearing pressure q_b of each soil layer. In the present case, this bearing capacity was calculated according to the Menard specifications version 3 (2017), from pressuremeter and penetrometer tests. The bearing capacity of IR1 was estimated at 1246 kN using the pressuremeter method and 1132 kN using the penetrometer method.

3.7.5 Experimental protocol

The SLT consists of applying an axial compressive force to the head of the rigid inclusion and measuring the corresponding vertical displacement at the head of the inclusion according to a program defined by the French code NF P 94-150-1 (Figure 3-42). As shown in Figure 3-42, two loading cycles were performed. During the first loading cycle, the load was applied from initial 0 kN to 600 kN in four increments and subsequently unloaded in two loading steps. During the second loading cycle, the load was applied from 0 kN to 1200 kN where the failure occurred. The load of the first and second cycle was maintained for a period of 15 or 60 minutes, and the unloading lasted for 5 minutes. The loading was performed in accordance with the recommendations of the ASIRI (2013) allowing the possibility to apply the next increment loading level if the vertical displacement within 15 minutes of loading is less than 0.02 mm.

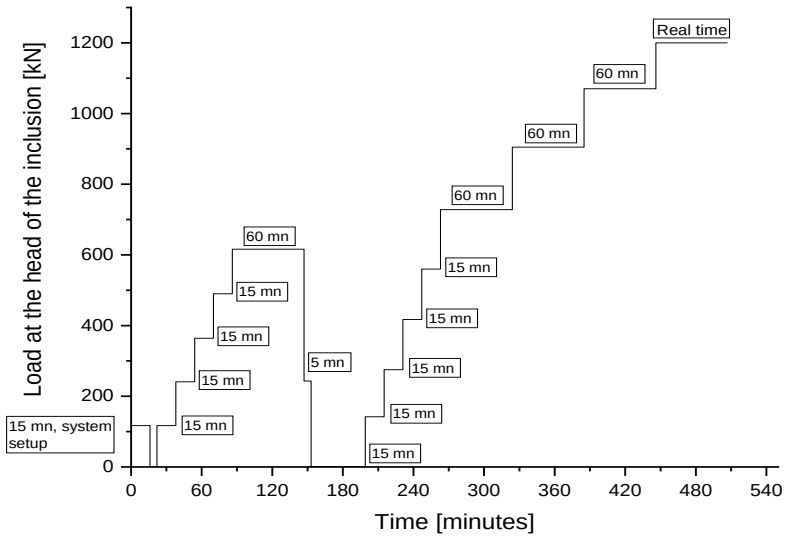

Figure 3-42: Schedule of the SLT.

3.7.6 Analytical approaches

In order to characterize the soil-structure interaction in a soil reinforced by isolated columns, Frank and Zhao (1982) proposed two semi-empirical mobilization laws for skin friction at the interface of the column and for end bearing at the toe of the column. This semi-empirical model is proposed in ASIRI (2013)which also recommends calibrating the numerical models in finite

elements with respect to the curves (t-z) of Frank & Zhao in the absence of experimental values during the design phase. This model is based on pressuremeter data:

- The skin friction mobilization law is defined according to the relationship between the shear stress τ and the relative displacement S_{s-i} between the rigid inclusion and the soil around the shaft of the column (Figure 3-43 (a)). This law depends directly on the limit value of skin friction q_s correlated from the limit pressure P_L
- The end-bearing mobilization law is defined according to the relationship between the stress at the column toe q and the vertical displacement at the inclusion toe S_b in the anchor layer (Figure 3-43 (b)). This law depends directly on the limit value of the end-bearing resistance q_b, correlated from the limit pressure P_L.

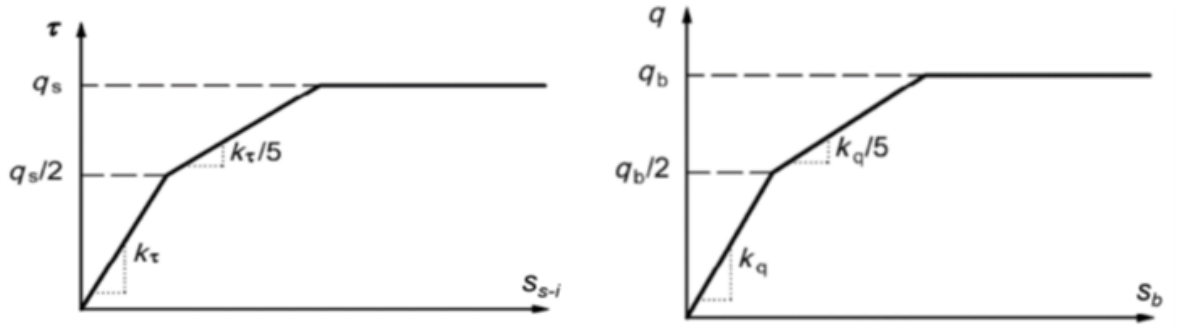

(a) (b)

Figure 3-43: (a) Semi-empirical mobilization law for skin friction, (b) Semi-empirical mobilization law for end-bearing (NF P94-262, 2012).

The parameters of the slopes k_τ and k_q depend on the type of soil, the pressuremeter modulus E_M and the diameter of the isolated column B (Table 3.10).

Table 3.10: Parameters of the k_τ and k_q slopes of Frank & Zhao according to the type of soil

Slope of the Trilines	Fine grained soil	Coarse grained soil
k_τ	$2.0\ E_m/B$	$0.8\ E_m/B$
k_q	$11.0\ E_m/B$	$4.8\ E_m/B$

3.7.7 Results

The loading curve of the test (Figure 3-44) shows that the ultimate capacity measured are very closed to the analytical estimated bearing capacity (Section 3.7.4). The DFOS inside the test RI (Figure 3-45) shows the evolution of the measured deformation with respect to the load phases.

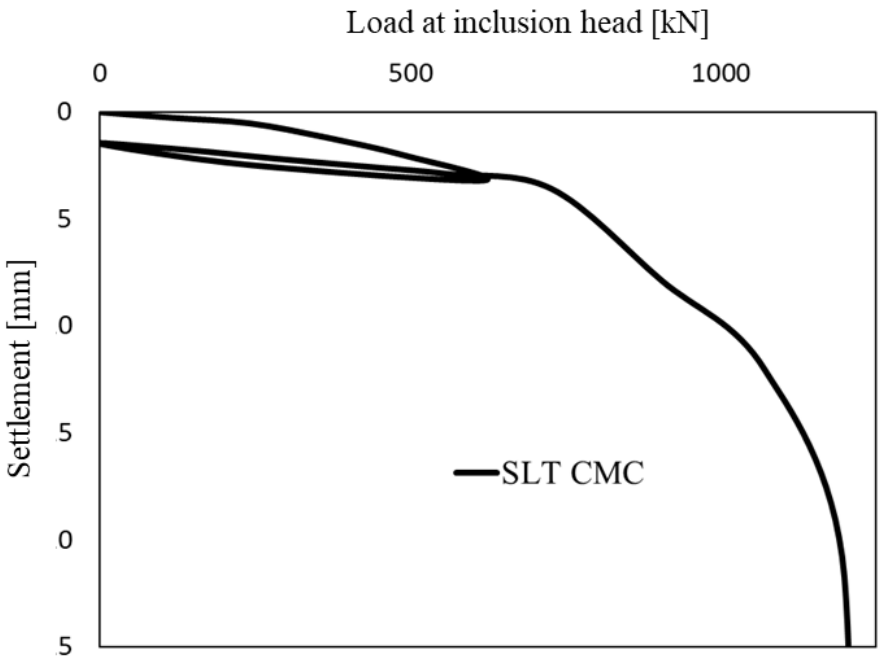

Figure 3-44: Settlement at the IR1 head.

One of the direct physical quantities that could be derived from the DFOS is the shaft skin friction calculated for layer 1 and layer 2 (LS & CS) of the compressible soil adjacent to the rigid inclusion (Figure 3-46). All results were compared with analytical solutions and finite element model and discussed in detail in the following chapter.

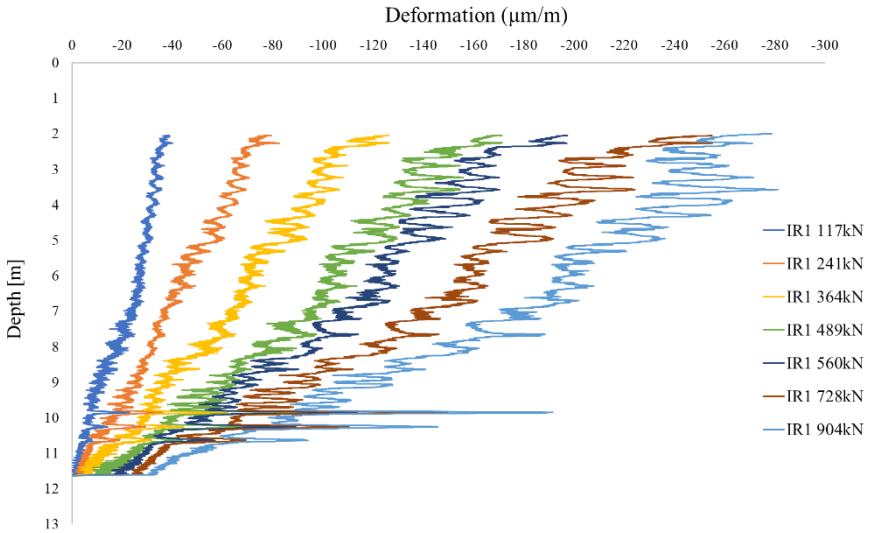

Figure 3-45: Axial load distribution.

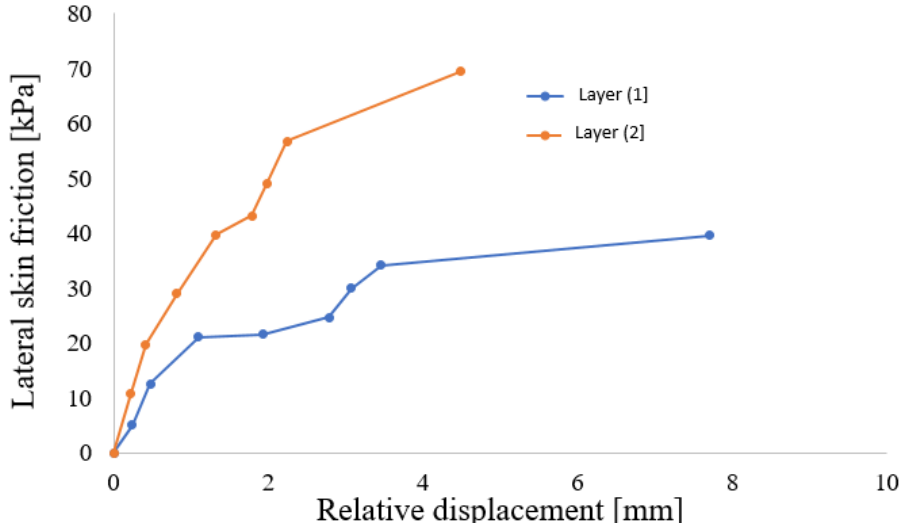

Figure 3-46: Raw data of the lateral skin friction calculation based on the measurements.

3.8 Conclusions

In September 2019, a full-scale wind turbine foundation reinforced with RIs-type CMC was instrumented in northern France. The objective of the instrumentation is to record measurements over an extended period of time (several years) to observe and analyse the load transfers from the foundations to the inclusions in order to optimize future wind turbines and to determine the capacity of an existing foundation to be retrofitted. When monitored during construction phases, initial earth pressure measurements show differences before and after wind turbine commissioning. A ON / OFF test confirmed this hypothesis. Furthermore, a statistical method (PCA) was used to qualitatively illustrate the overall behaviour of the CMC under the wind turbine foundation. In addition, a post-processing method that combined the measurements with SCADA allowed the quantitative description of the CMC behaviour under the wind turbine.

Further data analysis was performed to quantify the CMC behaviour and it is possible to derive the descending load for different speeds from the measurements. These analyses will be presented in the next papers with multiple 3D models calibrated thanks to the monitoring and compared with the measurements.

CHAPTER 4

Finite Element Method

4.1 Introduction

Advances in computer processing have revolutionized the field of geotechnical engineering, enabling the use of numerical modelling techniques as essential tools for predicting and analysing foundation behaviour under various loading conditions. Among these numerical methods, the finite element method (FEM), the finite difference method (FDM), and the boundary element method (BEM) have become widely used and valuable in geotechnical engineering practice.

This chapter is primarily concerned with the application of numerical modelling, particularly nonlinear FEM, to simulate the behaviour of a soil reinforced by rigid inclusions under the action of a wind turbine foundation. The objective is to compare the numerical simulation results with the available measurements from Chapter 3. Numerical modelling approaches involve a methodology relying on the de-complexing and de-coupling of the various soil-structure interactions in this system before simulating the overall behaviour in three-dimensional modelling. The terms "de-complexing" and "de-coupling" practically refer to identifying and breaking down the various components of soil reinforcement, determining their properties, and simplifying their analysis, in the following form:

- Soil properties. FEM modelling of the laboratory tests to determine the mathematical soil models suitable for the loading cases and soil type.
- Inclusion – soil interface. An axisymmetric modelling approach to reproduce an instrumented static load test until failure on an isolated rigid inclusion
- Foundation – LTP – Soil – Inclusion network interactions. An axisymmetric model to replicate a unit cell of a rigid inclusion under a wind turbine gravity foundation.
- Wind turbine loading. The modelling includes the loading conditions exerted by the onshore wind turbine. This involves considering the overturning moment due to the wind, including wind speed, direction, and their influence on the system.
- Three-dimensional modelling to reproduce the E6 wind turbine supported by a gravity foundation underlined by rigid inclusions.

The main findings of this chapter lie in the successful pre-calibration phases of the above component and the comparison of the global model with the available measurements. The results obtained from these analyses were satisfactory. The chapter also serves as a background and validation of rigid inclusions modelling in the case of onshore wind turbine foundations. The results presented here provide a crucial database for the calibration and comparison of the novel macro element developed in this dissertation.

It is important to note that this chapter did not address cyclic loading modelling. However, the discussion of cyclic loading is an interesting intriguing topic that warrants further exploration. We are aware of the importance of this aspect and intend to address it in one of our next publications.

4.2 Finite Element Method

In simple terms, FEM is a powerful method for solving complex problems that are difficult or impossible to solve analytically. The concept is based on the solution of partial differential equations of a domain Ω discretized into a finite number of elements under appropriate boundary conditions. The equations governing the behaviour of the system are derived using the Principle of Virtual Power (PVP) and then expressed in terms of matrices at nodal resolution. The formulations of a linear elastic FEM problem usually include the following steps:

- **Discretization:** The domain is divided into a finite number of smaller regions, called finite elements
- **Approximation method:** the behaviour of the finite elements is approximated by a set of simple functions, usually polynomials. The nodal values of the functions are determined by solving a set of linear equations derived by applying the PVP to each element of the system
- **Element formulation:** The element equations are composed into a system of linear equations that determine the behaviour of the entire system.
- **Solution**: The system of linear equations is solved to obtain the nodal values of the functions, which are then used to calculate the behaviour of the system.

The FEM can be used to solve problems involving different types of materials, such as elastic, elastic-plastic, hardening and softening, etc. The formulation of FEM depends on the constitutive laws that the user determines for the problem. In a nonlinear response of a domain, the nodal displacements are not solved directly, but iterations are performed at each loading step until the equilibrium of the system is reached. The iterations are controlled by a numerical value set by the user, which is related to the tolerance. It controls the accuracy of the solution by calculating the difference between external and internal forces and displacements at each iteration.

To illustrate the mathematical formulations of FEM on a practical problem, a numerical example in MATLAB for a 1D truss problem with bar elements is included in Appendix A. The materials are characterised as elastic-plastic using a linear hardening model. Therefore, the solution was derived based on iterations using the Newton-Raphson method.

4.3 Soil models

A constitutive model is a mathematical formulation that governs the stress-strain relationship of a material. The equations are often implemented in finite element codes such as PLAXIS, which contain several categories of models (Schweiger, 2009):

- **Elastic models, linear or non-linear:** largely applied in conventional soil mechanics because of their simplicity, but in some cases misrepresent actual soil behaviour.

- **Elastic-perfectly plastic model:** such as the Mohr-Coulomb model, which is the most practical and was first used in engineering for soils subjected to monotonic loading. However, it does not allow variation of the assigned stiffness and the dilatancy is not mobilized before fracture, which is generally observed for cyclic loading.
- **Isotropic hardening single surface plasticity models:** such as Modified Cam Clay, represents a non-linear elasticity and introduces the hardening/softening law. This model is known for soft soils, mainly normally consolidated Clay.
- **Isotropic hardening double surface plasticity models:** e.g., HSM, which was developed to determine the non-linear behaviour of soil (Duncan and Chang, 1970) with more reliable features of soil behaviour under load, including aspects such as densification, stress history, and dilatancy. It is suitable for modelling the dominance of plastic shear strains observed in non-cohesive and over consolidated cohesive soils, as well as the dominance of plastic compressive strains typical of soft soils(Schanz et al., 1999; Obrzud, 2010).

A linear-elastic correlation such as Hooke's law combined with Mohr-Coulomb's perfect plasticity criterion to calculate a single soil stiffness is insufficient for a variety of geotechnical applications (Schanz et al., 1999), including cyclic loading. However, an advanced constitutive model for reliable and more realistic predictions of soil response would be useful if a soil database is available, which is not always the case in engineering. In geotechnical engineering, an optimal solution for selecting an available constitutive law with an appropriate number of parameters is to find a compromise between the type of geotechnical application, the type of loading, the soil and the expected extent of deformation.

4.3.1 Elastoplastic "Mohr-Coulomb"

The theory of the Mohr-Coulomb (MC) model is used in geotechnical engineering to define the shear strength of soils and rocks at different states of effective stress. The behavioural law of this model is characterized by an isotropic Hooke linear elasticity (E, ν), a loading surface $f(\boldsymbol{\sigma})$, and a plastic potential $g(\boldsymbol{\sigma})$. It is a fracture model with three parameters: the cohesion c, the friction angle φ and the dilatancy angle ψ.

This model is based on the Coulomb hypothesis, which dates back to 1776 and assumes a linear relationship between the shear strength in a plane and the normal stress acting on it:

$$\tau = c - \sigma_n tan\varphi \qquad (4.1)$$

where τ is the shear strength, σ_n is the normal stress (tension positive), φ is in the angle of internal friction and c is the cohesion.

The equation of the load surface according extreme principal stresses is:

$$f(\boldsymbol{\sigma}) = (\sigma_1 - \sigma_3) - (\sigma_1 + \sigma_3)\sin\varphi - 2c\cos\varphi = 0 \qquad (4.2)$$

where σ_1 and σ_3 are the extreme principal stresses, so that $\sigma_1 \geq \sigma_2 \geq \sigma_3$, with the following sign convention: compressions are counted positively.

The plastic potential is written as a function of the extreme principal stresses:

$$g(\boldsymbol{\sigma}) = (\sigma_1 - \sigma_3) - (\sigma_1 + \sigma_3)\sin\psi \quad \textbf{(4.3)}$$

When $\varphi = \psi$, the flow is called associated.

The parameters of this model can be directly measured by routine laboratory experiments. Moreover, the numerical calculation for the constitutive model is quite simple and a constant average stiffness or a stiffness that increases linearly with depth is estimated by this model for each layer. Because of this constant stiffness, the calculations are usually relatively fast (Schanz et al., 1999). Accordingly, the time required for numerical computation with this model is reasonable. The results of existing studies on numerical simulation of problems using the constitutive model MC have shown that this model gives quite accurate results for friction materials such as sand and gravel and cured concrete (Vermeer and de Borst, 1984).

4.3.2 HSM

The Hardening Soil (HS) model, formulated by (Schanz et al. 1999), is an advanced isotropic non-linear elastoplastic model that takes into account the nonlinear response of soil, even at small loads. Unlike the purely elastic behaviour assumed in the MC model, the HS model introduces hardening plasticity in the pre-failure stress state. The HS model defines the soil stress states using shear strength parameters: effective cohesion (c'), effective friction angle (φ'), and dilatancy angle (ψ), which are used to establish the boundaries of the Mohr-Coulomb failure stress criterion. The model considers two expandable yield surfaces: the shear hardening yield surface and the compression hardening yield surface. These surfaces accurately account for irreversible shear straining due to deviatoric loading and volumetric straining due to isotropic loading, respectively. To determine the stiffness of the soil, the HS model incorporates three input stiffnesses: triaxial loading stiffness (E_{50}), oedometer loading stiffness (E_{oed}), and unloading-reloading stiffness (E_{ur}). These stiffnesses are formulated in a stress-dependent manner, following the principles outlined by Ohde in 1930. The use of E_{ur} allows for distinguishing between the soil stiffness during first loading and unloading-reloading conditions. It is important to note that in this formulation, compression is considered positive.

4.3.2.1 Definition of the stiffness moduli

In the Hardening Soil model, the behaviour of soil is represented by a set of ten parameters. These parameters capture various aspects of soil behaviour, including stiffness, plasticity, and failure criteria. Among these parameters, three stiffness parameters can be defined based on soil tests. These stiffness parameters are used to describe the mechanical response of the soil:

- Triaxial stiffness modulus for primary deviatoric loading (E50): This parameter, denoted as E50, is used to describe the shear hardening behaviour of the soil at small strains. It replaces the initial modulus Ei and represents the stiffness of the soil during primary deviatoric loading:

$$E_{50} = E_{50}^{ref}\left(\frac{c\,cot\varphi + \sigma_3}{c\,cot\varphi + p^{ref}}\right)^m \quad \textbf{(4.4)}$$

Where p^{ref} is the reference pressure.

- Triaxial stiffness modulus for unloading/reloading (Eur): The unloading/reloading path is assumed to be purely elastic in the HS model. The stiffness of the soil during this path is described by the parameter Eur, which represents the triaxial stiffness modulus for unloading/reloading. The elastic strains in this case are calculated using specific equations:

$$E_{ur} = E_{ur}^{ref}\left(\frac{c\ cot\varphi + \sigma_3}{c\ cot\varphi + p_{ref}}\right)^m \quad (4.5)$$

$$G_{ur} = \frac{E_{ur}}{2(1+\nu_{ur})} \quad (4.6)$$

$$\varepsilon_1^e = \frac{q}{E_{ur}};\ \varepsilon_2^e = \varepsilon_3^e = \nu_{ur}\frac{q}{E_{ur}} \quad (4.7)$$

- Tangent stiffness modulus for primary compressive loading (Eoed): The compression hardening behaviour of the soil is characterized by the tangent stiffness modulus for primary compressive loading, denoted as Eoed. This parameter describes the stiffness of the soil during primary compressive loading:

$$E_{oed} = E_{oed}^{ref}\left(\frac{c\ cot\varphi + \sigma_1}{c\ cot\varphi + p^{ref}}\right)^m \quad (4.8)$$

It is worth noting that the terms "E_{50}^{ref}", "E_{ur}^{ref}" and "E_{oed}^{ref}" refer to the reference stiffness moduli corresponding to a reference stress level (pref), conventionally set at 100 kPa. The stiffness values must be correlated with the actual stress level experienced by the soil. The change of stiffnesses according to the stress state (σ_3' for "E_{50}^{ref}" and "E_{ur}^{ref}" and σ_1' for "E_{oed}^{ref}") is related to the cohesion, and mainly the power "m" (see equation (4.9)). Typical values of "m" used by PLAXIS: 0.5 for sand, 0.5- 0.7 for silt and nearly 1 for clay. Calibration of the "m" value is essential in this context.

$$E = E^{ref}\left(\frac{c\ cos\varphi + \sigma\ sin\varphi}{c\ cos\varphi + p^{ref}\ sin\varphi}\right)^m \quad (4.9)$$

4.3.2.2 Hyperbolic stress-strain relationship

The HS model is based on the hyperbolic relationship between the vertical strain (ε_1) and the deviatoric stress ($q = \sigma_1 - \sigma_3$) during primary triaxial loading. When soil is subjected to primary deviatoric loading, its stiffness decreases, and irreversible plastic deformations occur simultaneously. This behaviour is represented by a hyperbolic shape in the stress-strain curve, as shown in Figure 4-1.

Kondner (1963) was the first to propose a hyperbolic relationship between q and ε_1 in drained triaxial tests. This relationship captures the general trend observed in the stress-strain curve. Later, Duncan and Chang (1970) presented a hyperbolic model that further refined the relationship. The HS model, which is an advanced constitutive model, also adopts the hyperbolic stress-strain relationship similar to the Duncan-Chang model. However, the HS model surpasses

the basic hyperbolic model by incorporating additional features and improvements. The HS model incorporates the theory of plasticity instead of elasticity, recognizing the irreversible nature of plastic strains that develop in soils under primary deviatoric loading. By using plasticity theory, the HS model provides a more accurate representation of soil behaviour. In addition, the HS model introduces the concept of soil dilatancy, which refers to the tendency of soils to expand in volume during shearing. By considering soil dilatancy, the HS model captures the influence of this behaviour on the stress-strain relationship. Furthermore, the HS model introduces a compression yield surface, also known as a yield cap. This yield surface represents the maximum stress state that the soil can sustain before undergoing plastic deformation. By incorporating the compression yield surface, the HS model accurately represents the limits of soil strength and its behaviour under compression.

The hyperbolic stress-strain relationship in the HS model can be expressed as follows:

$$\varepsilon_1 = \frac{1}{E_i}\frac{q}{1-q/q_a} \text{ for } q < q_f \tag{4.10}$$

The maximum failure stress q_f , the asymtotic failure stress q_a and the initial modulus E_i are defined by:

$$q_f = \frac{6\sin\varphi}{3-\sin\varphi}(p + c\cot\varphi) \tag{4.11}$$

$$q_a = \frac{q_f}{R_f};\ R_f < 1 \tag{4.12}$$

$$E_i = \frac{2E_{50}}{2-R_f} \tag{4.13}$$

Where p is the mean effective stress defined as:

$$p = \frac{1}{3}(\sigma_1 + 2\sigma_3) \tag{4.14}$$

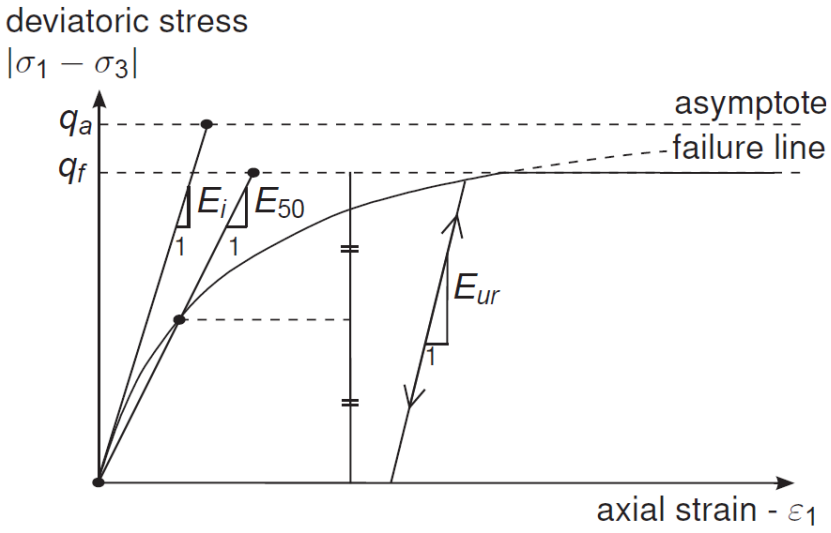

Figure 4-1: Hyperbolic stress-strain relation between deviatoric and axial strain from a drained triaxial test. (Brinkgreve et al., 2010).

4.3.2.3 Shear hardening yield function

The shear hardening is described by a yield function, denoted f^s, can be described by the following equation:

$$f^s = \frac{2 - R_f}{E_{50}} \frac{q}{1 - q/q_a} - \frac{2q}{E_{ur}} - \gamma^p = 0 \quad (4.15)$$

Where γ^p is the hardening parameter defined by:

$$\gamma^p = \varepsilon_1^p - \varepsilon_2^p - \varepsilon_3^p = 2\varepsilon_1^p - \varepsilon_v^p \approx 2\varepsilon_1^p \quad (4.16)$$

With ε_1^p, ε_2^p and ε_3^p are the plastic strains, and ε_v^p is the plastic volumetric strain.
To represent the yield condition $f^s = 0$ in the p'-q plane for a constant value of the hardening parameter (γ^p), yield loci are plotted. These yield loci are obtained using equations (4.4), (4.5) and (4.15) for the respective values of E_{50} and E_{ur}. The shape of the yield loci is influenced by the exponent value (m). When m = 1.0, the yield loci appear as straight lines, while lower values of the exponent result in slightly curved yield loci. Figure 4-2 illustrates the successive yield loci for m = 0.5, which is typical for hard soils. As loading increases, the failure surfaces approach the linear failure condition described by equation (4.11).

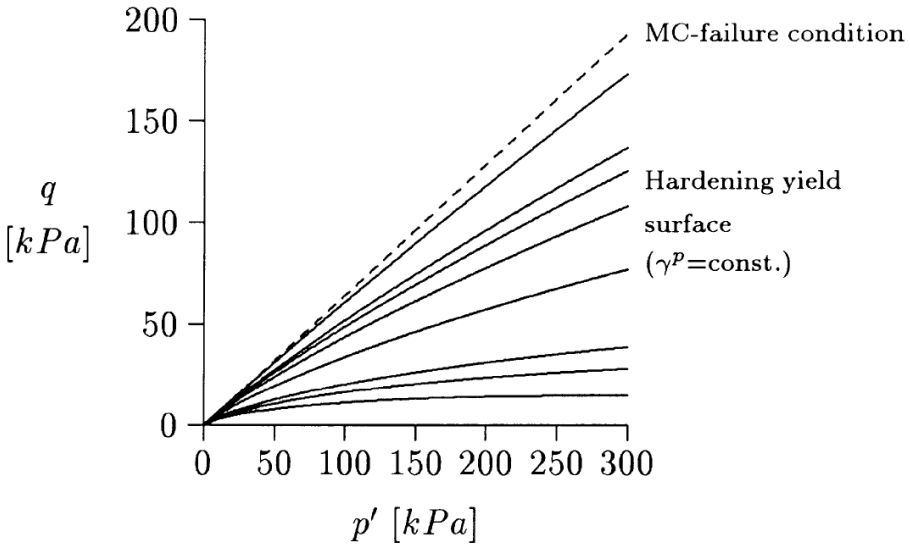

Figure 4-2: Variation of shear hardening yields with different values of γ^p (Schanz et al., 1999).

The flow rule used is non-associated, and the shear potential function is expressed by the following equation:

$$\dot{\varepsilon}_v^p = sin\psi_m \dot{\gamma}^p \quad (4.17)$$

The plastic potential functions g^s can be written as follow:

$$g^s = \frac{1}{2}(\sigma_1 - \sigma_3) - \frac{1}{2}(\sigma_1 + \sigma_3)\, sin\psi_m \quad (4.18)$$

Where ψ_m, the mobilized dilatancy angle, is defined according to Rowe (1962) and can be expressed as follows:

$$sin\psi_m = \max\left(\frac{sin\varphi_m - sin\varphi_{cv}}{1 - sin\varphi_m\, sin\varphi_{cv}}; 0\right) \quad (4.19)$$

The mobilized dilatancy angle is influenced by both the mobilized friction angle (φ_m) and the critical state of constant-volume friction angle (φ_{cv}). These angles are determined using the following equations:

$$\sin\varphi_m = \frac{\sigma_1 - \sigma_3}{\sigma_1 + \sigma_3 + c\cot\varphi} \tag{4.20}$$

$$\sin\varphi_{cv} = \frac{\sin\varphi - \sin\psi}{1 - \sin\varphi\sin\psi} \tag{4.21}$$

In the HS model, the behaviour of the material regarding contraction or dilation is determined by the relationship between the mobilized friction angle (φ_m) and the constant-volume friction angle (φ_{cv}). If φ_m is smaller than φ_{cv}, the material contracts. On the other hand, if the mobilized friction angle is equal to or greater than φ_{cv}, the material dilates (Schanz et al., 1999).

4.3.2.4 Compression hardening yield function

The existing shear-hardening yield surfaces shown in Figure 4-2 do not adequately explain the plastic volume strain observed during isotropic compression, especially for softer soil types. Therefore, an additional type of yield surface must be included to capture the elastic range for compressive stresses, especially for compaction hardening. The inclusion of this cap flow surface is necessary to achieve independent control of the E_{50}^{ref} and E_{oed}^{ref} parameters within the model. The shear yield surface depends primarily on the triaxial modulus, while the cap yield surface is influenced by the oedometer modulus. In particular, E_{50}^{ref} significantly determines the magnitude of the plastic strains associated with the shear flow area. Similarly, E_{oed}^{ref} is used to control the magnitude of plastic strains originating from the cap yield. The cap yield surface is defined by:

$$f^c = \frac{\tilde{q}^2}{\alpha^2} + (p')^2 - p_p^2 \tag{4.22}$$

Here α is a constant derived internally from other material parameters such as K_0^{NC} and p_p is the isotropic preconsolidation pressure, which also determines the magnitude of the yield cap, represented by an ellipse in the (p'- q) plane.
With:

$$p' = \frac{(\sigma_1' + \sigma_2' + \sigma_3')}{3} \tag{4.23}$$

$$\tilde{q} = \sigma_1' + (\delta - 1)\sigma_2' - \delta\sigma_3' \tag{4.24}$$

$$\delta = \frac{(3 + sin\varphi)}{(3 - sin\varphi)} \tag{4.25}$$

$\tilde{q}$ is a special stress measure for deviatoric stresses. In the specific case of triaxial compression, where the stress values are arranged as $-\sigma_1' > -\sigma_2' = -\sigma_3'$, the value of $\tilde{q}$ is calculated as $-(\sigma_1' - \sigma_3')$. Conversely, in the case of triaxial extension where $-\sigma_1' = -\sigma_2' > -\sigma_3'$, $\tilde{q}$ is given by the equation $\tilde{q} = -\delta(\sigma_1' - \sigma_3')$. The size of the yield cap, which represents the region of possible plastic deformation, is determined by p_p. The hardening law relating p_p to volumetric cap ε_v^{pc} is given by:

$$\varepsilon_v^{pc} = \frac{\beta}{1-m}\left(\frac{p_p}{p^{ref}}\right)^{1-m} \quad (4.26)$$

Similar to the parameter "α", the parameter "β" is also an internal parameter that influences the shape of the yield cap surface. The parameter "α" is associated with the lateral earth pressure at rest, including K_0^{NC}, E_{50}^{ref}, and E_{50}^{oed}. On the other hand, the parameter "β" is linked to E_{50}^{oed}, which can be determined through an odometer test, as shown in Figure 4-3. Both of these internal parameters are not considered as input parameters. In contrast to the shear hardening flow rule, the associated flow rule is applied to determine the strain rate in compression hardening. This means that the plastic potential function "f^c" is equal to the yield function "g^c". The plastic volumetric strain rate is determined as follows:

$$\dot{\boldsymbol{\varepsilon}}_v^{pc} = \lambda\frac{\partial f^c}{\partial \boldsymbol{\sigma}'} \quad (4.27)$$

Where λ is the plastic multiplier:

$$\lambda = \frac{\beta}{2p'}\left(\frac{p_p}{p^{ref}}\right)^m \frac{\dot{p}_p}{p^{ref}} \quad (4.28)$$

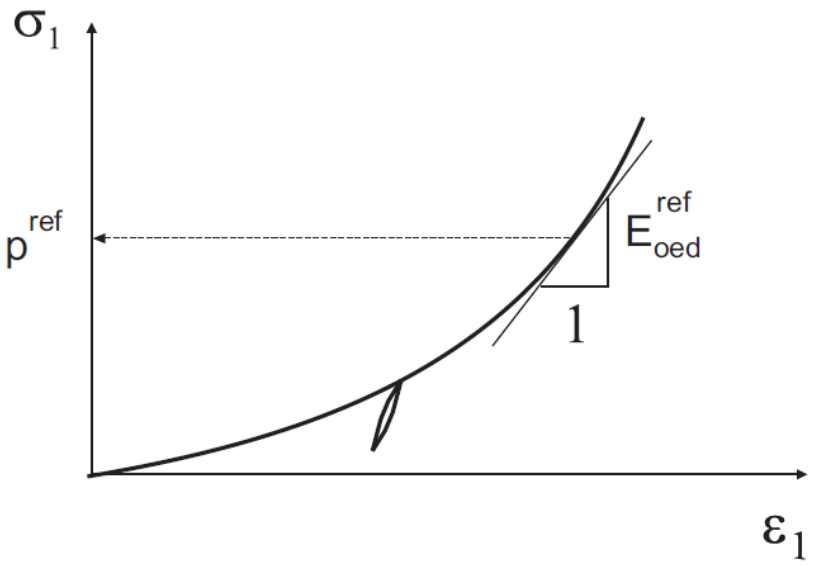

Figure 4-3: A characteristic stress-strain curve obtained from an oedometer test (PLAXIS Manual (2020) v8.2).

4.3.3 HSM small strain (HSS)

Meanwhile, The HSM represents a good approach to soil behaviour, it does not distinguish between large stiffness at small strains and reduced stiffness at engineering strains strain levels. This inability was overcome by the introduction of the small strain version of the model to the "HSS" small strain hardening model (Benz, 2007). It allows the integration of the degradation of the stiffness of the soil due to increased strains or cyclic loading and can also incorporate the hysteretic damping of the material, an aspect considered in the case of WT foundations. While the

unloading in HSM is purely elastic, as shown in Figure 4-4 (a). A typical hysteretic behaviour of HSS when the soil is subjected to cyclic shear is shown in Figure 4-4 (b).

The behaviour of soil at small strains has been a research interest on which many studies (Atkinson, 2000; Benz, 2007) have been carried out to improve the understanding of this phenomenon in various geotechnical applications. In the case of a wind turbine, this phenomenon could be observed due to the high number of cycles during its lifetime. A normalized stiffness degradation curve introduced by Atkinson and Sallfors (1991) explains the shear stiffness for a wide range of shear strains (Figure 4-5): a very small shear strain level where the stiffness modulus remains constant in the elastic range, a small strain level where the stiffness modulus varies nonlinearly with strain, and a large strain level where the soil is close to failure and the soil stiffness is relatively low. This definition was later modified by Diaz-Rodriguez and López-Molina, (2008) by dividing the three ranges into five. The deformation of a wind turbine is estimated to be between 0.001% and 0.1% (CFMS, 2011), which puts it in the low deformation range, so the HSS model is recommended in this case. The fact that soil deformation is reduced by the CMC technique results in a shift of the deformation level to a low range (Figure 4-5). This technique provides an efficient foundation system by reducing settlement and increasing bearing capacity and/or providing stability (Racinais et al., 2016).

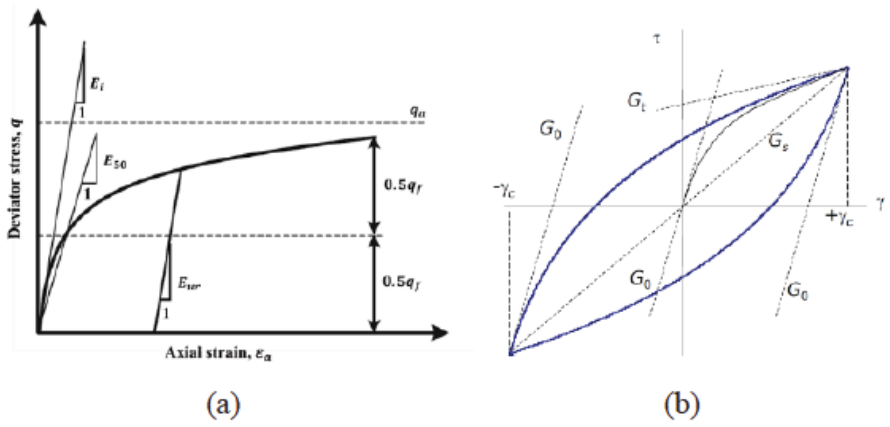

Figure 4-4: (a) Hyperbolic stress–strain relationship in primary loading for a standard drained triaxial test (Schanz et al., 1999), (b) Hysteretic behaviour in the HSS model (Brinkgreve and Vermeer, 2002).

Besides the input parameters of HSM, two additional variables are required for HSS model: shear modulus at initial or very small strain G_0^{ref} and the shear strain $\gamma_{0.7}$ at which the secant shear modulus is reduced about 70% from its initial reference modulus. By using a constant value for Poisson's ratio, as recommended in PLAXIS, the shear modulus could be calculated from Young's modulus for very small strains:

$$G_0^{ref} = \frac{E_0^{ref}}{2(1+\nu_{ur})} \qquad (4.29)$$

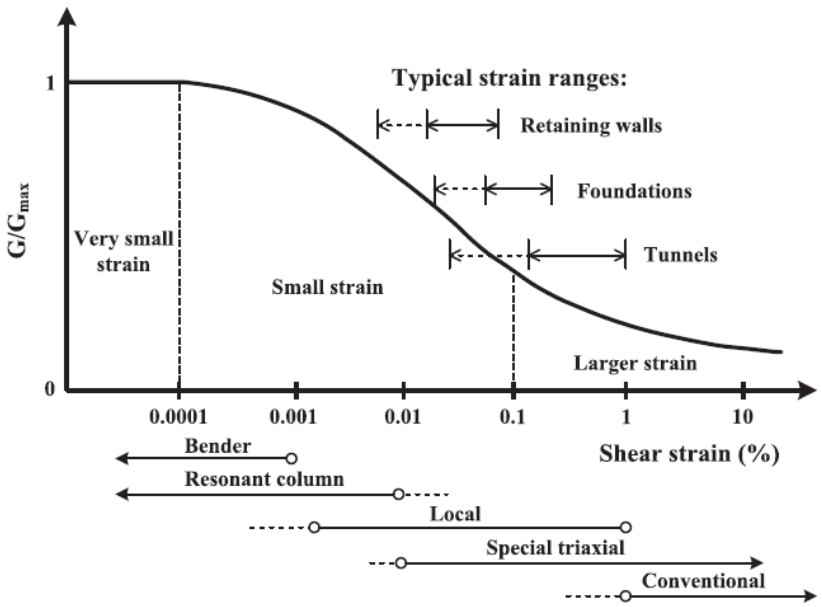

Figure 4-5: Normalized stiffness degradation (Atkinson and Sallfors, 1991).

The estimation of these parameters is more practical by using laboratory tests, despite the proven efficiency of empirical formulations and in-situ tests. Their estimation is more practical by using laboratory tests, despite the proven efficiency of empirical formulations and in-situ tests. Usually, $G_{max} = (6\ to\ 8)E_m$ indicated in CFMS (2011) was quite close to that obtained from laboratory results in FEDRE project. Down-hole seismic test (Ashford, et al., 2000) and seismic cone penetration test (Dong, 1998) are iBRIn-situ tests to characterize the shear modulus at small strain. The reference threshold shear strain $\gamma_{0.7}$ is correlated by (as written in equation (4.30)). It also could be found in a more complex representation for the stiffness degradation curve suggested by Ishibashi and Zhang (1993). For a precise estimation of HSS model parameters, a high resolution nearly 1 micro strain (Santagata et al., 2005) must be achieved. Cyclic triaxial test and resonant column devices are common to assess the dynamic properties of soils via laboratory experiments. They operate at a wide range of strain levels (10^{-5} % of γ to 10 %) and excitation frequencies (0.2 Hz of γ to 170 Hz) (Khan et al., 2011). The shortcoming of cyclic triaxial test is in its incapacity to impose a very low strain levels, this is therefore carried out by the resonant column in our case. Their results are usually merged to present the stiffness degradation curve.

$$\gamma_{0.7} = 0.0021 I_{\mathrm{p}} - 0.0055 \qquad \textbf{(4.30)}$$

$\gamma_{0.7}$ is calculated from the combined curve of the degradation of the shear modulus strain (Correia et al., 2001) level which constitutes 70% reduction from the initial shear modulus.

4.4 Geotechnical investigation

The loading complexity imposed by onshore wind turbines significantly influences the behaviour of the soil. Therefore, it is essential to establish an appropriate geotechnical investigation protocol. According to the guidelines of (CFMS, 2011), it is advisable to perform at least four soundings per wind turbine, by using weather pressuremeter test (PMT) or Cone Penetration Test (CPT). Additionally, coring at the centre of the wind turbine is necessary, and the quantity of coring

depends on the number of wind turbines being considered. In Risø and Veritas (2002) recommendations stipulate that performing CPT tests beneath the gravity foundation is imperative. The number of required boreholes is determined based on the prevailing soil conditions and the structural dimensions. Both sets of recommendations from underscore the importance of using cyclic triaxial tests to evaluate the degradation of soil strength under cyclic loading conditions.

Within this project, a comprehensive soil investigation was undertaken, encompassing a pressuremeter test, ten static penetrometer tests, and a total of 15 meters of core drilling (Figure 4-6). The soil stratigraphy is identified based on the

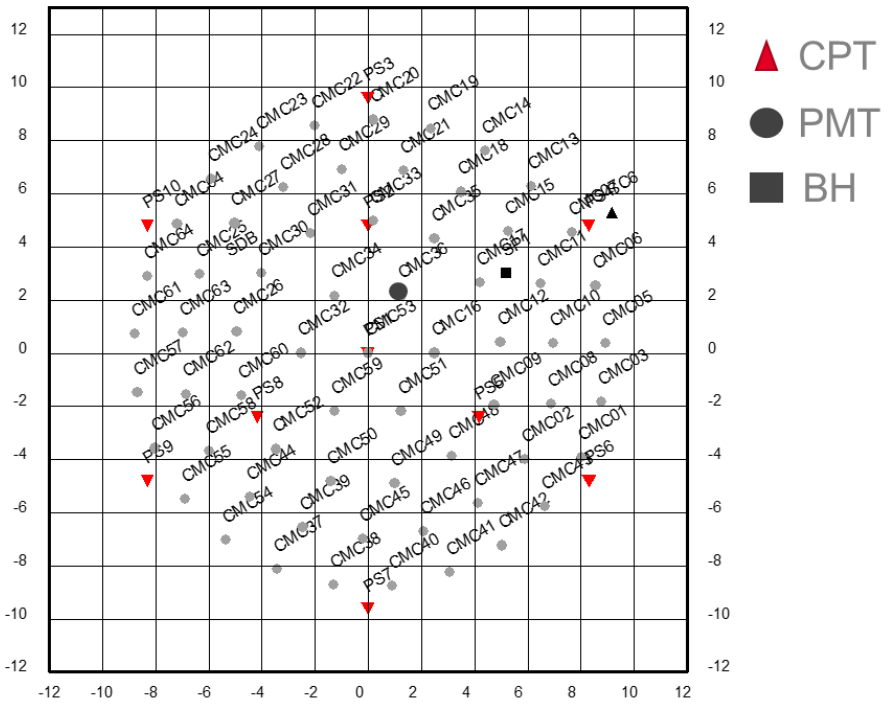

Figure 4-6: In-situ tests conducted under the footprint of the WTF (positions in relation to the CMC soil reinforcement.

The core drilling revealed a one-meter section of undisturbed soil (Figure 4-7). A range of laboratory evaluations were performed to study the soil's mechanical behaviour under both monotonic and cyclic conditions, including Oedometer tests, Static Triaxial tests, Cyclic Triaxial tests, and Resonant Columns. These tests were modelled using FEM to establish material parameters. This topic is not discussed in the current document.

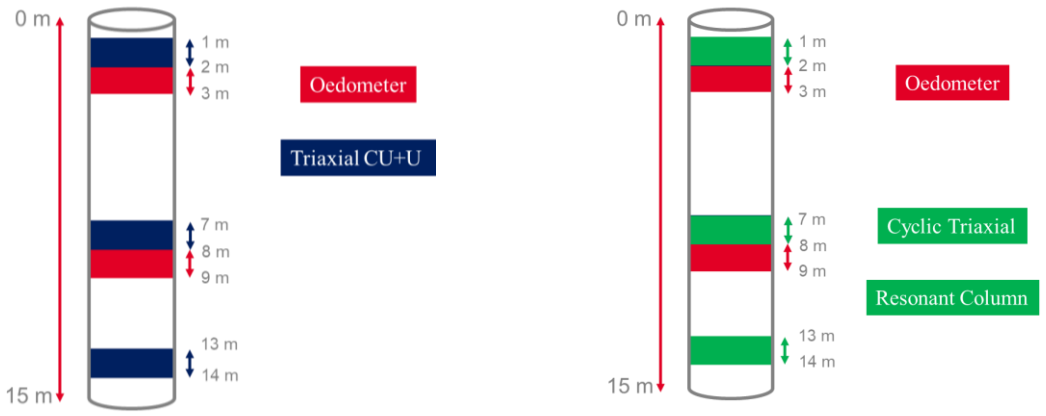

Figure 4-7: Tests in relation to core drilling.

4.5 Numerical modelling of the static load test on isolated rigid inclusion

In order to quantify the interaction between the soil and rigid inclusions, a static load test was conducted on instrumented CMC-type rigid inclusions. Using FEM, the static load test was simulated on a real-scale model. Verification of the original geotechnical parameters and characterization of the soil layers at the interface were critical to the accuracy of the numerical model. By comparing the simulated results with the measured responses from the static load test, a calibration process was performed at the rigid soil inclusion interfaces and base resistance to match the experimental measurements.

4.5.1 Model representation

The test was conducted close to the wind turbine "E6" (Figure 4-8 (a)) to replicate the lithological properties of the soil beneath the wind turbine foundation. The SLT was replicated in FEM using asymmetric modelling (Figure 4-8 (b)). The model is defined by a rigid inclusion centred in a natural soil volume. This environment converts the three-dimensional structures into a circular cell by preserving the area of the inclusion and the soil. This reduces the computational cost compared to full three-dimensional modelling while still capturing the essential characteristics of the problem. This type of modelling is suitable for circular structures with a uniform radial cross-section and load distribution around the central axis. It has been successfully used to represent the static load tests (Said et al., 2009; Satibi, 2009; Racinais and Burtin, 2017).

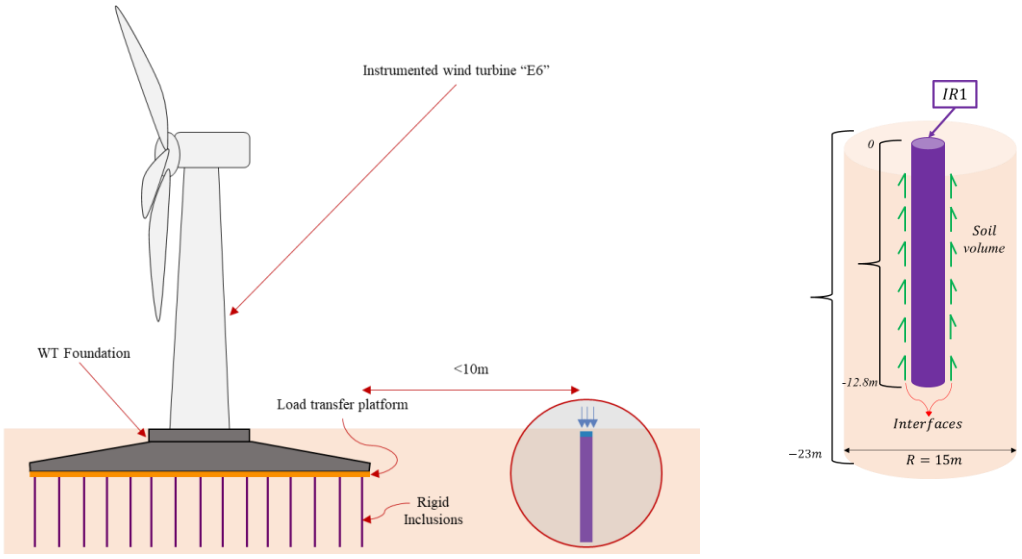

(a) (b)

Figure 4-8: (a) Schematic representation of the static load test next to the instrumented wind turbine (not to scale), (b) axisymmetric modelling representation.

4.5.2 Geotechnical parameters

In the static load test phase, geotechnical parameters were determined based on in-situ tests conducted directly under the footprint of the wind turbine. The tests performed included 10 electrical penetration tests (CPT), 1 Pressuremeter test (PMT), and one core boring (Figure 4-6). These tests were strategically distributed to gather information about the soil conditions near IR1.The soil layering are consistent with the following characteristics: 4.5 m of loose silt underlain by a 5.5 m thick compact layer of clayey silt ending in a compact horizon. The water table is estimated to be directly below the head level of IR1, as indicated by the soil identification tests and the observation during the test (Figure 4-9).

The evaluation of these tests in addition to the Menard database in the area allowed the characterization of the soil profile in the vicinity of IR1. The soil stratification was found to have the following characteristics:

- Loose Silt: The uppermost layer of the soil profile is approximately 4.5 meters thick and consists of loose silt.
- Clayey Silt: Below the loose silt layer, there is a compact layer approximately 5.5 meters thick composed of clayey silt.
- Compact Horizon: The clayey silt layer transitions into a compact horizon, which is the lowermost part of the soil profile.

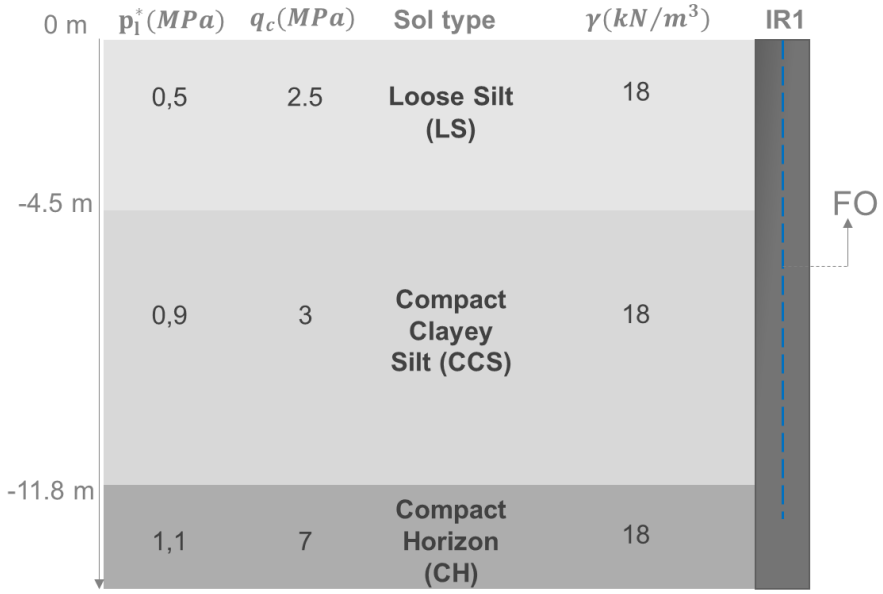

Figure 4-9: (a) Soil layering.

During the static load test of an isolated rigid inclusion, the mobilized resistance is mainly attributed to two physical phenomena: interfacial resistance and base resistance along the columns shaft. During the load test, conditions such as soil properties, rigid inclusion installation method, have a direct influence on the mobilization of column resistance.

The effective radial stress determines the contact friction between the rigid inclusion and the surrounding soil volume (Satibi, 2009). In the effective stress approach to simulate friction in static load tests, the contact friction between the rigid inclusion shaft and the surrounding soil volume is governed by the effective radial stress. This approach is commonly used in numerous studies to analyse the behaviour of such interactions. In this approach, the friction surface between the inclusion and the soil is assumed to be vertical. The frictional behaviour at the interface is based on the Mohr-Coulomb failure criterion, which is theoretically (Chandler, 1968; Kulhawy, 1984), been related by the following equation:

$$\tau_s = \sigma'.tan\delta = K_0.\sigma'_{v0}.tan\delta \qquad \textbf{(4.31)}$$

Where, σ' represents the effective radial stress acting on the interface, δ is the friction angle at the interface, σ'_{v0} is the effective vertical stress acting on the interface and K_0 is the lateral earth pressure coefficient.

In the presented model, it is assumed that the behaviour of the soil layers and the interface follows the linear-elastic, perfectly plastic law with the "Mohr-Coulomb" failure criterion. According to this criterion, failure occurs when the shear stress reaches the friction angle of the soil multiplied by the normal stress. The parameters required for the modelling are presented in Table 4.1 & Table 4.2. As mentioned previously, at this stage, the soil characteristics are directly correlated from the in-situ tests.

The Young's modulus was calculated by the following correlation from the PMT test (Combarieu, 2006):

$$E_Y = \mathrm{k}\frac{E_m}{\alpha} \tag{4.32}$$

Where, k represents the ratio between horizontal and vertical stresses, E_m represents Menard pressuremeter modulus, and α represents the rheological coefficient.

Table 4.1: Initial parameters of the interface Soil – RI

Soil Layer	$\gamma(kN/m^3)$	$c'(kPa)$	$\varphi'(°)$	$E_Y(MPa)$	R_{inter}
Loose Silt	18	5	25	$E_M/\alpha = 12$	1
Compact Clayey Silt	18	10	25	$E_M/\alpha = 24$	1
Compact Horizon	18	10	30	$E_M/\alpha = 33$	1

Table 4.2: Initial anchorage parameters

Soil Layer	$\gamma(kN/m^3)$	$c'(kPa)$	$\varphi'(°)$	$E_Y(MPa)$
Compact Horizon	18	10	30	$E_M/\alpha = 33$

We could distinguish three zones of input parameters:

(1) The natural soil was modelled using Mohr-Coulomb elastic-plastic model,
(2) The rigid inclusion was modelled using linear elastic model,
(3) The interface between the soil and the inclusion was set from the adjacent soil.

4.5.3 Meshing and boundary conditions

The mesh is refined at the head and base levels of the inclusion to capture the local behaviour more accurately. Coarser meshes are employed in the direction of the model boundary, where the overall behaviour is less influenced by local effects. The finite element mesh in the model is characterized by the following:

- Element type and connectivity: The model utilizes a triangular mesh with 15 nodes of 4th order interpolation, resulting in a total 30,189 nodes (Figure 4-10).
- Element size: The size of the elements in the mesh is represented in (Figure 4-11(a)), reflecting the smallest size next to the point of interest for the accuracy of the results.
- Mesh quality: The quality of the mesh is automatically checked (Figure 4-11(b)). It is shown with a scale range from 1 to 0, with 1 representing the best mesh quality.
- An interface is defined between the inclusion and the soil to model the interactions. Its thickness is set by default in Plaxis, which employs a virtual thickness to represent it (PLAXIS Manual, 2020).

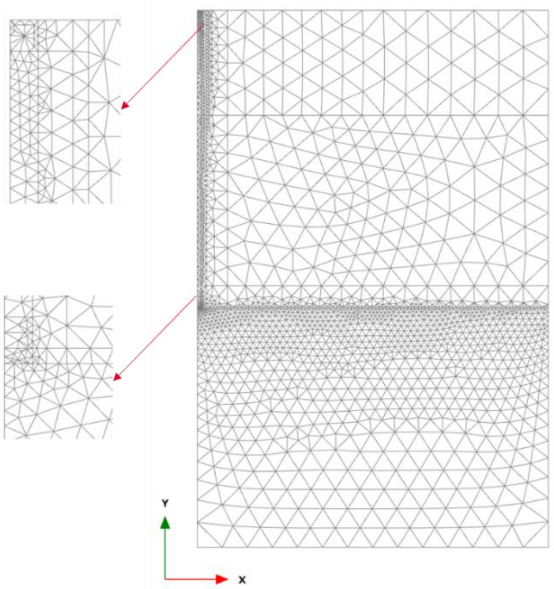

Figure 4-10: 2D mesh.

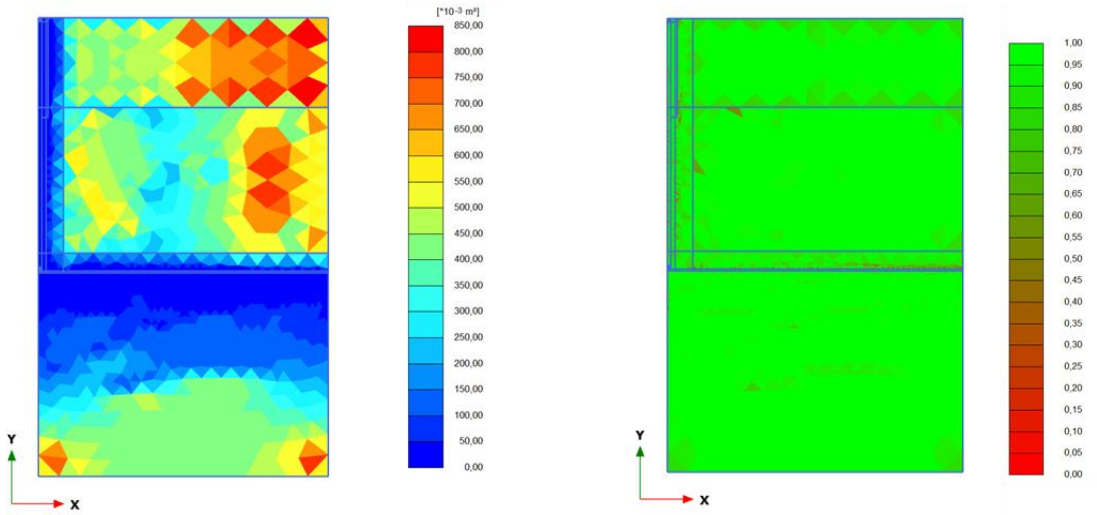

(a) (b)

Figure 4-11: (a) Element size, (b) Mesh quality.

The boundary conditions for the model are summarized as follow:

- The boundaries of the area under study are defined as 23 m along the Y axis and 15 m along the X axis. This defines the extent and dimensions of the modelled area.
- At the outer vertical boundary of the model, horizontal displacements are constrained to zero, implying that no horizontal movement is allowed at this boundary.
- At the lower boundary, displacements are constrained to zero, suggesting that the vertical and horizontal movements are restricted at this boundary.

4.5.4 Loading conditions

The loading applied to the rigid inclusion in the modelling is determined based on the obtained from the load cell installed on the top of the inclusion during the SLT. The load is uniformly applied to the head of the inclusion. The measurements help to ensure that the loading applied in the

numerical model accurately represents the real loading conditions experienced onsite. The loading schedule for the SLT is designed to replicate the loading conditions experienced on-site (Figure 3-42).

4.5.5 Phases

To accurately simulate the behaviour of rigid inclusion during the loading test, the analysis is divided into three phases, each representing a particular phase of the test. These phases are determined based on the sequence of events and the desired focus of the analysis (Figure 4-12).

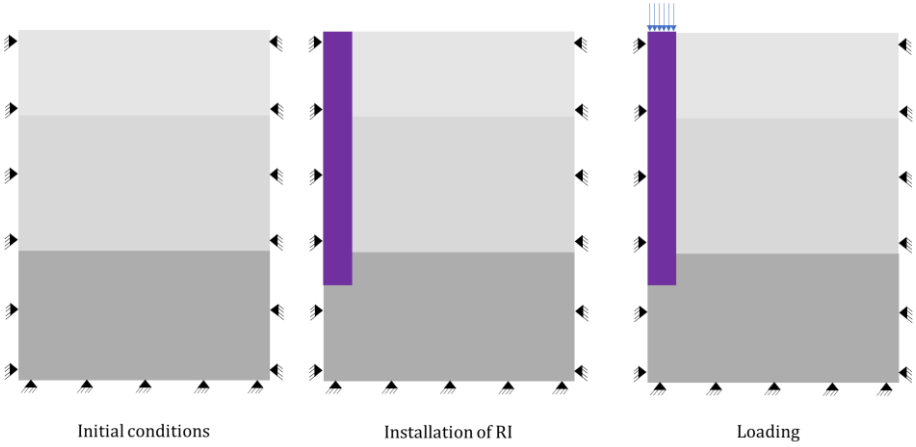

Figure 4-12: Calculation phases of the FEM.

4.6 Results

The simulation of the SLT with the initial parameters led to an underestimation of the stiffness and the bearing capacity of the rigid inclusion, which was significantly higher than the measured values (Figure 4-13). This discrepancy between the simulation and the actual test results indicates that the initial parameters used in the model do not accurately represent the behaviour of the soil and the interaction with the rigid inclusion.

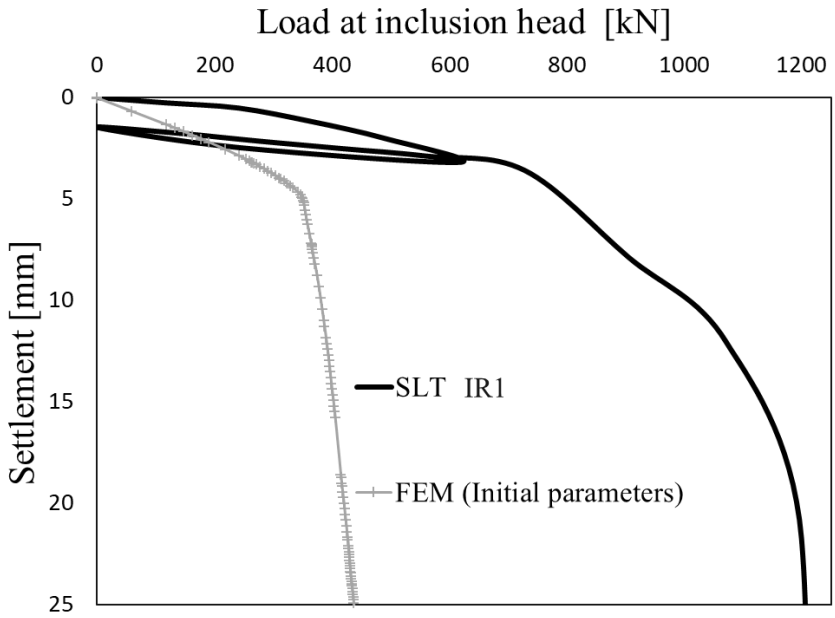

Figure 4-13: Settlement of IR1 (FEM vs Measurements).

To address this issue, further analysis and calibration of the model parameters are required. This can involve adjusting the material properties of the soil, such as the stiffness and strength parameters, as well as the interface properties between the inclusion and the soil. In addition to the choice of the soil model. Based on the literature review (Said et al., 2009; Satibi, 2009; Racinais and Burtin, 2017), it is recommended to perform a calibration of the interface parameters between the inclusion and the soil by targeting the soil stiffness and the allowable shear values. In addition to calibrating the base resistance, determining the interaction between the column tip and the anchorage layer.

Calibration of the FEM parameters:

The calibration process in this context focuses on adjusting the stiffness parameters and strength parameters of the soil at the interface and anchorage layer. These parameters are key components of the Mohr-Coulomb soil model, which operates in both the elastic and plastic domains. The elastic behaviour of the soil is primarily influenced by the Young's modulus. This allows the calibrated model to better capture the elastic response observed in the static load test. On the other hand, the plastic behaviour of the soil is governed by the strength parameters, such as cohesion and friction angle. By calibrating these parameters, the model can accurately reproduce the plastic deformation and failure mechanisms observed during the static load test (Figure 4-14).

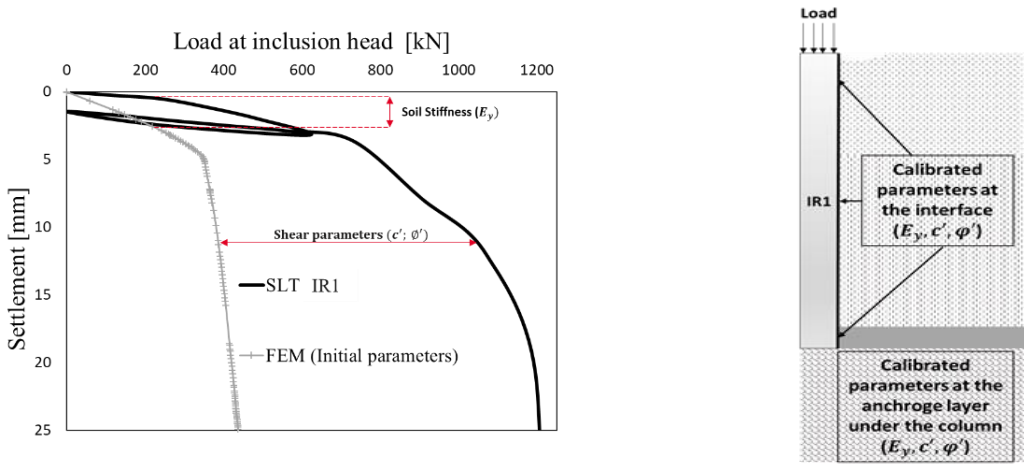

(a) (b)

Figure 4-14: (a) Calibration Strategy, (b) zones of calibration.

4.6.1.1 Skin friction mobilization

The comparison between experimental measurements, analytical analysis and numerical analysis is presented for the mobilization of lateral skin friction (Figure 4-15). The first two lines of the trilinear relationship proposed by Frank and Zhao (F&Z) have slopes similar to the measurements, indicating good agreement with respect to the overall trend of mobilization of skin friction. However, there is a slight difference in the level of the limit skin friction. On the other hand, the results of the finite element method analysis (FEM) show a significant deviation from the observed behaviour at the interface. This suggests that the numerical model used in the analysis of FEM may not accurately capture the mobilization of lateral skin friction.

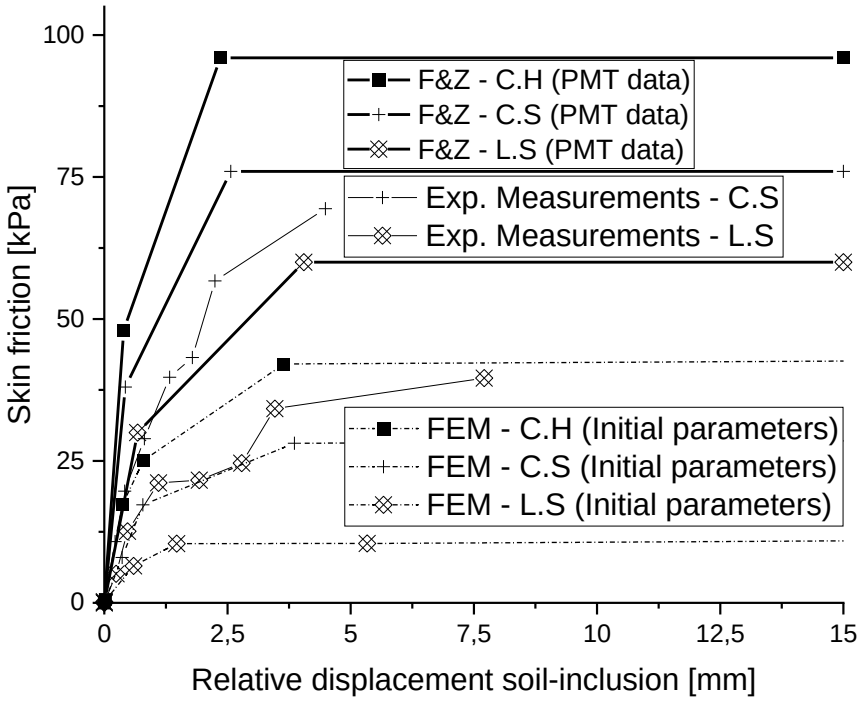

Figure 4-15: Lateral skin friction mobilization – Exp vs FEM and F&Z.

In the calibration process, the optimum values of the soil parameters at the interfaces were determined as follows:

To simulate the elastic behaviour of the column: $Ey = 6\frac{Em}{\alpha}$ (Multiplying the initial Young's modulus by (6)

To mobilize the maximum friction at the interface, following the equation (4.33), the mobilization the shear stress at the interface is manipulated to achieve the limit skin friction (q_s):

$$\tau_s = R_{inter}(c + \sigma'_v \tan(\varphi)) = q_s \quad \textbf{(4.34)}$$

Where, R_{inter} represents the mobilization of interface properties.

The ground near a localized spot of the column shaft plasticizes during the loading increment and prevents the friction from being properly mobilized. In order to address the issue, we have readjusted parameters of a thin layer of the soil at this spot. Using these parameters, the adopted model correctly simulates the mobilization of friction on all the layers considered (Figure 4-16).

The pressuremeter data, using the Frank & Zhao semi-empirical law, were also calibrated experimentally. For the initial results, we determined q_s of 60 kPa and 75 kPa for L.S and C.S, respectively, while the measurements reached a maximum of 40 kPa and 60 kPa, respectively.

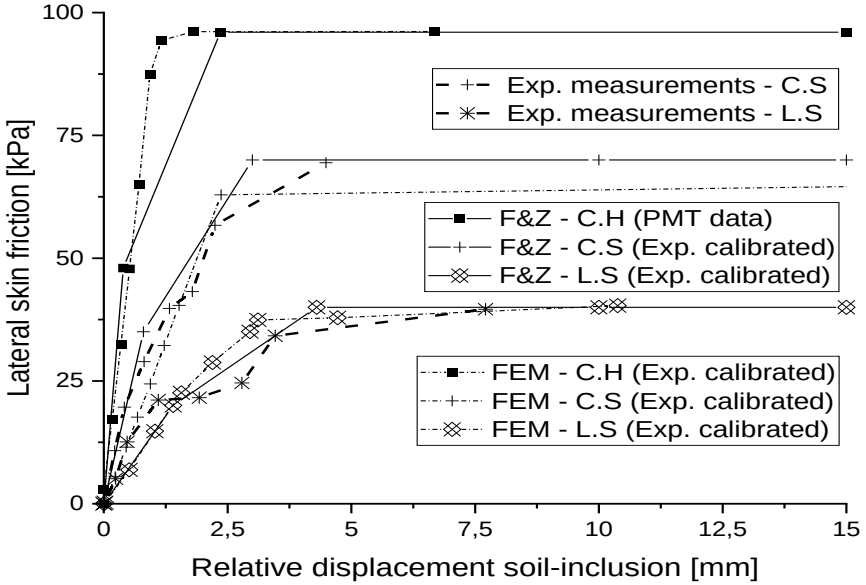

Figure 4-16: Lateral skin friction mobilization – Experimentally calibrated.

4.6.1.2 End bearing resistance mobilization

In the calibration process, the optimum values for the anchorage layer parameters were determined as follows:

- $Ey = 3\frac{Em}{\alpha}$ (multiplying the initial Young's modulus by 3)

- $c' = \frac{q_b}{9}$, the effective cohesion of the anchorage layer is set to be equal to the ultimate base resistance divided by a factor of 9, $c' = \frac{q_b}{9}$

The slope of the curve obtained from the readjusted parameters is equivalent to that of the analytical curve, indicating a good match between the numerical and analytical methods (Figure 4-17). This suggests that the calibration process successfully captured the behaviour of the anchorage layer.

It is important to note that there may still be a difference in the maximum load between the analytical and numerical methods. This difference can be attributed to the estimation of an infinite load and infinite displacement in the semi-empirical law of Frank & Zhao's law, which was used in the analytical approach. In contrast, the numerical method applied a maximum load of 1200 kN at the column head and calculated the corresponding displacement.

By calibrating the parameters and limiting the load in the numerical model, a more realistic estimation of the behaviour and response of the system was obtained. The calibrated parameters and the corresponding load-displacement relationship can provide valuable insights for further analysis and prediction of the system's behaviour under different loading conditions.

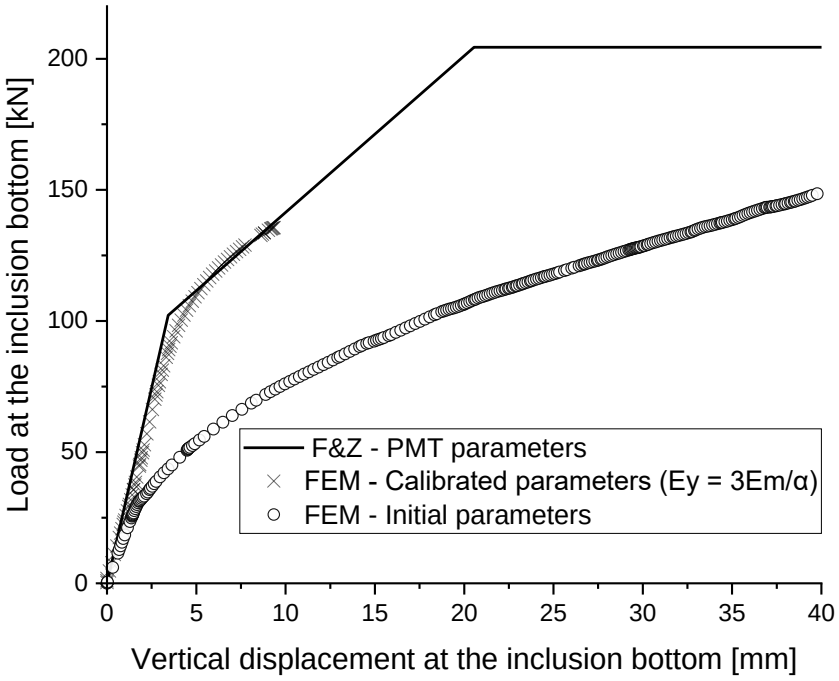

Figure 4-17: Base resistance F&Z vs FEM.

4.6.1.3 Load - displacement curve

The load-displacement behaviour at the column head level during the SLT, including the results obtained from Frank & Zhao's law, the initial parameters in the axisymmetric model using PLAXIS 2D, and the calibrated parameters are illustrated in (Figure 4-18). Initially, a good correlation is observed between the analytical output of Frank & Zhao's and the SLT measurements. However,

when using the initial parameters in the FEM modelling, there is a discrepancy in reproducing the loading test. The initial slope of the curve and the failure point simulated at 400 kN are significantly different from the other two curves. As a result of calibration, the FEM simulation approaches the test results more closely. The calibrated curve of Frank & Zhao's law based on the pressuremeter data exhibits a similar behaviour compared to the experimental measurements.

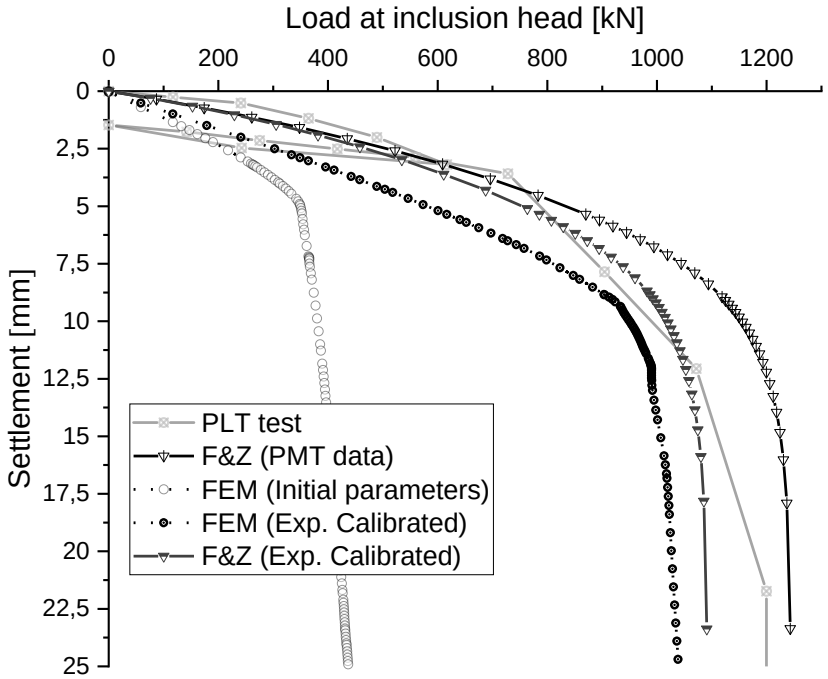

Figure 4-18: Settlement at the IR1 head. Comparison between FEM, F&Z values and measurements.

This indicates that by refining and calibrating the parameters in the FEM model, a better representation of the SLT behaviour can be achieved, leading to improved accuracy in predicting the load-displacement response of the system.

4.6.1.4 Deformation analysis – Axial load distribution

The first part of each experimental result shown in dotted lines (Figure 4-19). This adjustment is made to account for the noise present in the raw data of the measured load applied to the head of the rigid inclusion. The noise in the initial data can be caused by various factors such as instrumentation limitations or environmental influences. On the other hand, the remaining part of the experimental results, represented by solid lines, is directly transformed from the raw strain data measured by the optical fibre. The strain measurements provide information about the deformation and behaviour of the system during the static load test. By analysing the strain data, important parameters such as displacements and settlements can be determined.

In the analysis of the column behaviour during the static load test (SLT), both the axisymmetric model and the semi-empirical law of Frank & Zhao were calibrated to reproduce the skin friction and end bearing capacity based on experimental calculations and pressuremeter data, respectively. The axial distribution of the load from both methods was compared to the experimental data, as shown in (Figure 4-19). At an applied load of 904 kN at the head of the column, the calculated axial loading from both Frank & Zhao and PLAXIS (axisymmetric model)

closely matched the real data, indicating the successful adjustment of parameters in the numerical model and its convergence with the analytical approach. This validation of the numerical model strengthens the confidence in its ability to accurately simulate the behaviour of the column under load.

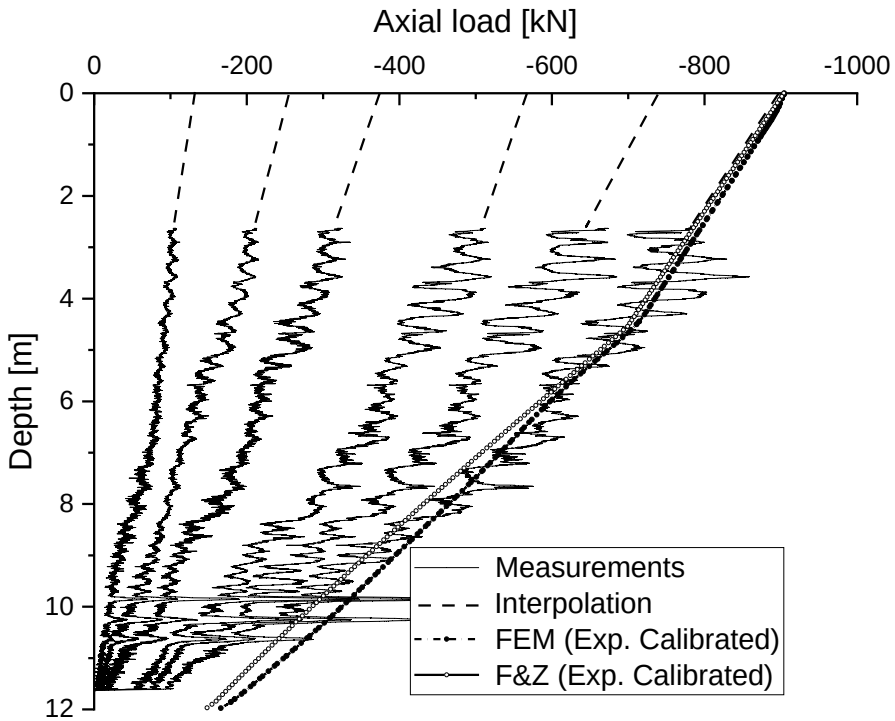

Figure 4-19: Axial load distribution.

It should be noted that during the SLT, the optical fibre signal inside the Cemented Mortar Column (CMC) was lost, resulting in the absence of experimental data under a load equal to 1071 kN. However, using the calibrated model, this value could be effectively estimated, providing valuable insights into the behaviour of the column at higher loads. The summary of the calibrated materials used in the FEM is summarixed in the table below:

Table 4.3: Calibrated parameters of the interface Soil – RI

Soil Layer	$\gamma(kN/m^3)$	$c'(kPa)$	$\varphi'(°)$	$E_Y(MPa)$	R_{inter}
Loose Silt	18	40	0	$6\frac{Em}{\alpha} = 72$	1
Compact Clayey Silt	18	70	0	$6\frac{Em}{\alpha} = 144$	1
Compact Horizon	18	96	0	$6\frac{Em}{\alpha} = 198$	1

Table 4.4: Initial anchorage parameters

Soil Layer	$\gamma(kN/m^3)$	$c'(kPa)$	$\varphi'(°)$	$E_Y(MPa)$
Compact Horizon	18	$\frac{q_b}{9} = 224$	0	$3\frac{Em}{\alpha}$=99

4.6.1.5 Displacement method impact

As highlighted earlier in this document, this project adopts the displacement technique for the installation of CMCs. This method embeds the columns into the earth by shifting the soil laterally instead of removing it entirely. This strategy diverges significantly from traditional methods like bored piling and the Continuous Flight Auger (CFA), which necessitate the excavation of soil to accommodate the pile. Renowned for its efficacy in foundation engineering, the displacement technique offers a sustainable alternative that significantly reduces the volume of spoil generated on-site.

The process of installing CMCs through lateral displacement can lead to disturbances in the surrounding terrain (Suleiman et al., 2016). This activity may escalate the radial stress within the vicinity of the CMCs, potentially improving the lateral resistance between the soil and the columns (Figure 4-21). However, the ability to accurately predict the increase in stress levels and its extent remains underdeveloped both in existing literature and within the scope of this dissertation. Consequently, this gap in understanding could lead to the underestimation of skin resistance during static load testing (Figure 4-18).

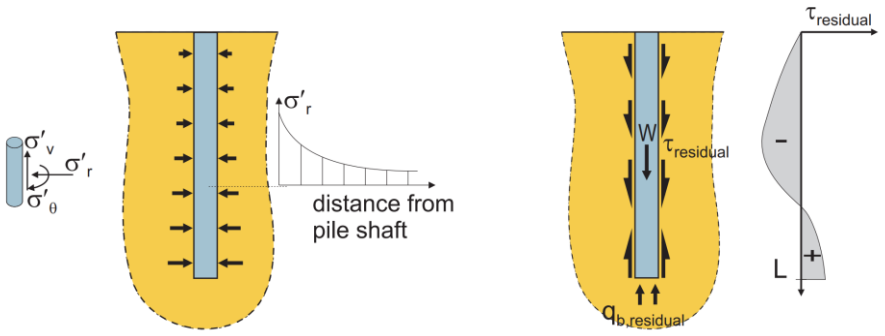

Figure 4-20: Impact of Pile Displacement Installation on Radial Stress, Skin Friction, and Tip Pressure (Satibi, 2009).

Most studies have focused on the load-deformation responses of CMCs or on determining shaft resistance, few have explored the impact of CMC installation. This includes considerations such as numerical simulations in granular soil, conducting field studies, and performing small-scale model tests. As an early analytical approach to predict the increase in lateral stress, several empirical methods were developed, and we can cite as example (Lancellotta, 1995). In numerical modelling, recent studies highlights this phenomena in finite difference method (Nguyen et al., 2016) and in FEM (Satibi, 2009).

4.7 Three-dimensional modelling of onshore wind turbine underlined by rigid inclusions

In the three-dimensional modelling of the reinforced soil domain under an onshore wind turbine, a comprehensive analysis using nonlinear finite element modelling was performed to capture the full complexity of the soil-structure interactions. This approach allows for a detailed assessment of the response of the reinforced domain to axial, rotational, and lateral loading acting on the wind turbine foundation.

The modelling process involves creating a virtual 3D environment where the wind turbine structure, including the tower and foundation, is represented. In addition to the soil layers, the load transfer platform, and the rigid inclusions within the soil mass. The material properties and the local soil-structures interactions are integrated into the model based on the calibrated data obtained from laboratory tests, in situ measurements and the FEM modelling at the level of unit cell axisymmetric modelling.

In the comparison between the results of the 3D modelling and the monitoring data, a good agreement was observed, particularly regarding the load transfer to the rigid inclusions under different loading conditions. The modelling output served as valuable databank for the macroelement modelling. We acknowledge that the presented 3D modelling has certain limitations. One notable limitation is the non-application of cyclic loading in the analysis, despite the capability of the soil modelling to capture this type of loading. However, the loading values employed in the model are directly derived from the measurements, taking into account the wind speed and wind direction acting on the wind turbine.

The research background on three-dimensional modelling of onshore wind turbine foundations with rigid inclusions is indeed limited, and only a few studies have specifically considered this aspect. Two notable works in the literature include the studies of (Plomteux, 2010; Pham et al., 2018). In the former (Plomteux, 2010), a full design methodology for rigid inclusions in onshore wind turbine foundations was developed using both analytical methods and three-dimensional finite element analysis. The study aimed to establish a comprehensive understanding of the behaviour and response of the foundation system underlined by rigid inclusions. However, both studies didn't focus cyclic axial loading, and their loading values were derived from the classical loading schedule typically applied to wind turbine foundations.

4.7.1 Model representation

The global geometry of the numerical model is based on the properties of the reference wind turbine as described in (Figure 3-4). In the numerical model certain simplifications and assumptions are made due to the computational costs and the focus of the research. Components of the wind turbine system, such as the blades, nacelle, and generator, are simplified. Their effects on the system are accounted for by considering their weight and applying appropriate external loads or simplified representations. In this approach, the resonance problem is not modelled, and the simplification suggested by (Nikitas et al., 2016) is therefore followed. The schematic in (Figure 4-21) serves as a visual representation of the general features of the model and the assumptions.

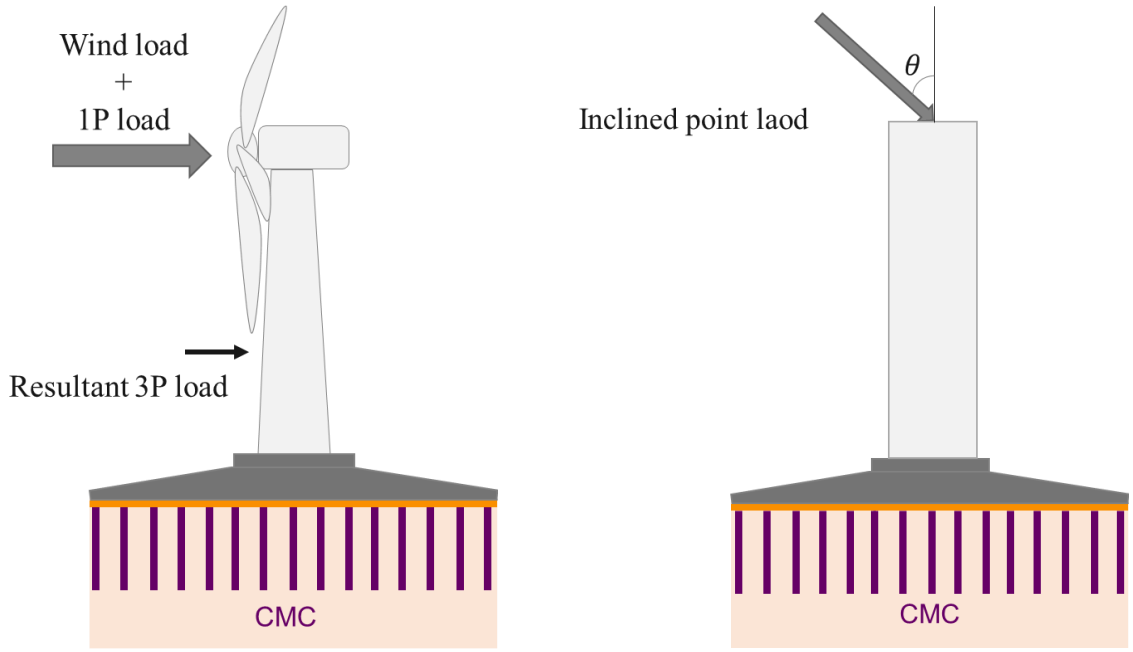

Figure 4-21: a) Schematic representation of the real scale, (b) 3D modelling simplification.

4.7.2 Structural modelling assumptions

The essential simplifications to be highlighted in this modelling are as follows:

- Inclined Point Loading: Instead of modelling the turbine components weight and wind loading directly, an inclined point loading with angle θ is applied to the tower. The vertical component of the load represents the equivalent vertical load of the structure, while the horizontal components represent the external horizontal load acting on the structure. The distance between the load and the foundation is multiplied by the force to represent the overturning moments. Several load configurations were tested before using this specific configuration (Figure 4-22).
- Modelling of Rigid Inclusions: The rigid inclusions are modelled using a calibrated embedded beam row instead of volumetric material. This approach is commonly used to model rigid inclusions in numerical simulations.

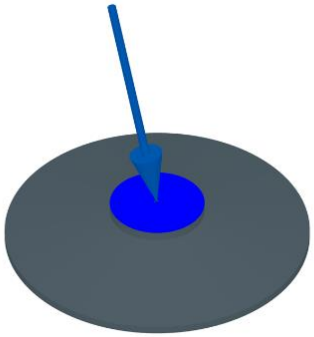

Figure 4-22: One of the tested loading configurations, not discussed in this document.

The model components adapted in this section are shown in (Figure 4-23): the load application, beam loading and the rigid inclusions.

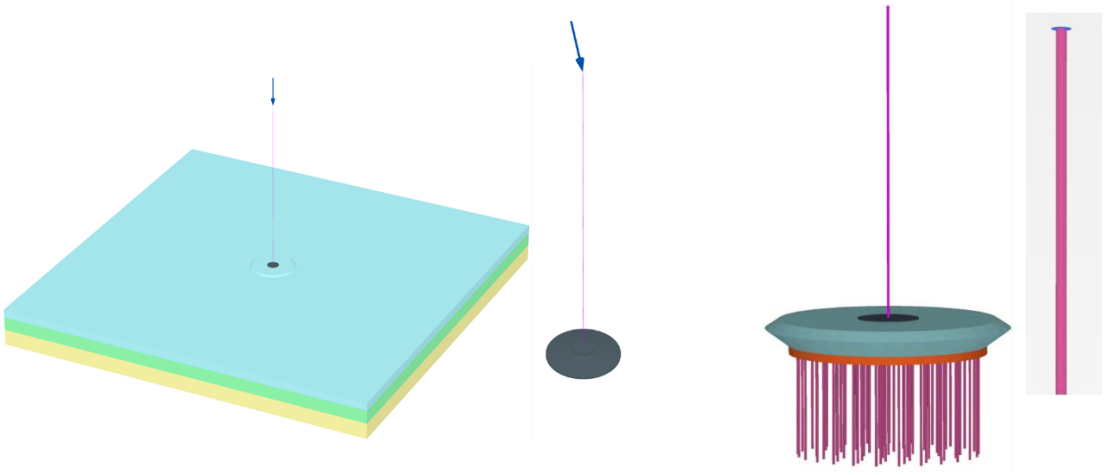

(a) (b)

Figure 4-23: (a) Load application (b), Rigid inclusions and beam loading representation.

4.8 Geotechnical parameters

In this phase of modelling, the geotechnical parameters (Table 4.5) were determined based on the conclusions from the individual parts of the dissertation:

- The SLT test: The interface parameters of Soil- Inclusion.
- Calibration of laboratory tests: The soil volume parameters are derived from the calibrated FE modelling of the tests.

4.8.1 Load transfer platform

In this project, the load transfer platform (LTP) is simulated with an elastic, perfectly plastic model based on the Mohr-Coulomb criterion. This model is commonly used for LTP (Jenck, 2005; Sloan, 2011). It assumes that the soil behaves elastically up to a certain point and then deforms plastically when the shear stresses exceed the shear strength parameters of the soil. This phenomenon strongly affects the load transfer to the head of the rigid inclusions.

4.8.2 Natural soil volume

The soil layering of the model follows the assumption made in section (4.5.2). The difference in this model is the soil models. Here is a summary of the soil models used for each layer.

Table 4.5: Soil layers parameters (HSS)

HSS parameters	Loose Silt	HSS parameters	Compact Clayey Silt	HSS parameters	Compact Horizon
$E_{50}{}^{ref}(kPa)$	11000	$E_{50}{}^{ref}(kPa)$	11000	$\boldsymbol{E_{50}{}^{ref}(kPa)}$	38000
$E_{oed}{}^{ref}(kPa)$	9000	$E_{oed}{}^{ref}(kPa)$	5000	$\boldsymbol{E_{oed}{}^{ref}(kPa)}$	40000
$E_{ur}{}^{ref}(kPa)$	40000	$E_{ur}{}^{ref}(kPa)$	60000	$\boldsymbol{E_{ur}{}^{ref}(kPa)}$	95000
m	0.7	m	0.85	m	0.85
c' (kPa)	15	c' (kPa)	17	c' $(\boldsymbol{kPa})$	35
ϕ'(°)	34	ϕ'(°)	28	ϕ'(°)	27
ψ (°)	0	ψ (°)	0	ψ (°)	0
$G_0{}^{ref}(kPa)$	22000	$G_0{}^{ref}(kPa)$	30000	$\boldsymbol{G_0{}^{ref}(kPa)}$	48000
$\gamma_{0.7}$	0.011	$\gamma_{0.7}$	0.026	$\boldsymbol{\gamma_{0.7}}$	0.027
$P^{ref}(kPa)$	100	$P^{ref}(kPa)$	100	$\boldsymbol{P^{ref}(kPa)}$	100
POP (kPa)	340	POP (kPa)	340	POP (kPa)	0
ν	0.3	ν	0.3	$\boldsymbol{\nu}$	0.3

In the model, the rigid inclusions and the concrete foundations (15 GPa, underestimated) are represented with a linear elastic model. The modulus of elasticity of the rigid inclusions material is measured in situ in the laboratory and provides accurate values for their stiffness.

4.8.3 Meshing and boundary conditions

In the three-dimensional modelling, meshing plays a crucial role in generating a homogeneous mesh throughout the model and refining the mesh around areas of interest. However, it is noted that generating an appropriate mesh for the wind turbine foundation shape can be challenging due to its complex geometry (Motallebiyan et al., 2020). The meshing is evaluated systematically before the simulations.

The mesh is refined next to the foundation, LTP, rigid inclusions interfaces and the soil volume between the inclusions (Figure 4-24). Coarser meshes are employed in the direction of the model boundary, where the overall behaviour is less influenced by local effects. The finite element mesh in the model is characterized by the following:

- Element type and connectivity: The model utilizes a tetrahedral mesh with 10 nodes of 2nd order interpolation, resulting in a total 608,977 nodes (Figure 4-24).
- Element size: The size of the elements in the mesh is represented in (Figure 4-25 (a)), reflecting the smallest size next to the point of interest for the accuracy of the results,

- Mesh quality: The quality of the mesh is automatically checked (Figure 4-25 (b)). It is shown with a scale range from 1 to -1, with 1 representing the best mesh quality.

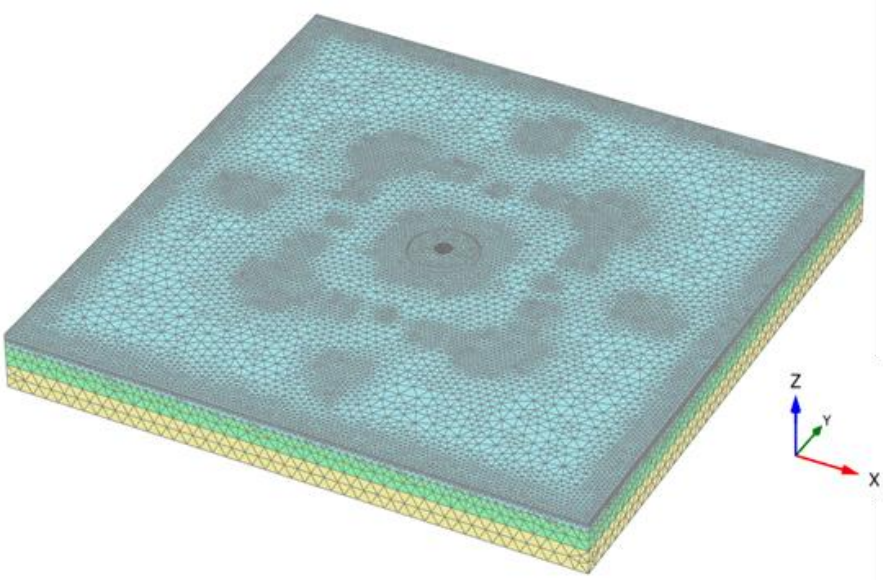

Figure 4-24: Meshing refinement (3D model)

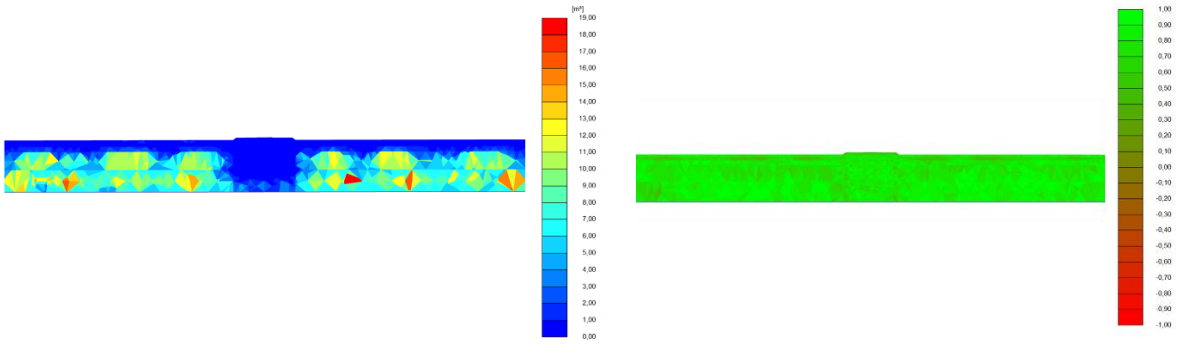

(a) (b)

Figure 4-25: (a) Element size, (b) Mesh quality

The boundary conditions for the model are summarized as follow:

- The boundaries of the area under study are defined as 100 m along the Y axis and 100 m along the X axis. This defines the extent and dimensions of the modelled area,
- At the outer vertical boundary of the model, horizontal displacements are constrained to zero, implying that no horizontal movement is allowed at this boundary,
- At the lower boundary, vertical and horizontal displacements are constrained to zero, suggesting that the movement is restricted at this boundary.

4.8.4 Loading conditions

The measurements of the load cells installed during the monitoring phase are then used to determine the load acting on the wind turbine foundation (Table 3.9). The loading conditions allow us to logically compare the results with the instruments since the same loading conditions are applied. This approach helps to verify the model's ability to capture the actual response of the wind turbine foundation and increases confidence in the accuracy of the numerical predictions.

4.8.5 Phases

To accurately simulate the behaviour of the global system, the analysis is determined based on the sequence of events during construction and the particular aspects that need to be captured in each phase (Table 4.6). By analysing each phase separately, the model can capture the incremental changes in stress and deformation as the construction progresses. This allows for a more comprehensive understanding of the behaviour of the system and helps identify potential issues or areas of concern during different stages of construction.

Table 4.6: Stage construction phases

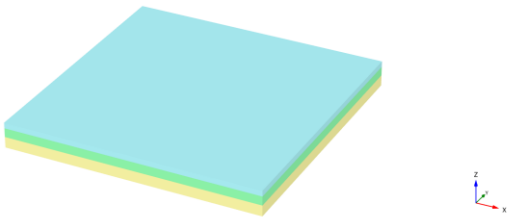

Initial phase

The initial state serves as a baseline for subsequent construction and loading phases. This means that the soil is assumed to be in its natural, undisturbed state before any excavation or loading takes place.

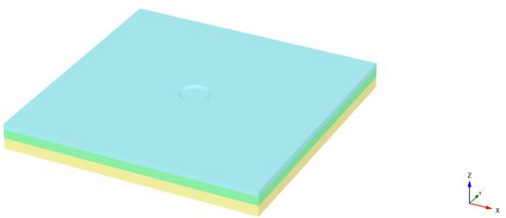

Excavation phase

During the excavation stage, the soil layers or volumes that are intended to be excavated are removed in the numerical model. The geometry and boundaries of the model are adjusted accordingly to reflect the excavated area. The analysis considers the changes in soil conditions and stress

redistribution that occur as a result of excavation.

LTP and rigid inclusions installation

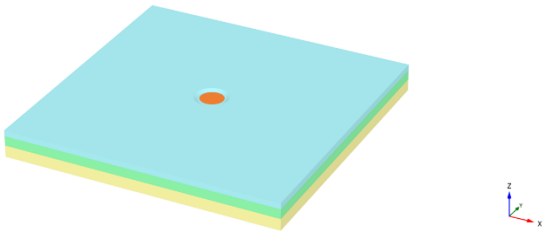

The load transfer platform is modelled as a distinct component that covers the area below the foundation.
Similarly, the rigid inclusions are modelled as separate elements that are installed into the ground according to the specified dimensions and layout from the actual site conditions.

Onshore wind turbine foundation

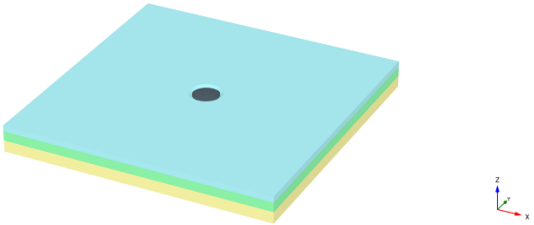

This phase of construction provided for a combination of the following sequence of construction in one step of modelling: Installation of lean concrete, and pouring of concrete. The equivalent weight and density of the foundation have been carefully modelled.

Backfilling

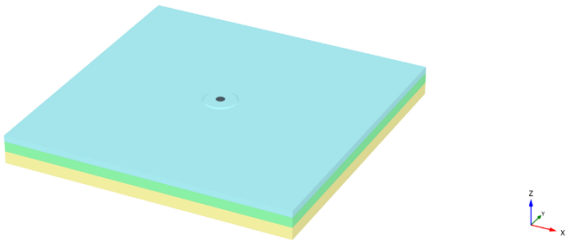

This construction phase is important for the stability of the wind turbine to resist the overturning moment. In this phase, the soil volume and density of the fill placed on site are reproduced.

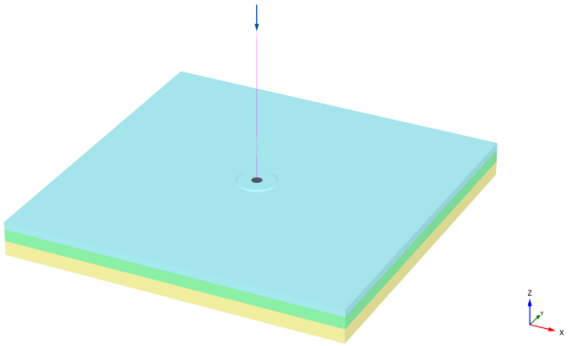

Wind turbine tower / Loading phase

In the model, the wind turbine tower is represented virtually. To simulate loading of the turbine as well as the external loads, a point load is applied at the top of the tower. By changing the magnitude and direction of the point loads, different loading scenarios can be simulated, allowing for a comprehensive analysis of the tower's response under different operating conditions.

4.8.6 Results

In the analysis of the three-dimensional modelling, the generated output provides a wealth of information regarding the behaviour of the system under consideration. To facilitate effective interpretation and understanding of the results, it is crucial to focus on the main physical phenomena that are of particular interest and relevance to the study. These phenomena are selected based on their significance and their comparison with the output of the macroelement modelling as well as the available measurements.

The following key aspects are typically studied and analysed within the different simulations:

- Settlement of the gravity foundation: The settlement of the gravity foundation, which includes both the overall settlement and any differential settlement across the foundation, is examined. This helps to evaluate the foundation's stability and the potential for uneven settlement, which can impact the structural integrity of the wind turbine.
- Settlement of the soil and rigid Inclusions: This includes assessing the magnitude and distribution of settlements in different areas of the system. Understanding the settlement patterns provides insights into the load transfer mechanisms and the effectiveness of the rigid inclusions in improving the soil's bearing capacity.
- Load Transfer to the rigid inclusions: The analysis focuses on quantifying the distribution of the load along the shafts of the inclusions. Therefore, identifying their behaviour under different loading conditions, and positions below the foundation.

4.9 Case study: Gravity foundation without ground improvement

The simulation represents the contact pressure at the base of the foundation as well as the differential settlement due to the loading from the wind turbine and without the presence of rigid inclusions (Figure 4-26). In this demonstration, the soil volume is modelled by MC.

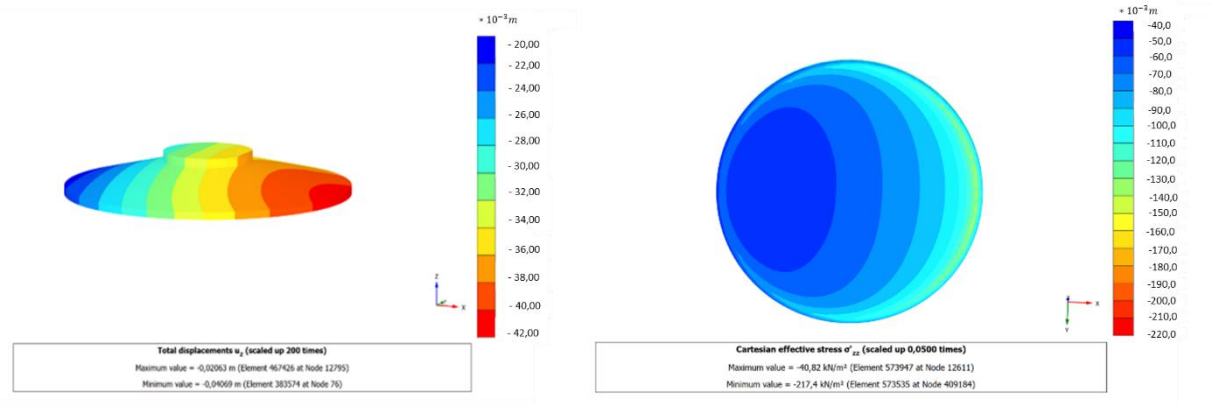

(a) (b)

Figure 4-26: (a) vertical settlement, (b) effective vertical stress.

In the simulation, the loading assigned to the wind turbine foundation is represented by the values of M_16: {V, H, M} = {4095 kN, 330 kN, 30000 kN.m}. It is important to note that the magnitude of the moment (M) in this specific case is smaller than the value of the service limit state (SLS) quasi-permanent condition indicated in the manufacture loading.

The foundation does not settle uniformly across its entire base, it experiences differential settlement at its edges, with settlements of 21 mm and 41 mm. The contact pressure distribution at the base of the foundation is characterized by a trapezoidal shape. The maximum contact pressure (qmax) is approximately -150 kN/m^2, while the minimum contact pressure (qmin) is -41 kN/m^2. This stress distribution reflects the mechanism of load transfer between the foundation and the underlying virgin soil.

4.10 Case study: Influence of rigid inclusions under WT foundation

The settlement of the foundation with soil reinforcement under the M_16 loading conditions is represented in (Figure 4-27). Two different soil models, the Mohr-Coulomb model (MC) and the Hardening Soil with Small Strain (HSS) model, are employed to characterize the soil volume. The simulation using the Mohr-Coulomb model (Figure 4-27 (a)) shows that the settlement of the foundation is reduced by approximately half compared to the simulation without soil reinforcement. Additionally, the effect of the soil model is significant in this case, by using the HSS, the foundation experiences less settlement. The effect of the soil modelling is studied in a form of sensitivity analysis in the following sections.

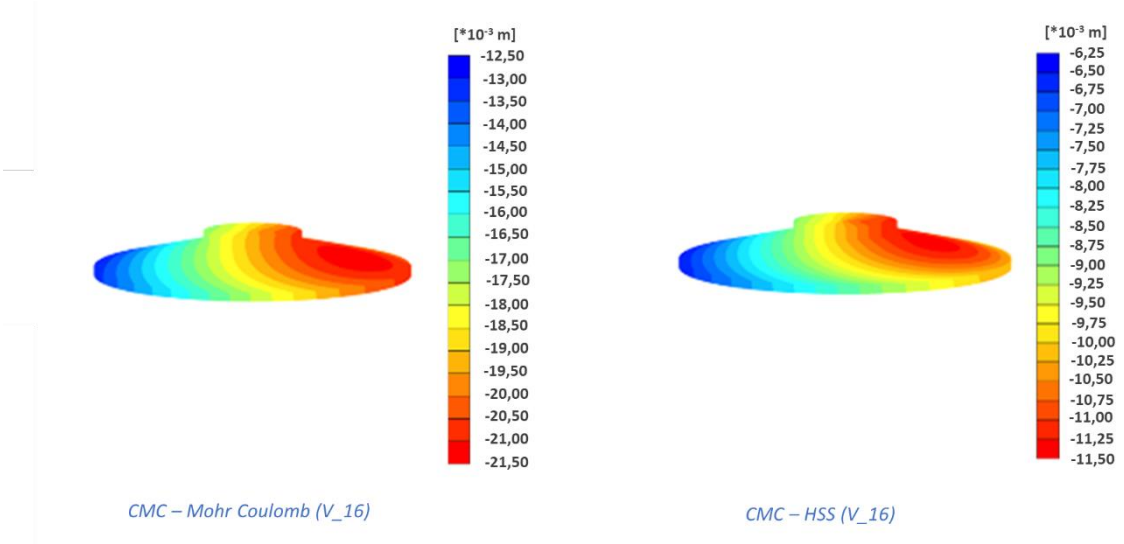

Figure 4-27: Vertical settlement (MC), (b) vertical settlement (HSS).

Furthermore, the effect of the soil model is studied by using the HSS model. The results show that when the HSS model is employed, the foundation experiences even less settlement compared to the Mohr-Coulomb model. This suggests that the choice of the soil model significantly affects the behaviour of the foundation and its response to applied loads. The sensitivity analysis of the soil modelling conducted in subsequent sections adds to the understanding of the impact of different soil models on the foundation behaviour and settlement response with rigid inclusions.

The presence of the rigid inclusions under the gravity foundation, separated by a granular load transfer platform will alter the stress path within soil. Due to the high relative rigidity of the inclusions compared to the surrounding soil, they bear a significant portion of the applied load, resulting in stress concentration at their heads and reducing the stress into the soil. This effect is illustrated in (Figure 4-28) under the dead load of the structure.

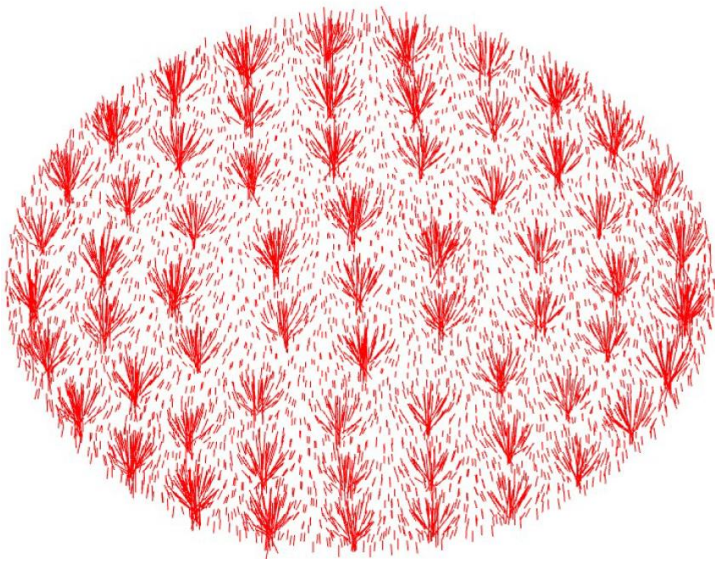

Figure 4-28: Stress concentration on the rigid inclusions.

Table 4.7 & Table 4.8summarize the results of a parametric study investigating the influence of different soil models on the foundation settlement and differential settlements. In Table 4.7, which represents the results without rigid inclusions, it can be observed that as the soil model

transitions from the Mohr-Coulomb model to the Hardening Small Strain (HSS) model, the settlement of the foundation progressively decreases. The same trend is observed for the differential settlements. In Table 4.8, which represents the results with rigid inclusions, a similar trend is observed. The foundation settlement and differential settlements decrease as the soil model transitions from the Mohr-Coulomb model to the Hardening Small Strain (HSS) model.

Table 4.7: Summary of Foundation Settlement and Differential Settlement (Without Rigid Inclusions)

Loading case	Vertical settlement (mm)	Differential settlement (mm/m)	Soil model
Dead load	33	0	MC
M_16	41– 21	1.05	
Dead load	13	0	HSS
M_16	15–9	0.32	
Dead load	17	0	HSM
M_16	20–13	0.37	

Table 4.8: Summary of Foundation Settlement and Differential Settlement (With Rigid Inclusions)

Loading case	Vertical settlement (mm)	Differential settlement (mm/m)	Soil model
Dead load	18	0	MC
M_16	20.5–13.5	0.37	
Dead load	9.2	0	HSS
M_16	11 – 6.75	0.22	
Dead load	12	0	HSM
M_16	13.5 – 8.5	0.26	

The difference in results obtained with different soil models can be influenced by various factors. The Mohr-Coulomb (MC) soil model, being derived directly from in-situ tests at the design stage, may lead to conservative calculations as it does not consider the specific laboratory soil data. On the other hand, the Hardening Soil Model (HSM) and Hardening Small Strain Model (HSS) take the available laboratory soil data into account. However, it is important to note that the laboratory soil data may be limited to a certain depth, and the soil model parameters are generalized to the entire corresponding soil layer. This generalization can introduce some uncertainties and may not accurately capture the variation in soil behaviour with depth. Additionally, the settlements originating from the soil layers beneath the rigid inclusions aren't influenced by the columns, meaning they can't be mitigated in such scenarios.

In the following three-dimensional simulations, the behaviour of the rigid inclusions under quasi-static loading of the wind turbine foundation can be effectively highlighted.

Load transfer and axial loading:

Using the finite element simulations with different soil models for the surrounding soil volume, the influence of the latter on the axial loading inside the rigid inclusion can be observed. Typically, the differences in axial loading are more pronounced at the head level of the inclusion and at the maximum loading point (neutral point) along its depth (Figure 4-29). However, as we

move towards the base resistance of the inclusion, the differences in axial loading between different soil models tend to diminish.

The axial load inside the rigid inclusion (13) is identified thanks to the fibre optic cable embedded inside the inclusion. Furthermore, the rigid inclusion (14) is equipped with a load cell at its head, which provides direct measurement of the axial load applied to the inclusion. To compare the experimental measurements with the finite element (FE) results, the vertical stress variation can be used as a basis for comparison. This involves comparing the stress measured at a certain point in time (instant t) with the stress measured at the time when the fibre optic measurements were tared (zeroed). By subtracting the stress at the tare time from the stress at instant t, the change in stress can be calculated. This change in stress corresponds to the load applied to the inclusion and can be compared with the axial load obtained from the FE results. By comparing the experimental measurements of the axial load inside the inclusion with the finite element (FE) results, it is observed that the Hardening Soil with Small Strain (HSS) model better represents the behaviour of the rigid inclusion based on the measurements (Figure 4-29). In the comparison, a red zone is identified as a region where the stress measurements may be less accurate. This zone is located near the surface, where the fibre optic cables are attached to an aluminium thin bar. The presence of the thin bar may introduce some inaccuracies in the stress measurements near the surface. Even thought, the decrease in the axial loading inside the RI_13 follows a similar trend as the numerical modelling, approximately 25% of difference in the loading is detected between the experimental and numerical results. Different reasons can be causing this difference. (1), the experimental vertical stress is not measured, it is directly calculated by applying Hook's law on the measured deformation. The calculations might be inaccurate. (2), regarding the finite element modelling, there could be various factors contributing to the differences observed. One possible reason is the incorrect modelling of the evolution of the over consolidation ratio of the soil along the depth. In the current modelling approach, each soil layer has a fixed over consolidation ratio, which may not accurately represent the actual soil conditions. The assessment of the soil characteristics might led to an underestimation given that we're concentrating on a single mechanical test for each layer, for a soil presenting a lot of heterogeneities.

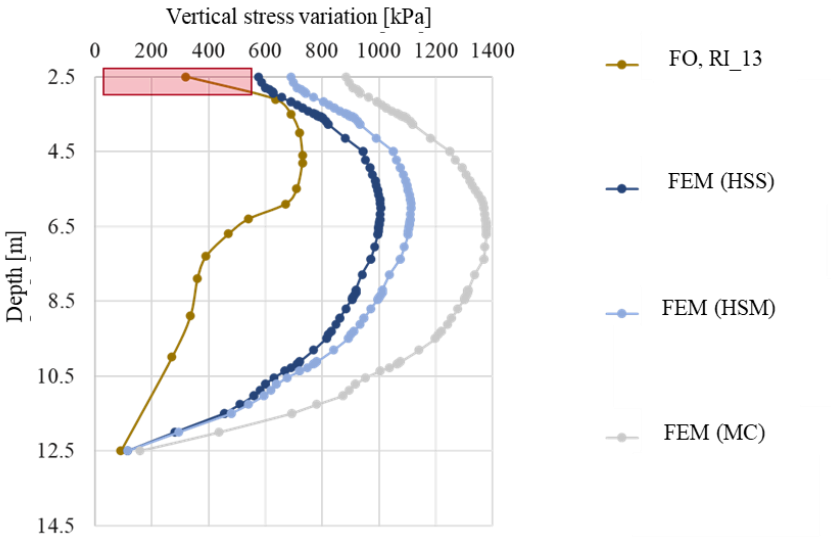

Figure 4-29: Axial load inside the rigid inclusion (Soil model impact).

One of the most important parameters affecting the load transfer to the rigid inclusion is the modulus of elasticity of the Load Transfer Platform (LTP). Different values of Young's modulus were considered for the LTP, namely 80 MPa, 60 MPa and 40 MPa (Figure 4-30). It can be observed that as the elastic modulus of the LTP increases more load is transferred to the head of the rigid inclusion. The axial stress of the RI_13 calculated from the fibre optic measurements is also shown in the analysis to illustrate the influence of the modelling of the LTP. Although several soil models for the LTP were considered in the simulations, the results for the axial stress of the rigid inclusions are not presented in this context. This is because the soil parameters of the LTP were not accurately measured, but rather estimated. The accuracy of the results is highly dependent on the accuracy of the LTP soil parameters, which were not available in this case.

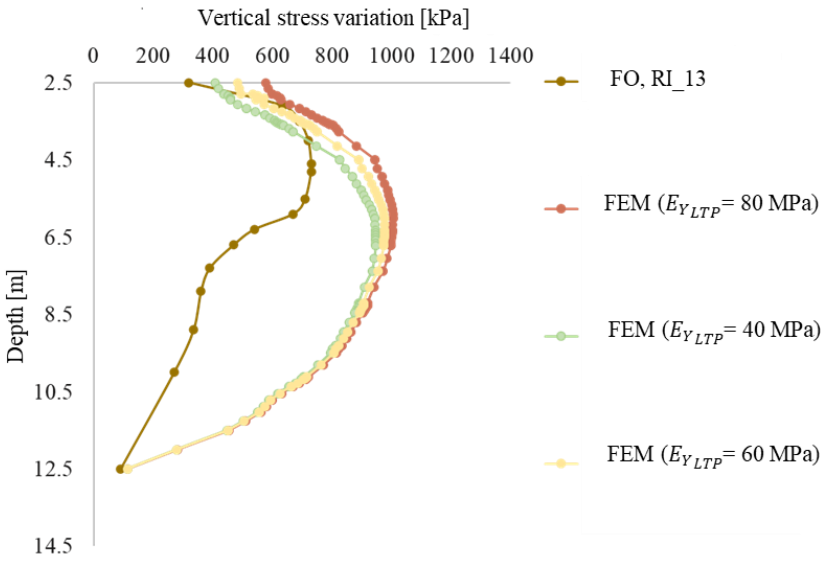

Figure 4-30: Axial load inside the rigid inclusion (LTP influence).

Overturning moment:

The behaviour of the rigid inclusions under the wind turbine foundation is assessed under different loading conditions, including different values of the overturning moment. Using HSS model for the soil volume, the axial loading of selected rigid inclusions along the direction of the dominant wind are presented in (Figure 4-31 (a)). The positions of the columns with respect to the wind direction, as shown in (Figure 4-31 (b)), are the main factors influencing the axial vertical stress distribution. It is observed that the columns located opposite to the wind direction experienced a significant increase in vertical stress compared to the columns on the opposite axes. This indicates that the columns facing the wind direction bear a higher load, which is reflected in the modelling through the magnitude and direction of the overturning moment. The variations in vertical stress along the wind line can be visualized as a trapezoidal distribution, with the vertical stress gradually decreasing from RI_14 to RI_36. Additionally, the vertical stress distribution of the RIs, as depicted in (Figure 4-31 (a)), indicates that the neutral plane deepens as approaching the centre of the foundation.

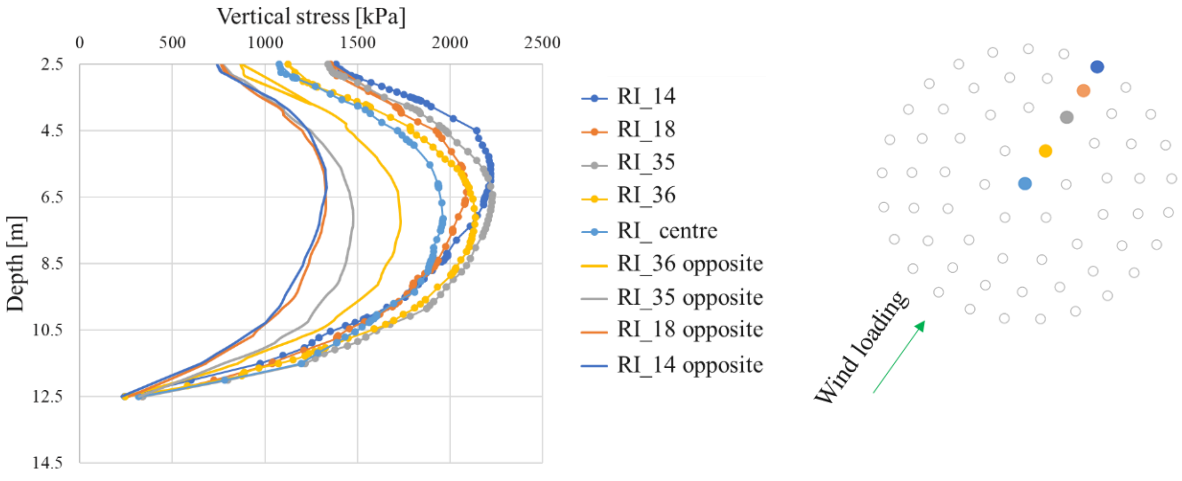

(a) (b)

Figure 4-31: Axial loading inside the rigid inclusions (overturning moment impact).

In Chapter 2, experimental measurements of stress variation at the head level of the rigid inclusions were conducted independently of the wind direction and in relation to the wind speed. These measurements were then compared to the corresponding FE results obtained under similar load conditions (Figure 4-32). The comparison between the FE results and the experimental measurements revealed a good agreement. This suggests that the FE model effectively replicated an approximate behaviour of the system under the given loading conditions and wind speeds.

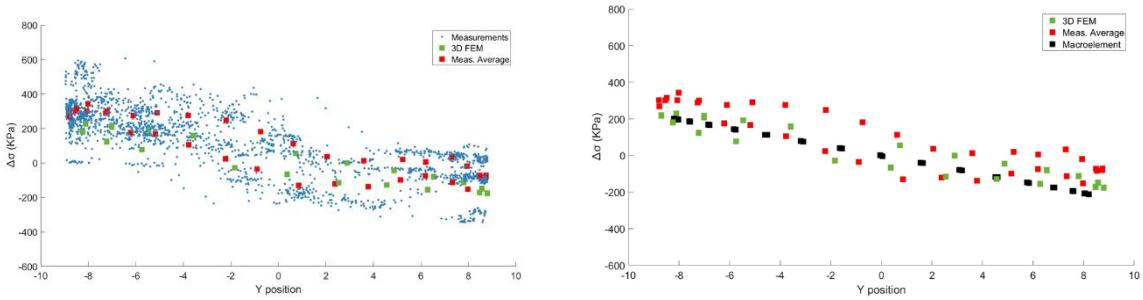

(a) (b)

Figure 4-32: Stress distribution under identical load conditions as derived from the measurements.

4.11 Conclusions

This chapter presented the FEM of the soil reinforced by rigid inclusions in case of onshore wind turbine foundation. The following numerical strategy (Figure 4-33) were followed to achieve the following purposes:

- Identifying the soil-structure interaction at the interface between the rigid inclusion and the surrounding soil.
- Identifying complex soil models to reproduce the soil behaviour. It has been performed through modelling the laboratory soil tests using FEM.
- Three-dimensional modelling of the soil reinforcement system under the wind turbine, including all identified soil-structure interactions using FEM. The comparison of the

results with the available measurements under defined load conditions reflects a satisfactory agreement.

- Creating of data bank for the macroelement modelling.

In this chapter, we were also able to highlight the importance of selecting an appropriate soil model, as it can significantly affect the predictions. The lack of information on load distribution platform (LTP) modelling highlights the need for further study and investigation on the soil parameters of this critical structural element. Accurate characterization of the behaviour and properties of the LTP is essential for more reliable predictions and evaluations of the wind turbine foundation system. In addition, cyclic loading analysis can provide insight into the accumulation of stresses in the soil and the effects on the interfaces between soil and rigid inclusion. The use of HSS may be appropriate for this purpose.

Following the FEM, the next Chapter presents the development of a macroelement modelling approach that is based on the FEM to provide a reliable numerical tool for the engineering.

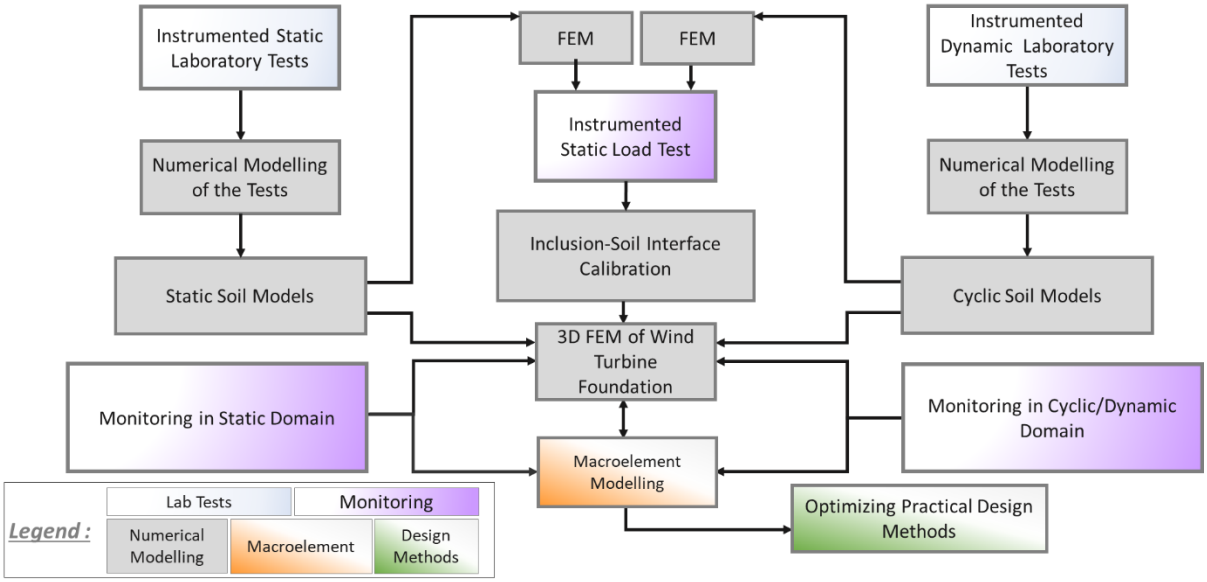

Figure 4-33: Numerical strategy.

CHAPTER 5

Macroelement

5.1 Introductions

Soil reinforcement by rigid inclusions is a well-known method, intermediate between shallow and deep foundations, to reduce settlement and increase the bearing capacity of soil foundations of various superstructures that transfer static loads and more complex loads such as cyclic loads, as well as a technique designed to resist natural hazards such as earthquakes. In this work, we have shown how this technique significantly reduces construction time and material costs for projects in almost all areas of construction, including revolutionary projects. The design methods used for this technique usually take into account the complex physical phenomena inherent in soil reinforcement. These phenomena have been the subject of several research projects, most notably the (ASIRI, 2013), in which the technique has been studied multiaxially and in depth. One of the principles in soil reinforcement is to identify and quantify the mechanism of load transfer from the superstructure to the reinforced soil, as well as the interaction between the rigid inclusions and the surrounding soil, in order to achieve an optimal design considering the complexity of the soil and the loading type of the superstructure. Although the technique is usually conceded to strengthen the mechanical properties of the soil and thus its ability to create a homogeneous soil medium with higher stiffness than in the initial phase, the complexity of the interactions at the level of a unit cell of a rigid inclusion and the group of inclusions cannot be neglected when the load transferred to the soil is not only a vertical centred axial load and a more complex load is applied, as is the case with wind turbines. When the foundation is subjected to such loading, the choice of design method becomes narrower. Various approaches can be employed in the design, particularly those based on the FEM or finite difference method, the so-called direct methods. These methods are used to account for soil nonlinearity, geometry, and load eccentricity in the context of soil-structure interaction. This leads to local nonlinearity on the order of a rigid inclusion interacting with the soil volume surrounding it, and global nonlinearity of the system (inclusions – soil – LTP – foundation), as well as control of load transfer from the foundation to the inclusions by modelling the load transfer platform between the columns and the foundation. However, the application of these methods in this context could be complex due to the selection of appropriate constitutive soil models to represent the behaviour of the soil, the interface between the inclusions and the soil, and the large-scale geometry of the model. Calibration of the parameters also adds to the already long computation time of the simulations. The usefulness of these methods is not always obvious, as they are an important part of the design process, usually under time pressure, as is common in civil engineering. There are other important methods in design and in the literature, such as the analytical methods, which are able to reproduce the complex mechanisms at the different levels of interaction. They have demonstrated their robustness and suitability to instrumentation and advanced numerical modelling in several soil reinforcement projects, but their application in the case of an overturning moment or a three-dimensional problem is still challenging. Other methods, also called hybrid methods, so-called

multiphase models, are an advanced homogenization method developed for rigid inclusions to capture the interactions between the rigid inclusion domain and the soil matrix region in a static, dynamic, and three-dimensional framework. Such methods are sometimes complex for use in engineering design and do not provide access to all the data related to the individual rigid inclusion and the associated soil volume within the reinforced matrix. However, these methods open the door for various research advances in soil reinforcement and provide a basis for the development of various analytical methods.

As a contribution to the design methods, this chapter presents a new numerical tool based on the concept of the macroelement, which allows efficient time calculation, is practically applicable, and is suitable for the design of soil reinforcement by rigid inclusions. In the case of the OWT foundation, this model is able to evaluate the general design limits defined in the guidelines for wind turbines, such as the stability, and the high eccentricity of the foundation, as well as the load transfer from the foundation to the reinforced soil, considering the different interaction phenomena. Moreover, and more importantly, it allows the prediction of forces and displacements under the concrete foundation and in each of the rigid inclusions as well as the soil in a corresponding area geometrically defined by the designer with a good approximation in a three-dimensional configuration, which is very simplified using the classical analytical approach. The constitutive laws implemented in the model provide the possibility of physical calibration at the level of rigid inclusions and their interface with the surrounding soil, as well as the interaction between the foundation and the soil, which affect the phenomena of load transfer or otherwise the arching effect. The macroscale 1D model is developed in the MATLAB environment using the ATL4S platform (Grange, 2018) to simulate a rigid foundation underlined by soil reinforced with rigid inclusions. The key outcome of the model is its ability to represent the complex phenomena of interaction of soils reinforced with rigid inclusions within the conceptual framework of commonly used inclusion-soil interaction methods. The scope of the work, from the constitutive laws to the simplified numerical resolution to the analysis of the model and the kinematics of the applied load, is presented synthetically. The notion of local macroelement in the model refers to a unit cell model in which a rigid inclusion is centred in a soil volume that represents its tributary area under the foundation. The set of different unit cells located under the gravity foundation of the wind turbine considered in the FEDRE project reconstructs a global multiscale model of the final version of the macroelement. In order to take into account the different types of superstructures and the resulting loads, an interchangeable friction law at the interface between the rigid inclusion and the soil and the base resistance law at the tip of the column have been considered in the model, allowing the user to adjust the chosen constitutive law according to the type of load. The current version of the programme is therefore suitable for all types of structures founded on a rigid foundation and a soil reinforced by rigid inclusions, where the vertical behaviour is the most important part to be calculated.

The choice of the macroelement concept in this dissertation is consistent with soil improvement by rigid inclusions. This chapter briefly addresses soil-structure interaction (SSI) in a soil reinforced by rigid inclusions, mainly distinguishing three levels of interaction: inclusion vs soil, inclusion-soil vs LTP-foundation, and global reinforced soil vs structure interaction. The purpose of the bibliography in this chapter is to first explain the concept of SSI and the methods used to express it, from indirect to direct methods, also considering hybrid methods such as multiphase modelling and the macroelement approach. Second, this chapter presents the new multiscale macroelement approach for rigid inclusions, from the mathematical background to the

numerical implementation. Finally, this chapter presents the results of the model in detail by comparing them with the finite element methods using PLAXIS and the appropriate analytical methods in the field of soil improvement, especially the methods recommended in (ASIRI, 2013), as well as with the available monitoring measurements carried out in this work.

5.2 Background

The term macroelement refers to a macroscale representation of the soil-foundation system in which the soil behaviour acting on a foundation is constrained by a nonlinear connecting element located in the so-called "near field," where the "far field" refers to the soil profile far enough away from the soil-foundation-structure system to consider the nonlinearities induced by the soil-foundation interaction negligible. The main objective of the model was to replace the traditional semi-empirical method for calculating bearing capacity with a new approach that can capture the nonlinearity of the problem and is suitable for numerical simulations. This approach was first introduced in geotechnical engineering by Nova and Montrasio, (1991) to study the bearing capacity of an infinitely rigid surface foundation with in-plane deformations resting on loose sand under eccentric static loading. The authors represented the loading by a series of generalised forces that produced a series of generalised displacements of the foundation due to the condensation of nonlinearities at a single point at the centre of the foundation. In a finite element framework, the macroelement is a tool used to impose the displacement in order to calculate the initial stiffness matrix of the associated forces considering various nonlinearities. The size and shape of the stiffness matrix and the load and displacement vectors depend on the degrees of freedom studied. The key element for modelling some fundamental features of the global behaviour of the soil-foundation system is the formulation of the constitutive equations of the macroelement the so-called "phenomenological constitutive law", in incremental form, i.e., in the form of evolution laws for the variables of the system. Thus, the problem can be treated much more simply as a point relating forces and displacements using stiffness parameters and a phenomenological constitutive law (Figure 5-1). The following sections briefly review the various approaches to macroelement models. The focus is on three different directions, such as the geometry of the problem, the phenomenological constitutive law, and the application to real case studies.

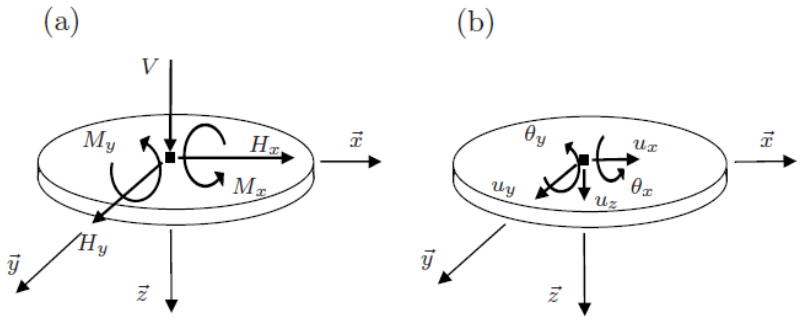

Figure 5-1: Presentation of the global variables: (a) forces and (b) displacements on the circular foundation (Grange et al., 2008).

5.2.1 Shallow foundation

5.2.1.1 Monotonic loading, 2D framework

The model of (Nova and Montrasio, 1991) targets the shallow strip foundation under a homogeneous soil layer using a 2D loading by introducing a vertical load "*V*", a horizontal load *"H"* and an overturning moment *"M"* with a corresponding kinematic variable of a vertical and horizontal displacement in addition to the foundation rotation. The constitutive law used in this model was derived from a classical elasto-plastic model with an isotropic hardening. The validity of the model was then extended by Montrasio and Nova (1997) through a series of experimental tests on different shallow foundations instead of strip foundations, ending with the proposal of empirical parameters to calculate the constitutive parameters of the already proposed model. Following this model, Tan (1990); Butterfield and Gottardi (1994); Gottardi et al. (1999); Byrne and Houlsby (2001); Cassidy and Bienen (2002) models further developed the failure envelope resulting from plasticity theory by introducing the concept of "swipe tests" resulting from an experimental test consisting in creating a loading space { *V* - *H* – *M* } as a failure envelope (Figure 5-2). The tests consist in controlling the displacement of the foundation by first forcing a vertical displacement of the foundation to obtain a corresponding vertical load. The imposed vertical displacement remains constant until the end of the experimental test. Now the foundation is subjected to a horizontal force or rotation or both together. By performing a systematic series of tests with different ratios between horizontal displacement and rotation, it is possible to obtain a comprehensive picture of the shape of the yield surface. Thus, this type of testing has made it possible to perform a complete study of the failure criteria for circular foundations in the space { *V* - *H* - *M*} for 2D loads and then in the space {V - Hx - My - Hy - Mx – T} (where *T* is the torsional moment) for 3D loads (Cassidy et al., 2004).

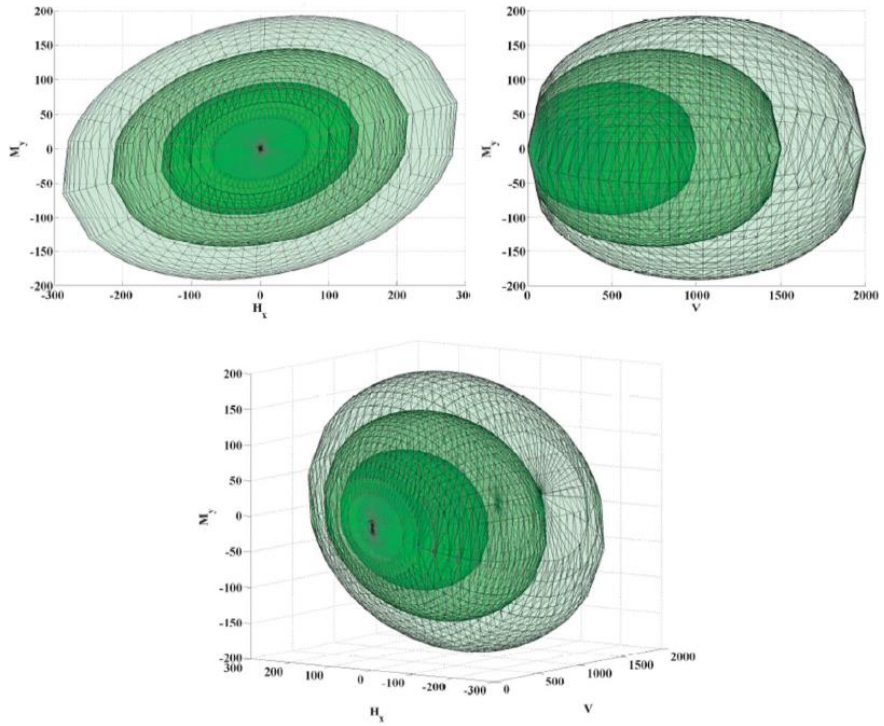

Figure 5-2: Failure criterion and load surface for the macroelement (Grange, 2008) after the swipe tests (Gottardi et al., 1999; Cassidy and Bienen, 2002).

5.2.1.2 Dynamic loading, 2D framework

At this stage in the development of macroelement models, the limitation is the use of dynamic-cyclic loading, which was limited due to the nature of the constitutive law used in the previously cited models. The model of Cremer (2001)was introduced to simulate the cyclic and dynamic behaviour of a strip footing on a cohesive soil subjected to a 2D loading by considering a multi-surface plasticity through two types of hardening variables, "kinematic and isotropic", and adding radiative damping phenomena. Another peculiarity of this model is that it integrates the geometrical nonlinearities through a nonlinear and nonreversible mechanism, theoretically resulting from the overturning phenomena of the foundation at its centre. In the dynamic-cyclic domain, several models available in the literature have been built in a 2D framework for dynamic/cyclic loading (Paolucci and Pecker, 1997; Shirato et al., 2008; Abboud, 2017). The following models (Di Prisco et al., 2003, 2006; Chatzigogos et al., 2009) have the particularity of introducing a bounding surface as an alternative to the failure criterion described for the classical laws of plasticity, allowing to develop permanent strains to better describe cyclic loading.

5.2.1.3 Dynamic loading, 3D framework

The first extension to a 3D problem was made in the model of Bienen et al., (2006) by introducing 6 degrees of freedom. The model was validated experimentally through a series of tests on a rough circular flat foundation using a classical plasticity law with an isotropic hardening law with radial hardening components, similar to the work of Byrne and Houlsby, (2001). The 3D model presented by Grange et al., (2008), which considers 5 degrees of freedom defined by (My, Mx, Hx, Hy, V), represents the nonlinearities at the centre of the foundation in a generalised load-displacement model. A special feature of the model is that it is suitable for different superficial foundation types such as rectangular, circular, and strip foundations. The phenomenological law proposed in the model assumes classical plasticity and differs by a new formulation of the uplift phenomena based on the model of Cremer, (2001) and Cremer et al., (2002), which takes the nonlinearity of the soil and the geometric nonlinearities into account. The model was tested using experimental tests with static, cyclic and dynamic loading. The phenomenological model consists of the elastic behaviour of the soil and the subsequent uplift on an elastic soil to finally study the coupling between the plasticity and the uplift. The hypoplastic macroelement is characterised by the absence of an elastic region in the space of generalised stresses and by a continuous change of the stiffness matrix of the system as a function of the direction of the generalised velocity (Grange and Salciarini, 2022). This model was adopted by Salciarini and Tamagnini (2009), who used the principles of generalised hypoplasticity theory instead of classical plasticity in a 3D framework to extend the basic macro-element formulation to the cyclic/dynamic loading conditions by inserting a suitable kinematic internal variable (internal displacement) and adopting the approach proposed for continuous media. This model was followed by Salciarini et al., (2011) and Tamagnini et al., (2013), which included torsional loading based on the hypoplastic phenomenological law for a shallow foundation on sands. The 3D models of Grange (2008) and Salciarini et al., (2011) with their phenomenological laws of hardening plasticity and hypoplasticity were compared in the simulation of SSI in the pre-compressed reinforced concrete viaduct under dynamic loading (Grange and Salciarini, 2022). The results were very similar in terms of both horizontal forces/moments and horizontal displacements/rotations, which can be attributed to the successful representation of the hysteretic behaviour of the soil-foundation system.

5.2.1.4 Deep foundation

The concept of macroelements was extended to deep foundations, more specifically pile foundations, with the model of Correia (2011), which simulates a single vertical pile in a cohesive soil subjected to lateral seismic loading. The constitutive law of the model is based on a kinematic plasticity approach and the loading is limited to a moment and a horizontal loading, without considering a vertical load. Following the hypoplasticity approach of Salciarini and Tamagnini (2009), a series of models (Li et al., 2016, 2018) were proposed for a single vertical pile and a single inclined pile. These models were presented by a combination of {V-H-M} after estimating the 3D failure surface by several numerical tests using the radial displacement method and swipe tests to represent the behaviour of the pile at its head.

Given the limitations of the cited models in reproducing the pile group effect under static and dynamic loading, the model of (Pérez-Herreros, 2020)proposes a multiscale macroelement consisting of three levels of interaction (Figure 5-3): (1) a single pile model to reproduce the nonlinear static response of each pile based on the failure surface, the hypoplasticity failure surface proposed by Li et al., (2016) and inspired by Salciarini and Tamagnini (2009), (2) static group effects (pile-soil-pile interactions) by introducing static interaction factors to reproduce the nonlinear static response of a group of piles, (3) dynamic response by adding dynamic interaction factors. The model is characterized by a rigid pile cap connecting all piles to the control node of the pile group via rigid connections. To reproduce the behaviour of a monopile under an offshore wind turbine, Gupta (2020) proposed a 1D macroelement to represent the pile-soil interaction using an elastoplastic constitutive law. The monopile was simulated under the combined action of V-H-M under static and cyclic conditions. For this purpose, “p-y”, “t-z”, and interface drag elements are used in a single macroelement that spans the entire length of the pile (Figure 5-4).

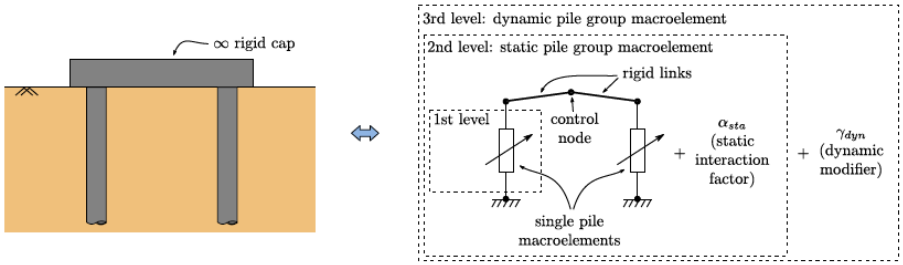

Figure 5-3: Modular macroelement concept for a pile group (Pérez-Herreros, 2020).

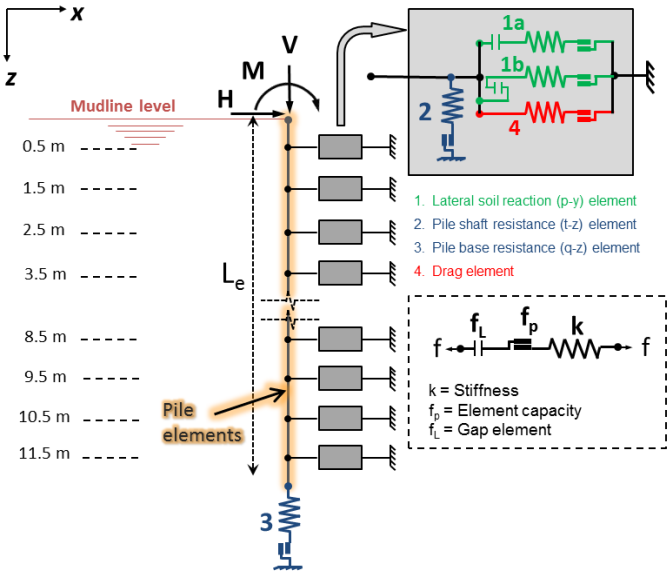

Figure 5-4: Local macroelement model assembly (Gupta, 2020).

5.2.2 Partial conclusions

As we have seen, the main purpose of the macroelement approach is to reproduce the response of the soil-foundation system under complex loading conditions by combining all nonlinearities (material and geometry) in a FEM framework to minimise the time required compared to competing methods. Soil reinforcement by RIs technique is considered between shallow and deep foundations, so such an approach could be very beneficial to improve field design and go beyond classical methods (direct and indirect approaches). On this basis, in addition to the two-phase modelling approach, a multiscale macroelement has been developed and is presented in the following sections. It is (to our knowledge) the first macroelement approach to model rigid inclusion technology. The approach borrows from the multiscale model of (Pérez-Herreros, 2020), which distinguishes between three scales of interaction at the level of piles and pile groups, and rigid connections between piles. The main difference is that the individual pile level is modelled with a modified two-phase interaction model based on the two-phase conceptual model of Hassen and De Buhan (2005), which allows direct access to the response of each rigid inclusion by itself and in the context of the group effect.

5.3 Multi-scale Macroelement

In this chapter, we present a novel 1D multiscale macroelement that models soil reinforcement by rigid inclusions in a 3D geometric implementation based on the finite element method using Atl4S (Grange, 2022) "A Tool and Language for Simplified Structural Solution Strategy" for use in nonlinear dynamic and seismic risk analyses. The macroelement approach allows us to consider the various aspects that control the response to the group effect of rigid inclusions by different features:

- Each rigid inclusion represents a "two-phase" model in a local macroelement reproduced in a FEM environment. The interaction between these two domains is described by the t-z method (Figure 5-5), which represents the first level of interaction: inclusion-soil;

- the interaction between the group of rigid inclusions (inclusion-soil-inclusion) is described by a constitutive law of the type shear friction between soil-soil, which separates a single rigid inclusion from the surrounding inclusions and considers their geometrical positions on the pre-execution plan.3D effects are respected through diffusing the load of the reinforced soil to the external unreinforced soil mass beyond the perimeter of the foundation due to the friction between these two components;
- the load is applied through a kinematic relationship that connects all parent nodes of the to a master node that controls the vertical displacement and rotation of the foundation through a predefined equation controlled by the degree of freedom of the system and the assumption of infinite stiffness of the foundation (Figure 5-5).

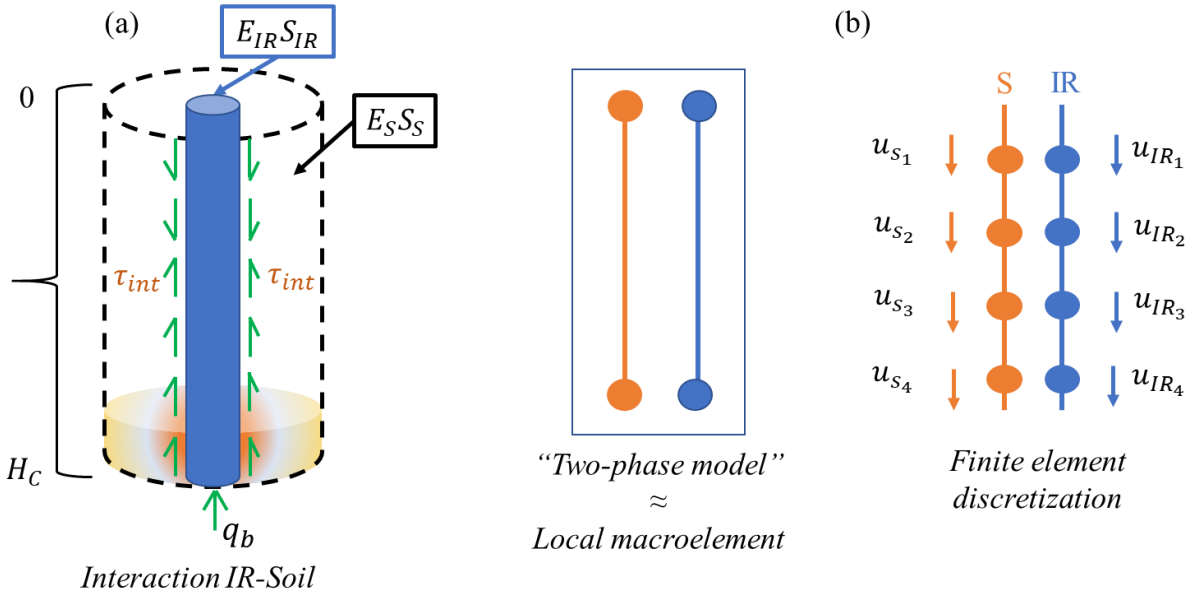

Figure 5-5: (a) Interaction of the two domains with interaction force mobilization laws, (b) Finite element discretization of the soil and RI elements in a macroelement approach.

5.3.1 Model Framework

The principle of virtual power (PVP) postulates a balance of forces within a virtual movement. It can be used as a basis for all finite element formulations and more generally for continuous media. A simple way to understand the PVP is to observe that when a solid has reached mechanical equilibrium (static or dynamic), the sum of the internal, external, and inertial forces is zero. Thus, when a "virtual" displacement field acts on the solid, the sum of the powers of the forces and moments (internal, external, and inertial forces) is also zero (Langlade, 2021). This chapter describes the formulation of an element to treat the axial behaviour of a two-phase medium with inclusion-soil interaction law at the interface. The two media have the properties $(E_{IR}\ , S_{IR})$ and $(E_S\ , S_S)$ and are of height H. The general form of the PPV could be described:

$$\int_{\Omega_{el}} {}^{t}\bar{\bar{\varepsilon}}^{*}\,\bar{\bar{\sigma}}\, d\Omega_{el} = \boldsymbol{W}^{*}_{\boldsymbol{ext}} \qquad (5.1)$$

With, $\Omega_{el} = \Omega_{IR} + \Omega_S$

5.3.2 Variational formulation of the model

It is assumed that the two media have their own kinematics, they are projected into two independent virtual fields. The mobilized frictional load at the interface is represented as an external input, $\tau_s(y_{IR} - y_s) = -\tau_{IR}(y_{IR} - y_s)$. The equilibrium equation (5.2) of the two-phase model, integrated at a height "H" of the model, could be written as follows:

$$\int_0^H \varepsilon_{IR}^* E_{IR} S_{IR} \varepsilon_{IR} + \varepsilon_s^* E_s S_s \varepsilon_s dz = \int_0^H y_s^* \tau_s + y_{IR}^* \varepsilon_{IR} dz + P_{ext}^* \quad (5.2)$$

Thus,

$$\int_0^H \varepsilon_{IR}^* E_{IR} S_{IR} \varepsilon_{IR} + \varepsilon_s^* E_s S_s \varepsilon_s dz = \int_0^H (y_s^* - y_{IR}^*) \tau_s (y_{IR} - y_s) dz + P_{ext}^* \quad (5.3)$$

And so, finally, the power term of the internal efforts that allow to maintain the internal forces necessary for the resolution of the equilibrium of the element can be considered as, $P_{int}^* = P_{ext}^*$:

$$\int_0^H \varepsilon_{IR}^* E_{IR} S_{IR} \varepsilon_{IR} + \varepsilon_s^* E_s S_s \varepsilon_s dz - \int_0^H (y_s^* - y_{IR}^*) \tau_s (y_s - y_{IR}) dz = P_{ext}^* \quad (5.4)$$

5.3.3 Finite element resolution

This equation can be discretized with a displacement distributed along the z-axis in the nodes (in the manner of a finite element method), provided that the continuous fields can be approximated by interpolation functions. Due to the distributed forces induced by the frictional forces, elements with interpolation functions of order 2 are chosen (3-node bar elements). This is how the displacement and deformation fields are written:

$$\begin{aligned} y_{IR}(z) = &= \mathbf{N}(z)\boldsymbol{u_{IR}} \\ y_s(z) &= \mathbf{N}(z)\boldsymbol{u_s} \end{aligned} \quad (5.5)$$

The matrix of the shape functions $\boldsymbol{N}$ are thus written as follows:

$$\mathbf{N} = \left[\frac{1}{2}\xi(\xi - 1),\ 1 - \xi^2,\ \frac{1}{2}\xi(\xi + 1)\right] \quad (5.6)$$

with the geometrical transformation relation, $z = \frac{1+\xi}{2}H$

The matrix of derivatives of the shape functions $\boldsymbol{B}$ with which $\frac{\partial y_{IR}}{\partial z}$ & $\frac{\partial y_s}{\partial z}$ can be calculated is expressed as:

$$\mathbf{B} = \left[\xi - \frac{1}{2},\ 2\xi,\ \xi + \frac{1}{2}\right] \quad (5.7)$$

If the element under consideration has length H, Equation (5.4) is written in discretized form:

$$\int_0^H {}^t\boldsymbol{u}_{IR}^* {}^t\boldsymbol{B} E_{IR} S_{IR} \boldsymbol{B} \boldsymbol{u}_{IR} + {}^t\boldsymbol{u}_s^* {}^t\boldsymbol{B} E_s S_s \boldsymbol{B} \boldsymbol{u}_s dz + \int_0^H {}^t(\boldsymbol{u}_s^* - \boldsymbol{u}_{IR}^*) {}^t N \tau_s (y_s - y_{IR}) dz = P_{ext}^* \tag{5.8}$$

Since the 2 virtual fields are independent, we find the following internal force term governing the equilibrium of each element:

$$\boldsymbol{p}^{el} = \begin{bmatrix} \int_0^H {}^t\boldsymbol{B} E_{IR} S_{IR} \boldsymbol{B}\, dz & 0 \\ 0 & \int_0^H {}^t\boldsymbol{B} E_S S_S \boldsymbol{B} dz \end{bmatrix} \begin{bmatrix} u_{IR} \\ u_s \end{bmatrix} + \begin{bmatrix} \int_0^H - {}^t\boldsymbol{N} \tau_s (y_s - y_{IR}) dz \\ \int_0^H - {}^t\boldsymbol{N} \tau_s (y_s - y_{IR}) dz \end{bmatrix} \tag{5.9}$$

On the elementary level, the equation has the following form:

$$\boldsymbol{p}^{el} = \underbrace{\int_0^H \begin{bmatrix} {}^t\boldsymbol{B} E_{IR} S_{IR} \boldsymbol{B} & 0 \\ 0 & {}^t\boldsymbol{B} E_S S_S \boldsymbol{B} \end{bmatrix} dz}_{k_1^{el}} \underbrace{\begin{bmatrix} u_{IR} \\ u_s \end{bmatrix}}_{u^{el}} + \int_0^H {}^t[-\boldsymbol{N} \quad \boldsymbol{N}]\, \tau_s (y_s - y_{IR}) dz \tag{5.10}$$

Where:

$$y_s - y_{IR} = [-\boldsymbol{N} \quad \boldsymbol{N}] \boldsymbol{u}^{el} \tag{5.11}$$

The elementary tangent operator is thus written as:

$$\frac{\partial \boldsymbol{p}^{el}}{\partial \boldsymbol{u}^{el}} = \int_0^H \begin{bmatrix} {}^t\boldsymbol{B} E_{IR} S_{IR} \boldsymbol{B} & 0 \\ 0 & {}^t\boldsymbol{B} E_S S_S \boldsymbol{B} \end{bmatrix} dz + \int_0^H \begin{bmatrix} -{}^t\boldsymbol{N} \\ {}^t\boldsymbol{N} \end{bmatrix} \frac{\partial \tau_s}{\partial (y_s - y_{IR})} [-\boldsymbol{N} \quad \boldsymbol{N}] dz \tag{5.12}$$

5.3.4 Internal condensation for degrees of freedom

Let "b" be the list of 4 degrees of freedom of the edge of a two-phase element and let "r" be the list of internal degrees of freedom. Then we could write down the set of degrees of freedom of the element in the form:

$$u_a = \begin{bmatrix} u_b \\ u_r \end{bmatrix} \tag{5.13}$$

At the scale of an element, the degrees of freedom "b" are the boundary conditions applied by the global code, and the internal system is solved with the internal degrees of freedom "r". We note

$\boldsymbol{P}_b$ and $\boldsymbol{P}_r$ the internal forces on each degrees of freedom and $\boldsymbol{F}_b$ the external forces on the "b" nodes. The sum of the internal forces P_r is zero.

$$\begin{bmatrix} \boldsymbol{P}_b(u_a) \\ \boldsymbol{P}_r(u_a) \end{bmatrix} = \begin{bmatrix} \boldsymbol{F}_b \\ 0 \end{bmatrix} \quad \textbf{(5.14)}$$

For a given u_b, the u_r is solved using the 2nd equation of the system with the Newton-Raphson method and with a time integration scheme (in dynamics) and with a tangential algorithmic operator $\frac{\partial P_r}{\partial u_r} = \boldsymbol{K}_{rr}$. Once u_r is solved, the u_a vector is completely known and the forces can then be derived at the boundary nodes of the two-phase element $\boldsymbol{F}_b$. The tangent operator of the two-phase element necessary for the resolution of a global Newton-Raphson is obtained by linearization of the system (5.14)(5.15).

$$\begin{bmatrix} \delta\boldsymbol{P}_b(u_a) \\ \delta\boldsymbol{P}_r(u_a) \end{bmatrix} = \begin{bmatrix} \delta\boldsymbol{F}_b \\ \boldsymbol{0} \end{bmatrix} \quad \textbf{(5.15)}$$

Whether:

$$\begin{bmatrix} \frac{\partial P_b}{\partial u_b} & \frac{\partial P_b}{\partial u_r} \\ \frac{\partial P_r}{\partial u_b} & \frac{\partial P_r}{\partial u_r} \end{bmatrix} \begin{bmatrix} \delta u_b \\ \delta u_r \end{bmatrix} = \begin{bmatrix} \delta\boldsymbol{F}_b \\ \boldsymbol{0} \end{bmatrix} \quad \textbf{(5.16)}$$

Whether:

$$\begin{bmatrix} \boldsymbol{K}_{bb} & \boldsymbol{K}_{br} \\ \boldsymbol{K}_{rb} & \boldsymbol{K}_{rr} \end{bmatrix} \begin{bmatrix} \delta u_b \\ \delta u_r \end{bmatrix} = \begin{bmatrix} \delta\boldsymbol{F}_b \\ 0 \end{bmatrix} \quad \textbf{(5.17)}$$

Thus, by convergence, the operator is condensed to obtain the relation $\widetilde{\boldsymbol{K}} = \frac{\delta \boldsymbol{F}_b}{\delta u_b}$ such that:

$$\widetilde{\boldsymbol{K}} = \boldsymbol{K}_{bb} - \boldsymbol{K}_{br}\boldsymbol{K}_{rr}^{-1}\boldsymbol{K}_{rb} \quad \textbf{(5.18)}$$

5.3.5 Kinematic relationship

In a computational FEM environment, kinematic relations are usually defined by Lagrange multipliers. The method implemented in ATL4S by Grange (2022) allows the user to handle kinematic relations based on projection methods inspired by the methodology of model reduction in FEM by sub-structuring to reduce the numerical task and projecting each substructure using vectors related to the degrees of freedom. Therefore, the kinematic relations are implemented using the projection matrix "$\boldsymbol{B}$" which contains the global degrees of freedom of the two-phase model, including those controlled by the boundary conditions by replacing their multiplier with "0".

According to the hypothesis of an equal settlement plan at the base of the LTP (Figure 2-19), the parent nodes of the two-phase model (soil and inclusions) are subjected to the same

displacement by connecting their 3 degrees of freedom via a kinematic relationship with a master node that pilots the displacement of the foundation assumed to be infinitely rigid (Figure 5-6). The multiphase macroelement model is implemented in a 3D configuration, but with a 1D response, so the geometric projection of the relationship between the master node "M" and the superior nodes of the model could be written as follows:

$$\begin{bmatrix} U_M \\ V_M \\ W_M \end{bmatrix} = \begin{bmatrix} u_i \\ v_i \\ w_i \end{bmatrix} + \begin{bmatrix} x_m \\ y_m \\ z_m \end{bmatrix} \wedge \begin{bmatrix} \theta_x \\ \theta_y \\ \theta_z \end{bmatrix} \tag{5.19}$$

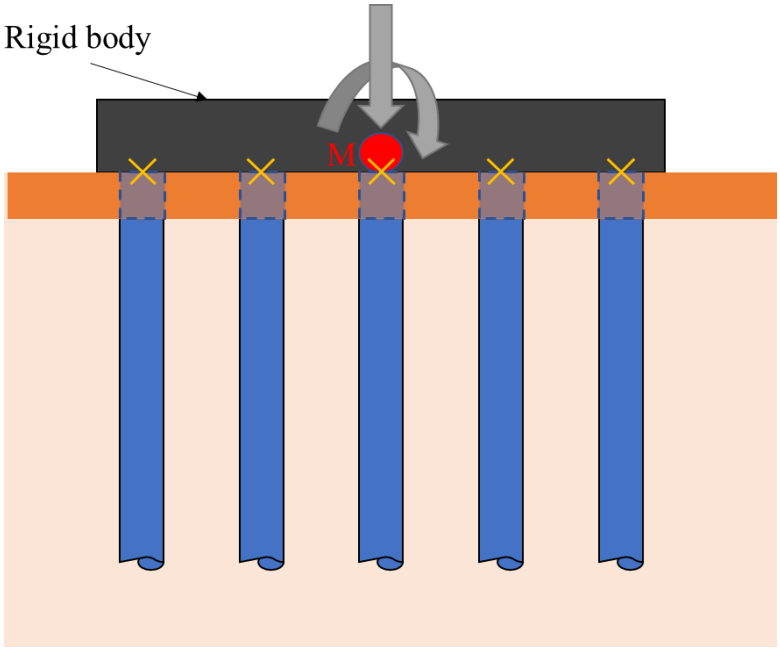

Figure 5-6. The connection of the superior nodes (X) of the two-phase model with the master node (M) in a rigid body movement.

5.3.6 Constitutive laws for the interaction forces

To characterise the soil-structure interaction between the domains of the two-phase model, the load transfer curves of (Frank and Zhao, 1982) are implemented in the macroelement model. These semi-empirical models, which are recommended in (ASIRI, 2013; NF P94-262, 2012) for rigid inclusions, piles and were also used as a successful reference for reproducing the behaviour of the tested column in Chapter 3 of this dissertation, are based on pressuremeter test data (PMT) and are therefore practical for engineering design. We should note that these laws are represented independently in the model, i.e., they are interchangeable depending on the type of loading and the application for which the rigid inclusions are being designed for. The intention to start with such laws is to validate the model with an experimental and numerical reference, since the interaction soil-inclusion in this strategy, which has been followed throughout the project in all research axes, is very closed as the behaviour of such laws:

- The load transfer of the skin friction at the column shaft-soil, called "τ_{int}" is mobilized by the equilibrium of the evolution of the force exerted on each domain, considering the differential settlement of both domains

- the load transfer of the base resistance force at the tip of the inclusion "q_b" whose mobilization depends as well on the system equilibrium between the evolution of the force at the interface, considering the differential settlement of both domains.

5.3.7 Interaction with the external soil mass

The work began with a series of general interactions that may occur in soil reinforcement by rigid inclusions under a rigid foundation (Figure 2-21). After considering the first family of these interactions (inclusion-soil) at the level of the local macroelement, consideration of other interactions is carried out at the 3D geometric scale. In this section, the interaction with the external, unloaded soil mass, which is critical for dissipating a portion of the load to the outside (Figure 2-20 (b)), is introduced into the macroelement model. For this purpose, additional elements are modelled to represent the external soil. A friction element was inserted between the local macroelements at the periphery of the model and connected between the soil domain of the model and the external soil (Figure 5-7). The friction law in such elements is exponential with a predefined asymptote and initial rigidity that considers the shear modulus of the soil, the maximum allowable shear friction and the thickness of the interface between the two elements, as classically modelled by virtual interfaces in the software FEM (Section 6.1.7 in PLAXIS Manual, (2020)). In a previous work by Cuira and Simon (2013), the interaction with the external soil on a foundation reinforced by rigid inclusions was simulated by defining a parameter "β" in their model. When this parameter is equal to 1, interaction with the external soil occurs based on pure shear over the entire corresponding extent of their local two-phase model, and when it is equal to 0, there is no interaction at all (Figure 5-8). This could be easier in case of rectangular foundation rather than circular shape. Therefore, in the developed model, this interaction is placed on the entire perimeter of the foundation, where the external soil area interacts with the external soil for all local macroelements located on the perimeter. Instead of defining coefficients for this, the external soil is modelled with a linear elastic element, in addition to modelling friction elements between the added elements and the soil domain of the local macroelements. The friction law is characterised by a parameter called "τ_{s-s}", acting on the soil-soil interface according to an elasto-plastic law that considers the shear modulus of the soil and the thickness of the interface. The contact area acted upon by friction is determined using the Voroni diagrams (Okabe et al., 2009), which directly represent a corresponding portion of the perimeter where a local macroelement interacts with the external soil.

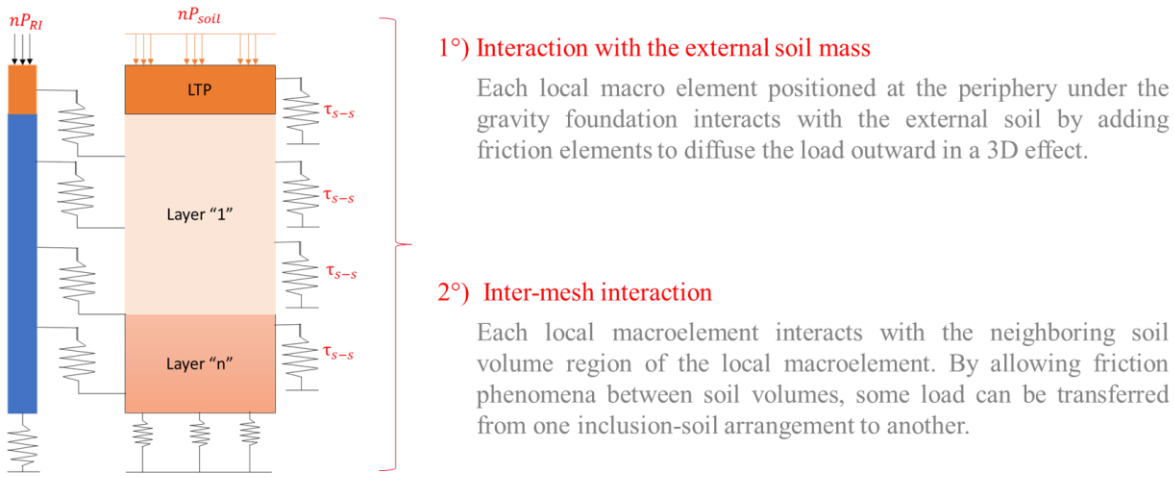

Figure 5-7: The concept followed for soil-soil interaction with the external soil mass and within the group of rigid inclusions (inclusion-soil-soil-inclusion)

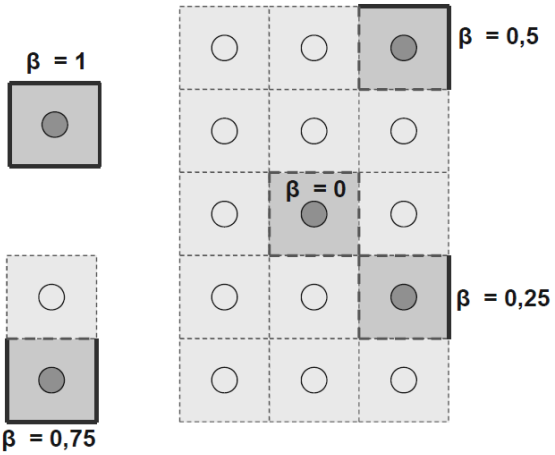

Figure 5-8: Choice of the parameter β for the case of a rectangular mesh (Cuira and Simon, 2013).

5.3.8 Intermesh interaction

In the literature review in this chapter, we have seen that among the available indirect methods for modelling the rigid inclusions under a gravity foundation, there are some that can account for the overturning moment and horizontal loading (such as the combined models MV3, MH3). When extending the application of such methods to simulate a rigid inclusion grid, they are accompanied by a checklist of tests and checks to control their results, boundary conditions, and assumptions. These models do not account for the geometry variations of the implementation of the CMCs as well as the trapezoidal loading acting at the base of the foundation. In the three-dimensional representation of the problem, where all local macroelements are assembled and connected to the master node, interaction between these macroelements is required to simulate possible differential settlements that may occur due to the overturning moment. To model this, a similar constitutive law as in the previous section (soil-external-soil interaction) is employed (Figure 5-7).

Since the positioning of rigid inclusions leads to a network of interconnections between rigid inclusions and thus to a complicated contact surface that plays the role of the terrain on which

shear occurs, it is important to model these interactions accurately. Voroni diagrams (Okabe et al., 2009) have been used to determine how each of the local macroelements interacts with other macroelements over a minimum distance required to reach another macroelement that forms a contact surface (Figure 5-9(a). We can think of this surface function as an analogy of the pile diameter such that shear ultimately acts on this surface multiplied by the corresponding depth of the soil layer. Each surface determined by the Voroni diagram was modelled in the multiscale macroelement (Figure 5-9 (b)).

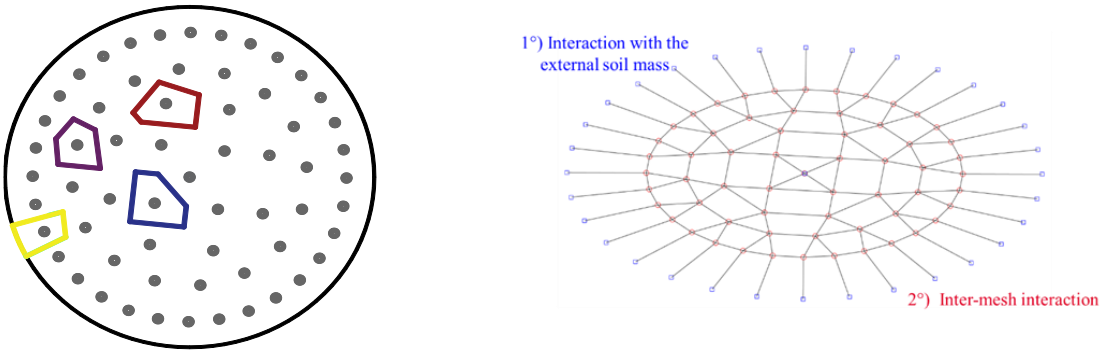

(a) (b)

Figure 5-9: (a) Voroni diagram projected into the intermesh connections of rigid inclusions, (b) projection of Voroni into the microelement (top view).

5.3.9 Strategy of validation

To validate the robustness of the model, three different applications were performed: (1) static load test on an isolated rigid inclusion, (2) axisymmetric model of a rigid inclusion centred in a soil volume under the wind turbine foundation, (3) a 3D configuration of the rigid inclusions under the wind turbine foundation. At each time point, at least one of the following methods is compared: experimental, numerical, and analytical.

5.4 Case study: Static Load Test on isolated column

In a first validation step, this work introduces the macroelement by simulating a static load test on the isolated rigid inclusion "IR1", in order to benefit from the experimental results, we obtained in the FEDRE project (Sahyouni et al., 2022). All the details related to the execution, instrumentation and modelling of this test are described in detail in Chapter 3 of this dissertation. In order to simulate the static load test of the rigid inclusion "IR1" with the current macroelement, it is sufficient to apply a load on the inclusion domain corresponding to the load steps performed during the experimental test. The results of the macroelement are compared with the finite element modelling conducted in PLAXIS, with the analytical method "CMCPLT" applied by Menard and with the measurements. The parameters of the macroelement and of CMCPLT can be easily calibrated by the experimental data, in particular by the values of "q_s" measured with the optical fibre. However, the initial parameters derived from the PMT test, which form the parameters of the macro element, were relatively close to the parameters derived from the measurements.

5.4.1 Loading curve

The load curve (Figure 5-10) shows the settlement at the head of the inclusion as a function of the applied load. It can be seen that there is a very good correlation between the results obtained with the CMCPLT, the macro element and the test measurements. On the other hand, the PLAXIS model with the initial parameters does not correctly reproduce the measurement behaviour. The shear parameters of the macroelement and the CMCPLT take the analysis of the fibre optic measurements inside the column into account. By calibrating the interface parameters of the PLAXIS model (Young's modulus and the maximum shear stress at the interface), the simulation approaches the test results.

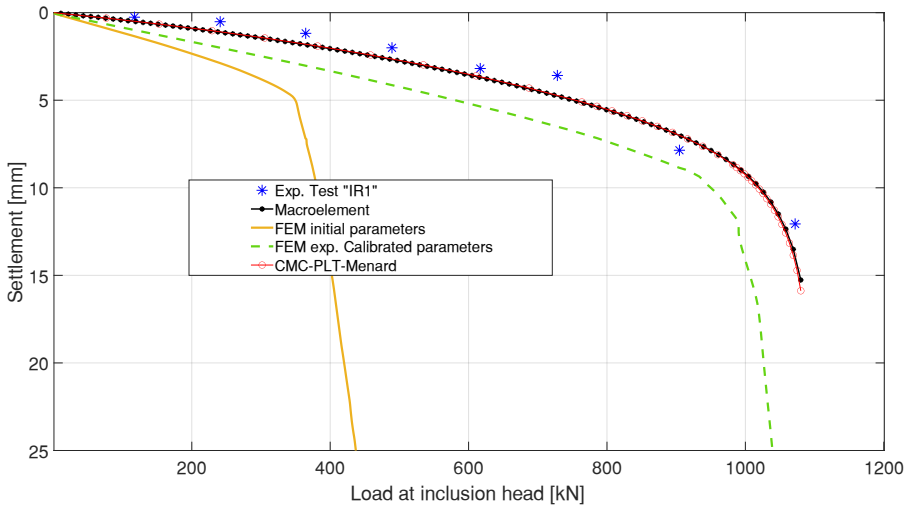

Figure 5-10: Settlement at the IR1 head. Comparison between FEM, Menard analytical method, macroelement and measurements.

5.4.2 Mobilized friction

Comparison of the skin friction results at the inclusion-soil interface shows that the transfer laws used (Frank and Zhao, 1982) are very close to the measurements (Figure 5-11) . After parametric calibration, the threshold value of mobilised friction in each layer agrees with the friction values calculated by the fibre optics: Loose Silt (LS) at 40 kPa, Compact Silt (CS) at 70 kPa, and Compact Horizon (CH) at 96 kPa. The slight difference between the macroelement and the measurements (Exp LL and Exp LC) could be related to the elevation considered in the analysis. The measurements consider the average of each layer, while the macroelement considers their geometric centre.

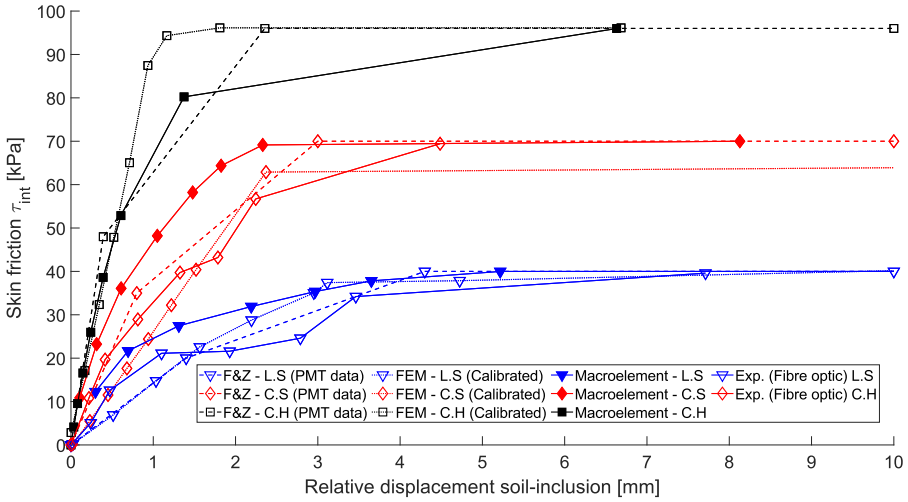

Figure 5-11: Lateral skin friction mobilization – Experimentally calibrated.

5.4.3 Base resistance

For the base resistance at the tip of the column, the macro element succeeded in reproducing the behaviour of the tested column compared to the other methods. The difference in peak load in the Frank and Zhao curve is due to the semi-empirical method, which estimates the peak load for an infinite load and displacement. For the other two curves, the load at the top of the column was limited to 1071 kN and the corresponding displacement was calculated (Figure 5-12).

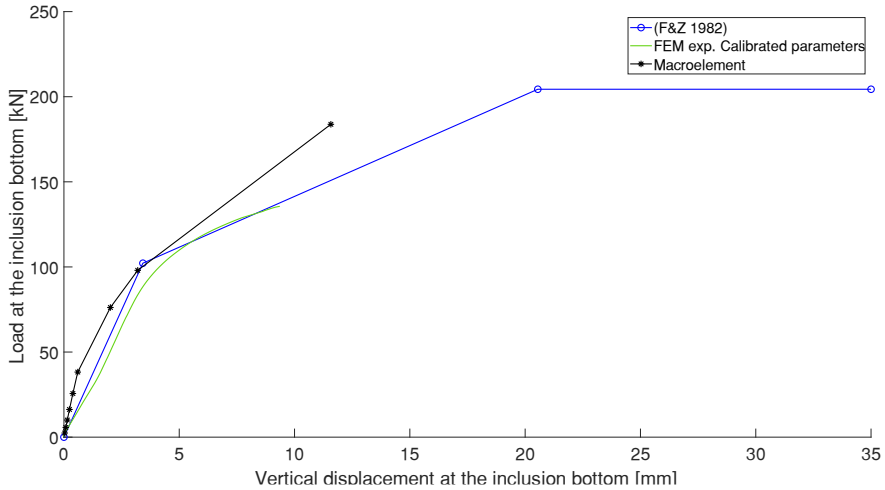

Figure 5-12: Base resistance (FEM, analytical method, macroelement).

5.4.4 Axial load in the column

The interesting part of the instrumentation of the static load test is the optical fibre that was placed in the centre of the tested column and along its depth. It allowed to measure the deformations of the material and to derive the forces in the column. After calculating the lateral friction unit at the interface and estimating the base resistance, the behaviour of the column is correctly reproduced. The results of the axial load distribution obtained by the three methods were compared with the experimental data (Figure 5-13).

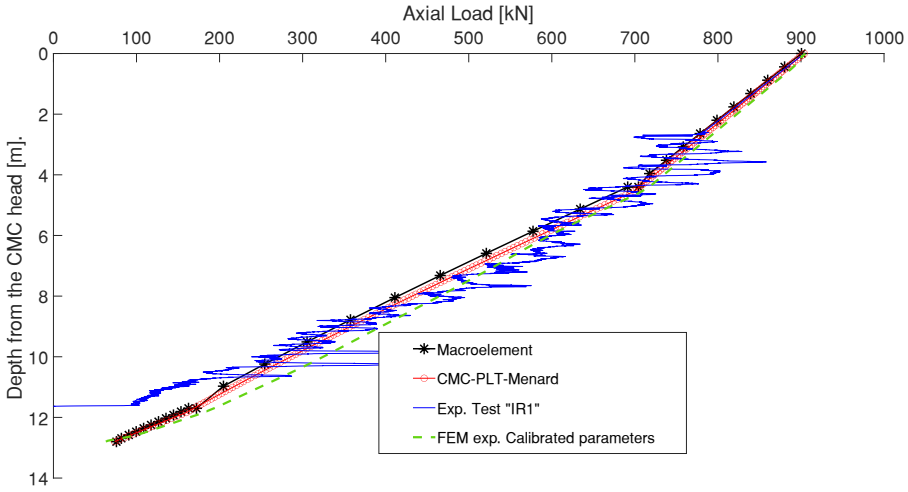

Figure 5-13: Axial load distribution.

5.4.5 Partial conclusions

The multiscale macroelement successfully simulated an isolated rigid inclusion during a static load test. The model was validated by the "IR1" exercise, the instrumented test performed as part of this work, and comparison with FEM. The model was also compared to the computational methods used by CMC-PLT-Menard by including the semi-empirical method of (Frank and Zhao, 1982).

The multiscale macroelemet will next simulate a unit cell model of a rigid inclusion centred in a soil volume to reproduce the SSI within this model.

5.5 Case study: Unit cell model

One of the most efficient methods for designing rigid inclusions under a gravity foundation is to simulate a unit cell model (Simon, 2012). The idea is to simulate the conditions faced by a rigid inclusion in an infinite grid of rigid inclusions under a uniformly distributed vertical load, assuming that there is no lateral displacement at the model boundaries. This elementary cell modelling procedure results in a less complex model than one that covers the entire grid layout. It is often further simplified by adding to the associated soil volume a cylinder that lies on the same axis as the column and has the same cross-sectional area as the grid. The result is an axisymmetric model suitable for analytical or numerical methods. The current state of the art of this design method is presented in Chapter 1 of this dissertation.

The axisymmetric model is shown in (Figure 5-14), and its equivalent tributary area expressed by the equivalent radius, which represents the rigid inclusion at the centre of the wind turbine foundation. The model shown is fundamentally different from the static load test model, where in this case the soil volume is a percentage of the total load distributed *"q"* to the unit cell model. As shown schematically, the LTP layer is located between the top of the column and the base of the foundation and is modelled using the fictious column technique according to (Combarieu, 2008). The macroelement replicates the model by assembling several soil layers, listed in Table 4.1 & Table 4.2.

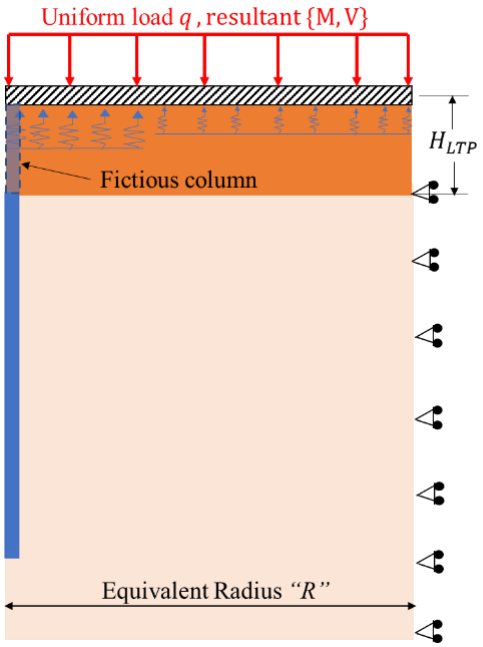

Figure 5-14: Axisymmetric model reproduced in the microelement.

5.5.1 Comparison with FEM and Simplified methods

To validate this step of the modelling, the conventional methods for this particular case were run in parallel to compare their results within the macroelement model. The analytical MV2 model is presented as the analytical method that reproduces the interaction between the rigid inclusion and the soil based on simplified iterative two-phase modelling. Moreover, the axisymmetric model can be perfectly represented in FEM software such as PLAXIS. In this part, the three approaches were simulated and compiled for comparison.

In the macroelement model, the interface between the inclusion and the soil is designed by its τ_{int}, where it is carefully entered into the model. The consequence of the load acting on the soil volume is the settlement of the latter, which leads to a negative skin friction. In this case, the maximum mobilizable friction become $k\,tan(\delta)\sigma'_v$. Along the length of positive skin friction (below the neutral plane), τ_{int} again assumes the values of the maximum shear stress of the corresponding layer.

The interactions between gravity foundation, LTP, rigid inclusion, and soil, corresponding to interactions 1 through 4 (Figure 2-21), result in a specific deformation and loading scheme. The comparison of the settlements of the inclusion and the soil is shown in (Figure 5-15). The assumption of equal settlements at the base of the foundation was used for both models (analytical and macroelement). We can interpret the results in terms of: (1) The punching of the inclusion within the LTP is approximately the same results with 7 mm. (2) The settlements in the deep layer derived from the settlements at the end of the RI profile and the soil profile were almost identical for the three methods. (3) The overall settlement profile of the RI and soil is around 23 mm in the three methods and clearly shows the inverse behaviour of the soil and RI settlements above and below the neutral plane.

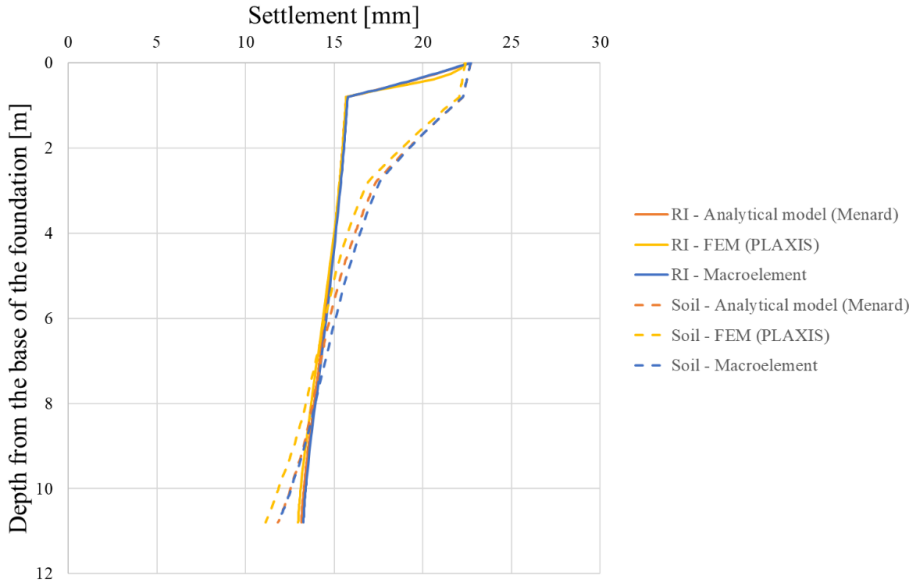

Figure 5-15: Settlement profile of the RI&Soil (FEM, analytical method and macroelement).

The load in the column increases with depth in the upper part due to negative skin friction, reaches its maximum in the neutral plane, and then decreases by load transfer to the soil by positive skin friction. The macroelement successfully reproduced this particularity of load transfer (Figure 5-16). The comparison between the methods reflects the similarity in the overall behaviour of both domains: RI & soil. Looking more closely at the interpretation of the results, we can see that the load transfer at the head of the inclusion is very similar for all methods. This similarity also applies to the base resistance of the RI, i.e., the mobilisation of this physical variable was similar for all methods. However, as for the difference in maximum between the macroelement and PLAXIS, it is directly related to the values of friction mobilisation at the interface, noting that the macroelement was not calibrated by PLAXIS, but only by its raw data. In the perspective work on the macroelement model, it is expected that the vertical effective stress of the soil layers will be added so that the values of negative skin friction in the compressible soil will be more accurate. Since the mobilisation of the law of the τ_{int} is independent of the weight of the materials, it is taken directly from the maximum values of friction, which is an asymptote in the shear law at the interface, this problem is not present.

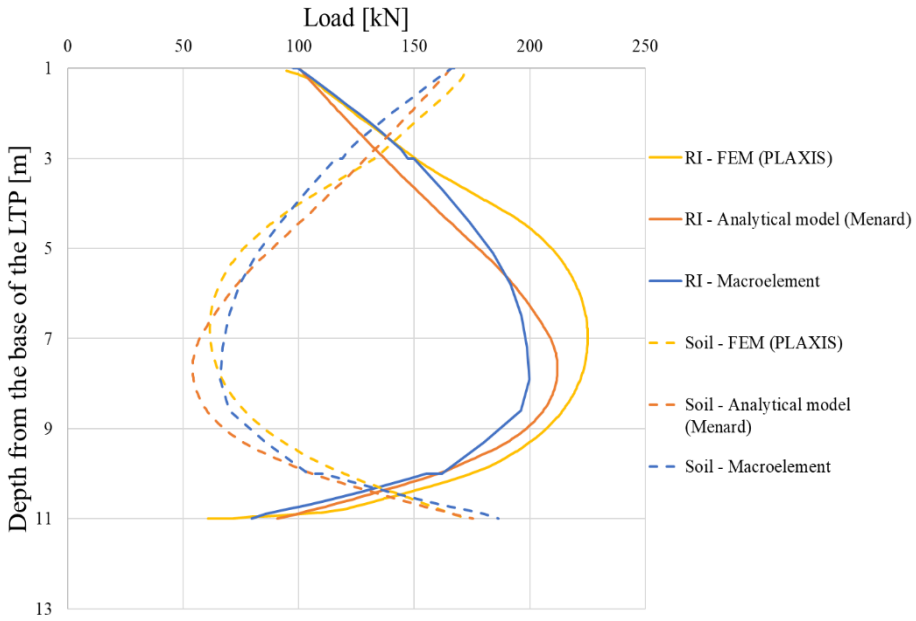

Figure 5-16: Load inside the RI, and the corresponding soil volume.

5.6 Case study: 3D Configuration

The main interest in developing the macroelement is to reproduce the behaviour of rigid inclusions under a gravity foundation. To be able add a load combination of {V, H, M} and thus overcome the shortening of the unit cell model of only applying a uniform vertical loading derived from {V, M}. Although the current model takes the 3D geometry aspect into account but not the 3D loading, since it is formulated in a 1D framework, we could perform the analogy with a 1D embedding of fibres in a 3D support volume, as is a common approach. In this case, the rigid inclusions can be viewed as fibres embedded in a finite soil volume. What makes this analogy even more valid is that the rigid inclusions are not connected to the foundation. Thus, they should only be subjected to cyclic loading in one direction. In other words, the inclusions can be compressed, but never pulled out of the structure.

The unit cell model represents very well the interaction between foundation-LTP-soil-inclusion, subjected to uniform vertical loading, forming a local multiscale macroelement at the level of an axisymmetric model. Therefore, a compilation of these models in a 3D geometric configuration (Figure 5-17) could be a good solution to reproduce the same interaction under the total load applied at the base of the foundation through the kinematic relationship without having to simulate each unit cell individually.

The 3D configuration of the model includes the interaction with the external soil mass and the interaction between the meshes, as described in the previous sections.

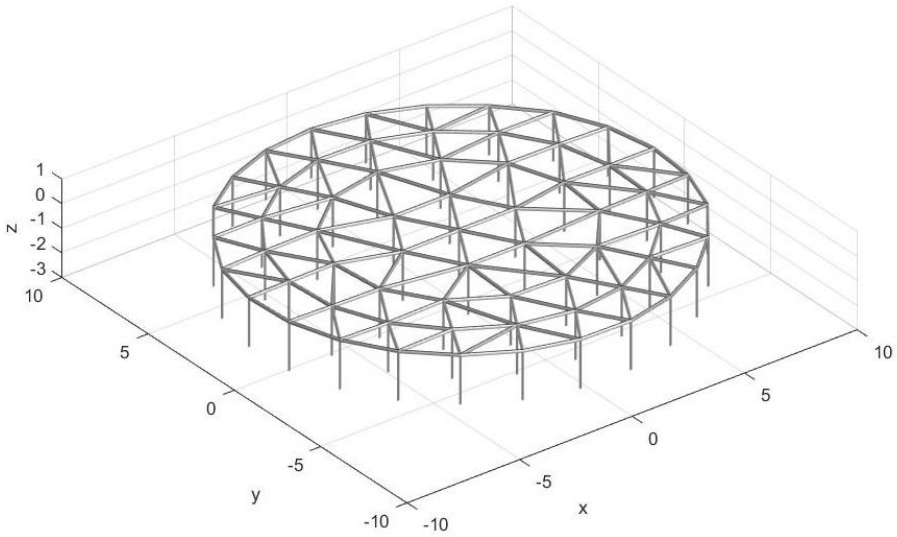

Figure 5-17: Compilation of the local multiscale macroelements in a 3D geometric configuration.

5.6.1 Vertical load

Since the model is built in 3D configuration and designed for a vertical response, a vertical load representing the total dead load at the base of the foundation is first applied to the master node "M". The result of this simulation is presented in terms of settlements of the foundation and settlements of the RI located at the centre of the foundation and its corresponding soil volume. To highlight the importance of the interaction with the external soil mass for the load diffusing, two versions of the macroelement are compared with a 3D FEM performed using PLAXIS 3D. The results directly reflect the importance of considering load distribution as it affects the overall settlement of the foundation. The settlement for this case was reduced by 23% relatively significant based on the diameter of the foundation equal to 19.3 m and a compressible soil of 10 m depth. This adjustment leads to a very similar result compared to the 3D FEM (Figure 5-18). The difference between the results of the FEM and the macroelement can be seen in the deformed part of the gravity foundation. The concrete volume is modelled without considering the massive density of the steel reinforcement, which could be the reason for this low deformation. On the other hand, the foundation is estimated to be infinitely rigid throughout the kinematic relationship in the macroelement, so the settlement of the foundation under vertical centred loading is a horizontal line, as expected.

In all upcoming results, we will point out that the macroelements were not calibrated to compare with PLAXIS 3D. The same parameters used in the unit cell are extended to the 3D macroelement version.

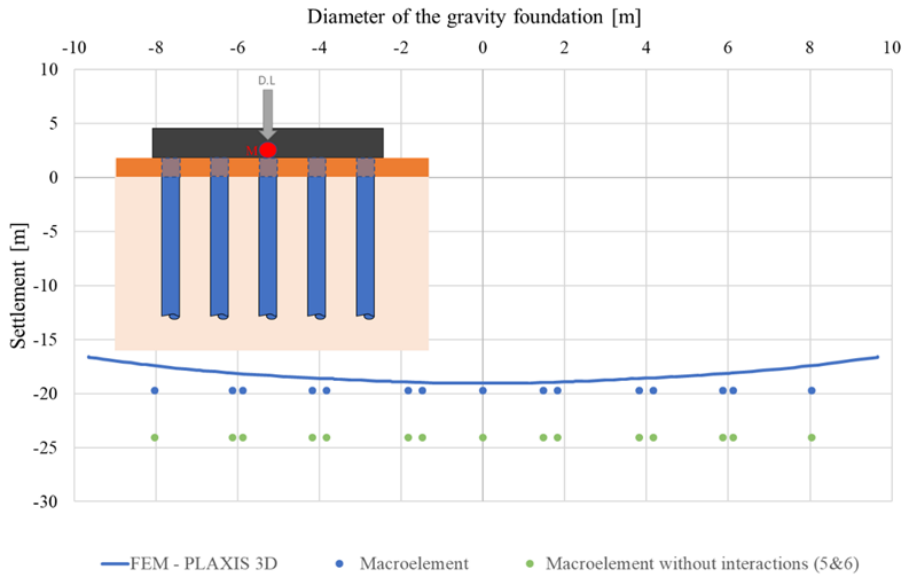

Figure 5-18: Settlements of the foundation under the dead load.

The settlement result of the RI at the centre of the gravity foundation and its complementary soil volume is compared between the macroelement and the 3D FEM. The settlements at the head of the inclusion are almost identical for the two methods. We could notice a difference in the settlement profile in the LTP. This difference could be due to the different modelling technique of the LTP. In FEM, the LTP is modelled as an independent soil layer with an elasto-plastic soil model. However, in the macroelement, a different modelling technique was used, namely the fictitious column technique (Figure 5-19), which was extended in the LTP to transfer the load by friction to the soil and the RI domain, taking their different stiffness into account. At the base resistance level, both approaches give very similar results. The very small difference between the two profiles for the LTP and base resistance is due to the different soil model used at the interfaces, however both have the same shape with a small offset factor.

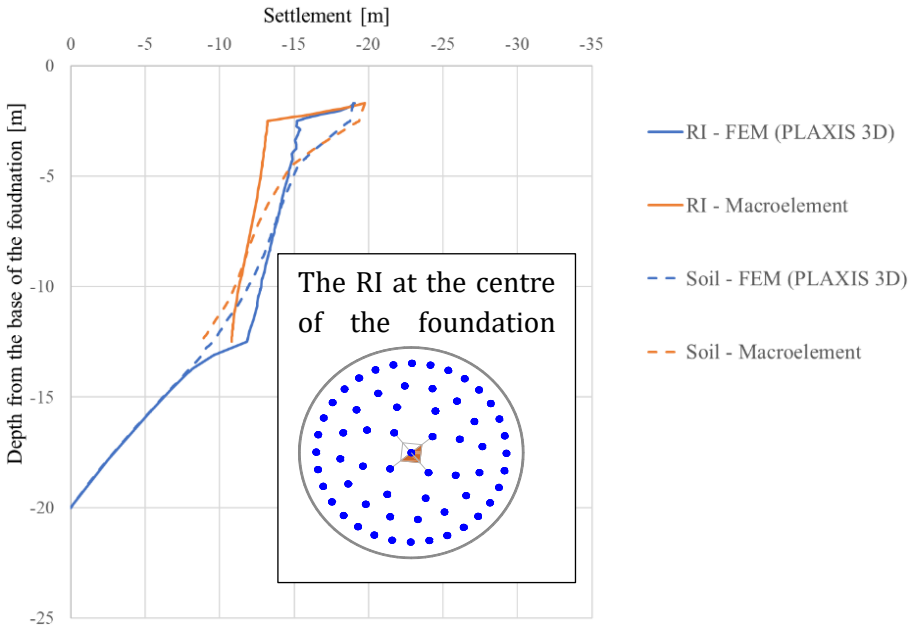

Figure 5-19: Settlement of the tributary area in the middle of the foundation (RI + soil).

The comparison of the maximum axial load in the selected rigid inclusions with the 3D FEM (Figure 5-20) shows, first, the similarity of the values in both methods and, second, that the variation of the axial load in the rigid inclusions is diametrically opposite to the example (R1 and R1*) almost null, since in this case only a vertical load is applied. We could notice that the biggest difference between the axial load in the macroelement and in the 3D FEM occurs in the rigid inclusions at the edge of the foundation (R1 and R1*), which could be related to the geometry effect and the particular shape of the gravity foundation, leading to a slight dissymmetry in the transfer of the axial load to the rigid inclusions, which cannot be replicated in the same way in the macroelement with the current definition of the kinematic relationship.

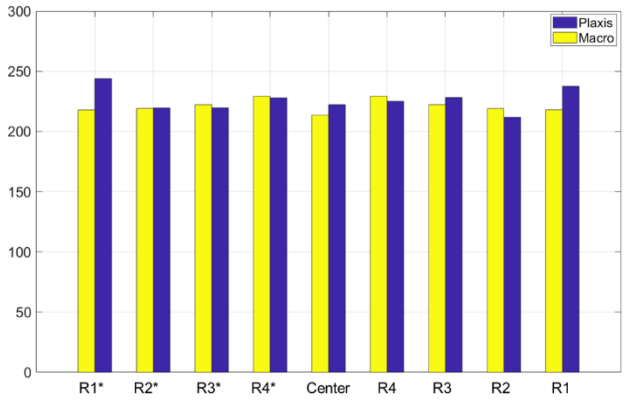

Figure 5-20: Maximum axial load along the line of RIs aligned with the wind direction, under the self-weight.

5.6.2 Overturning moment

The multiscale macroelement model is subjected to a vertical load, a horizontal load, and an overturning moment. The values of the overturning moment derived from instrumentation and used in the FEM chapter are also used for this approach. Two values are used: *M_12* and *M_16*, i.e. the moments for a wind speed of 12 m/s and 16 m/s.

In this case, the settlement of the foundation is no longer horizontal on the line. We could see that the overturning moment effect on both the macroelement and the 3D FEM is almost the same in terms of the inclination of the two approaches (Figure 5-21). On the one hand, the points representing the macroelement *M_12* and *M_16* coincide with the corresponding moment values of the 3D FEM. The difference on the other side results from the deformation (deflection) of the foundation that occurs in the FEM. The rotation of the foundation due to the overturning moment increases the differential settlement, i.e., while the small difference between the differential settlements of the two approaches over the entire foundation diameter, the (Table 5.1) with its calculation of the differential settlement, we could notice how the two approaches are relatively closed and also both are very far from the maximum differential settlement criteria of 3 mm/m.

Table 5.1: Comparison between the two approaches

Differential settlement (mm/m)		
Load case	3D FEM	Macroelement
M_12	0.23	0.37
M_16	0.61	0.68

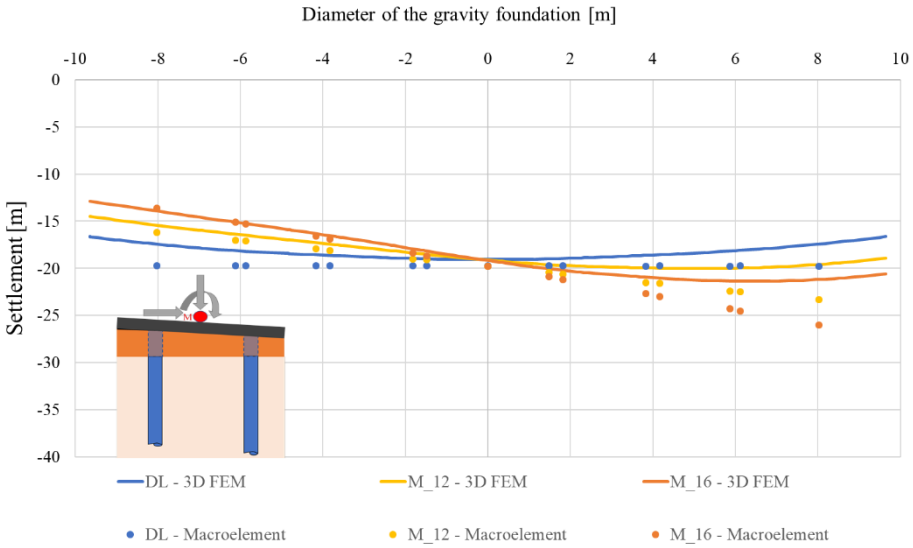

Figure 5-21: Settlements of the foundation under different load cases.

One of the main advantages of the macroelement model is the access to loading and settlement in all components of the model. Due to the overturning moment, the load transfer to the rigid inclusions varies depending on the position of the inclusions with respect to the main wind direction, as we saw in the chapter on installation. Figure 5-22 shows the comparison between the 3D FEM and the macroelement for the axial load within the RIs on the line of the main wind direction. As an example, R1 represents the inclusions that are most loaded due to their position at the edge of the foundation against the wind direction, while the (*) represent the diametrically opposite direction, which is the least loaded in this case.

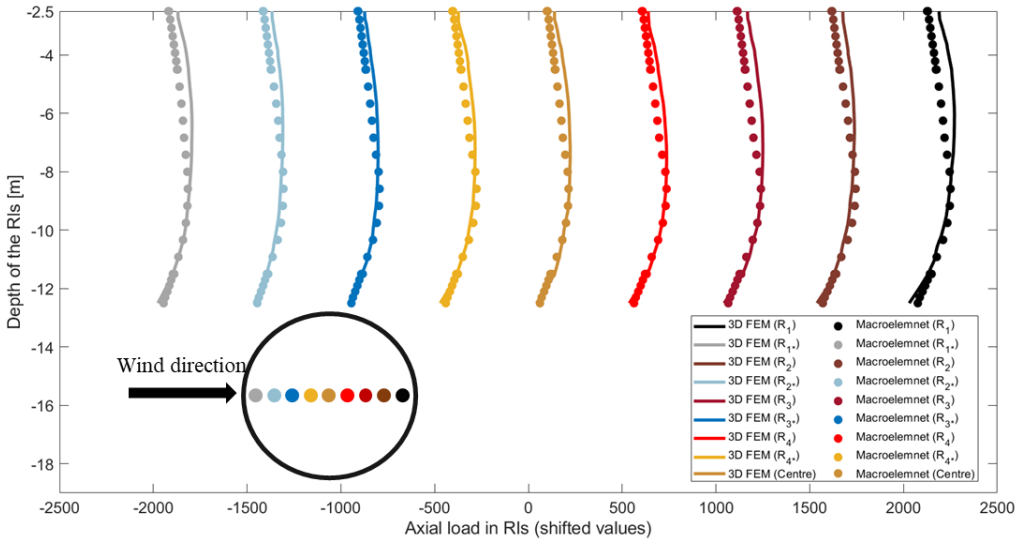

Figure 5-22: Axial load within rigid inclusions located on the same line of the main wind direction.

For rigid inclusions perpendicular to the wind direction, the results for axial loading are similar to FEM. In this case, the effect of wind is relatively less impactful in terms of load transfer for the diametrically opposed rigid inclusions. The results shown in (Figure 5-23) represent this comparison, but the values are offset in a plot similar to (Figure 5-22) to show all rigid inclusions in one graph. The results from the macroelement mode for this set of RIs also reproduce their behaviour very well, with high quantitative and qualitative similarity compared to PLAXIS 3D.

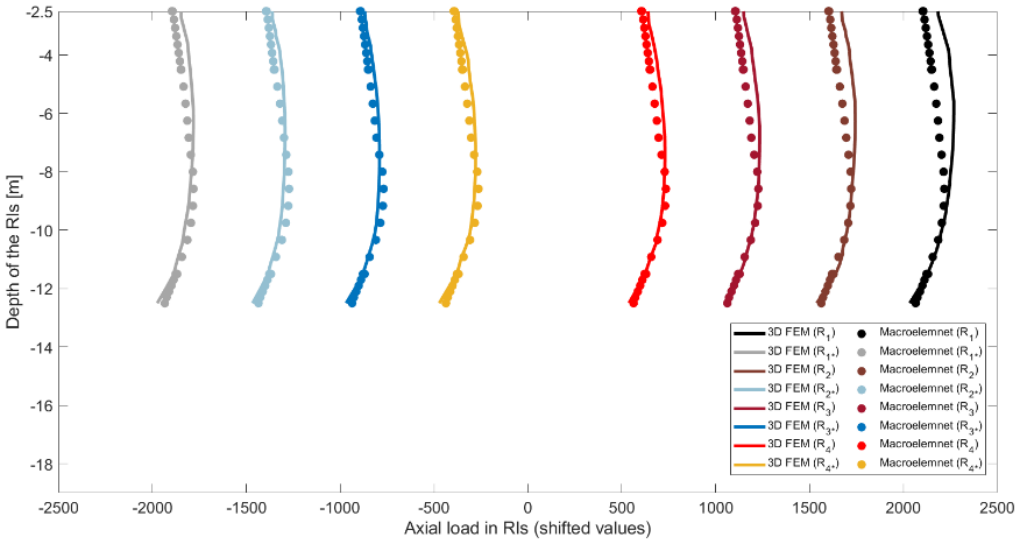

Figure 5-23: Axial load within rigid inclusions located on the same line of the main wind direction.

To narrow down the quantitative comparison of results between the three-dimensional macroelement model and the 3D FEM. The following results represent a cross-section of rigid inclusions located within the axis of the wind direction at their maximum axial loading, also called the "neutral plane," and are presented in a histogram (Figure 5-24). The comparison between the two methods reflects the accuracy of the macroelement in handling the overturning moment, since we can see that the total axial loads on the left side of the table (against the wind direction) are larger than the values of the rigid inclusions aligned with the wind direction (Figure 5-25). The R_1 opposite to the wind direction started from values near 250 KN, while the values of the R_1* diameterally opposite, the values are around 190 KN. When moving from R_1 to R_4 the maximum axial load in the rigid inclusions reduced in both methods. While when moving from R_1* to R_4* the axial load increases to than stabilize at the rigid inclusion located in the centre (M_12 and DL) Moreover, and more importantly, the results of the macroelement model are very close to those calculated by the finite element method, which gives the macroelement model a high credibility.

When the RI is situated at the centre of the Wind Turbine foundation, the stress fluctuations induced by the overturning moment are relatively restrained in comparison to the RIs positioned at the perimeter of the WT foundation. Both the macroelement analysis and the 3D FEM display nearly equivalent stress variation values for the WT's self-weight and when subjected to a moment value of M_12 (Figure 5-26).

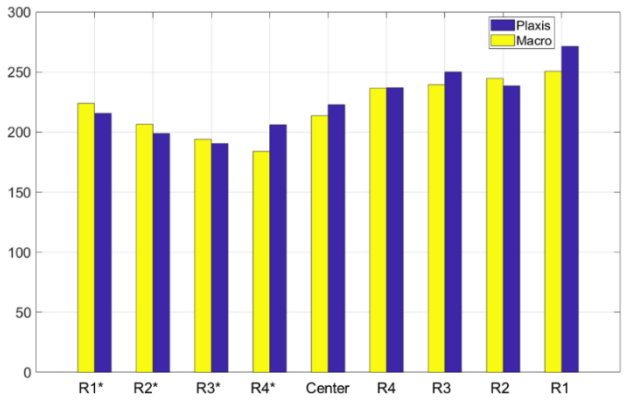

Figure 5-24: Maximum Axial Load at the line of RIs aligned with the wind direction, under an overturning moment of M_12.

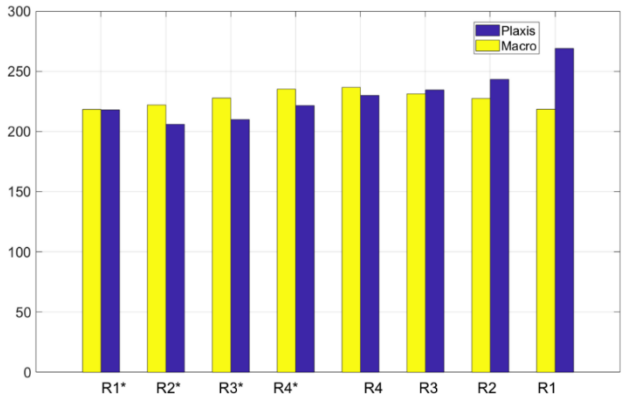

Figure 5-25: Maximum Axial Load at the line of RIs orthogonal to the wind direction, under an overturning moment of M_12.

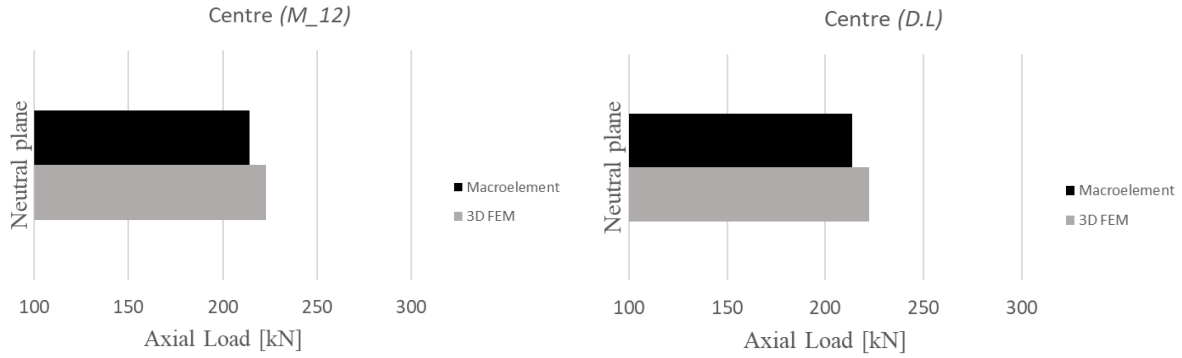

Figure 5-26: Maximum Axial Load of the RI at the centre of the foundation (Macroelement vs 3D FEM).

5.6.3 Comparison with FEM and Instrumentation

One of the most useful tools for validating a numerical model is comparison with a real scale instrumentation. In this project, the macroelement model is compared to available measurements of the instrumented wind turbine foundation, which in some ways immensely more beneficial than the usual methods of validating the macroelements by comparing results to direct methods. Figure 5-27 shows the stress variation of the rigid inclusions under the wind turbine foundation for a wind speed between 11 m/s and 13 m/s and compares it with the 3D FEM and the

macroelement results under M_12 overturning moment. The results for both numerical methods are very close to the measurements. We could see that the positive and negative stress variations in the macroelement are well calculated, and the results are in concordance with the measurements.

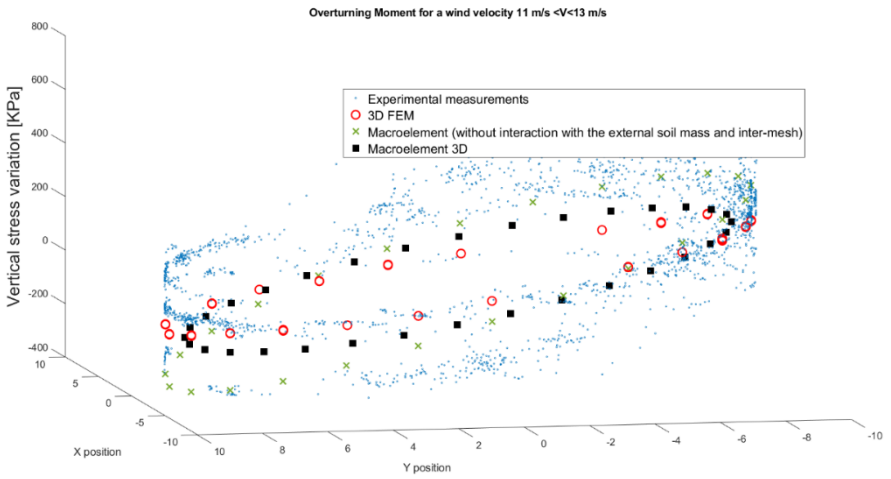

Figure 5-27: Vertical stress variations at the head level of the outer perimeter of the rigid inclusions (Measurements, 3D FEM and macroelement).

5.7 Conclusions

This chapter presents a novel macroelement developed for soil reinforcement by rigid inclusions. The model is based on two fundamental concepts of modelling, multiphase modelling and the macroelement approach. The developed approach has successfully simulated (1) a static load test on an isolated rigid inclusion. (2) An axisymmetric model of a rigid inclusion centred in the soil volume, a unit cell of a rigid inclusions grid. (3) A three-dimensional configuration of rigid inclusions under the foundation of a wind turbine. For each simulation, the model was compared with experimental, finite element, and analytical methods, and a very good correlation was found between the macroelement results and the other methods. The novel model is considered an efficient alternative to the simplified design methods, since the user is able to implement the CMCs positions and introduce the trapezoidal distributive uniform load under the gravity foundation, which is not possible with the current analytical methods that make the macroelement more complete model. In addition, the model is dramatically fast compared to direct methods such as FEM on PLAXIS, which was used in this work. One of the interesting results of the macroelement is that the model produces very closed-form results within its 1D behaviour of the reinforcement compared to the 3D model FEM. This suggests that the design of the soil reinforcement technique could be simplified to a 1D response depending on the project concepts, as in the case of the example of the fibres inside the beam. The developed macroelement model is less informative than the 3D FEM however, it is suitable for the RIs applications with the current output results.

CHAPTER 6

General Conclusions and Perspectives

The popularity of soil reinforcement by rigid inclusions has indeed increased significantly since the 1990s. The technique has proven to be effective in a wide range of geotechnical projects around the world, including infrastructure development, building construction, and renewable energy facilities such as wind turbines. The continuous increase in the number of projects using rigid inclusions is due to several reasons, such as its effectiveness and adaptability in different soil types and difficult ground conditions, lower costs and lower carbon emissions compared to classical geotechnical techniques.

On the other hand, there has been a significant advancement in wind turbine technology to increase electricity production and improve overall efficiency. As part of this advancement, wind turbine designs have been evolving to accommodate taller masts and larger turbine capacities.

As part of the FEDRE project FUI25, current research is focused on studying the behaviour of rigid inclusions under wind turbine foundations. One particular aspect that is of great interest and could benefit from the present study is the behaviour of rigid inclusions when existing gravity foundations are reused in wind turbine repowering projects. Logistically, it is possible to execute new columns to cover the additional area of the foundation, thus extending the reach of the rigid inclusions. This allows the foundation to be strengthened to meet the increased load requirements associated with wind turbine repowering. This research is conducted using a multiaxial approach that includes analytical, numerical, and experimental studies:

- Real scale monitoring of rigid inclusions, wind turbine foundation and real scale wind turbine
- Nonlinear FEM of the soil reinforced by rigid inclusions under wind turbine foundation
- Development of a novel multiscale macroelement for a soil reinforced by rigid inclusions

1) Instrumentation

The primary objective of the instrumentation was to monitor and record the behaviour of the soil reinforced by rigid inclusions under wind turbine loading. This involved carefully interpreting measurements obtained from various sensors during different phases of construction. The sensors were strategically placed during construction to capture the effects of wind on the readings. The use of earth pressure cells provided insights into the transfer of loads from foundations to the inclusions.

Initial measurements showed differences before and after the wind turbine was commissioned, which was further confirmed by conducting an ON/OFF test on the wind turbine with live measurements. To analyse the readings irrespective of wind direction, a statistical method known as Principal Component Analysis (PCA) was employed. This method qualitatively illustrated the overall behaviour of the rigid inclusions under the wind turbine foundation. The

analysis covered a range of wind directions, and the components reflected the behaviour of the rigid inclusions.

For quantitative analysis independent of wind direction, an algorithmic method was developed in the thesis. This method combined measurements with the Supervisory Control and Data Acquisition (SCADA) system to quantify global stress variations beneath the foundation caused by wind loading and direction. By using this method, the overturning moments were back-calculated from the measurements and associated with specific wind velocities.

Additionally, an instrumented static load test was performed near the wind turbine platform. The measurements from this test allowed the calibration of soil parameters in the numerical model to match the measurements and accurately represent the behaviour of isolated rigid inclusions. This calibration facilitated more precise modelling of the soil-structure interaction at the interface between the rigid inclusions and the soil.

The findings from this chapter were used to supplement and compare with the numerical models, contributing to a better understanding of the behaviour of reinforced soil with rigid inclusions under wind turbine loading.

2) Nonlinear finite element method

The finite element method plays a significant role in the design and research of rigid inclusions. This chapter introduces a comprehensive strategy for modelling that covers the essential soil-structure interactions identified in the literature review. The first focus of this chapter is on modelling the instrumented static load test conducted. The objective is to establish a reliable dataset of soil parameters at the inclusion-soil interface. Additionally, various soil tests were simulated using the finite element method and compared with experimental measurements from lab tests. Different soil models, such as MC, HSM, and HSSM, were calibrated to ensure accurate representation of soil behaviour.

Subsequently, a series of three-dimensional models were developed for sensitivity analysis and comparison with available measurements. The comparison results were satisfactory, affirming that the numerical models can serve as a reference for studying rigid inclusions under wind turbines. Moreover, these models contribute to the creation of a data bank for the macroelement tool developed in this thesis.

3) Macroelement

Finally, a novel multiscale macroelement has been developed to analyse the behaviour of soil reinforced by rigid inclusions under axial loading, horizontal loading, and moments. The model has been validated through numerical and experimental investigations. It employs an array of biphasic columns formulated using the MATLAB toolbox ATL4S, considering coupling at different embedment depths.

This macroelement model simulates the interaction between the rigid inclusions and the surrounding soil, as well as the intermesh interactions within the CMCs. It specifically addresses

a scenario where the CMCs experience higher loading compared to other elements, utilizing a trapezoidal loading scheme applied beneath the foundation of a wind turbine.

The model follows the global concept of the homogenization method commonly used in such cases, while also incorporating the conventional design principles for rigid inclusions. However, it adopts a unique approach and a robust treatment to enhance its capabilities. Notably, the model's internal programming allows for customization of the interface law to suit specific applications. Furthermore, its computational efficiency enables engineers to perform sensitivity analyses during the design phase, thereby deepening their understanding and knowledge of each construction site. Although the model presents significant advantages over existing design methods, it also holds potential for further development to handle more complex interactions.

Perspectives

The research presented in this document showcases significant potential for further exploration, especially when combined with the ongoing monitoring of the wind turbine. This potential is further strengthened by the anticipated outcomes of the FEDRE project, which aims to provide a repowering solution. Looking ahead, there are short-term and mid-term perspectives to consider.

1) Short term perspectives

The ongoing monitoring of the real-scale wind turbine has generated a diverse set of measurements, covering both static and dynamic aspects. Notably, the dynamic measurements were obtained more recently, adding an additional dimension to the data collected. Analysing these measurements presents a compelling opportunity to investigate the dynamic impact of the superstructure on the soil reinforced by rigid inclusions. This analysis has the potential to provide valuable insights into the behaviour and interaction of the system under dynamic loading conditions.

The nonlinear Finite Element Method employs a calibrated soil model that is capable of simulating cyclic effects in the soil. A promising avenue for near future study involves applying cyclic loads from wind turbines to the model and comparing the resulting measurements to dynamic experimental outputs. This comparative analysis can provide valuable insights into the model's ability to replicate the dynamic behaviour of the soil under wind turbine loading conditions.

2) Long term perspectives

The successfully developed macroelement in this thesis aimed to detect the behaviour of the rigid inclusions due to the vertical, horizontal and overturning moment. Although the current model takes into account the 3D geometry aspect but not the 3D loading, since it is formulated in a 1D framework, we could perform the analogy with a 1D embedding of fibres in a 3D support volume, as is a common approach. In this case, the rigid inclusions can be viewed as fibres embedded in a finite soil volume. What makes this analogy even more valid is that the rigid inclusions are not connected to the foundation. Thus, they should only be subjected to cyclic loading in one direction.

In other words, the inclusions can be compressed, but never pulled out of the structure. The macroelement could be developed to extend to 3D frame in order to take into account all the complexity in the soil-structure interaction.

The macroelement developed in this thesis successfully captures the behaviour of rigid inclusions under vertical, horizontal, and overturning moment loads. While the current model considers the 3D geometry aspect, it does not incorporate 3D loading as it is formulated within a 1D framework. However, an analogy can be drawn by envisioning a 1D embedding of fibers within a 3D support volume, which is a commonly adopted approach. To account for the complexities of soil-structure interaction, there is potential to expand the macroelement to a 3D framework. This expansion would enable consideration of the full three-dimensional aspects and enhance the model's accuracy and comprehensiveness.

The outcome of this research will be studied by the national French project ASIRI+ for the rigid inclusions in case of wind turbines.

The algorithm developed in this thesis will be able to utilize the ongoing continuous measurements from the real-scale monitoring as input for analysis. The primary objective of incorporating these measurements into the algorithm is to enhance the curve fitting process and enable the simulation of the wind turbine's future behaviour using machine learning techniques. By integrating real-time data into the algorithm, the model's accuracy and predictive capabilities can be significantly improved.

The main objective of the FEDRE project is to provide a repowering solution by utilizing the existing gravity foundation. One potential approach is to enhance the concrete foundation by constructing a mushroom-shaped canopy on top of the current structure. This method allows the rigid inclusions that reinforce the original foundation's footprint to remain intact. Additionally, it is feasible to install new columns to cover the expanded area of the foundation, facilitating the implementation of the repowering solution within the existing infrastructure. This perspective emphasizes a design and construction focus for the future.

Bibliography

Abboud, Y., 2017. Développement d'un macroélément pour l'étude des fondations superficielles sous charge sismique. Paris Est.

Abdelrazaq, A., 2012. Validating the Structural Behavior and Response of Burj Khalifa: Synopsis of the Full Scale Structural Health Monitoring Programs. International Journal of High-Rise Buildings 1, 37–51. https://doi.org/10.21022/IJHRB.2012.1.1.037

Adekoya, O.B., Olabode, J.K., Rafi, S.K., 2021. Renewable energy consumption, carbon emissions and human development: Empirical comparison of the trajectories of world regions. Renewable Energy 179, 1836–1848. https://doi.org/10.1016/j.renene.2021.08.019

Aguado, P., Berthelot, P., Carpinteiro, L., Durand, F., Glandy, M., Liausu, P., Pezot, B., Poilpre, C., Lambert, S., Volcke, J.-P., 2012. Recommandations sur la conception, le calcul, l'exécution et le contrôle des fondations d'éoliennes, par les membres du groupe de travail CFMS « Fondations d'éoliennes ». Revue Française de Géotechnique 71–86.

Alexiew, D., Vogel, W., 2002. Remblais ferroviaires renforcés sur pieux en Allemagne : projets phares., in: Travaux. pp. 47–52.

Allagnat, D., 2005. La méthode observationnelle pour le dimensionnement interactif des ouvrages. Presses de l'école nationale des Ponts et chaussées.

Antoinet, E., Marthe, M., 2016. L'amélioration des sols par inclusions rigides. Retours d'expérience depuis ASIRI.

Apergis, N., Pinar, M., 2021. The role of party polarization in renewable energy consumption: Fresh evidence across the EU countries. Energy Policy 157, 112518. https://doi.org/10.1016/j.enpol.2021.112518

API, 2GEO, 2011. Recommended practice for geotechnical foundation design consideration.

API RP2A-WSD, 2007. American petroleum institute recom-mended practice for planning, designing and constructing fixed offshore platforms–working stress design.

Arany, L., Bhattacharya, S., Macdonald, J., Hogan, S.J., 2015. Simplified critical mudline bending moment spectra of offshore wind turbine support structures: Simplified critical bending moment spectra of offshore wind turbines. Wind Energ. 18, 2171–2197. https://doi.org/10.1002/we.1812

ASCE–AWEA, 2011. Recommended practice for compliance of large land-based wind turbine support structures. American Wind Energy Association: Reston, VA, USA.

Ashford, S.A., Jakrapiyanun, W., Lukkunaprasit, P., 2000. Amplification of earthquake ground motions in Bangkok. Presented at the 12th World Conference on Earthquake Engineering, Auckland, New Zealand.

ASIRI+, 2018. Etat de l'art.

ASIRI, 2013. Recommendations for the design, construction and control of rigid inclusion ground improvements.

Atkinson, J.H., 2000. Non-linear soil stiffness in routine design. Géotechnique 50, 487–508.

Atkinson, J.H., Sallfors, G., 1991. Experimental determination of soil properties. General Report to Session 1. Presented at the 10th ECSMFE, Florence, pp. 915–956.

Awad, E.A., 2001. Basics of Fiber Optics - Fiber Optics Technician's Manual, Book, Hayes Jim, 2nd Edition. ed. Delmar, USA.

Awwad, T., Donia, M., 2016. The efficiency of using a seismic base isolation system for a 2D concrete frame founded upon improved soft soil with rigid inclusions. Earthq. Eng. Eng. Vib. 15, 49–60. https://doi.org/10.1007/s11803-016-0304-6

Bado, M.F., Casas, J.R., 2021. A Review of Recent Distributed Optical Fiber Sensors Applications for Civil Engineering Structural Health Monitoring. Sensors 21, 1818. https://doi.org/10.3390/s21051818

Bailly, C., 2014. Wind turbine dynamic-application to foundations.

Bao, X., Li, W., Qin, Z., Chen, L., 2014. OTDR and OFDR for distributed multi-parameter sensing, in: Ecke, W., Peters, K.J., Meyendorf, N.G., Matikas, T.E. (Eds.), . Presented at the SPIE Smart Structures and Materials + Nondestructive Evaluation and Health Monitoring, San Diego, California, USA, p. 906202. https://doi.org/10.1117/12.2045807

Barnoski, J.K., Jensen, S.M., 1976. Fiber waveguides: A novel technique for investigating attenuation characteristics. Applied optics 15, 2112–2115.

Baroni, M., Briançon, L., Racinais, J., Scache, H., 2016. Semelles Sur inclusions rigides: Validation Du Nouveau Cahier Des Charges De Menard-Footings over rigid inclusions: Experimental validation of the menard new specifications. Presented at the Journées Nationales de Géotechnique et de Géologie de l'Ingénieur, Nancy, pp. 1–8.

Bartz, J.R., Blatz, J.A., 2022. Considerations for measuring residual stresses in driven piles with vibrating wire strain gauges. Can. Geotech. J. 59, 441–446. https://doi.org/10.1139/cgj-2020-0614

Bennis, M., De Buhan, P., 2003. A multiphase constitutive model of reinforced soils accounting for soil-inclusion interaction behaviour. Mathematical and Computer Modelling 37, 469–475. https://doi.org/10.1016/S0895-7177(03)00039-6

Benz, T., 2007. Small-strain stiffness of soils and its numerical consequences. Univ. Stuttgart, Inst. f. Geotechnik.

Bersan, S., Bergamo, O., Palmieri, L., Schenato, L., Simonini, P., 2018. Distributed strain measurements in a CFA pile using high spatial resolution fibre optic sensors. Engineering Structures 160, 554–565. https://doi.org/10.1016/j.engstruct.2018.01.046

Bhattacharya, S., Nikitas, N., Garnsey, J., Alexander, N.A., Cox, J., Lombardi, D., Muir Wood, D., Nash, D.F.T., 2013. Observed dynamic soil–structure interaction in scale testing of offshore wind turbine foundations. Soil Dynamics and Earthquake Engineering 54, 47–60. https://doi.org/10.1016/j.soildyn.2013.07.012

Bienen, B., Byrne, B.W., Houlsby, G.T., Cassidy, M.J., 2006. Investigating six-degree-of-freedom loading of shallow foundations on sand. Géotechnique 56, 367–379. https://doi.org/10.1680/geot.2006.56.6.367

Bird, J.F., Boulanger, R.W., Idriss, I.M., 2005. ENGINEERING GEOLOGY | Liquefaction, in: Encyclopedia of Geology. Elsevier, pp. 525–534. https://doi.org/10.1016/B0-12-369396-9/00217-3

Bishop, A.W., Henkel, D.J., 1957. The measurement of soil properties in the triaxial test. E. Arnold.

Blanco-M., A., Gibert, K., Marti-Puig, P., Cusidó, J., Solé-Casals, J., 2018. Identifying health status of wind turbines by using self organizing maps and interpretation-oriented post-processing tools. Energies 11, 723. https://doi.org/10.3390/en11040723

Bohn, C., 2015. Serviceability and safety in the design of rigid inclusions and combined pile-raft foundations. Paris Est.

Bohn, C., Szymkiewicz, F., Briançon, L., Lambert, S., Carpinteiro, L., 2022. Essais de chargement de semelles sur inclusions rigides. Presented at the 11emes Journées Nationales de Géotechnique et de Géologie de l'Ingénieur, Lyon.

Boldyreva, E., 2016. Mesures réparties par réflectométrie fréquentielle sur fibres optiques (Doctoral dissertation).

Bordes, J.L., Debreuille, P.J., 1984. Some facts about long-term reliability of vibrating wire instruments. Reliability of geotechnical instrumentation 20–27.

Bourgeois, E., De Buhan, P., Hassen, G., 2012. Settlement analysis of piled-raft foundations by means of a multiphase model accounting for soil-pile interactions. Computers and Geotechnics 46, 26–38. https://doi.org/10.1016/j.compgeo.2012.05.015

Bourgeois, E., Rospars, C., Humbert, P., De Buhan, P., 2006. A 'multi-phase'model for finite element analysis of traction forces in bolts used in the reinforcement of tunnels walls. Taylor & Francis: London.

Briançon, L., 2020. Instrumentation in situ, un outil pour les techniques d'amélioration des sols. Rev. Fr. Geotech. 4. https://doi.org/10.1051/geotech/2020002

Briançon, L., 2002. Renforcement des sols par inclusions rigides. Etat de l'art en France et à l'étranger. Irex, Opération du réseau Génie Civil et urbain.

Briançon, L., Cazaudumec, B., Pincent, B., 2016. Auscultation géotechnique. Technique de l'Ingénieur C 229.
Briançon, L., Dias, D., Simon, C., 2015. Monitoring and numerical investigation of a rigid inclusions–reinforced industrial building. Can. Geotech. J. 52, 1592–1604. https://doi.org/10.1139/cgj-2014-0262
Briançon, L., Liausu, P., Plumelle, P., Simon, B., 2018. Amélioration et renforcement des sols-Tome 2, in: Le Moniteur.
Briançon, L., Simon, B., 2017. Pile-supported embankment over soft soil for a high-speed line. Geosynthetics International 293–305. https://doi.org/10.1680/jgein.17.00002
Briançon, L., Simon, B., 2011. Renforcement d'un remblai par inclusions rigides: approche expérimentale. Revue française de géotechnique 3–14.
Briet, S., Plomteux, C., 2010. Integrated Ground Improvement Solution for Windmill Foundation Support in soft soils. Presented at the Proc. 63rd Canadian Geotechnical Conference & 6th Canadian Permafrost Conference.
Brinkgreve, R.B.J., Swolfs, W.M., Engin, E., Waterman, D., Chesaru, A., Bonnier, P.G., Galavi, V., 2010. PLAXIS 2D 2010 User manual, Plaxis bv.
Brinkgreve, R.B.J., Vermeer, P.A., 2002. Plaxis finite element code for soil and rock analyses, Version 8. Balkema, Rotterdam.
BURLON, S., FRANK, R., BAGUELIN, F., HABERT, J., LEGRAND, S., 2014. Model factor for the bearing capacity of piles from pressuremeter test results – Eurocode 7 approach. Géotechnique 64, 513–525. https://doi.org/10.1680/geot.13.P.061
Burtin, P., Racinais, J., 2016. Embankment on Soft Soil Reinforced by CMC Semi-Rigid Inclusions for the High-speed Railway SEA. Procedia Engineering 143, 355–362. https://doi.org/10.1016/j.proeng.2016.06.045
Burton, T., Jenkins, N., Sharpe, D., Bossanyi, E., 2011. Wind energy handbook, Second Edition. ed. Wiley, Chichester , West Sussex.
Butterfield, R., Gottardi, G., 1994. A complete three-dimensional failure envelope for shallow footings on sand. Géotechnique 44, 181–184. https://doi.org/10.1680/geot.1994.44.1.181
Byrne, B., McAdam, R., Burd, H., Houlsby, G., Martin, C., C, L., Taborda, D., Potts, D., Jardine, R., Sideri, M., Schroeder, F., Gavin, K., Doherty, P., Igoe, D., Wood, A., Kallehave, D., Gretlund, J., 2015. New design methods for large diameter piles under lateral loading for offshore wind applications, in: Meyer, V. (Ed.), Frontiers in Offshore Geotechnics III. CRC Press, pp. 705–710. https://doi.org/10.1201/b18442-96
Byrne, B.W., Houlsby, G.T., 2001. Observations of footing behaviour on loose carbonate sands. Géotechnique 51, 463–466. https://doi.org/10.1680/geot.2001.51.5.463
Byrne, B.W., Houlsby, G.T., Martin, C.M., 2002. Cyclic loading of shallow offshore foundations on sand. Presented at the Physical Modelling in Geotechnics: Proceedings of the International Conference ICPGM'02, Taylor & Francis, St John's, Newfoundland, Canada, p. 277.
Caponero, M.A., 2020. Special Issue "Fibre Optic Sensors for Structural and Geotechnical Monitoring." Sensors 20, 2415. https://doi.org/10.3390/s20082415
Cassidy, M.J., Bienen, B., 2002. Three-dimensional numerical analysis of jack-up structures on sand. Presented at the ISOPE International Ocean and Polar Engineering Conference, p. ISOPE-I.
Cassidy, M.J., Martin, C.M., Houlsby, G.T., 2004. Development and application of force resultant models describing jack-up foundation behaviour. Marine Structures 17, 165–193. https://doi.org/10.1016/j.marstruc.2004.08.002
CFMS, 2011. Recommandations sur la conception, le calcul, l'exécution et le contrôle des fondations d'éoliennes (Comité Français de Mécanique des Sols et de géotechnique: CFMS).
Chandler, R., 1968. The shaft friction of piles in cohesive soils in terms of effective stress. Civil Eng & Public Works Review/UK 60.

Chatzigogos, C.T., Pecker, A., Salençon, J., 2009. Macroelement modeling of shallow foundations. Soil Dynamics and Earthquake Engineering 29, 765–781. https://doi.org/10.1016/j.soildyn.2008.08.009
Chen, C., Habert, G., Bouzidi, Y., Jullien, A., 2010. Environmental impact of cement production: detail of the different processes and cement plant variability evaluation. Journal of Cleaner Production 18, 478–485. https://doi.org/10.1016/j.jclepro.2009.12.014
Chow, V.T., 1986. Open-channel hydraulics. McGraw-Hill Inc, New York.
Chu, J., Varaksin, S., Klotz, U., Menge, P., 2009. State of the art report: construction processes. Presented at the 17th International Conference on Soil Mechanics & Geotechnical Engineering: TC17 meeting ground improvement.
Clancy, P., Randolph, M.F., 1993. An approximate analysis procedure for piled raft foundations. Int. J. Numer. Anal. Methods Geomech. 17, 849–869. https://doi.org/10.1002/nag.1610171203
Cohen, J.J., Azarova, V., Kollmann, A., Reichl, J., 2021. Preferences for community renewable energy investments in Europe. Energy Economics 100, 105386. https://doi.org/10.1016/j.eneco.2021.105386
Combarieu, O., 2008. Remblais sur sol compressible et inclusions rigides. Amélioration de l'approche du dimensionnement. Révue française de géotechnique 45–54.
Combarieu, O., 2007. Remblais sur sol médiocre et inclusions rigides. Nouvelle approche du dimensionnement (No. Rapport 1-07-5-01).
Combarieu, O., 2006. L'usage des modules de déformation en géotechnique. Rev. Fr. Geotech. 3–32. https://doi.org/10.1051/geotech/2006114003
Combarieu, O., 1990. Fondations superficielles sur sol amélioré par inclusions rigides verticales. Revue française de géotechnique 33–44.
Combarieu, O., 1988. Amélioration des sols par inclusions rigides verticales application à l'édification de remblais sur sols médiocres. Revue française de géotechnique 57–79.
Combarieu, O., Frossard, A., 2003. Amélioration des sols des berges de Loire par inclusions rigides pour stabiliser les remblais d'accès d'un poste à quai. Presented at the Geotechnical problems with man-made and man influenced grounds, Prague, Czech Republic, 25-28th August 2003, pp. 625–630.
Correia, A.A., 2011. A pile-head macro-element approach to seismic design of monoshaft-supported bridges. Unpublished PhD thesis). European School for Advanced Studies in Reduction of Seismic Risk (ROSE School), Pavia, Italy.
Correia, A.G., Santos, J., Barros, J.M.C., Niyama, S., 2001. An Approach to Predict Shear Modulus of Soils in the Range of 10-6 to 10-2 Strain Levels.
Cremer, C., 2001. Modelisation du comportement non lineaire des fondations superficielles sous seisme: macro-element d'interaction sol-structure. Ecole normale supérieure., Cachan,.
Cremer, C., Pecker, A., Davenne, L., 2002. Modelling of nonlinear dynamic behaviour of a shallow strip foundation with macro-element. Journal of Earthquake Engineering 6, 175–211.
Cuira, F., Simon, B., 2016. Benefits of soil structure interaction to the design of foundation structures. Journées Nationales de Géotechnique et de Géologie de l'Ingénieur.
Cuira, F., Simon, B., 2013. Prise en compte des effets de bord dans un massif renforcé par inclusions rigides. Presented at the Proceedings, 18th International Conference on Soil Mechanics and Geotechnical Engineering, pp. 1955–1962.
Cuira, F., Simon, B., 2009. Deux outils simples pour traiter des interactions complexes d'un massif renforcé par inclusions rigides. Presented at the Proceedings of the 17th International Conference on Soil Mechanics and Geotechnical Engineering, IOS Press, pp. 1550–1553.
Culshaw, B., 2000. Fiber optics in sensing and measurement. IEEE J. Select. Topics Quantum Electron. 6, 1014–1021. https://doi.org/10.1109/2944.902150
Currie, M., Saafi, M., Tachtatzis, C., Quail, F., 2015. Structural integrity monitoring of onshore wind turbine concrete foundations. Renewable Energy 83, 1131–1138. https://doi.org/10.1016/j.renene.2015.05.006
De Buhan, P., 2005. De l'approche par homogénéisation au développement d'un modele multiphasique: le cas des sols renforcés par inclusions linéaires.

De Buhan, P., Sudret, B., 2000. Micropolar multiphase model for materials reinforced by linear inclusions. European Journal of Mechanics - A/Solids 19, 669–687. https://doi.org/10.1016/S0997-7538(00)00181-9
Di Prisco, C.G., Massimino, M.R., Maugeri, M., Nicolosi, M., Nova, R., 2006. Cyclic numerical analysis of Noto Cathedral: soil–structure interaction modelling. Rivista Italiana di Geotecnica 48, 49–64.
Di Prisco, C.G., Nova, R., Sibilia, A., 2003. Shallow footings under cyclic loading: experimental behaviour and constitutive modelling, in: Geotechnical Analysis of Seismic Vulnerability of Historical Monuments. Pàtron.
Diaz-Rodriguez, J.A., López-Molina, J.A., 2008. Strain thresholds in soil dynamics. Presented at the roceedings of the 14th World Conference on Earthquake Engineering, Beijing, China, pp. 12–17.
DNV-ST-0126, n.d. Support structures for wind turbines.
Dong, N.P., 1998. In-situ Investigation of Soft and Stiff Clay in Bangkok (Masters thesis). Asian Institute of Technology (Masters thesis), Bangkok.
Duncan, J.M., Chang, C.-Y., 1970. Nonlinear Analysis of Stress and Strain in Soils. J. Soil Mech. and Found. Div. 96, 1629–1653. https://doi.org/10.1061/JSFEAQ.0001458
Dunnicliff, J., 1993. Geotechnical instrumentation for monitoring field performance, Synthesis of highway practice. Transportation Research Board, National Research Council, Washington, D.C.
Edenhofer, O., Pichs-Madruga, R., Sokona, Y., Seyboth, K., Matschoss, P., Kadner, S., et al., 2011. IPCC special report on renewable energy sources and climate change mitigation (Prepared By Working Group III of the Intergovernmental Panel on Climate Change). Cambridge University Press, Cambridge, UK.
Eickhoff, W., Ulrich, R., 1981. Optical frequency domain reflectometry in single-mode fiber. Appl. Phys. Lett. 39, 693–695. https://doi.org/10.1063/1.92872
EN ISO 18674-1, 2015. Allgemeine Regeln.
EN ISO 19674-3, 2017. Mesurages des déplacements perpendiculairement à une ligne par inclinomètre.
Energy, D.G., 2018. EU energy in figures: statistical pocketbook. Publications Office of the European Union, Luxembourg.
Enevoldsen, P., Xydis, G., 2019. Examining the trends of 35 years growth of key wind turbine components. Energy for Sustainable Development 50, 18–26. https://doi.org/10.1016/j.esd.2019.02.003
EU Climate Action, 2018. Climate strategies & targets.
Eurocode 7, 2007. Eurocode 7 - Geotechnical design - Part 2: Ground investigation and testing.
Eurocode 7 EN 1997-1, 2013. Eurocode 7: Geotechnical design - Part 1: General rules. European Committee for Standardization (CEN).
Eurocode 7 EN 1997-1, 2009. Eurocode 7: Geotechnical design - Part 1: General rules. European Committee for Standardization (CEN).
Eurocode 7 EN 1997-1, 2005. Eurocode 7: Geotechnical Design - Part 1: General Rules.
Eurocode 7 EN 1997-1, 2004. Eurocode 7: Geotechnical design - Part 1: General rules. European Committee for Standardization (CEN).
EWA, 2009. Wind Energy – The Facts: Part 2. European Wind Energy Association.
Fellenius, B.H., 2002. Determining the true distributions of load in instrumented piles. Geotechnical special publication 2, 1455–1470.
Frank, R., Zhao, S.R., 1982. Estimation par les paramètres pressiométriques de l'enfoncement sous charge axiale de pieux forés dans des sols fins. Bull. Liaison Labo. P. et Ch. 17–24.
Garcia, J.A.B., Rodríguez Rebolledo, J.F., dos Santos Mützenberg, D.V., Caicedo, B., de Farias Neves Gitirana, G., 2021. Experimental Investigation of a Load-Transfer Material for Foundations Reinforced by Rigid Inclusions. J. Geotech. Geoenviron. Eng. 147, 04021110. https://doi.org/10.1061/(ASCE)GT.1943-5606.0002649
Gazetas, G., Mylonakis, G., 1998. Seismic soil-structure interaction: New evidence and emerging issues. Geotechnical Special Publication 1119–1174.

Glandy, M., Frossard, A., 2002. Justification d'une fondation superficielle sur un sol renforcé d'inclusions. Annales du bâtiment et des travaux publics (Paris) 45–53.
González, J.S., Lacal-Arántegui, R., 2016. A review of regulatory framework for wind energy in European Union countries: Current state and expected developments. Renewable and Sustainable Energy Reviews 56, 588–602. https://doi.org/10.1016/j.rser.2015.11.091
Göransson, F., Nordenmark, A., 2011. Fatigue assessment of concrete foundations for wind power plants.
Gottardi, G., Houlsby, G.T., Butterfield, R., 1999. Plastic response of circular footings on sand under general planar loading. Géotechnique 49, 453–469. https://doi.org/10.1680/geot.1999.49.4.453
Grange, S., 2022. ATL4S–A Tool and Language for Simplified Structural Solution Strategy–Internal Report.
Grange, S., 2018. ATL4S—a tool and language for simplified structATL4S|A Tool and Language for Simplied Structural Solution Strategy.ural solution strategy (Internal Report). Technical report, GEOMAS, INSA-Lyon, Villeurbanne, France.
Grange, S., 2008. Modélisation simplifiée 3D de l'interaction sol-structure: application au génie parasismique. Institut National Polytechnique de Grenoble-INPG.
Grange, S., Kotronis, P., Mazars, J., 2008. A macro-element for a circular foundation to simulate 3D soil–structure interaction. Int. J. Numer. Anal. Meth. Geomech. 32, 1205–1227. https://doi.org/10.1002/nag.664
Grange, S., Salciarini, D. (Eds.), 2022. Deterministic Numerical Modeling of Soil–Structure Interaction, 1st ed. Wiley. https://doi.org/10.1002/9781119887690
Gravett, D.Z., Markou, G., 2021. State-of-the-art investigation of wind turbine structures founded on soft clay by considering the soil-foundation-structure interaction phenomenon – Optimization of battered RC piles. Engineering Structures 235, 112013. https://doi.org/10.1016/j.engstruct.2021.112013
Griffiths, D.V., Clancy, P., Randolph, M.F., 1991. Piled raft foundation analysis by finite elements, in: International Conference on Computer Methods and Advances in Geomechanics. 7. pp. 1153–1157.
Guo, Z., Yu, L., Wang, L., Bhattacharya, S., Nikitas, G., Xing, Y., 2015. Model Tests on the Long-Term Dynamic Performance of Offshore Wind Turbines Founded on Monopiles in Sand. Journal of Offshore Mechanics and Arctic Engineering 137, 041902. https://doi.org/10.1115/1.4030682
Gupta, R., 2020. Behaviour of monopile under combined cyclic load. Université Grenoble Alpes.
Hansen, M.O.L., 2015. Aerodynamics of wind turbines, 2nd ed., repr. ed. Routledge.
Harte, M., Basu, B., Nielsen, S.R.K., 2012. Dynamic analysis of wind turbines including soil-structure interaction. Engineering Structures 45, 509–518. https://doi.org/10.1016/j.engstruct.2012.06.041
Hassen, G., De Buhan, P., 2005. A two-phase model and related numerical tool for the design of soil structures reinforced by stiff linear inclusions. European Journal of Mechanics - A/Solids 24, 987–1001. https://doi.org/10.1016/j.euromechsol.2005.06.009
Hassine, J.B., 2011. Foundation condition monitoring. Presented at the Wind turbine condition monitoring workshop, Broomfield, CO: RES Americas, pp. 1–24.
Hatem, A., 2009. Comportement en zone sismique des inclusions rigides: Analyse de l'interaction sol-inclusion-matelas de répartition–structure. Lille 1.
Haza Rozier, E., Vinceslas, G., Le Kouby, A., Duprez, T., 2012. Instumentation des fondations d'une éolienne : Cas des inclusions rigides. Presented at the JNGG 2012, p. 9.
He, M., Bai, X., Ma, R., Huang, D., 2019. Structural monitoring of an onshore wind turbine foundation using strain sensors. Structure and Infrastructure Engineering 15, 314–333. https://doi.org/10.1080/15732479.2018.1546325
IEA, 2013. Technology roadmap: Wind energy. Technical report, IEA. (Tech. Rep). International Energy Agency.
IEC 61400-1, n.d. 61400-1: Wind turbines part 1: Design requirements.

IEC 61400-1 (Edition 3) (Ed.), 2005. Design requirements: = Exigences de conception, Ed. 3.0, 2005-08. ed, Wind turbines. IEC, Geneva.
IEC 61400-3, 2005. Wind turbinespart 1: Design requirements. International Electrotechnical Commission, Geneva.
Indicator, S., 2004. Guide to geotechnical instrumentation. Washington, USA.
IRENA, 2018. Statistics Data.
Ishibashi, I., Zhang, X., 1993. Unified dynamic shear moduli and damping ratios of sand and clay. Soils and foundations 33, 182–191.
Iten, M., 2012. Novel applications of distributed fiber-optic sensing in geotechnical engineering. vdf Hochschulverlag AG.
Janssen, L.G.J., Brøndsted, P., Thibaux, P., Gimondo, P., Klimpel, A., Johansen, B.B., 2012. Scientific assessment in support of the materials roadmap enabling low carbon energy technologies: wind energy. Publications Office, LU.
Jawad, H.S.H.A., Mashhour, I.M., Akl, S.A.Y., Abu-keifa, M.A., 2023. Effectiveness of concrete rigid inclusions for coastal reclaimed liquefiable soils. Ain Shams Engineering Journal 14, 101857. https://doi.org/10.1016/j.asej.2022.101857
Jenck, O., 2005. Le renforcement des sols compressibles par inclusions rigides verticales. Modélisation physique et numérique. INSA de Lyon.
Jimenez, G.A.L., 2019. Static and Dynamic behaviour of pile supported structures in soft soil.
Kania, J.G., Sorensen, K.K., Fellenius, B.H., 2020. Application of Distributed Fibre Optic Cables in Piles 51.
Karabalis, D.L., Beskos, D.E., 1984. Dynamic response of 3-D rigid surface foundations by time domain boundary element method. Earthquake Engng. Struct. Dyn. 12, 73–93. https://doi.org/10.1002/eqe.4290120106
Kausel, E., 2010. Early history of soil–structure interaction. Soil Dynamics and Earthquake Engineering 30, 822–832. https://doi.org/10.1016/j.soildyn.2009.11.001
Kechavarzi, C., Soga, K., de Battista, N., Pelecanos, L., Elshafie, M.Z.E.B., Mair, R.J., 2015. Distributed fibre optic strain sensing for monitoring civil infrastructure: a practical guide. ICE Publishing, London.
Khadour, A., Waeytens, J., 2018. Monitoring of concrete structures with optical fiber sensors, in: Eco-Efficient Repair and Rehabilitation of Concrete Infrastructures. Elsevier, pp. 97–121. https://doi.org/10.1016/B978-0-08-102181-1.00005-8
Khan, Z., El Naggar, M.H., Cascante, G., 2011. Frequency dependent dynamic properties from resonant column and cyclic triaxial tests. Journal of the Franklin Institute 348, 1363–1376. https://doi.org/10.1016/j.jfranklin.2010.04.003
Kondner, R.L., 1963. Hyperbolic Stress-Strain Response: Cohesive Soils. J. Soil Mech. and Found. Div. 89, 115–143. https://doi.org/10.1061/JSFEAQ.0000479
Kramer, S.L., 1996. Geotechnical earthquake engineering, Prentice-Hall international series in civil engineering and engineering mechanics. Prentice Hall, Upper Saddle River, NJ.
Kulhawy, F.H., 1984. Limiting tip and side resistance: fact or fallacy?, in: Analysis and Design of Pile Foundations. ASCE, pp. 80–98.
Lancellotta, R., 1995. Geotechnical engineering. AA Balkema, Rotterdam.
Langlade, T., 2021. Vulnerability and risk analyzes of structures subjected to earthquake-induced building pounding with a non-smooth contact dynamics method (Doctoral dissertation). Université de Lyon.
Li, Z., Kotronis, P., Escoffier, S., Tamagnini, C., 2018. A hypoplastic macroelement formulation for single batter piles in sand. Num Anal Meth Geomechanics 42, 1346–1365. https://doi.org/10.1002/nag.2794
Li, Z., Kotronis, P., Escoffier, S., Tamagnini, C., 2016. A hypoplastic macroelement for single vertical piles in sand subject to three-dimensional loading conditions. Acta Geotech. 11, 373–390. https://doi.org/10.1007/s11440-015-0415-7
Liu, Z., Lacasse, S., 2022. Machine learning in geotechnical engineering: Opportunities and applications. Presented at the Australian Geomechanics Society, Sydney, Australia.

Lombardi, D., Bhattacharya, S., Muir Wood, D., 2013. Dynamic soil–structure interaction of monopile supported wind turbines in cohesive soil. Soil Dynamics and Earthquake Engineering 49, 165–180. https://doi.org/10.1016/j.soildyn.2013.01.015

Lopez-Querol, S., Cui, L., Bhattacharya, S., 2017. Numerical Methods for SSI Analysis of Offshore Wind Turbine Foundations, in: Wind Energy Engineering. Elsevier, pp. 275–297. https://doi.org/10.1016/B978-0-12-809451-8.00014-X

Mánica Malcom, M.Á., Ovando-Shelley, E., Botero Jaramillo, E., 2016. Numerical Study of the Seismic Behavior of Rigid Inclusions in Soft Mexico City Clay. Journal of Earthquake Engineering 20, 447–475. https://doi.org/10.1080/13632469.2015.1085462

Marques, A.C., Fuinhas, J.A., Manso, J.P., 2011. A Quantile Approach to Identify Factors Promoting Renewable Energy in European Countries. Environ Resource Econ 49, 351–366. https://doi.org/10.1007/s10640-010-9436-8

Martínez, E., Latorre-Biel, J.I., Jiménez, E., Sanz, F., Blanco, J., 2018. Life cycle assessment of a wind farm repowering process. Renewable and Sustainable Energy Reviews 93, 260–271. https://doi.org/10.1016/j.rser.2018.05.044

Menard Group, n.d. https://www.menard-group.com/.

Michel, P., Butenweg, C., Klinkel, S., 2018. Pile-grid foundations of onshore wind turbines considering soil-structure-interaction under seismic loading. Soil Dynamics and Earthquake Engineering 109, 299–311. https://doi.org/10.1016/j.soildyn.2018.03.009

Milane, R., 2021. Deep foundations of a high-rise building: An in-situ testing and numerical study. Université de Lyon.

Mirza, S.A., Brant, W., 2009. Footing design, in: ACI Design Handbook. pp. 189–204.

Modu, J., 2022. Physical and numerical modeling of transfer mechanisms of onshore wind turbine foundations. Insa Lyon.

Mohamad, H., Tee, B.P., Chong, M.F., Ang, K.A., 2017. Investigation of shaft friction mechanisms of bored piles through distributed optical fibre strain sensing. Presented at the 9th International Conference on Soil Mechanics and Geotechnical Engineering.

Mohamed, W., Austrell, P.-E., 2018. A comparative study of three onshore wind turbine foundation solutions. Computers and Geotechnics 94, 46–57. https://doi.org/10.1016/j.compgeo.2017.08.022

Montrasio, L., Nova, R., 1997. Settlements of shallow foundations on sand: geometrical effects. Géotechnique 47, 49–60. https://doi.org/10.1680/geot.1997.47.1.49

Motallebiyan, A., Bayat, M., Nadi, B., 2020. Analyzing the Effects of Soil-Structure Interactions on the Static Response of Onshore Wind Turbine Foundations Using Finite Element Method. Civ. Eng. Infrastruct. J. 53. https://doi.org/10.22059/ceij.2020.281914.1586

Nardelli, A., 2019. The shaft friction degradation of piles under cyclic axial loading in wind turbine foundations (Doctoral dissertation). Universidade de São Paulo.

NF P 94-150-1, n.d. Essai statique de pieu isolé sous un effort axial.

NF P94-261, 2012. Justification des ouvrages géotechniques, Normes d'application nationale de l'Eurocode 7, Fondations superficielles.

NF P94-262, 2012. Justification des ouvrages géotechniques, Normes d'application nationale de l'Eurocode 7, Fondations profondes.

Nguyen, V.T., Hassen, G., De Buhan, P., 2016. Assessing the dynamic stiffness of piled-raft foundations by means of a multiphase model. Computers and Geotechnics 71, 124–135. https://doi.org/10.1016/j.compgeo.2015.08.014

Nicholson, P., 2014. Soil improvement & ground modification methods, 1st edition. ed. Elsevier, Waltham, MA.

Nikitas, G., Vimalan, N.J., Bhattacharya, S., 2016. An innovative cyclic loading device to study long term performance of offshore wind turbines. Soil Dynamics and Earthquake Engineering 82, 154–160. https://doi.org/10.1016/j.soildyn.2015.12.008

Nova, R., Montrasio, L., 1991. Settlements of shallow foundations on sand. Géotechnique 41, 243–256. https://doi.org/10.1680/geot.1991.41.2.243

Novak, M., El Hifnawy, L., 1988. Structural response to wind with soil-structure interaction. Journal of Wind Engineering and Industrial Aerodynamics 28, 329–338. https://doi.org/10.1016/0167-6105(88)90129-8
NREL, 2014. Wind Energy Foundation Systems: Overview and Comparison. National Renewable Energy Laboratory.
Obrzud, R.F., 2010. On the use of the Hardening Soil Small Strain model in geotechnical practice. Numerics in geotechnics and structures 16, 1–17.
Okabe, A., Boots, B., Sugihara, K., Chiu, S.N., 2009. Spatial tessellations: concepts and applications of Voronoi diagrams.
Okyay, U. S., Briançon, L., 2012. Monitoring and numerical investigations of rigid inclusion reinforced concrete water tank. Presented at the 3rd International Conference on New Developments in Soil Mechanics and Geotechnical Engineering, Near East University, Nicosia, North Cyprus, pp. 28–30.
Okyay, Umur Salih, Briançon, L., 2012. Monitoring and numerical investigations of rigid inclusion reinforced concrete water tanks. Presented at the 3rd International Conference on New Developments in Soil Mechanics and Geotechnical Engineering, pp. 28–30.
Paniagua, W.I., Ibarra, E., Valle, J.A., 2007. Rigid inclusions for soil improvement in a 76 building complex.
Paolucci, R., Pecker, A., 1997. Seismic Bearing Capacity of Shallow Strip Foundations on Dry Soils. Soils and Foundations 37, 95–105. https://doi.org/10.3208/sandf.37.3_95
Peck, R.B., 1993. The Coming of Age of Soil Mechanics: 1920-1970.
Peck, R.B., 1969. Advantages and Limitations of the Observational Method in Applied Soil Mechanics. Géotechnique 19, 171–187. https://doi.org/10.1680/geot.1969.19.2.171
Pecker, A., 2011. Dynamique des structures et des ouvrages, Ecole des Ponts-ParisTech. ed.
Pecker, A., 2004. Design and Construction of the Rion Antirion Bridge, in: Geotechnical Engineering for Transportation Projects. Presented at the GeoTrans 2004, American Society of Civil Engineers, Los Angeles, California, United States, pp. 216–240. https://doi.org/10.1061/40744(154)7
Pecker, A., 2000. Le pont de Rion-Antirion: fiabilite et conception parasismique des foundations. La sécurité des grands ouvrages. Hommage aPierre Londe. Presses de l'Ecole Nationale des Ponts et Chaussée 21–37.
Peralta, P., Achmus, M., 2010. An experimental investigation of piles in sand subjected to lateral cyclic loads, in: Physical Modelling in Geotechnics, Two Volume Set. CRC Press, pp. 1009–1014.
Pérez-Herreros, J., 2020. Dynamic soil-structure interaction of pile foundations: experimental and numerical study. École centrale de Nantes.
Perry, M., McAlorum, J., Fusiek, G., Niewczas, P., McKeeman, I., Rubert, T., 2017. Crack Monitoring of Operational Wind Turbine Foundations. Sensors 17, 1925. https://doi.org/10.3390/s17081925
Pham, H.V., Briançon, L., Dias, D., Racinais, J., 2019. Investigation of behavior of footings over rigid inclusion-reinforced soft soil: experimental and numerical approaches. Can. Geotech. J. 56, 1940–1952. https://doi.org/10.1139/cgj-2018-0495
Pham, H.V., Dias, D., Miranda, T., Cristelo, N., Araújo, N., 2018. 3D Numerical Modeling of Foundation Solutions for Wind Turbines. International Journal of Geomechanics 18, 04018164. https://doi.org/10.1061/(ASCE)GM.1943-5622.0001318
Pham, V.H., 2018. 3D modelling of Soft soil Improvement by Rigid Inclusions-Complex and Cyclic loading. Université Grenoble Alpes (ComUE).
PLAXIS Manual, 2020. PLAXIS 2D-Reference Manual.
Plomteux, C., 2010. Approche pour le dimensionnement des renforcements de sol par inclusions rigides.
Plomteux, C., Ciortan, R., 2010. Integrated Ground Improvement solution for the largest wind farm project in Europe. Research to Design in European Practice, Bratislava, Slovak Republic, June 2, 4, 2010.

Plomteux, C., Lacazedieu, M., 2007. Embankment construction on extremely soft soils using controlled modulus columns for Highway 2000 project in Jamaica. Presented at the Proceedings of the 16th Southeast Asian Geotechnical Conference.
Puech, A., Garnier, J. (Eds.), 2017. Design of piles under cyclic loading: SOLCYP recommendations. ISTE, Ltd. ; Wiley, London, UK, Hoboken, NJ.
Pytlik, R., 2016. DOCTEUR DE L'UNIVERSITÉ DU LUXEMBOURG EN SCIENCES DE L'INGÉNIEUR.
Racinais, J., Burtin, P., 2017. Ground improvement solutions for transport infrastructure: philosophy and case histories. Improvement, Reinforcement and Rehabilitation of Transport Infrastructures 54.
Racinais, J., Plomteux, C., 2011. Design of slab-on-grades supported with soil reinforced by rigid inclusions, in: Geotechnical Engineering: New Horizons. IOS Press, pp. 105–112.
Racinais, J, Thomas, B., Ong, R., 2016. Twenty years of CMC successful application. Presented at the Retrieved from 19th Southeast Asian Geotechnical Conference.
Racinais, Jérôme, Thomas, B., Ong, R., 2016. Twenty years of CMC successful application. Presented at the Retrieved from 19th Southeast Asian Geotechnical Conference.
Rangel-Núñez, J.L., Gómez-Bernal, A., Aguirre-González, J., Sordo-Zabay, E., Ibarra-Razo, E., 2008. Dynamic response of soft soil deposits improved with rigid inclusions. Presented at the 14th World Conference on Earthquake Engineering (14WCEE), pp. 1–8.
Risø, D.N.V., Veritas, N., 2002. Guidelines for design of wind turbines. Wind Energy Department.
Rivera Rojas, A.J., 2019. Lateral response of stiff column-supported shallow foundations. Virginia Tech.
Rubert, T., Perry, M., Fusiek, G., McAlorum, J., Niewczas, P., Brotherston, A., McCallum, D., 2017. Field demonstration of real-time wind turbine foundation strain monitoring. Sensors 18, 97. https://doi.org/10.3390/s18010097
Russo, G., Abagnara, V., Poulos, H.G., Small, J.C., 2013. Re-assessment of foundation settlements for the Burj Khalifa, Dubai. Acta Geotech. 8, 3–15. https://doi.org/10.1007/s11440-012-0193-4
Sahyouni, A., Briançon, L., Grange, S., Burtin, P., Racinais, J., 2022. Instrumentation of a real-scale wind turbine foundation underlined by rigid inclusions. Presented at the 11th International Symposium on Field Monitoring in Geomechanics, Imperial College London.
Said, I., De Gennaro, V., Frank, R., 2009. Axisymmetric finite element analysis of pile loading tests. Computers and Geotechnics 36, 6–19. https://doi.org/10.1016/j.compgeo.2008.02.011
Salciarini, D., Bienen, B., Tamagnini, C., 2011. A hypoplastic macroelement for shallow foundations subject to six-dimensional loading paths. Presented at the roceedings of the Second International Symposium on Computational Geomechanics (ComGeo II), International Centre for Computational Engineering, pp. 721–733.
Salciarini, D., Tamagnini, C., 2009. A hypoplastic macroelement model for shallow foundations under monotonic and cyclic loads. Acta Geotech. 4, 163–176. https://doi.org/10.1007/s11440-009-0087-2
Salm, S., Hille, S.L., Wüstenhagen, R., 2016. What are retail investors' risk-return preferences towards renewable energy projects? A choice experiment in Germany. Energy Policy 97, 310–320. https://doi.org/10.1016/j.enpol.2016.07.042
Santagata, M., Germaine, J.T., Ladd, C.C., 2005. Factors Affecting the Initial Stiffness of Cohesive Soils. J. Geotech. Geoenviron. Eng. 131, 430–441. https://doi.org/10.1061/(ASCE)1090-0241(2005)131:4(430)
Santamarina, J.C., Park, J., Terzariol, M., Cardona, A., Castro, G.M., Cha, W., Garcia, A., Hakiki, F., Lyu, C., Salva, M., Shen, Y., Sun, Z., Chong, S.-H., 2019. Soil Properties: Physics Inspired, Data Driven, in: Lu, N., Mitchell, J.K. (Eds.), Geotechnical Fundamentals for Addressing New World Challenges, Springer Series in Geomechanics and Geoengineering. Springer International Publishing, Cham, pp. 67–91. https://doi.org/10.1007/978-3-030-06249-1_3
Satibi, S., 2009. Numerical analysis and design criteria of embankments on floating piles, Mitteilung ... des Instituts für Geotechnik. Inst. für Geotechnik, Stuttgart.

Schaefer, V.R., Mitchell, J.K., Berg, R.R., Filz, G.M., Douglas, S.C., 2012. Ground Improvement in the 21st Century: A Comprehensive Web-Based Information System, in: Geotechnical Engineering State of the Art and Practice. Presented at the GeoCongress 2012, American Society of Civil Engineers, Oakland, California, United States, pp. 272–293. https://doi.org/10.1061/9780784412138.0011

Schanz, T., Vermeer, P.A., Bonnier, P.G., 1999. The hardening soil model: Formulation and verification, in: Beyond 2000 in Computational Geotechnics. p. 16.

Schlosser, F., Juran, I., Jacobsen, H.M., 1983. Soil Reinforcement: general report: session no. 5. Presented at the Proc. of VIII ECSMFE: Helsinki, pp. 159–1180.

Schweiger, H.F., 2009. Influence of constitutive model and EC7 design approach in FE analysis of deep excavations. Presented at the Proceeding of ISSMGE International Seminar on Deep Excavations and Retaining Structures, pp. 99–114.

Seymour, S., 2018. Numerical modelling of onshore wind turbine gravity foundations susceptible to cyclic soil degradation. University of Cape Town.

Shirato, M., Paolucci, R., Kouno, T., Nakatani, S., Fukui, J., Nova, R., Di Prisco, C., 2008. Numerical Simulation of Model Tests of Pier-Shallow Foundation Systems Subjected to Earthquake Loads Using an Elasto-Uplift-Plastic Macro Element. Soils and Foundations 48, 693–711. https://doi.org/10.3208/sandf.48.693

Siegel, T., McGillivray, A., 2009. Interpreted residual load in an augered cast-in-place pile. Presented at the Proceedings of the Deep Foundations Institute 34th annual conference on deep foundations, Kansas City, MO.

Sienko, R., Bednarski, L., Kanty, P., Howiacki, T., 2019. Application of Distributed Optical Fibre Sensor for Strain and Temperature Monitoring within Continuous Flight Auger Columns. IOP Conf. Ser.: Earth Environ. Sci. 221, 012006. https://doi.org/10.1088/1755-1315/221/1/012006

Simon, A., Courtois, A., Clauzon, T., Coustabeau, E., Vinit, S., 2015. Long-term measurement of strain in concrete: durability and accuracy of embedded vibrating wire strain gauges. SMAR.

Simon, B., 2012. General report S5 Rigid Inclusions and Stone Columns.

Simon, B., 2010. Une méthode simplifiée pour le calcul des semelles sur sol renforcé par inclusions rigides. Presented at the JNGG, pp. 529–536.

Sloan, J.A., 2011. Column-supported embankments: full-scale tests and design recommendations. Virginia Tech.

Spross, J., Johansson, F., 2017. When is the observational method in geotechnical engineering favourable? Structural Safety 66, 17–26. https://doi.org/10.1016/j.strusafe.2017.01.006

Steigen, T., 2018. Solar PhotoVoltaics in Norway: a state of the art study (Master's Thesis). Norwegian University of Life Sciences.

Sudret, B., 1999. Multiphase model for inclusion-reinforced structures. ENPC, Paris.

Sudret, B., De Buhan, P., 2001. Multiphase model for inclusion-reinforced geostructures: Application to rock-bolted tunnels and piled raft foundations. Int. J. Numer. Anal. Meth. Geomech. 25, 155–182. https://doi.org/10.1002/nag.123

Suleiman, M.T., Ni, L., Davis, C., Lin, H., Xiao, S., 2016. Installation Effects of Controlled Modulus Column Ground Improvement Piles on Surrounding Soil. J. Geotech. Geoenviron. Eng. 142, 04015059. https://doi.org/10.1061/(ASCE)GT.1943-5606.0001384

Tamagnini, C., Salciarini, D., Ragni, R., 2013. Implementation of 6–dof hypoplastic macroelement in a finite element code. Presented at the Proceedings of third international symposium on computational geomechanics (ComGeo III). Berlin: Springer.

Tan, F.S.C., 1990. Centrifuge and theoretical modelling of conical footings on sand. https://doi.org/10.17863/CAM.31036

Tan, X., Bao, Y., Zhang, Q., Nassif, H., Chen, G., 2021. Strain transfer effect in distributed fiber optic sensors under an arbitrary field. Automation in Construction 124, 103597. https://doi.org/10.1016/j.autcon.2021.103597

Thai Son, Q., 2009. Développements théorique et numérique d'un modèle multiphasique pour le calcul des ouvrages renforcés par inclusions. ENPC, Paris.

Thai Son, Q., Hassen, G., De Buhan, P., Okyay, U., Dias, D., 2009. Dimensionnement sous sollicitation sismique de sols de fondations renforcés par inclusions rigides, in: Proceedings of the 17th International Conference on Soil Mechanics and Geotechnical Engineering. IOS Press, pp. 606–609.

Thévenaz, L., Niklès, M., 2007. Recent progress in Brillouin distributed fibre sensing. Presented at the The 2nd International Workshop on Opto-electronic Sensor-based Monitoring in Geoengineering, Nanjing, China, pp. 12–19.

Thomas H, H., 1985. Field instrumentation in geotechnical engineering.

Turner, J.A., 1999. A realizable renewable energy future. Science 285, 687–689.

UNFCCC, 2015. Adoption Of The Paris Agreement.

Van Eekelen, S.J., Brugman, M.H., 2016. Design guideline basal reinforced piled embankments. CRC Press.

Varaksin, S., Hamidi, B., Racinais, J., 2014. The Thin Line between Deep Foundations and Soil Improvement.

Vetter, K., 1998. Untersuchungen zum Tragverhalten der Kombinierten Pfahl-Plattengr ndung des Messeturms in Frankfurt am Main auf der Basis von Messungen und numerischen Computersimulation. echnische Universit t Darmstadt, Institut fr Geotechnik.

Wehnert, M., Vermeer, P.A., 2004. Numerical analyses of load tests on bored piles. Numerical methods in geomechanics–NUMOG IX 505–511.

WindEurope, 2017. Annual combined onshore and offshore wind energy statistics.

Wolf, J.P., 1985. Dynamic soil-structure interaction, Prentice-Hall international series in civil engineering and engineering mechanics. Prentice-Hall, Englewood Cliffs, N.J.

Yang, W., Court, R., Jiang, J., 2013. Wind turbine condition monitoring by the approach of SCADA data analysis. Renewable Energy 53, 365–376. https://doi.org/10.1016/j.renene.2012.11.030

Yilmaz, M., Eun, J., Tinjum, J.M., Fratta, D., 2022. In-Service Response of Shallow On-Shore Wind Turbine Generator Foundation. Geotech Geol Eng 40, 977–994. https://doi.org/10.1007/s10706-021-01938-1

Yu, J., Meng, X., Yan, B., Xu, B., Fan, Q., Xie, Y., 2020. Global Navigation Satellite System-based positioning technology for structural health monitoring: a review. Struct Control Health Monit 27. https://doi.org/10.1002/stc.2467

Yu, L.-Q., Wang, L.-Z., Guo, Z., Bhattacharya, S., Nikitas, G., Li, L.-L., Xing, Y.-L., 2015. Long-term dynamic behavior of monopile supported offshore wind turbines in sand. Theoretical and Applied Mechanics Letters 5, 80–84. https://doi.org/10.1016/j.taml.2015.02.003

Zachert, H., Triantafyllidis, T., Wienbroer, H., 2011. Experimentelle Untersuchung der Verformungsakkumulation eines Flachgründungsmodells von Offshore-Windenergieanlagen. Bautechnik 88, 782–792. https://doi.org/10.1002/bate.201101515

Zachert, H., Wichtmann, T., 2020. Approaches for the Design of Foundations for Offshore Wind Turbines: A Review Based on Comparisons with HCA-Based Models, in: Triantafyllidis, T. (Ed.), Recent Developments of Soil Mechanics and Geotechnics in Theory and Practice, Lecture Notes in Applied and Computational Mechanics. Springer International Publishing, Cham, pp. 113–135. https://doi.org/10.1007/978-3-030-28516-6_7

Zachert, H., Wichtmann, T., Triantafyllidis, T., 2016. Soil Structure Interaction of Foundations for Offshore Wind Turbines. Presented at the The 26th International Ocean and Polar Engineering Conference, p. ISOPE-I-16-346.

Zhang, J., Jenck, O., Dias, D., 2022. 3D Numerical Analysis of a Single Footing on Soft Soil Reinforced by Rigid Inclusions. Int. J. Geomech. 22, 04022113. https://doi.org/10.1061/(ASCE)GM.1943-5622.0002412

Zhou, Y., Liu, X., Deng, Z., Gao, Q.-F., 2021. Field monitoring and numerical analysis of the reinforced concrete foundation of a large-scale wind turbine. Advances in Materials Science and Engineering 2021, 1–14. https://doi.org/10.1155/2021/7656613